Restoration of Aluminum Aerospace Parts and Coatings using Cold Gas Dynamic Spraying

By

Daniel MacDonald

Thesis submitted to the Department of Mechanical Engineering
in partial fulfillment of the requirements for the degree of
Master of Applied Science (Engineering)

University of Ottawa
Ottawa, Ontario, Canada
April 2014

ABSTRACT

The majority of the structural weight of many common commercial aircrafts is composed of high strength aluminum alloys. The properties of high performance aluminum alloys such as a high strength to weight ratio (specific strength), ease of recycling, crash energy absorption capacity, and corrosion resistance make them ideal for use in the aerospace field. As a result of the high performance nature of the parts and specific properties of the materials, manufacturing requires intricate casting, precision machining, and specific heat treatments – which results in expensive components. As a result of its excellent corrosion resistance properties, pure aluminum coatings are commonly used in the aerospace field for corrosion protection of steel, aluminum alloy components, and titanium alloy components. The common method to deposit these coatings is called ion vapour deposition (IVD). These IVD aluminum coatings provide the coating adhesion, coverage, thickness, and corrosion resistance required to protect the part.

The present study was motivated by the potential use of the cold gas dynamic spray (CGDS) process to repair a) damaged aluminum alloy aerospace parts and b) damaged pure aluminum IVD coatings. The primary research objective was to successfully produce these repairs using commercially available aluminum alloy feedstock powders deposited with commercially available CGDS equipment. This work was treated as prequalification work for The Boeing Company to commercialize this process and therefore the repairs aim to meet the same standards (military and industrial) required of the original aluminum alloy parts and IVD aluminum coatings.

The use of CGDS was shown in this research to be a very promising as a process for the restoration of aluminum alloy aerospace components. The adhesion strength of the repaired aluminum components was found to be well above the accepted range for thermally sprayed repairs according to industrial standards. The repairs were subjected to a highly corrosive environment and showed only minor pitting. These sites could be reduced in the future with improved machining techniques and attention to surface detail prior to exposure to the salt fog. The only requirement that the repaired components did not meet was for the wear properties of the anodized layer, measured thought Taber abrasion testing. The results of this test, at times, approached the desired values, and

it is believed that, in the future, the quality and consistency of the coatings could be improved and the test would meet industrial standards.

The results of this research show that the use of CGDS as a process for the restoration of damaged aluminum IVD coatings is possible and is a promising alternative to conventional methods. The CGDS coatings were scrutinized to the same level as required of IVD coatings when they replaced toxic cadmium coatings in the late 1980s. The coating adhesion, demonstrated through glass bead abrasion and strip rupture testing, was shown to meet the current industrial standards. The corrosion testing of the repairs resulted in no visible red rust of the steel components, even when the steel was exposed.

ACKNOWLEDGEMENTS

First, I would like to take this opportunity to express my great appreciate to my thesis supervisor, Professor Bertrand Jodoin. His guidance and encouragement took me down the path I am now on and I am forever grateful for this. Thank you for being a mentor and a friend.

I am very grateful to have worked with so many industrial partners during my studies. I would like to offer my special thanks to Stephen Gaydos and all of our collaborators at the Boeing Company, Centerline, and Mitacs. I am also thankful for opportunity to work with NWMO and apply my skills in a new industry.

I wish to acknowledge the help provided the technicians from the machine shop at the University of Ottawa. Having access to skilled technicians was crucial in completing this research, thank you. I would also like to thank Dr. Mohammed Yandouzi for his involvement throughout my work and for the all of his help in materials science and analysis.

Thank you Ramin Ghelichi and those at Politecnico di Milano for the opportunity to work on other interesting projects.

I would like to thank my colleagues for making this an amazing experience both in and outside of the lab. Ruben Fernandez, Jamil Assaad, Tyler Samson, Antoine Bacciochini, Mathieu Bolduc, Jean-Louis Pelletier, Bu Hengyong, Deliange (Leon) Goudl, Patrick Trahan, thank you for your help with this research.

I wish to thank my family for showing me so much support and encouragement during my studies. Lastly, I would like to thank Bryn for supporting me all these years; I couldn't have done it without you.

This page has intentionally been left blank.

Table of Contents

List of Tables

List of Figures

This page has intentionally been left blank.

1 INTRODUCTION

1.1 Background

High strength aluminum alloys constitute the majority of the structural weight of many common commercial aircrafts [1]–[3]. A breakdown of structural weight percentages of different materials in commercial aircrafts is shown in Figure 1.1.

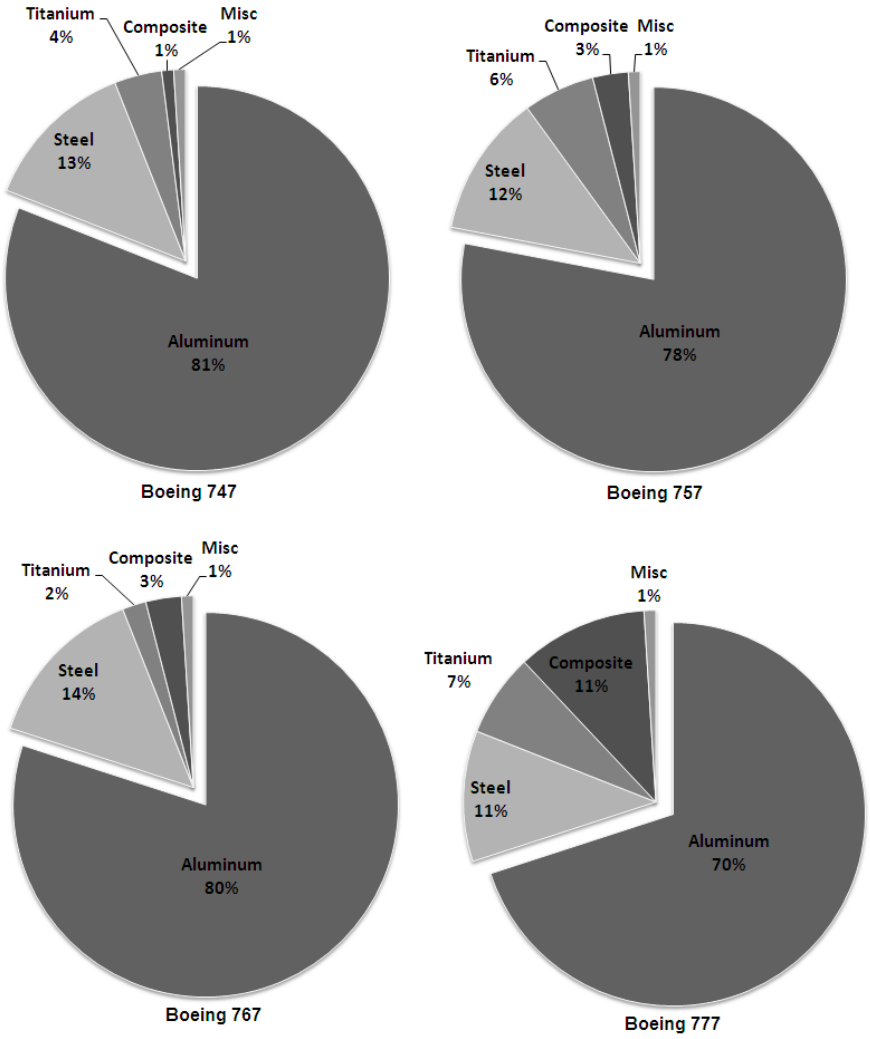

Figure 1.1: Structural weight percentage of different materials in common Boeing commercial aircraft [1].

The properties of high performance aluminum alloys such as a high strength to weight ratio (specific strength), ease of recycling, crash energy absorption capacity, and corrosion resistance

make them ideal for use in the aerospace field [2]–[4]. The specific strength, in particular, is a key feature for the aerospace sector, where weight reduction directly translates into fuel saving [1]. As a result of the high performance nature of the parts and specific properties of the materials, manufacturing requires intricate casting, precision machining, and specific heat treatments – which results in expensive components [1], [3], [4].

As a result of its excellent corrosion resistance properties, pure aluminum coatings are commonly used in the aerospace field for corrosion protection of steel, aluminum alloy components, and titanium alloy components. The common method to deposit these coatings is called ion vapour deposition (IVD) [5]. In the IVD process, a vacuum chamber is backfilled with argon gas, and a high negative potential is applied between the parts and an evaporation source. Metal (in this case, aluminum) is evaporated and becomes ionized and is accelerated towards the part surface, resulting in excellent uniformity and adhesion [5]–[7]. These thin (25μm to 50 μm) IVD aluminum coatings provide the coating adhesion, coverage, thickness, and corrosion resistance required to protect the part [5], [8].

During operation and manufacturing, the aluminum alloy components and IVD aluminum coatings regularly sustain damage. There is no approved rework/ repair process for the aluminum components; the parts are scrapped/ recycled and new parts must be manufactured. In order to repair the damaged aluminum coatings, the rework process consists of exposing the entire component with a caustic solution that selectively dissolves the coating. The bare component is then masked and recoating using the IVD process [5]. These repairs are time consuming, labour intensive, not environmentally sound, and expensive.

This research proposes a potential repair solution for these aerospace parts and coatings using a thermal spray process known as cold gas dynamic spraying (CGDS). CGDS is a solid state spray process that relies on the kinetic energy (at impact) of solid particles to plastically deform upon impact and form coatings [9]. This coating process is particularly well suited for ductile materials such as aluminum and its alloys [10].

1.2 Motivation and Research Objectives

The present study was motivated by the potential use of the CGDS process to repair a) damaged aluminum alloy aerospace parts and b) damaged pure aluminum IVD coatings. The primary research objective was to successfully produce these repairs using commercially available aluminum alloy feedstock powders deposited with commercially available CGDS equipment. This work is being treated as prequalification work for The Boeing Company to commercialize this process and therefore the repairs aim to meet the same standards (military and industrial) required of the original aluminum alloy parts and IVD aluminum coatings. In order to achieve the goals of this research, the following procedure was undertaken:

1) Creation of CGDS coatings using an array of different process parameters using aluminum alloy powders on relevant substrates.
2) Investigation of the coatings to isolate the CGDS parameters best suited to produce the required repairs.
3) Evaluation of the mechanical/ chemical properties of repairs (sprayed using the chosen parameters) and comparison with existing commercial/ military standards.

1.3 Thesis Arrangement

The material in this thesis is organized in seven chapters. Chapter 1 presents a general introduction to the background information relevant to the research project including the general motivation and research objectives.

A summary of relevant literature is provided in Chapter 2. This includes: background material on relevant aluminum and aluminum alloys, aluminum IVD, and conversion coating processes; a detailed description of the CGDS process and a brief description of other commonly used thermal spray processes; and a summary of existing studies using CGDS to deposit aluminum.

Chapter 3 provides a detailed description of the specific objectives of the research. This chapter demonstrates the importance of the specific objectives in satisfying the main motivation of this research.

The method of investigation and the experimental research approach is detailed in Chapter 4. This includes detailed information on the experimental materials, experimental equipment, characterization equipment, characterization techniques, and industrial/ military standards required to complete the specific research objectives outlined in Chapter 3.

Chapter 5 details the experimental design, including test plans, CGDS parameters and number of samples. It also provides the results of the feasibility study in order to determine the CGDS parameters to be used for the characterization of the repairs. A discussion of these results is found inside this chapter.

Chapter 6 provides the results and discussion of the full characterization of the repairs. This chapter involves iterations (including repeating of tests) from the original plans outlined in chapter 4.

Chapter 7 provides any conclusions of the results found in Chapter 5 and Chapter 6. It also outlines the work that should be undertaken in the future in order to continue towards the research objectives. A complete list of references and appendices follow this chapter.

2 LITERATURE REVIEW

This chapter reviews up to date theory of relevant repair technology, aerospace materials, national and international standards, and current industry practices and trends. The purpose of this literature review is to gain adequate background knowledge to complete the goal of this research.

2.1 Aerospace Aluminum Components

2.1.1 Background

High strength aluminum alloys contribute over 60-80 percent of the structural weight of modern commercial aircrafts [1]–[3]. These alloys are prized for their high strength to weight ratios (see Figure 2.1) and good corrosion performance [1]–[3], [11]. Other exotic materials (e.g. titanium, composite materials (PMCs), and superalloys) may have higher specific strength and higher temperature tolerance than aluminum alloys (Figure 2.2), but they are prohibitively expensive. For example, titanium alloy (Ti-6Al-4V) cost 55.0-130 USD/kg compared to 9-9.70 USD/KG for aluminum 7075 (2003 cost estimate [4]). As a result of high availability and relatively low cost, aluminum alloys have come to dominate the commercial aerospace market, only recently being replaced with composite materials [1], [3].

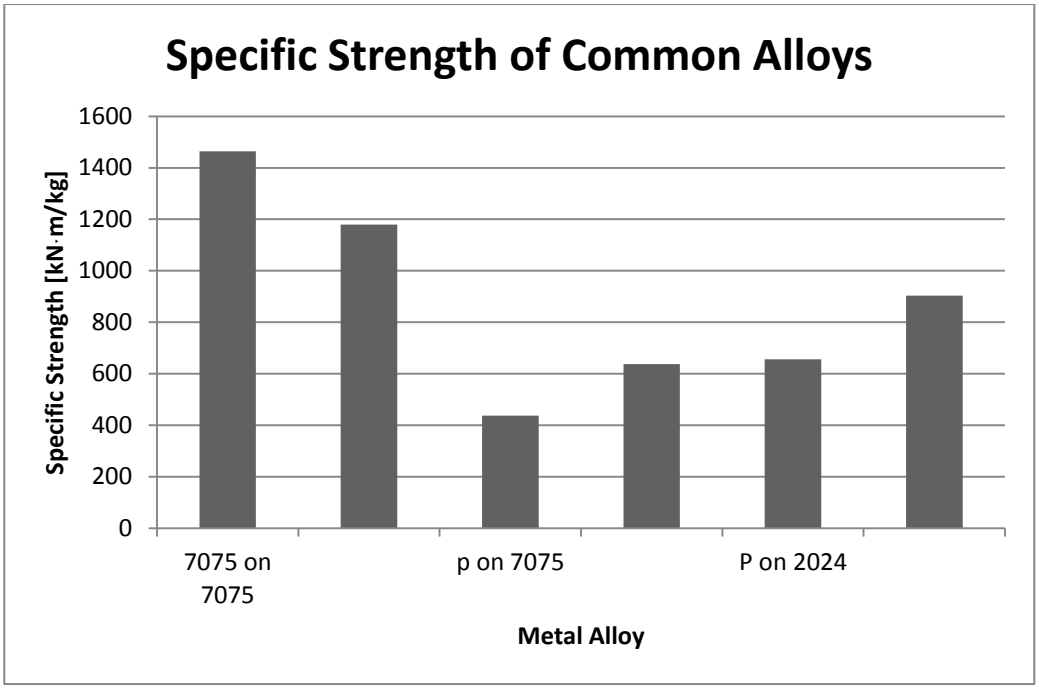

Figure 2.1: Specific strength of common metal alloys. Data acquired from [4], [12], [13].

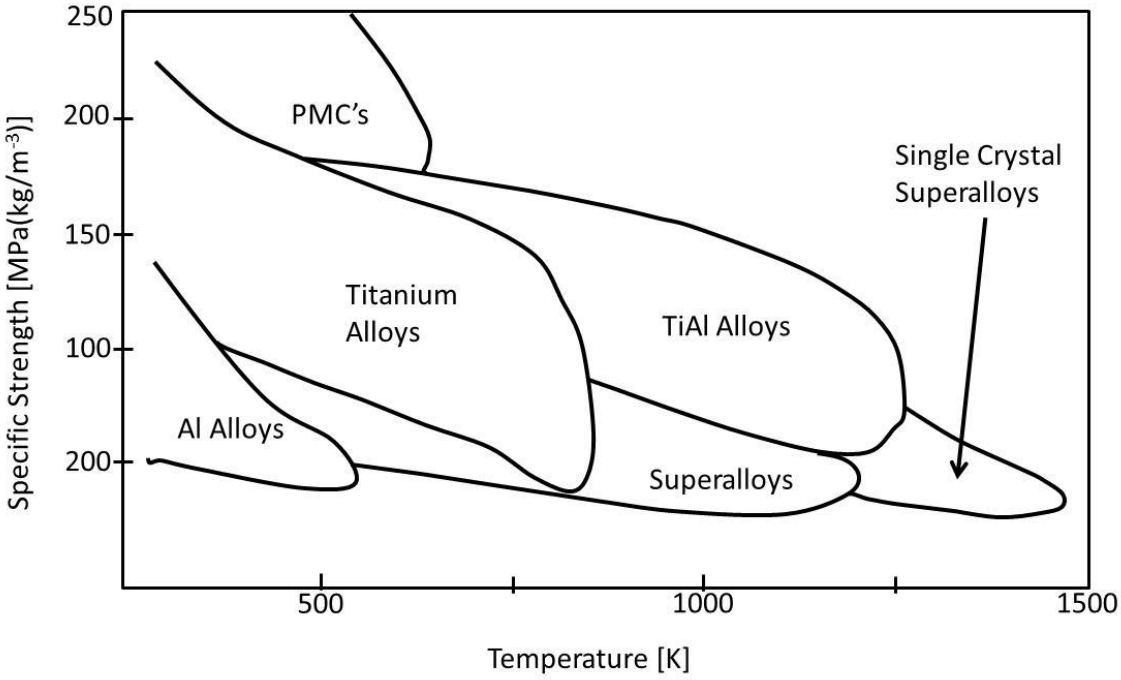

Figure 2.2: Specific strength vs. operating temperature for high performance aerospace materials (adapted from [2]).

2.1.2 Aluminum Alloys

For the last 100 years of commercial flight, the aerospace industry has relied on aluminum alloys to meet the need for light weight components. With the aerospace industry pushing advancement in materials, aluminum alloy castings (Al-Cu) were replaced with new high performance alloys in the early 1900s. Aluminum 2024, introduced in 1935, was the first of these alloys to dominate the aerospace sector, followed 20 years later by aluminum 7075 [1], [11]. These alloys still constitute the majority of the aluminum components in service.

Although higher strength aluminum alloys (such as aluminum 7055 and aluminum 2324) have been developed, this project focuses only on aluminum 2024 and aluminum 7075 for component repair. The reason for this being that access to these advanced alloys (in substrate and powder form) is restricted and prohibitively difficult. Aluminum 2024 and aluminum 7075 also demonstrate opposite ends of the fracture toughness and yield strength spectrum (Figure 2.3) [1], [11]. This study will also focus on pure aluminum and aluminum 5083 for their corrosion properties.

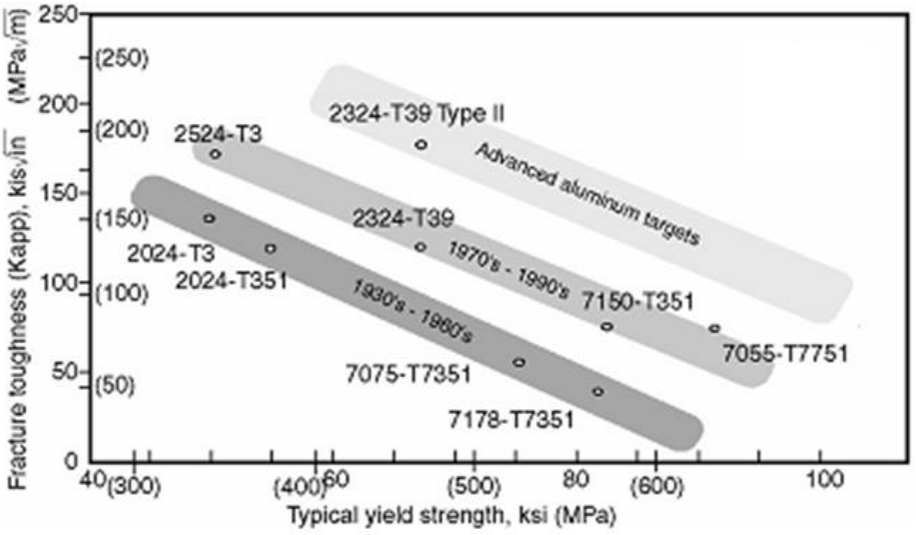

Figure 2.3: Strength-toughness development of aluminum alloys [1]

Aluminum alloys contain elements such as magnesium, chromium, copper, silicon, zinc, tin, lithium, and manganese. Copper is one of the most important additions and found in most

alloys. It has a substantial hardening effect though solid solution and precipitate hardening. Tin is added for antifriction characteristics and lithium is added to lower the density while increasing the elastic modulus. The other alloying elements, in proper concentrations, add hardness in a similar way as copper [11]. The real strength in these alloys comes from proper concentration of multiple elements combined with a heat treatment. This heat treatment (age hardening) allows for the formation of precipitates to pin dislocations, increasing strength [4], [11].

2.1.2.1 Aluminum 7075

The zinc rich 7000 series of aluminum alloys are known for their high specific strength (see Figure 2.1) and are commonly used for upper wing surfaces, spars and ribs, in sheets, plates, and extrusions [1], [3]. Developed in the 1950s, aluminum 7075 is an alloy of Al-5.7Zn-2.3Mg-1.5Cu-0.2Cr [4]. The alloy gains its strength through precipitates that form during heat treatment (commonly T6) [3], [4], [11], i.e. zinc and magnesium found in this alloy form $MgZn_2$ precipitates. The precipitates and alloying found in aluminum 7075 make it more susceptible to pitting corrosion, in comparison to pure aluminum [11]. Most aluminum 7075 surfaces must be converted into protective oxides in order to improve this property.

2.1.2.2 Aluminum 2024

In the 1920s, aluminum 2024, an alloy of Al-4.4Cu-1.5Mg-0.6Mn, was developed [1], [4]. A copper rich 2000 series aluminum alloy, aluminum 2024 was the most common aluminum alloy in aerospace applications before phased out by aluminum 7075. It is still common on aircraft to this day due to its high toughness and is primarily used for fuselage skins and lower wing surfaces [1], [3]. Aluminum 2024 owes its strength to precipitates (Al_2CuMg) formed during heat treatment (commonly T3) [3], [4]. Similar to aluminum 7075, the alloying makes it more susceptible to corrosion when compared to pure aluminum [11].

2.1.2.3 Aluminum 5083

Aluminum 5083, an alloy of Al-4.5Mg-0.7Mn, is not normally used as an aerospace alloy as its specific strength is not as high as aluminum 7075 or aluminum 2024 (see Figure 2.1) [4]. Unlike

aluminum 7075 and aluminum 2024, aluminum 5083 does not gain its strength from precipitate hardening, but rather from solid solution and strain hardening [11]. As a result of this, pitting corrosion does not occur as readily as the other alloys and results excellent corrosion performance in seawater and chemical environments [11], [14].

2.1.2.4 Pure Aluminum

Pure aluminum is not used as a structural component in the aerospace industry, but as a coating. The corrosion resistance of pure aluminum is superior to all other alloys, as pitting corrosion is uncommon. Pure aluminum develops a passive, uniform, oxide film which results in slow, even corrosion [4], [11], [14].

2.1.3 Heat Treatments and Temperature Limitations

Aluminum has a relatively low melting temperature (approximately 660°C) compared to other aerospace materials (e.g. titanium has a melting point of 1668°C) [4]. This limits aluminum to low temperature applications. Aluminum 2024 and aluminum 7075 also rely on precipitates for strengthening. These precipitates may coarsen or dissolve into solution if held at high temperatures for extended periods of time [1], [4]. A coarsening of precipitate size increases the dislocation energy required for cutting, strengthening the material, but at the same time increases the space between precipitates. Increasing this space reduces the Orowan (bowing) stress required for the dislocations to pass the precipitates – reducing the overall strength of the material (see Figure 2.4). Therefore, there is a precipitate size that maximizes strength and hardness - the further the precipitates are from this ideal size, the softer the material becomes [15]–[17].

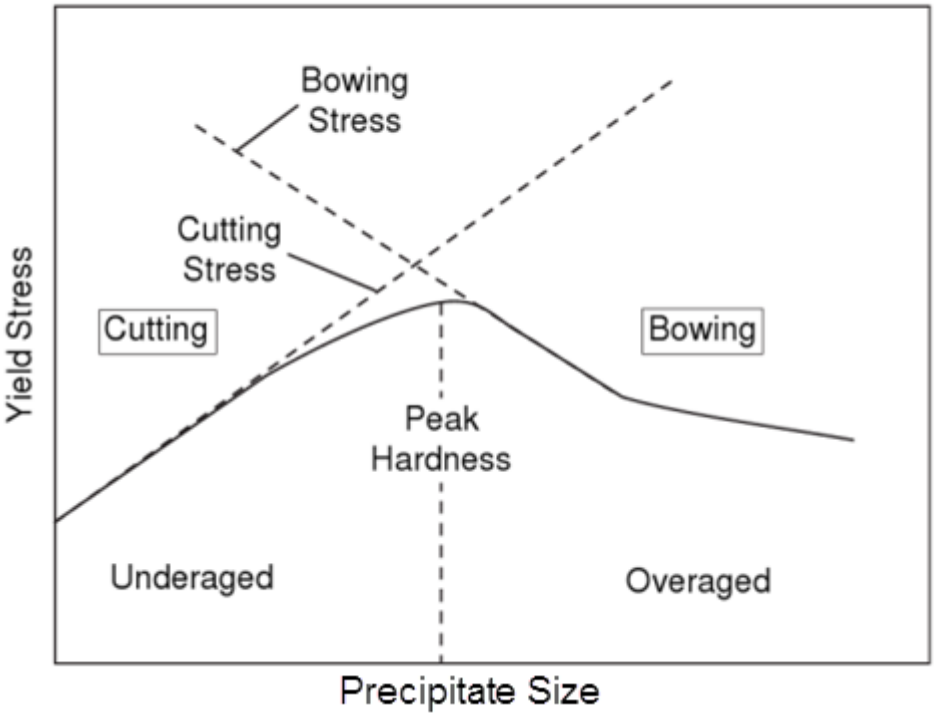

Figure 2.4: Relationship between yield strength vs. precipitate size showing the influence of cutting and bowing stresses. Modifed from *[17]*.

This limits the temperature at which parts can be exposed to. There is no exact value for a ceiling temperature for this to occur, but general guidelines are available (see Appendix I). If these components exceed their temperature limitations during operation (or during repairs) they will experience softening. This softening can be used as an indication that the heat treatment (precipitate size) has been modified [15].

2.1.4 Conversion Coating

Aluminum components are naturally covered by a protective, thin (5 to 15 nanometers) oxide (Al_2O_3) layer from being exposed to air [17]. This thin oxide layer provides adequate short term corrosion protection, but may be insufficient for long term corrosion prevention that is required for aerospace components. Therefore, the majority of aluminum aerospace components and coatings undergo a finishing process, likely a conversion coating, to improve the corrosion performance before use. Unlike conventional coatings, a conversion coating is not a protective

layer bonded to a surface; but rather, a conversion coating is any coating in which the surface itself is converted into the coating through a chemical (e.g. chromate conversion coating) or electro-chemical (e.g. anodizing) process. Conversion coatings increase corrosion resistance and surface hardness, add colour, and act as a paint primer for the metals to which they are applied [17]–[20].

2.1.4.1 Chromate Conversion Coating

Chromate conversion coatings (CCC) are the most common for aluminum components in non-wear applications. In this process, aluminum components are exposed to a hexavalent chromium (Chromium VI) bath. This caustic environment partially dissolves the existing alumina layer before creating a very thin layer of chromium oxide (CrO_3) on the remaining alumina surface. These chromium oxide films are inert, hydrophobic, and stable over a broad pH range; making them excellent coatings for corrosion resistance. The coatings are also slightly porous and residual hexavalent chromium can be found in these pores, resulting in a self-healing coating [20]–[22]. The coating porosity also makes these coatings excellent paint primers.

The chemical conversion coatings of aluminum aerospace parts for this research will be governed by MIL-C-5541F [23], in which the coatings are separated into different types and classes.

Type I: Coatings applied using hexavalent chromium. The coatings generally appear brown or gold in colour.
Type II: Coatings applied without hexavalent chromium. Coatings generally appear to add no colour (clear).
Class 1A: Coatings specified for maximum protection against corrosion. These coatings can be used as a finished component or may be painted. This type of coating is required for all non-anodized external aluminum surfaces in aircraft.
Class 3: A much thinner coating compared to Class 1A that provides corrosion protection with minimal electrical resistance.

The conversion coatings applicable to this study are Type 1, Class 1A. This is a common conversion coating used by The Boeing Company for commercial and military applications [23]. These coatings can range from a few nanometres to a few micrometres in thickness, depending on the strength of the solution and the length of exposure [20].

2.1.4.2 Anodization

A method to increase surface hardness and improve corrosion resistance is to make the naturally formed oxide layer thicker and more uniform. This can be accomplished through anodization; which creates a thicker passive oxide layer than can be produced in chemical conversion coatings [11], [17]. The process is a controlled form of oxidation and results in a thick, highly ordered, porous, aluminum structure that resists chipping and peeling. The honeycomb shaped porosity allows the components to be dyed easily; because of this property many commercial products are anodized for cosmetic reasons [11], [17], [18], [24], [25].

The anodization process increases the natural oxide layer on the surface of a component through electrolytic passivation. In the process, the part becomes the anode of an electrical circuit. The oxygen ions are released from the electrolyte and combine with the atoms at the surface of the part being anodized. The type of electrolyte and the voltage controls the properties of the anodized layer [11], [17], [18], [24], [25].

For this research, the governing document for anodic coatings on aluminum and aluminum alloys is MIL-A-8625F [24], where they are separated into different types and classes.

Type I: Conventional chromic acid anodizing.
Type IB: Low voltage chromic acid anodizing.
Type IC: Non-chromic acid anodizing acting as an alternative for Type I and Type IB.
Type II: Conventional sulfuric acid anodizing.
Type IIB: Thin sulfuric acid anodizing (often used as a Type IC).
Type III: Hardcoat sulfuric acid anodizing.
Class 1: Non-dyed.
Class 2: Dyed.

For this research, some components will undergo the common types of anodization used by The Boeing Company; Type II Class 1 and Type III Class 1. Type II coatings are the conventional sulfuric acid anodized coatings used often in commercial non-wear applications. The alumina layer will range between 1.8 μm to 25.4 μm. For wear applications Type III coatings are used [24]. These coatings follow a similar process as Type II except the process occurs at lower temperatures (approximately 0°C) [18]. The result of this cold process is an alumina layer that is between 12.7 μm to 114.3 μm thick [1]. This added thickness greatly increases the wear resistance of the coating [25].

2.2 Aluminum IVD Coatings

2.2.1 Background

In the late 1980s McDonnell Aircraft Company proposed the replacement of toxic cadmium coatings with aluminum coatings applied using the IVD process [2]. IVD aluminum coatings provided the adhesion, coverage, thickness, and corrosion resistance required of the original cadmium coatings [5]–[7]. These pure aluminum IVD coatings allowed any metallic component to have the surface properties of pure aluminum (such as a corrosion resistant, naturally occurring passive oxide layer and the ability to be conversion coated) without a significant effect on the mechanical properties of the base material [26]. The focus of this research will deal with the IVD of pure aluminum used by the Boeing Company to protect high strength steel components, often found in landing gear [6], [7], [17], [18].

2.2.2 Process

Ion vapour deposition is a plating process developed in the mid-1960s. In the IVD process, a vacuum chamber is backfilled with inert (often argon) gas, and a high negative potential is applied between the parts and the evaporation source. Metal (aluminum) is evaporated and a portion becomes ionized as it nears the cathode (substrate). The ionized metal then accelerates towards the substrate surface, resulting in excellent uniformity and adhesion[5]–[7], [26], [27].

High purity aluminum coatings are separated into types and classes in the governing document MIL-DTL-83488D [8].

Class 1: 0.025mm minimum thickness.
Class 2: 0.013mm minimum thickness.
Class 3: 0.008mm minimum thickness.
Type I: as coated.
Type II: with supplementary chromate treatment (see Section 2.1.4.1).

The IVD coatings relevant to this research are of Class 1, Type I and Class 1, Type II. This standard also the governing document for specific tests required of the coatings [7], including strip rupture (MIL-DTL-83488D - 4.4.2.2.), glass bead burnishing (MIL-DTL-83488D - 4.4.2.3), and corrosion resistance (MIL-DTL-83488D - 4.4.3) [8].

2.2.3 Damage and Restoration

Aluminum IVD coatings are thin and soft. These coatings are readily damaged during operation and manufacturing. There is no current technology that is being used with regularity for repairing damaged IVD components. Components are stripped of their coatings using a caustic chemical solution before being recoated entirely. This is a costly, environmentally damaging, and time consuming process [6], [7].

In recent years, there has been research into the reparation of these coatings as new technologies emerge. A study has been done by Tapphorn et al. into the reparation of aluminum IVD using kinetic metallization [28]. This research differs from the goals of the current investigation as it uses a different deposition process and a blend of metal and oxides as the repair material (Al-Trans™ [29]) [28].

2.3 Cold Gas Dynamic Spray

This study proposes a potential repair solution for aluminum alloy aerospace parts and pure aluminum IVD coatings using a thermal spray process known as cold gas dynamic spraying

(CGDS). CGDS is a solid state spray process that relies on the kinetic energy (at impact) of solid particles to form coatings. Particles are injected into an inert gas stream (normally nitrogen or helium) that is accelerated though a converging-diverging (de Laval) nozzle (see Figure 2.5) [9], [30], [31]. Particles in this stream are accelerated to high velocities before impacting the substrate to create coatings. Coating formation and adhesion in CGDS requires that the particles locally deform by experiencing adiabatic shear instabilities. In order for this type of deformation to occur, the impact velocity must be sufficiently high; this is known as the critical velocity [32]. These impacting particles form dense coatings with low oxide content, in comparison to other thermal spray processes [30], [33].

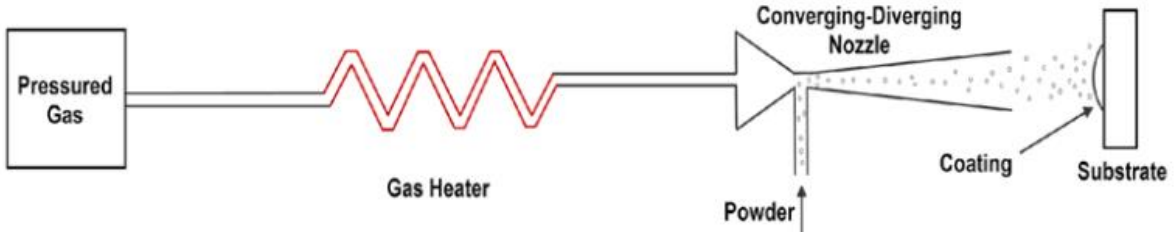

Figure 2.5: Schematic of a typical low pressure cold gas dynamic spray system

2.3.1 Background

In the mid-1980's Russian scientists at the Institute of Theoretical and Applied Mechanics of the Siberian Division of the Russian Academy of Science developed a process for depositing metallic particles using a high velocity gas stream. The process was discovered accidently when scientists noticed that trace particles were depositing on the leading edge of models in supersonic wind tunnel experiments [9], [34]. This process was further refined with by the development of a powder injection, gas heating, and nozzle design into what is now known as cold gas dynamic spraying. This design became the basis for the original patent that was approved in 1994 [31], [34]. A schematic of the original system from the patent can be found in Figure 2.6 [31].

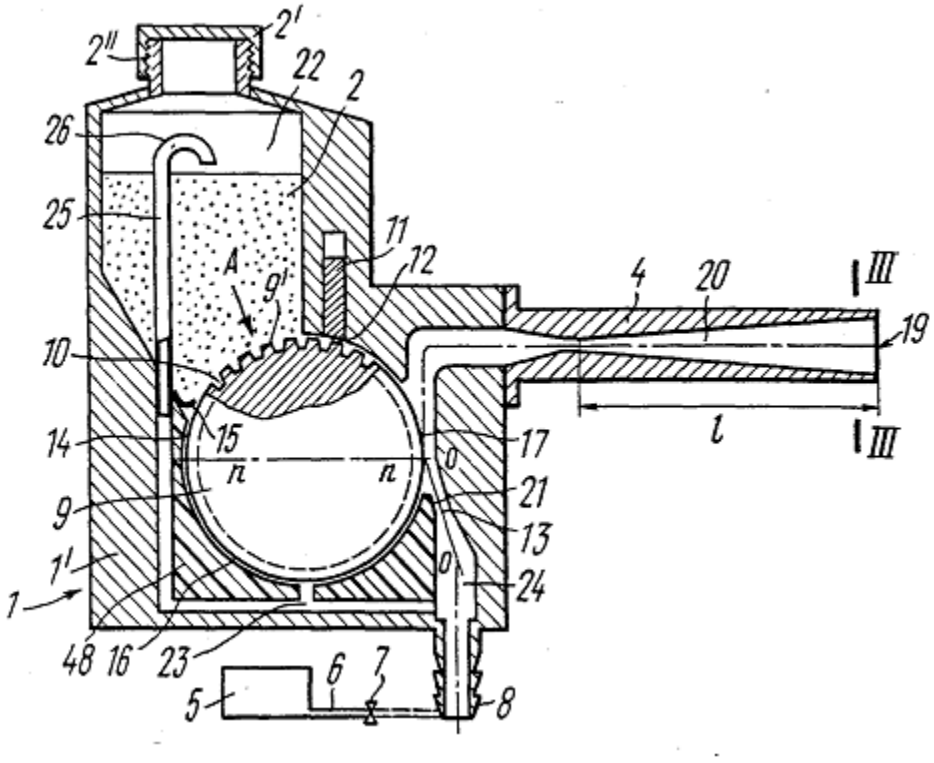

Figure 2.6: Original patent schematic for cold gas dynamic spraying *[31]*

2.3.2 Coating Mechanism

The kinetic energy of the fast moving particles must be converted to another form as it strikes the substrate in order for energy to be conserved. In the CGDS process, the majority of the energy is transferred into deformation and heat. Since this impact occurs over such a short period of time, the heat cannot transfer evenly throughout the particle and substrate, resulting in local heating (often approaching the melting temperature of the metal). This locally heated zone undergoes deformation, resulting in outward jetting of metal from both the particle and substrate (see Figure 2.7). This phenomenon is known as adiabatic shear instability [33], [35]–[37].

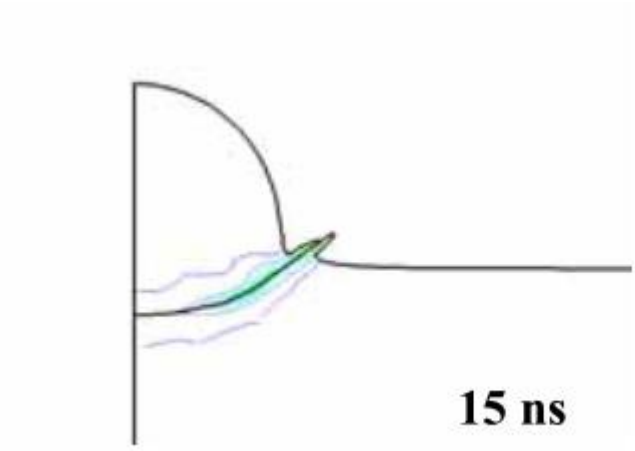

Figure 2.7: Gärtner et al. simulation of a copper particle impacting a copper substrate. Colour contours indicate the temperature distribution *[38]*.

The intertwining of these metal jets can result in mechanical anchoring (or mechanical bonding). This bonding mechanism requires both the substrate and the particles to deform upon impact [39], [40] (see Figure 2.8). Often, to improve mechanical bonding, substrates are pre-deformed through grit blasting processes to improve sites for mechanical anchoring of the particles [41].

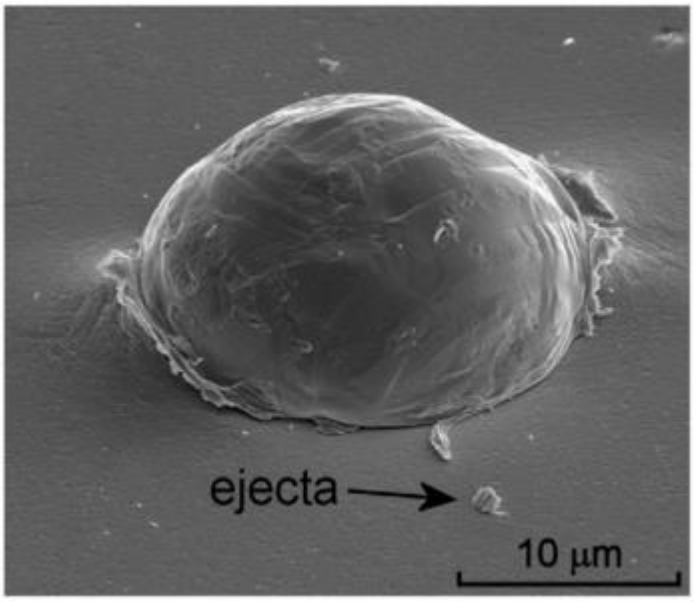

Figure 2.8: P. King et al.SEM image of a titanium particle after an impact*[42]*.

During an impact, the protective oxide layers in the locally heated zone may break or dissolve; creating pure metal to metal contact. Depending on the materials, temperature, time, and force of impact- this intimate contact can result in metallurgical bonding between the substrate and the particles[37], [39] (see Figure 2.9). A full understanding of the bonding mechanism in cold spray is still being investigated, but it is assumed to be a combination of both mechanical anchoring and metallurgical bonding [37].

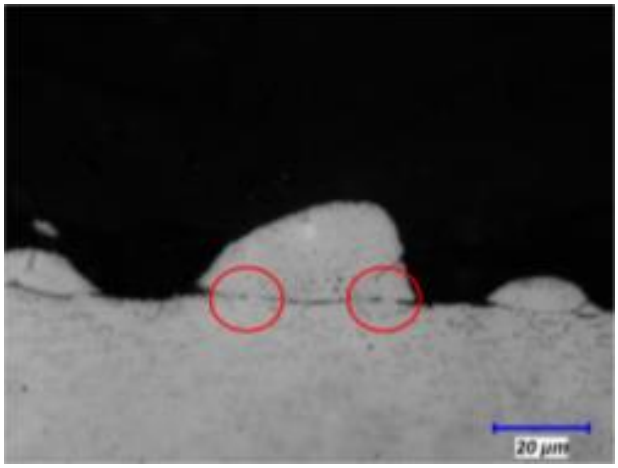

Figure 2.9: Optical image of an etched single commercially pure titanium particle after impact with a titanium alloy substrate showing metallurgical bonding (image courtesy of Mathieu Bolduc).

2.3.3 Critical Velocities

In order to have either metallurgical or mechanical bonding, between the impacting particle and the substrate, a certain particle velocity (kinetic energy) must be present. This velocity is known as the critical velocity[31], [35], [37], [43]. There have been a number of studies attempting to identify equations for critical velocities through semi-empirical and numerical methods. These relationships usually involve material properties, temperatures (of the powder and substrates), and particle sizes [32], [35], [37], [44]–[46]. Often the studies focus only on the powder properties; this neglects the potentially significant role of substrate material, temperature, and finish. Above this critical velocity, deposition occurs, below this velocity only abrasion of the substrate will occur.

After the initial particles have deposited on the substrate, subsequent particles will impact the previously deposited particles. The velocity at which impacting particles adhere to previously deposited particles can be considered a second critical velocity. This velocity is also material and temperature dependent. The particles may also reach what is known as the erosion velocity [32], [36], [47]. Above this velocity, particles have too much energy and remove previously deposited particles. Figure 2.10 demonstrates the trends observed in CGDS when particle velocity and particle temperature are taken into account.

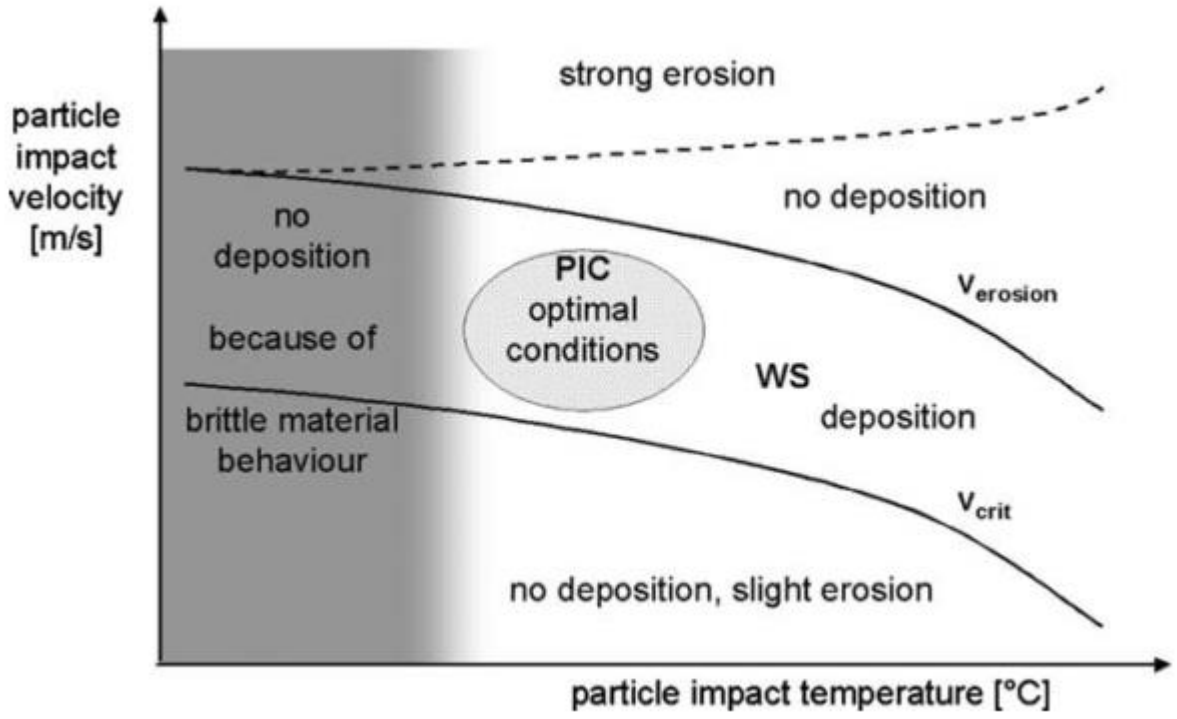

Figure 2.10: Particle velocity vs. particle impacting temperature showing the window of sprayablitly *[32]*.

2.3.4 Deposition Efficiency

Deposition efficiency (DE) describes the mass of particles that deposit on the substrate as a percentage of the overall mass of particles sprayed. The deposition efficiency is often linked to the velocity; the higher the particle velocities are above the critical velocity, the higher the deposition efficiency. Since increasing particle temperatures (and substrate temperatures) lowers

the critical velocity, DE is also shown to be higher for elevated temperatures for the same particle velocity. This trend continues until hitting the erosion velocity [39], [48]–[50].

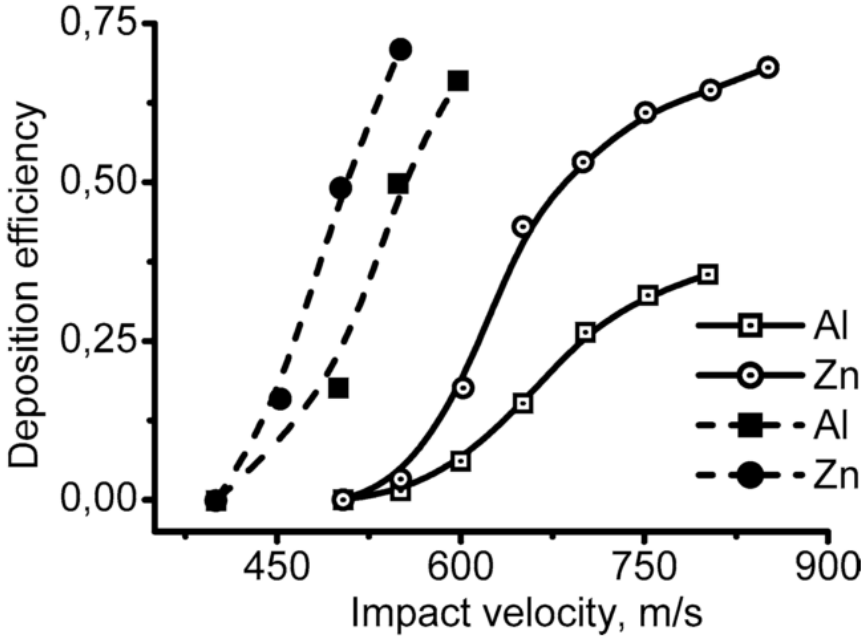

Figure 2.11: Deposition efficiency of different powders vs. impact velocity*[39]*.

2.3.5 Powder Injection Location

The CGDS process can be further defined depending where in the flow the particles are injected. In upstream injection CGDS, also known as high pressure cold spray (HPCS), the particles are injected in the high pressure / high temperature section of the nozzle upstream of the throat. This process results in the particles being exposed to the hot gas. The longer the particles are exposed to this hot gas, the higher the particle temperature as they exit the nozzle (Figure 2.12) [51]. This increased particle temperature lowers the critical velocity and increases DE. The downfall of this injection is that it requires a powder feeding gas pressure higher than the process pressure and may result in throat clogging.

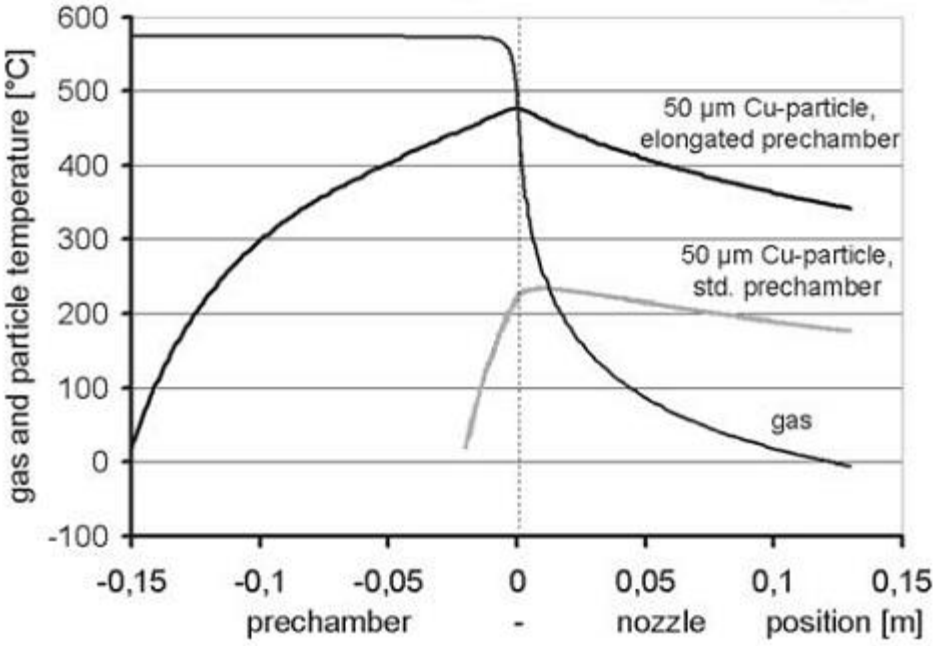

Figure 2.12: Temperature of particles and gas in upstream injection CGDS (showing two different powder injection locations) *[51]*.

In downstream injection cold spray, also known as low pressure cold spray (LPCS), the particles are injected after the throat in the low pressure/ low temperature section of the nozzle. This requires significantly lower powder feeding pressures and avoids throat clogging. Unlike HPCS, the downstream injected particles do not interact with the gas before it is cooled, and is therefore will have lower particle temperature than the upstream injection.

2.3.6 Gas Dynamics Principles present in CGDS

The particles gain there kinetic energy from the supersonic gas stream that is created in the de Laval nozzle. This subsection will briefly review the gas dynamic principles present in CGDS, in order to understand the influence of different parameters. The order and presentation of these equations is designed specifically for understanding the CGDS process and does not cover all gas dynamics principles. A basic understanding of compressible flows is assumed. All equations in this section are directly from (or derived from) known fluid and gas dynamics equations, as can be found in Fox and McDonald's Introduction to Fluid Mechanics [52].

A critical aspect of CGDS is the particle velocity. The velocity of the particles, as a result of their acceleration, is determined by a force that is imparted on them, through the relationship,

$$F = ma$$

where F is the force applied on the particle, m is the mass of the particle, and a is the acceleration of the particle. This force can be assumed to be a result of pressure drag, which is represented with the equation,

$$F_d = \frac{1}{2}\rho V^2 C_d A_p$$

where $F_d$is the drag force, ρ is the density of the fluid, V is the velocity of the fluid, C_d is the drag coefficient, and A_p is the cross sectional area of the particle. This equation for drag only takes into account a non-moving particle. In reality, the drag at any point in the nozzle would be relative to the difference between the gas velocity and particle velocity at that point, i.e.,

$$F_d = \frac{1}{2}\rho (V - V_p)^2 C_d A_p$$

where V_p is the velocity of the particle. At this point it is clear that these calculations cannot be solved linearly, as the velocity of the particle is related to the drag force applied for an amount of time. This force is constantly changing as the density, flow velocity, particle velocity, and drag coefficient are constantly changing along the nozzle length. The goal of this subsection is not to solve these calculations but show the effect of different parameters on the final velocity of the particle.

The Mach number represents the ratio of the flow velocity over the local speed of sound in the fluid. The velocity of the fluid can therefore be represented as a function of the Mach number and the speed of sound,

$$F_d = \frac{1}{2}\rho (MC - V_p)^2 C_d A_p$$

where M is the Mach number of the fluid and C is the speed of sound in the fluid. The speed of sound is influenced by the type of gas and the temperature of the gas through the equation,

$$C = \sqrt{kRT}$$

where R the specific is gas constant, T is the temperature, and k is the heat capacity ratio of the fluid. Combining these equations the drag force becomes,

$$F_d = \frac{1}{2}\rho(M\sqrt{kRT} - V_p)^2 C_d A_p$$

The drag force involves the density of the fluid. This density is related to the Mach number of the fluid and the stagnation density through the equation,

$$\frac{\rho_o}{\rho} = \left(1 + \frac{(k-1)}{2}M^2\right)^{\frac{1}{k-1}}$$

where ρ_o is the stagnation density. Assuming that at stagnation conditions the gas can be treated as an ideal gas, stagnation density can be related to stagnation pressure through,

$$P_o = \rho_o R T_o$$

where $P_o$is the stagnation pressure and T_o is the stagnation temperature. This shows that an increase in stagnation pressure, increases stagnation density, which increases the flow density, which increases the drag force.

The fluid temperature plays a role in determining the speed of sound in the fluid, which would increase the gas velocity for a given Mach number, and therefore increase the drag force. The temperature of the fluid is related to the Mach number and the stagnation temperature through the equation,

$$\frac{T_o}{T} = 1 + \frac{(k-1)}{2} M^2$$

This equation demonstrates that an increase in stagnation temperature will increase the downstream temperature, increasing the speed of sound, and therefore increase drag force. There is a tradeoff here as an inverse correlation was shown between stagnation temperature and stagnation density. Therefore an increase of stagnation temperature may decrease drag force by decreasing the density of the fluid. Combining all of these equations, an equation for drag force can be shown as,

$$F_d = \frac{1}{2} \frac{P_o}{RT_o \left(1 + \frac{k-1}{2} M^2\right)^{\frac{1}{k-1}}} \left(M \sqrt{kR \frac{T_o}{1 + \frac{k-1}{2} M^2}} - V_p \right)^2 C_d A$$

This relationship demonstrates that the drag force at any point in the nozzle is related to the Mach number, the stagnation temperature, the stagnation pressure, and the velocity of the particle. The Mach number of the flow is predetermined by the nozzle geometry for supersonic flows. The area ratio of the nozzle is the ratio between the area of a nozzle at any point and the area of the throat. It can be used to calculate the Mach number through the equation,

$$\frac{A}{A^*} = \frac{1}{M} \left[\left(\frac{2}{k+1} \right) \left(1 + \frac{(k-1)}{2} M \right) \right]^{k+1/2(k-1)}$$

where A is the nozzle area, A^* is the throat area. This equation demonstrates that the nozzle geometry (i.e. the area ratio) determines the Mach number of the fluid at any point downstream of the throat, regardless of all other parameters. The nozzle length has no effect on the Mach number, but determines the length of time the particles are exposed to the flow.

It is helpful to remember that the goal of the CGDS process is to accelerate the particles above their critical velocities. Although increasing stagnation temperature may decrease the density of the flow, it raises the overall velocity of the flow by increasing the speed of sound. This can be a

crucial factor in the selection of parameters in CGDS, as a particle can only be accelerated to a maximum of the fluid velocity.

The above equations show how the major parameters in cold spray can potentially affect the particle velocity. Another important element in cold spray is the mass of gas that is being sprayed. This can be determined through the equation,

$$\dot{m} = \frac{A^* P_o}{\sqrt{T_o}} \sqrt{\frac{k}{R}} \left(\frac{k+1}{2}\right)^{-\frac{k+1}{2(k-1)}}$$

where $\dot{m}$ is the mass flow rate of gas. This equation shows that decreasing stagnation pressure, and increasing stagnation temperature will decrease mass flow rate, which may be a significant cost factor in CGDS.

2.3.7 Summary of the Effects of Different Gas Dynamics Parameters in CGDS

This subsection summarizes the effects of different parameters in the CGDS process. These effects can be related to the equations derived in Section 2.3.6.

Area ratio: Affects the Mach number of the flow.

Nozzle length: Affects the length of time the particles are accelerated and exchange heat with the fluid.

Injection point: Affects the temperature at which the particle begins interacting with the fluid.

Gas nature: The properties of the gas, k and R, significantly affect the drag force and maximum velocity of the particles.

Stagnation temperature: Stagnation temperature is positively correlated to the velocity of the fluid. It is negatively correlated to density of the fluid and mass flow rate.

Stagnation pressure: Stagnation pressure is positively correlated to the drag on the particles and to mass flow rate.

2.3.8 Summary of the Effects other Known CGDS Parameters

This subsection summarizes the effects of different parameters in the CGDS process. These effects are known in literature and are referenced accordingly.

Traverse velocity: Effects substrate temperatures, as lower velocities give more time to transfer heat to the substrate, which can have an effect on coating quality [53].

Powder feed rate: Powder feed rate is positively correlated to the deposition rate. Accelerating the particles requires energy from the flow, too many particles results in oversaturation of the flow, decreasing coating quality [54].

Powder feeder gas flow: A minimum quantity of carrier gas is required in order to fluidize the powder and carry it to the nozzle. The effects of this gas on the flow are not well known, but are assumed to be minimal.

Standoff distance: The standoff distance must be in a certain range to effectively deposit particles on a substrate. Too small of a standoff distance may result in the impacting gas flow effecting the output of the nozzle. Too large a standoff distance and the particles may decelerate before impact[55].

2.4 Alternate Repair Technologies to CGDS

This section presents a brief overview of the existing technologies that could potentially be used to achieve the goal of the research and the reasoning for choosing CGDS technology.

2.4.1 Other Thermal Spray Processes

Thermal spray processes, other than CGDS, exist for depositing metallic coatings. Powder flame, wire arc, plasma arc, high velocity oxy-fuel (HVOF), and detonation gun are commonly found in industrial applications. These processes rely on a combination of particle velocity and temperatures that exceed melting point of the materials. These high temperatures allow for the spraying of non-ductile ceramic coatings, but are often result in high levels of oxides, thermally induced residual stresses, and detrimental substrate temperatures [30]. Of the alternative thermal spray processes, plasma deposition and HVOF are the most common.

2.4.1.1 Plasma Deposition

Plasma deposition relies on the thermal energy of the particles to deposit material to create coatings. An electric arc is generated by passing a direct current between a cathode and an anode. A mixture of gases (e.g. argon, nitrogen, helium, hydrogen) is passed through the arc, where it is heated, dissociated, and ionized into a plasma state. Feedstock powders are injected into this plasma jet where they are melted and projected onto the substrate where they quickly solidify into a coating [30], [56]. Typically plasma temperatures range from 5000°C to 25000°C, with particle velocities of 80 to 400 m/s. Theses extremely high temperatures allow for the deposition of high melting point ceramics, but metallic coatings from this process are often very high in oxides [30], [56].

2.4.1.2 High Velocity Oxygen Fuel (HVOF)

HVOF is similar to CGDS in that it uses the kinetic energy of particles to create coatings. Fuel and oxygen are combusted to create a high temperature and high pressure gas that is expanded through a converging-diverging nozzle. Particles are injected into this stream where they are heated and accelerated. The gas temperatures used in HVOF tend to be higher than CGDS, resulting in particles that are often partially or fully molten. This partial melting lowers the critical velocity required for coatings, but generally results in high levels of oxides present in the coatings [30], [56]. In recent years, HVOF coatings have been able to decrease these oxide levels through process control and nozzle optimization, resulting in low temperature sprays similar to CGDS[57].

2.4.2 Weld Overlays

Although uncommon, aluminum may be repaired by feeding aluminum stock into a locally melted area. This repair has the same drawbacks seen in conventional welding of aluminum alloys – high thermal stresses, oxide content, and the component would require heat treatment after welding [18].

2.4.3 Advantages of CGDS

The main advantage for CGDS for this application is the lower process temperature. Aluminum will readily oxidize during the other processes, while it is kept at a minimum during CGDS. The lower temperature also keeps the substrate temperature much lower, which is very important when dealing with aluminum alloys (see Section 2.1.3).

3 RESEARCH OBJECTIVES

3.1 General

The goal of this thesis is to develop a methodology to repair a) aluminum aerospace components and b) aluminum IVD coatings using commercially available CGDS technology and feedstock powders. Two separate development streams were required for this research: one for the reparation of aluminum parts (Figure 3.1) and one for the reparation of aluminum IVD coatings (Figure 3.2). Each of these streams has been separated into two phases: i) feasibility and coating development and ii) repair characterization.

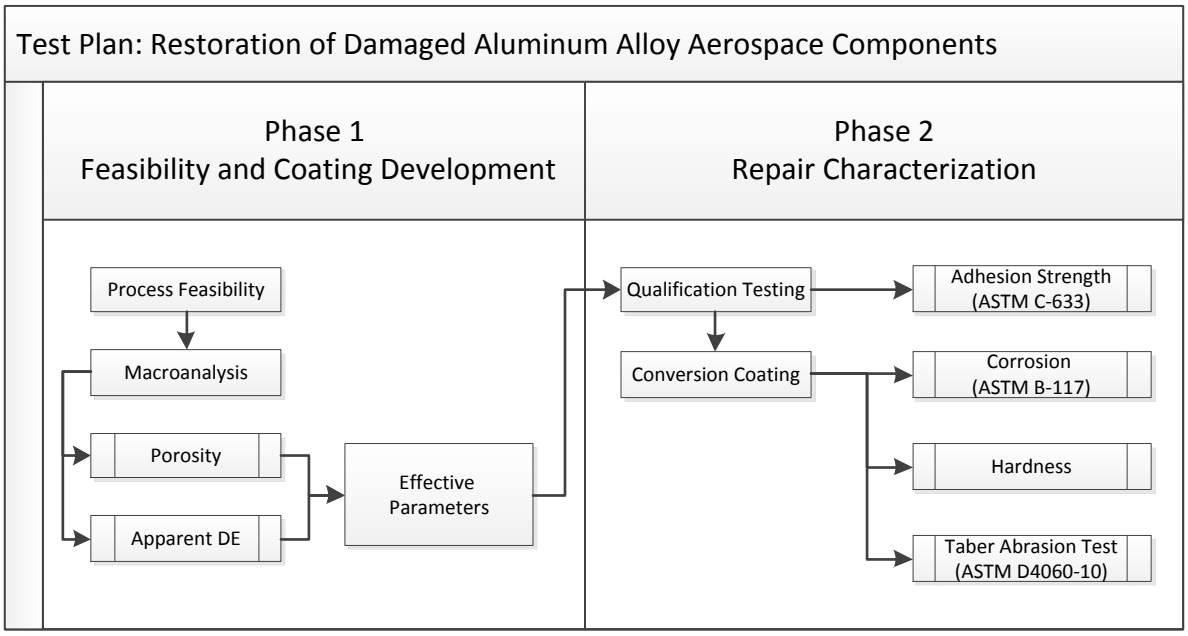

Figure 3.1: Overall test plan for damaged aluminum alloy aerospace component repair.

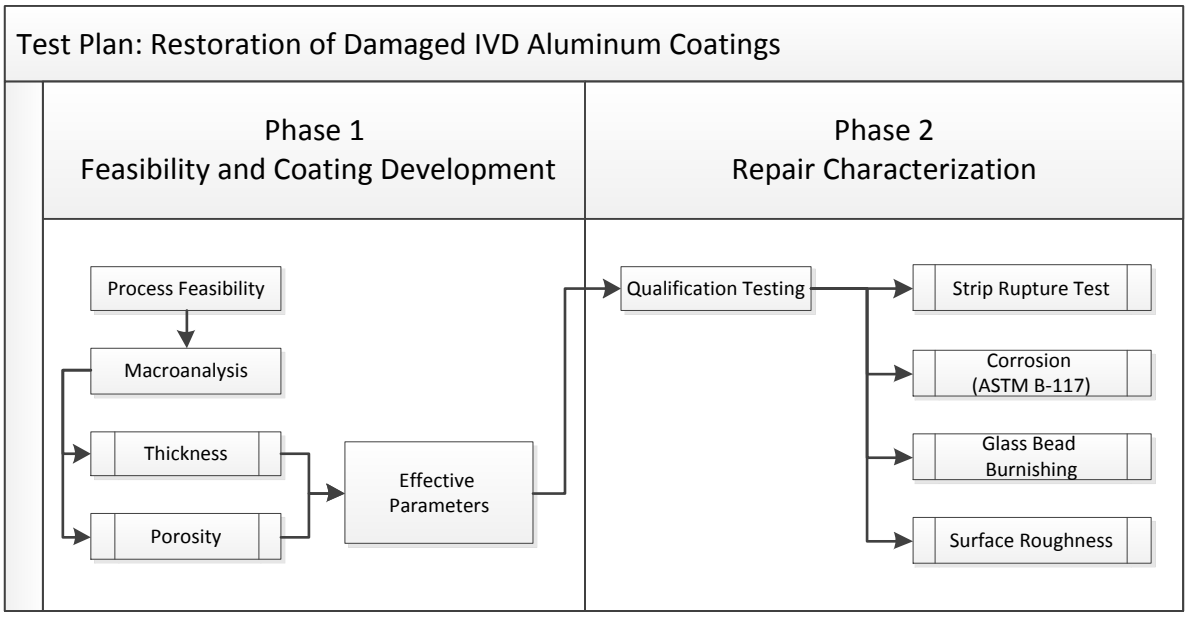

Figure 3.2: Overall test plan for damaged aluminum IVD repair.

Feasibility and coating development consisted of a series of experimental trials designed to identify a set of CGDS parameters that could be used to create the repairs. These parameters were then used to spray coatings for common preliminary qualifications for the aerospace repairs, namely, adhesion, corrosion, and wear. This phase was thought of as a preliminary qualification testing phase, as it aimed to meet the standards set by industry (The Boeing Company).

3.2 Feasibility and Coating Development for the Restoration of Damaged Aluminum Alloy Components

For the reasons discussed in the literature review, two common aerospace aluminum alloys were chosen to be the focus of this project; aluminum 2024 and aluminum 7075. The main deposition objective was to spray aluminum 7075 powder onto aluminum 7075-T6 substrates and aluminum 2024 powder on aluminum 2034-T3 substrates. Development of parameters for pure aluminum powder was also to be researched for both substrates. The deposition of pure aluminum using CGDS has been documented extensively; therefore if the alloy powders did not work, research could continue with pure aluminum as a superficial (non-structural) repair. See Figure 3.3 for a flow chart of deposition objectives.

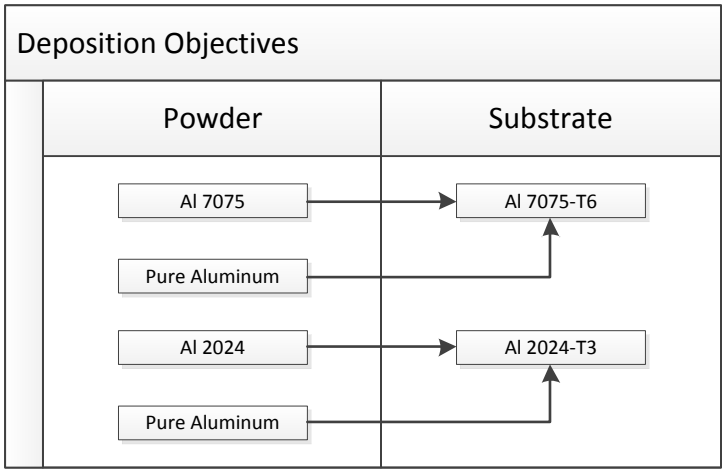

Figure 3.3: Deposition objectives for the damaged aluminum alloy component repair.

3.3 Feasibility and Coating Development for the Restoration of Damaged Aluminum IVD Coatings

The main purpose of the IVD aluminum coatings is corrosion protection and therefore the target powder to deposit on was pure aluminum. Aluminum 5083 was also investigated, since it has known corrosion resistance in saline environments. Aluminum 7075 was investigated because it could potentially have improved mechanical properties over the other alloys. Figure 3.3 shows the deposition objectives for the restoration of damaged aluminum IVD coatings.

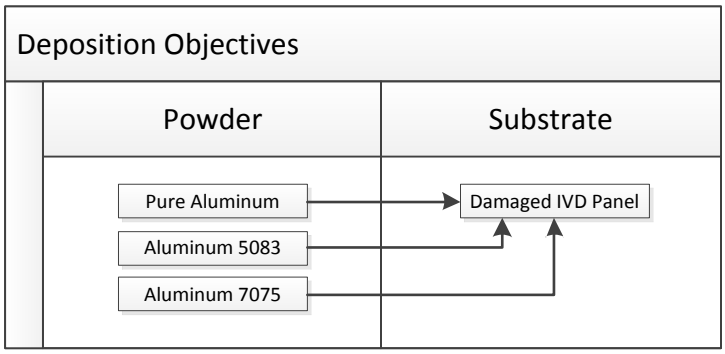

Figure 3.4: Deposition objectives for damaged aluminum IVD repair.

3.4 Characterization of CGDS Restorations of Damaged Aluminum Alloy Components

In order determine the suitability of CGDS for the reparation of aluminum alloy aerospace components; the repairs must undergo the same scrutiny as non-repaired components. Adhesion strength, the ability to be anodized, wear properties, and adhesion properties were examined. In addition to the repaired areas meeting the industry requirements, the reparation process must leave the base material properties intact.

3.4.1 Anodization Behavior and Wear Resistance

As was discussed in the literature review, components that experience wear must undergo a hardcoat anodization process prior to use in the field. The repairs in this study must also be able to undergo the anodization process. In this step, repaired components underwent both hardcoat and regular anodization. The quality of the hardcoat anodized layer was evaluated through a Taber abrasion testing. This test (shown in detail in Chapter 4) is designed to quantitatively measure the wear quality of the anodized layer.

3.4.2 Adhesion

The adhesion of the repairs is a crucial factor in the repairs of aerospace components. Without adequate adhesion, the repairs may delaminate from their parts. This delamination would mean a catastrophic failure of the repair. Since research in this field is novel, the adhesion values required are based on existing industrial specifications for other thermal spray processes. The testing procedure itself will follow ASTM C633, which is a thermal spray industry standard. A detailed outline of the procedure can be found in Section 4.

3.4.3 Corrosion

The repairs must also withstand the same environmental conditions of the original components. In industry, these components are tested for their corrosion properties through a neutral salt fog

test (ASTM B117) [58]. In this test, components are placed in a corrosive environment. The corroded components are examined visually for signs of excessive corrosion and are comparatively evaluated. For this study, the repairs will placed under the same conditions as the undamaged components and must perform in a similar manner.

3.5 Characterization of CGDS Restorations of Damaged Aluminum IVD Coatings

In order to qualify the repairs of IVD coatings the repairs must withstand the same scrutiny as IVD coatings. The standards are set in the military standard MIL-DTL-83488D [8]. The applicable tests will be for corrosion performance and adhesion through glass bead burnishing and strip rupture testing.

3.5.1 Corrosion Testing

Similarly to the aluminum alloy component repair, the IVD aluminum repairs must also undergo a neutral salt fog corrosion test. As is the standard protocol for testing thin aluminum coatings, the repaired IVD panels will be tested.

3.5.2 Adhesion Testing

Due to the thin nature of these coatings, standard thermal spray adhesion tests were not applicable as ASTM C633 states that the coating must be at least 0.38mm [58]. Additional adhesion testing methods, such as glass bead burnishing and strip rupture testing were undertaken in accordance with industry.

Glass bead burnishing creates residual stress in the coating that will expose areas of poor adhesion strength through delamination. The repaired samples will be tested in accordance with MIL-DTL-83488D [8].

Another method used to determine the adhesion strength of thin aluminum coatings is strip rupture testing. Repaired samples will be bent repeatedly until rupture where they will be examined for delamination as described in MIL-DTL-83488D [8]

3.5.3 Surface Roughness

The surface roughness of the finished repairs must be similar to that of existing pure aluminum IVD coatings. The coatings surface finish was analyzed using a VHX-2000 Series Digital Microscope, where Ra values will be compared.

4 EXPERIMENTAL DETAILS

4.1 Feedstock Material

Four different feedstock powder compositions were used for this investigation: pure aluminum, aluminum 5083, aluminum 7075, and aluminum 2024 for reasons discussed in the previous chapters. Laser diffraction analysis (Microtrac S3500, Nikkiso, Japan) was used to determine the mean particle size based on volume (MV), number of particles (MN), and area (MA) [59]. (Note: Aluminum 2024 had been eliminated from the project prior to particle size measurements). The results are found in Table 4.1.

Table 4.1: Mean particle size for pure aluminum, aluminum 5083, and aluminum 7075.

Powder	**Mean Particle Diameter (μm)**		
	MV	MN	MA
Pure Aluminum	29.33	14.36	22.52
Aluminum 5083	21.89	5.20	12.88
Aluminum 7075	42.10	13.46	29.62

The powder size chosen are in the optimal range for CGDS. Particles must be above a certain size (approx. 5 μm for aluminum) for thermal diffusion to be slow enough to allow for localized shear instability [32]. These particles are found to be above this critical size, but small enough that they can still be accelerated in the gas flow to the critical velocity.

The pure aluminum powder for this project is SST-A5001 from Centerline (Windsor) Ltd. The powder is irregularly shaped (non-spherical) which is uncommon for gas atomized powders (see Figure 4.1). The powder morphology closely matches those of water atomized powders, but the supplier (Centerline (Windsor) Ltd.) of the powder has ensured that it is gas atomized. The irregularly shaped particles have been shown to have a larger drag force compared to spherical, therefore increasing the potential for particles to reach the critical velocity by the end of the nozzle [60].

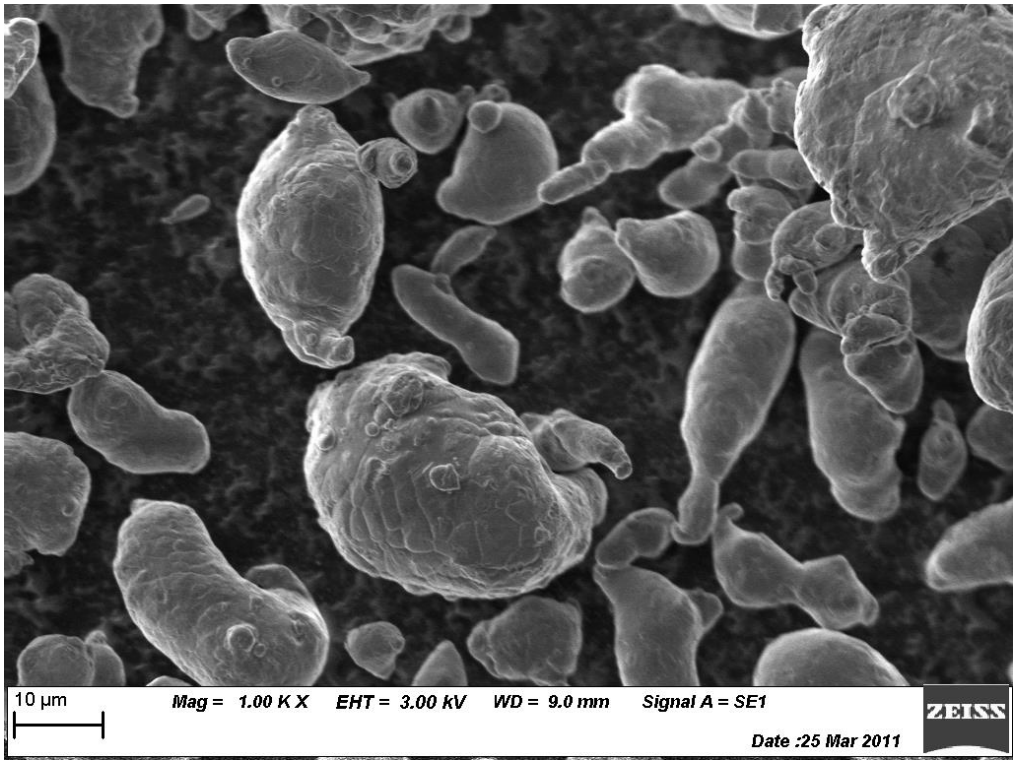

Figure 4.1: SEM image of pure aluminum powder (SST A5001)

The aluminum 7075 powder for this study is AA7075 -200 mesh from Valimet (Stockton, CA, USA). The particles are gas atomized and spherical (Figure 4.2). The high hardness and large size of these particles may reduce the deposition rate of the powder, but decreases the chances of clogging.

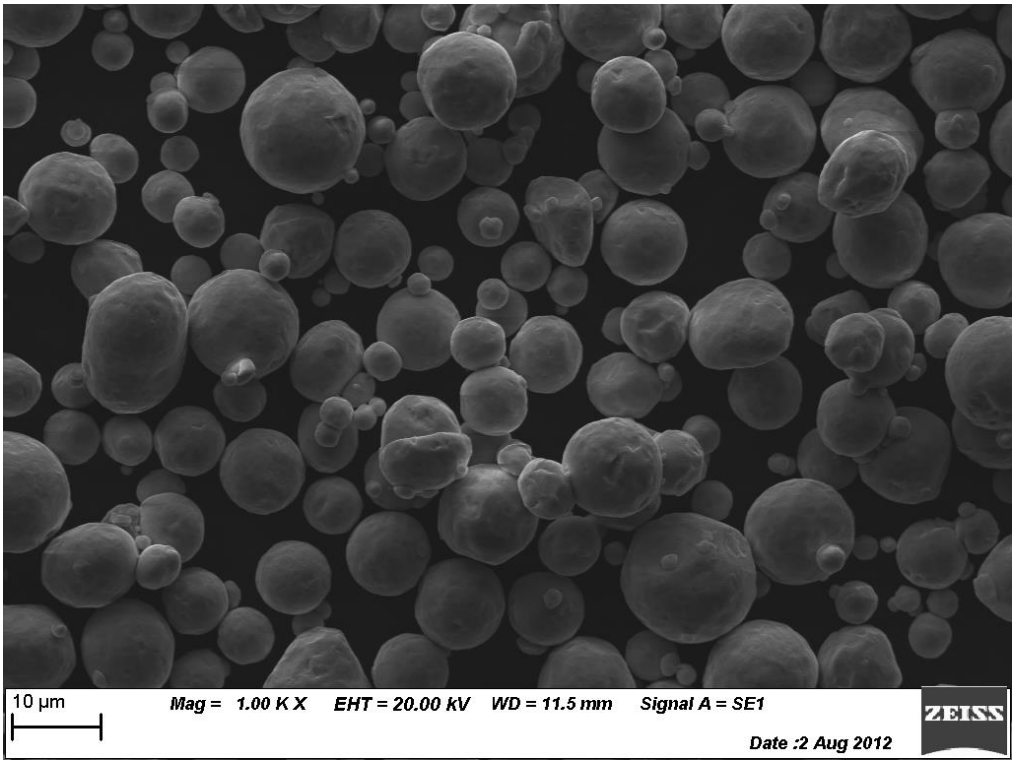

Figure 4.2 SEM Image of Aluminum 7075 powder (AA7075 -200 mesh (Valimet)).

The aluminum 5083 powder is AA5083 -200 mesh from Valimet (Stockton, CA, USA). The particles were gas atomized and are spherical. This powder contained an abundance of smaller particles (known as satellites) which can be seen in Figure 4.3. These small particles tend to induce clogging inside the nozzle.

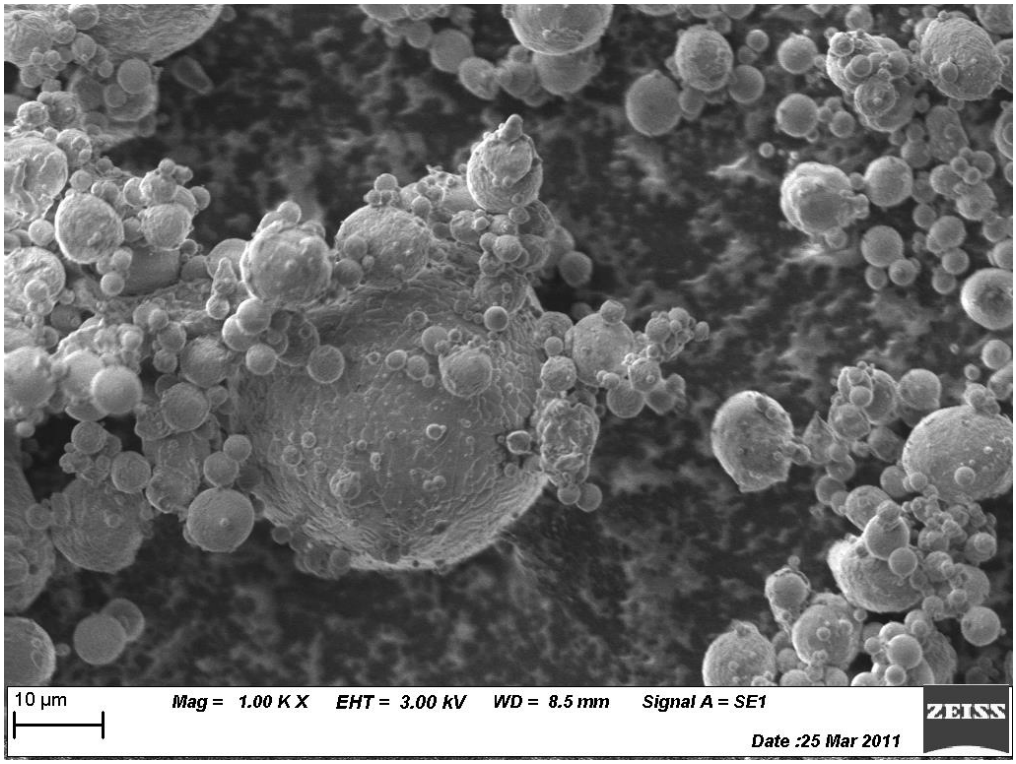

Figure 4.3: SEM Image of Aluminum 5084 powder (AA5083 -200 mesh (Valimet)).

Aluminum 2024 powder was F27131 atomized aluminum powder from Poudres Hermillon. According to the manufacturer, the powder has a D10, D50, and D90 of 6.8 µm, 31.8µm, and 74.4µm particle size, respectively (taken with a MALVERN laser gradulometer). This powder was not found to be suitable for cold spray because the extremely small particles (Figure 4.4) clogged the nozzle immediately after the spray began. These small particles could not be separated during sieving as they tended to stick together. Aluminum 2024 powder is not widely available and this is the only supplier that could be found, therefore research using aluminum 2024 powder was halted after initial trials.

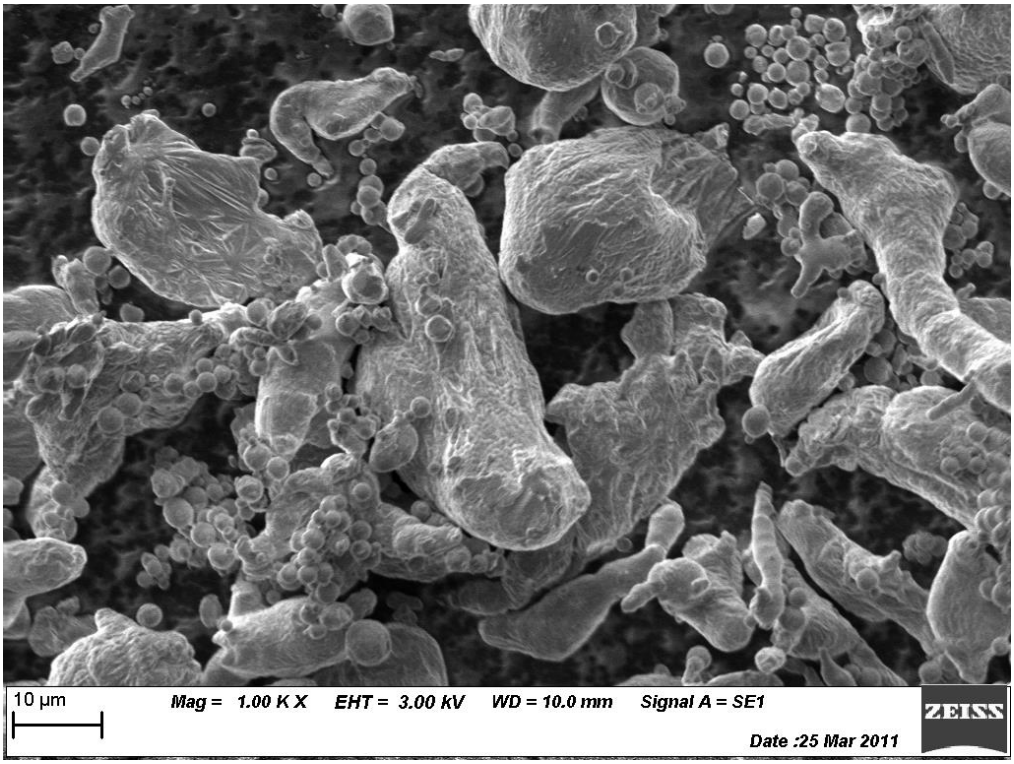

Figure 4.4 SEM Image of Aluminum 2024 powder.

4.2 Substrates

4.2.1 Restoration of Damaged Aluminum Alloy Components

Substrates were cut from ¼" (6.35 mm) plates of mill finished aluminum 2024-T3 and aluminum 7075-T6. These plates were procured from Metal Supermarket Ottawa and came without certification.

4.2.2 Restoration of Damaged Aluminum IVD Coatings

The substrates were 40 thou (1.0 mm) thick 4130 steel. In some cases, the 4130 steel is covered with a Class 1, Type I pure aluminum IVD coating. A section of this coating was masked during deposition in order to simulate damage to be repaired. These sheets (both bare and IVD coated) were supplied by the Boeing Company (St-Louis, USA).

4.2.3 Substrate Surface Preparation

All substrate surfaces underwent a grit blasting procedure using air as the process gas. The grit blasting unit was a hand held, gravity fed gun with a 13/64" (5.2mm) I.D. steel nozzle. All blasting was done at approximately a 45° angle with a standoff distance of approximately 2 inches. This unit had an average air consumption of 6CFM (170 l/min) at a max pressure of 90 psi (621 kPa) (Princess Auto SKU: 8140709). The air pressure could be regulated from 0 to 80 PSI (551 kPa).

Two types of abrasive were used in this study, one fine and one course. The courser grit was a 20 mesh (0.853 mm) ferrosilicate (Ebonygrit from Opta Minerals Inc). The finer grit is an 80 mesh (0.178 mm) aluminum oxide (Opta Minerals Inc). Both the course and fine abrasives were procured from Princess Auto with the SKUs 8200594 and 8200578, respectively. The parameters for the surface preparations can be found in Table 4.2.

Table 4.2: Surface preparation parameters for aluminum alloy and steel substrates.

Parameter	Aluminum Alloy Substrates	Steel Substrates
Abrasive	Aluminum Oxide	Ferroscilicate
Size	80 mesh	20 mesh
Process Gas	Filtered/Dry Air	Filtered/Dry Air
Spraying Pressure	60 psi	60 psi
Spray Angle	45°	45°
Standoff Distance	2 inch	2 inch

After grit blasting, aluminum samples were blown with compressed air and cleaned with acetone. Steel samples were immersed in a vibratory bath of ethanol for a minimum of 20 minutes in order to remove embedded grit. To avoid oxide formation, samples were only removed from the ethanol bath immediately prior to spraying.

4.3 CGDS Equipment

4.3.1 Heater and Controls

The system used for this research was the commercially available Centerline SST Low Pressure Cold Spray system from Centerline (Windsor) Ltd. An image of the system is shown in Figure 4.5. The system consists of a 4.3 kW heater with a maximum gas temperature of 500°C and a maximum gas pressure of 1.72 MPa (250 psi). Temperature is controlled digitally using the touch screen on the control panel, while pressure is controlled through a valve on the side of the cabinet. Pressure and temperature of the system is calibrated regularly using Centerline (Windsor) Ltd approved equipment.

Figure 4.5: Control cabinet (left) and heater cabinet (right) from Centerline (Windsor) Ltd.

4.3.2 Orifice

The orifice is the component of the cold spray system that contains the throat and holds the nozzle. It connects to the heater directly. The throat size used in this study was 2 mm in

diameter. This diameter was chosen over the 2.5 mm in order to reach full temperature and pressure without exceeding the 4.3 kW maximum. Only 2 mm and 2.5 mm throat size orifices were available from Centerline (Windsor) Ltd.

Two different orifices were used depending on the nozzle type that was connected. A brass orifice with a tungsten carbide throat insert (Figure 4.6 left) was used to hold the stainless steel nozzles. An aluminum orifice with a tungsten carbide throat insert (Figure 4.6 right) was used to hold the polymer nozzle. The two designs differ in the way they connect to the nozzle and the angle that the powder is injected, but should function in a similar manner.

Figure 4.6: Image of brass orifice (left) and aluminum orifice (right).

4.3.3 Nozzle

Two diverging nozzles were used in this study. A stainless steel nozzle was used for the spraying of aluminum alloy powders (Figure 4.7 left). This nozzle was capable of reaching 500°C but is prone to clogging, especially while using pure aluminum powders. A polymer nozzle was used

for spraying the pure aluminum powder (Figure 4.7 right). This nozzle was extremely resistant to clogging but could tolerate a maximum temperature of only 350°C.

Figure 4.7: Image of stainless steel nozzle (left) and polymer nozzle (right) from Centerline (Windsor) Ltd.

4.3.4 Spray Gun Traverse System

The spraying nozzle was moved by an automated X-Y traverse from IAI America Incorporated (shown in Figure 4.8). The slider type actuators were capable of velocities between 1mm/s and 500mm/s, with a minimum step size of 1 mm between passes. This unit is controlled through commercial software provided by IAI.

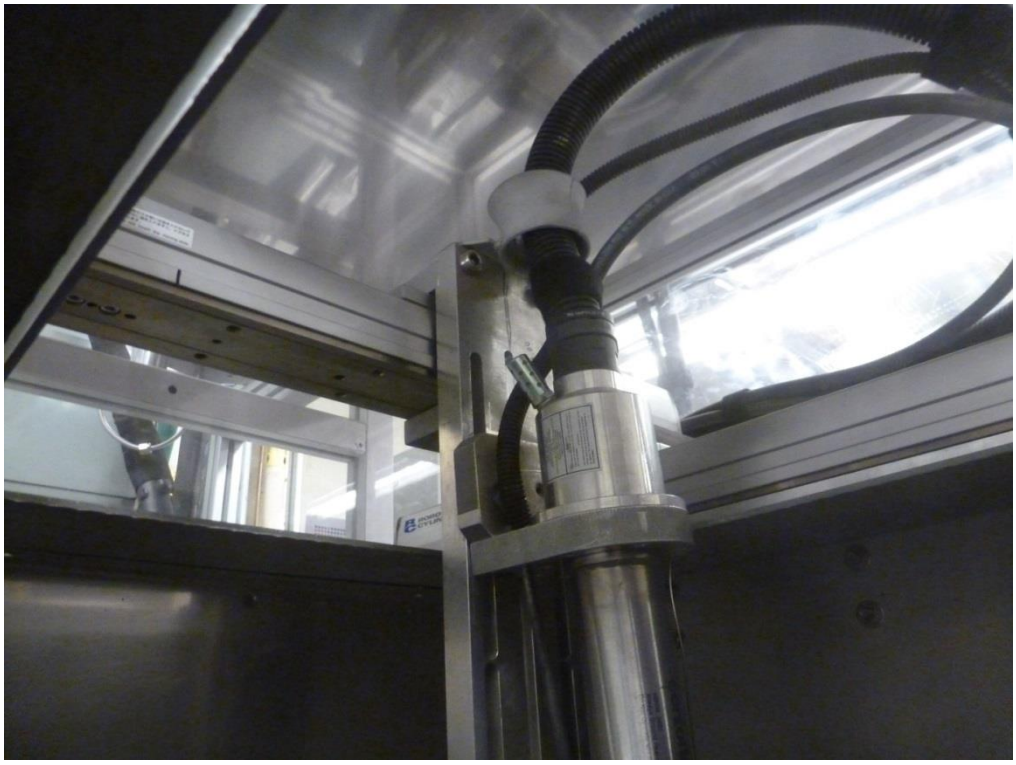

Figure 4.8: Image of traverse system.

4.3.5 Powder Feeding Equipment

The powder feeding equipment used in this research was the commercially available powder feeder from Praxair Surface Technologies (Model 1264, Praxair Surface Technologies, Concord, NH, USA) (see Figure 4.9). The powder is delivered through a rotating disk, where the powder is deposited into small holes in the wheel. As the wheel turns, the holes align with a carrier gas stream and are carried into the flow. The rotational velocity of the wheel and the size/frequency of the holes determine the flow rate of the powder. For this research, a wheel with 120 large holes was used for the reparation of aluminum alloy components (Figure 4.10) and a 320 small hole wheel (Figure 4.11) was used for the reparation of damaged aluminum IVD. This small holed wheel was found to be necessary in order to spray an even coating at the thickness required.

Figure 4.9: Praxair powder feeder.

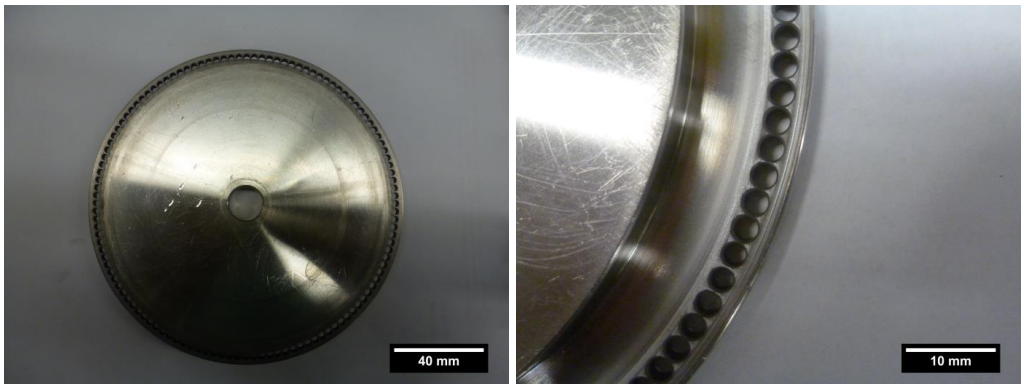

Figure 4.10: Large hole powder feeder wheel (120 holes).

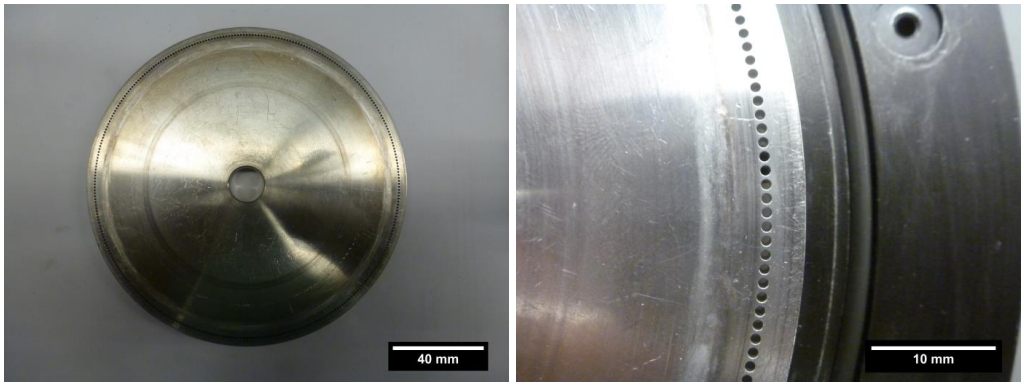

Figure 4.11:Small hole powder feeder wheel (320 holes).

4.3.6 Spray Chamber

The chamber that surrounded the CGDS deposition zone was custom built by Centerline (Windsor) Ltd (Figure 4.12). A dust collection system pulls the air and non-depositing powders through a water filter where the water traps the powders safely. The remaining air is pushed through a HEPA filter before being released to the room.

Figure 4.12: Centerline (Windsor) Ltd custom built spray chamber.

4.3.7 Gas Delivery System

Both nitrogen and helium gas was delivered to the CGDS system from a preassembled 11 bottle reservoir (bottle pack) at approximately 18 MPa. An example of a nitrogen bottle pack can be seen in Figure 4.13. These packs provided enough nitrogen for spray times up to 2.5 hours at full parameters. The system could also be connected to compressed air which could be supplied continuously at approximately 550 kPa.

Figure 4.13: Nitrogen bottle reservoir (bottle pack).

4.4 Analysis Equipment

In order to characterize the coatings and repaired areas, cross-sectional images must be taken and analyzed. The following equipment was used for this task.

4.4.1 Processing and Polishing

The samples were cut using the Struers Secotom-10 (Figure 4.14 left), following manufacturer recommended blade speeds and cutting parameters. The cut samples (Figure 4.14 right) were then mounted in thermosetting epoxy resin using the Struers LaboPress-3 (Figure 4.15 left). The mounted samples were polished using a Struers Tegrapol (Figure 4.15 right) using the recommended procedures from Struers. A mounted and polished sample can be seen in Figure 4.16 left. If samples were to be investigated using the SEM, they were gold sputtered prior to investigation using a Denton Vacuum Desk IV (Figure 4.16 right).

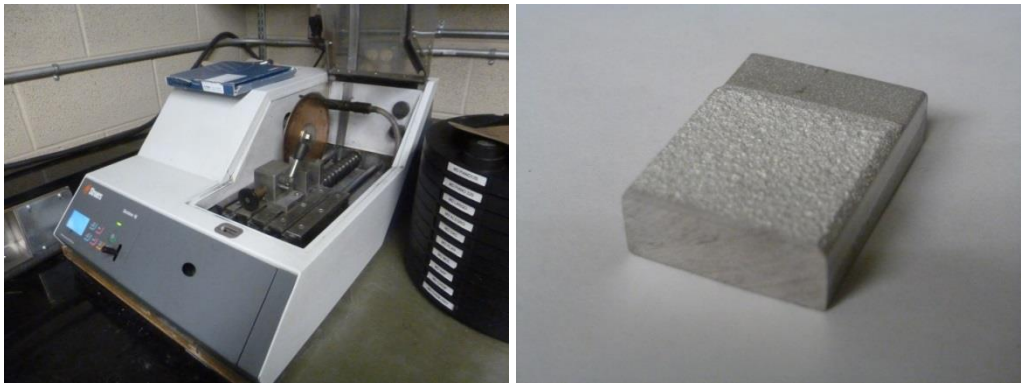

Figure 4.14: Struers Sectoctom-10 cutting machine (left) and cut aluminum alloy sample (right).

Figure 4.15: Struers Labopress 3 mounting machine (left) and Struers Tegrapol polishing machine (right).

Figure 4.16: Mounted and polished sample (left) and Denton Vacuum Desk IV gold sputtering machine (right).

4.4.2 Optical Imaging

The coatings were examined using an optical microscope (Kingdak NMM-800) shown in Figure 4.17. From these images, coatings could be qualitatively and quantitatively characterized. Porosity measurements were done with using commercially available software (Vision-Lite, Clemex, Montreal, Canada). This software can determine area ratios using the different contrasts of porosities and coating. A minimum of 10 porosity measurements were done on each sample from various areas of the coatings.

Figure 4.17: Kingdak NMM-800 Optical microscope.

4.4.3 Scanning Electron Microscope

Coatings and powders were investigated using a scanning electron microscope (EVO-MA10, Zeiss, UK), This SEM is equipped with secondary electron (SE), back-scattered electron (BSE), energy dispersive spectroscopy (EDS), electron backscatter diffraction (EBSD) and X-ray computed tomography (CT) detectors.

The secondary electron detector was used to take high quality images of the coatings and powders. BSE was used in order to clearly differentiate the alumina layer from the coating layer of the Taber abrasion test samples.

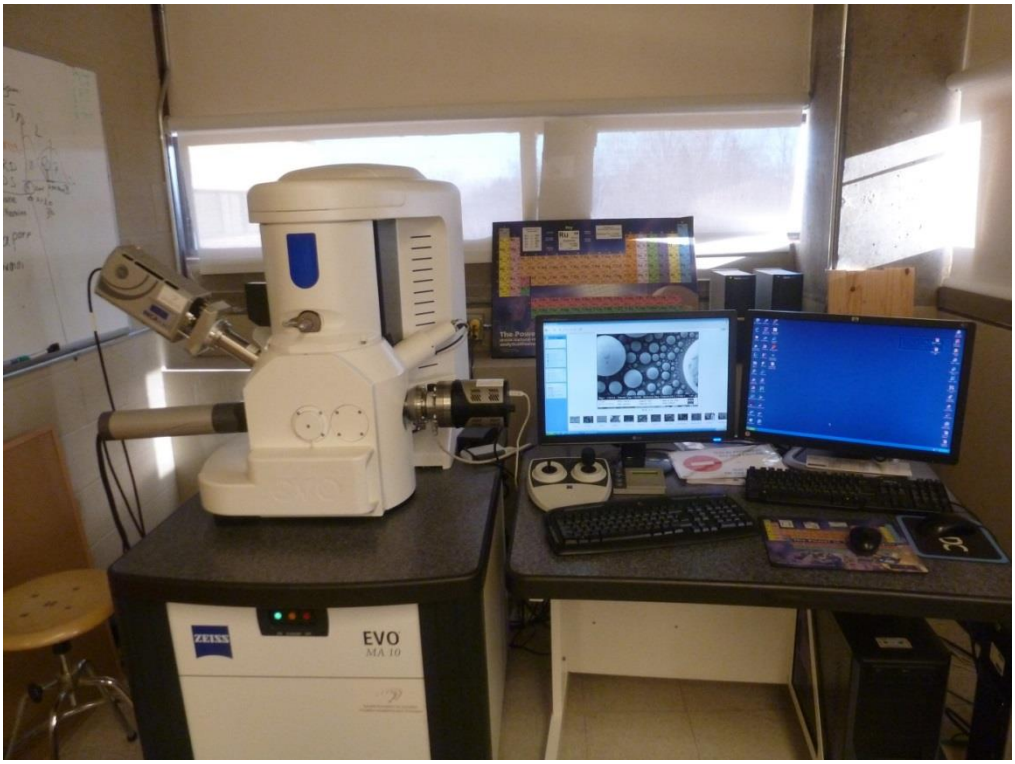

Figure 4.18: Scanning electron microscope (EVO-MA10, Zeiss, UK).

4.4.4 Indentation Hardness

Microhardness measurements were performed on the aluminum part repairs to assess the hardness of the sprayed coatings, the converted oxide layer, and the substrate. The microhardness tests were conducted on polished samples using a Vickers microhardness tester (Struers Duramin-1, pictured in Figure 4.19 left). The Taber abrasion panels had an oxide layer too thin to measure with the Vickers hardness tester and therefore a knoop hardness tester was used (Buehler Micromet 6030, pictured in Figure 4.19 right).

Figure 4.19: Struers Deramin 1 (left) and Buehler MIcromet 6030 (right) hardness testers.

4.5 Repair Characterization Equipment and Procedures

4.5.1 Corrosion Testing

Corrosion testing was conducted under the ASTM B117 standard *'Standard Practice for Operating Salt Spray (Fog) Apparatus'* [61]. For this test, samples are exposed to a heated salt fog environment for a specified time. These conditions accelerate the corrosion process, but do not produce a quantitative corrosion result. The corroded samples must be analyzed at chosen time increments.

In order to test the corrosion properties of repaired aluminum alloy components, application specific corrosion panels were developed to simulate damaged and repaired parts. These corrosion panels were designed to simulate a scratch of 1 mm deep and 76.2 mm (3 inches) long in a 76.2 mm by 152.4 mm substrate. The damaged area is then machined in order to blend the damaged. Dimensions of the damaged and machine area can be found in Figure 4.20. This

machining is done using a special blending tool currently used by the Boeing Company for the reparation of ALCLAD components (a drawing is found in Figure 4.21).

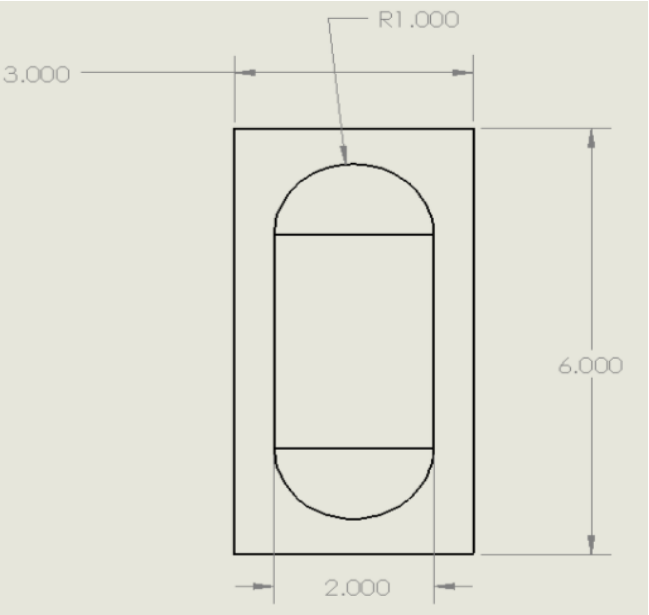

Figure 4.20: Dimensions of aluminum alloy repair corrosion panels containing damage area (dimensions in inches) [maximum depth of damage is 42 thou (1.06mm)].

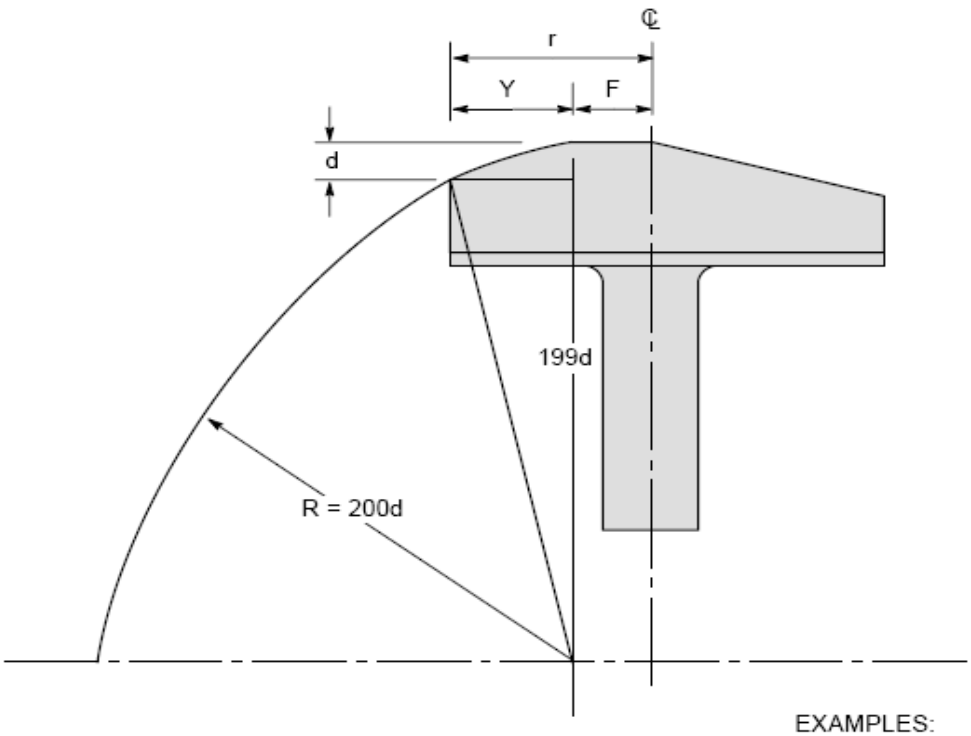

DEFINITIONS:

F	=	Flat
Y	=	Minimum route radius
r	=	Route radius = (Y + F)
W	=	Cutter width = 2 (Y + F)
d	=	Route depth
R	=	Blend radius (defined by Engineering as 200d)

EXAMPLES:

d (in.)	min. W=40d (F=0) (in.)
0.005	0.20
0.006	0.24
0.010	0.40
0.015	0.60
0.020	0.80
– –	– –

CALCULATIONS;

When F = 0,

$$Y = \sqrt{(200d)^2 - (199d)^2} = 20d$$

therefore,

$$W = 2(Y + F) = 2(20d + 0) = 40d => \textit{minimum cutter width}$$

FIGURE 3 ENGINEERING DIMENSIONS OF A BLENDOUT ROUTING BIT

Figure 4.21: Drawing of blendout routing bit used to blend damage from substrates before repair (credit to: The Boeing Company).

The damaged blended area (shown in Figure 4.20) is then repaired using CGDS and machined flat. This area is then conversion coated (Type I, Class 1A) or anodized (Type II, Class 1) prior to exposure to the corrosive environment. For this study, the repaired aluminum alloy components were scrutinized with a pass/fail observation at total of 640 hours, as requested by the industrial sponsor. In order for a sample to pass, a minimal amount of visible oxidation must have occurred.

For the restoration of damaged aluminum IVD coatings, the samples were 76.2 mm by 152.4 mm, 40 thou (1.0 mm) thick 4130 steel covered with a Class 1, Type I pure aluminum IVD coating. This coating has a 25.4 mm damaged region in which the substrate (steel) is exposed (Figure 4.22, top). The repairs will be done by coating the entire sample in CGDS aluminum (and aluminum alloy) coatings. According to the MIL-DTD-83488D standard, a class 1 aluminum coating with a Type II conversion coating must be tested up to 672 hours [8].

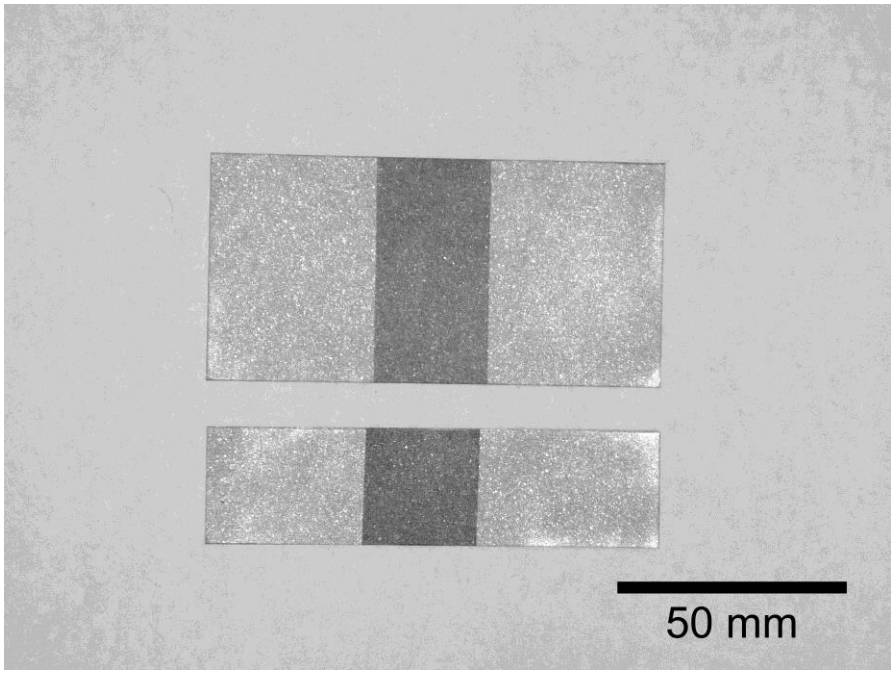

Figure 4.22: Example of simulated damaged IVD coatings on 4130 steel before coating after grit blasting (top: corrosion sample, bottom: strip rupture sample).

Half of the samples sprayed had an 'X' scored through the coating and into the substrate. This was done to verify that the aluminum coating offers proper sacrificial corrosion protection to the steel if the repaired area is ever damaged. This protection occurs because aluminum is more active (i.e. has a more negative corrosion potential) than the steel, which induces a galvanic current that protects the steel while creating a preferential dissolution of the aluminum near the scribe [62]. A test fails if corrosion products of the substrate are visible (red for the steel). White corrosion of the aluminum layer is not considered a cause for rejection.

4.5.2 Adhesion Strength

Adhesion strength for the reparation of aluminum alloy components was done according to ASTM C633: Standard Test Method for Adhesion of Cohesion Strength of Thermal Spray Coatings [58]. For this test, a coating was deposited on a one inch (25.4 mm) diameter rod (see Figure 4.23 left). The coating is then machined flat and glued (using FM-1000 Elastomeric Adhesive, Cytec Engineering Materials) to an identical rod the opposite side. The complete process for the gluing of adhesion strength samples can be found in APPENDIX II. The glued samples are then pulled axially in an Instron Universal Tensile Testing Machine (see Figure 4.23 right).

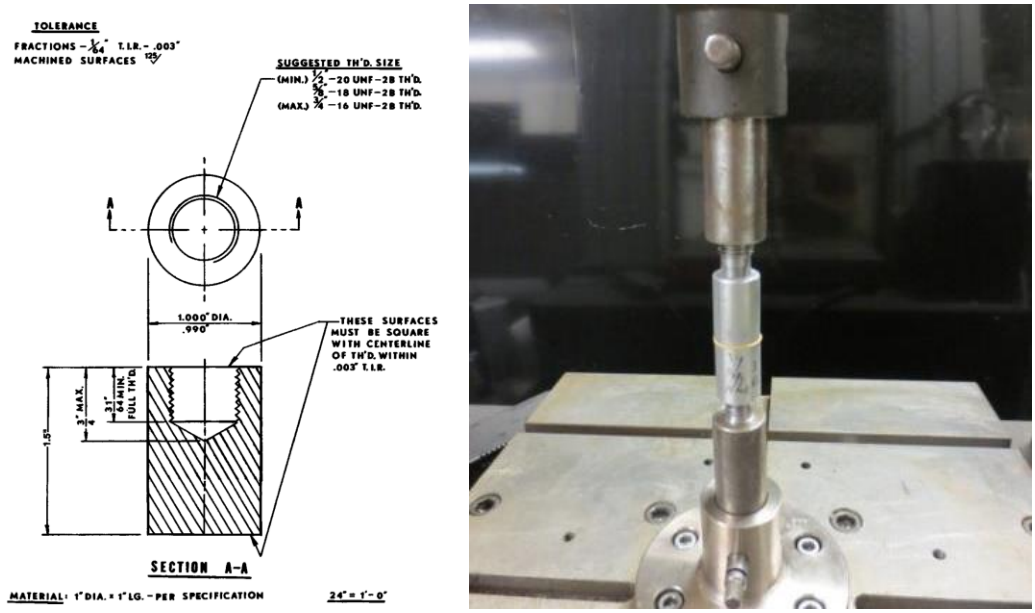

Figure 4.23: Diagram of an adhesion substrate (left) and a glued sample read to be pulled (right).

For this study, 5 adhesion tests per parameter set were performed. By dividing the average resulting force of these tests by the area of the substrate, the pressure required to remove the coating is found. In some cases, the glue delaminates before the coating; this value is considered the minimum adhesion strength of the coating. The coatings were sprayed the pattern shown in Figure 4.24

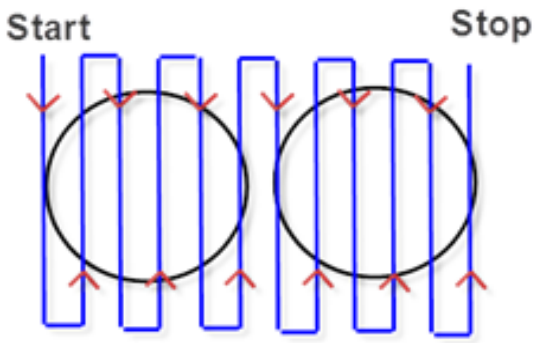

Figure 4.24: Adhesion test spray pattern.

For the restoration of pure aluminum IVD coatings the ASTM C633 adhesion standard cannot be followed as it states that the coating must be at least 0.38mm thick [58], which is much thicker than the Class 1, Type I and Class 1 IVD coatings to be repaired. In order to determine the adhesion of these coatings, additional testing methods such as glass bead burnishing and strip rupture testing were undertaken.

Glass bead burnishing was done in accordance with the MIL-DTL-83488D standard [8]. For this test, No. 10 glass beads are sprayed at the coating using an air pressure of 60 psi. If the coating peels from the substrate, it is deemed a fail. In practice, the glass bead burnishing is often done on all parts as a finishing step.

For strip rupture testing, tests strips (1"x4") were cut from the larger simulated damaged IVD panels (Figure 4.22 bottom). These samples were then coated in their entirety. This test, as described in MIL-DTL-83488D, states that the coated test strip (1"x4") is placed in a vice and bent back and forth until strip rupture occurs. If after the rupture the coating can be peeled back or has been separated from the substrate it is deemed a fail [8].

4.5.3 Taber Abrasion Testing

In order to test the quality of the hard coat anodized layer on the repaired aluminum alloy components, samples were tested via the Taber abrasion testing method. This testing followed the ASTM D4060: Standard Test Method for Abrasion Resistance of Organic Coatings by the Taber Abraser [63]. A schematic of the wear area is shown in Figure 4.25.

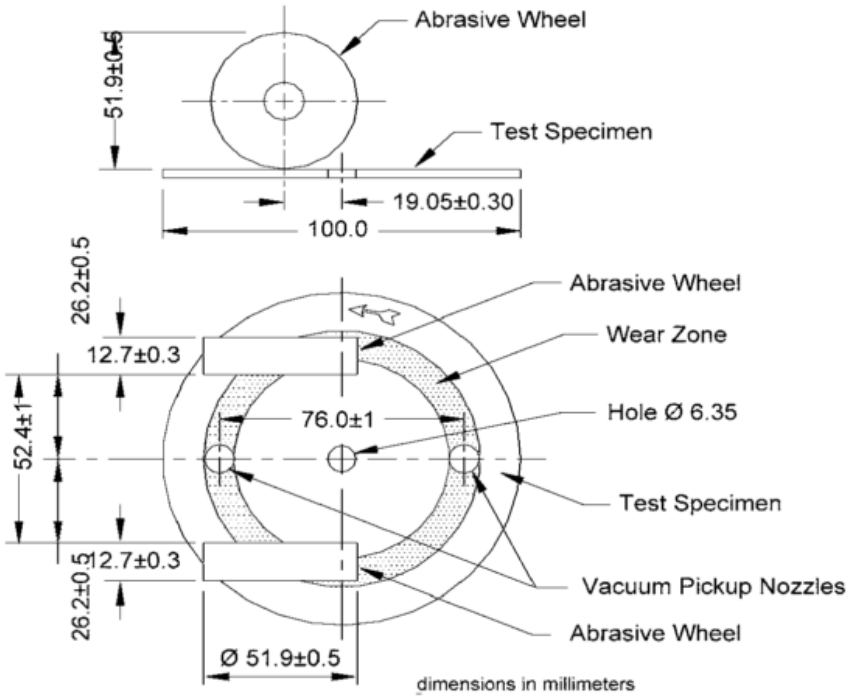

Figure 4.25: Taber abrasion schematic showing proper wheel position *[63]*.

Repairs were simulated by applying the coating on a ¼" aluminum alloy panel, before receiving a Type III Class I hardcoat sulphuric acid anodizng. The hardcoated panels were tested for 10,000 cycles on a Taber Abraser Model 140 using CS 17 wheels, 1000 gram load, and 70 rpm. Test panels may be lapped prior to the Taber Abraser without periodic resurfacing.

As a requirement of the Boeing Company, the weight loss of coated 2024 alloys and other copper bearing alloys shall not exceed 40 milligrams. The weight loss of all other alloys shall not exceed 20 milligrams.

5 FEASIBILITY AND COATING DEVELOPMENT

This chapter details the experimental design and development of the CGDS parameters to be used for the restoration of damaged parts and coatings. It includes test plans, results, perturbations based on those results, and finally a set of qualified parameters for each powder/substrate combination. This chapter is separated into sections according to powder and substrate material, based upon the deposition objectives shown in Figure 3.3 and Figure 3.4. The focus of each of these sections will be to determine a qualified set of parameters for each combination of powder and substrate.

5.1 Coating Development of Aluminum 7075 Powders on Aluminum 7075-T6 Substrates

As a result of the number of variables present in cold spray (see subsection 2.3.7) and the lack of literature involving the deposition of aluminum 7075 powders with low pressure CGDS, the initial stages of this project covered a very broad range of parameters. In order to identify the effect of the individual parameters, the variable being investigated was varied while holding the other parameters constant. All substrates were prepared using the parameters found in Table 5.1.

Table 5.1: Substrate surface preparation parameters for aluminum 7075-T6 and aluminum 2024-T3 substrates.

Parameter	Value
Abrasive	Aluminum Oxide
Size	80 mesh
Process Gas	Filtered/Dry Air
Pressure	60 psi (410 kPa)
Spray Angle	45°
Standoff Distance	2 inch (51 mm)
Post Treatment	Acetone

5.1.1 Pressure, Temperature, and Traverse Velocity

In CGDS, the process gas pressure and temperature are expected to have the most significant effect on particle velocity, and in turn, coating quality. The standoff distance, nozzle type, orifice diameter, powder feeder wheel, powder feeder gas rate, and powder feed rate were held constant at values recommended by the CGDS supplier (Centerline (Windsor) Ltd). These values can be found in Table 5.2.

Table 5.2: CGDS parameters held constant for the initial coating development test matrix for Al 7075 powder on Al 7075-T6 substrates.

CGDS Parameter	Value
Standoff Distance	15 mm
Nozzle Type	120 mm SS Nozzle
Orifice Diameter	2 mm
Powder Feeder Wheel	120 Large Hole
Powder Feeder Gas Rate	20 SCFH
Powder Feed Rate	3 RPM
Step Size	1 mm

This test also aims to identify the effect of traverse velocity on the resulting coatings. A high and low for each of the variable categories was chosen based on recommended ranges from the manufacturer and accumulated knowledge. A test matrix showing the velocities, temperatures, and pressures tested is found in Figure 5.1.

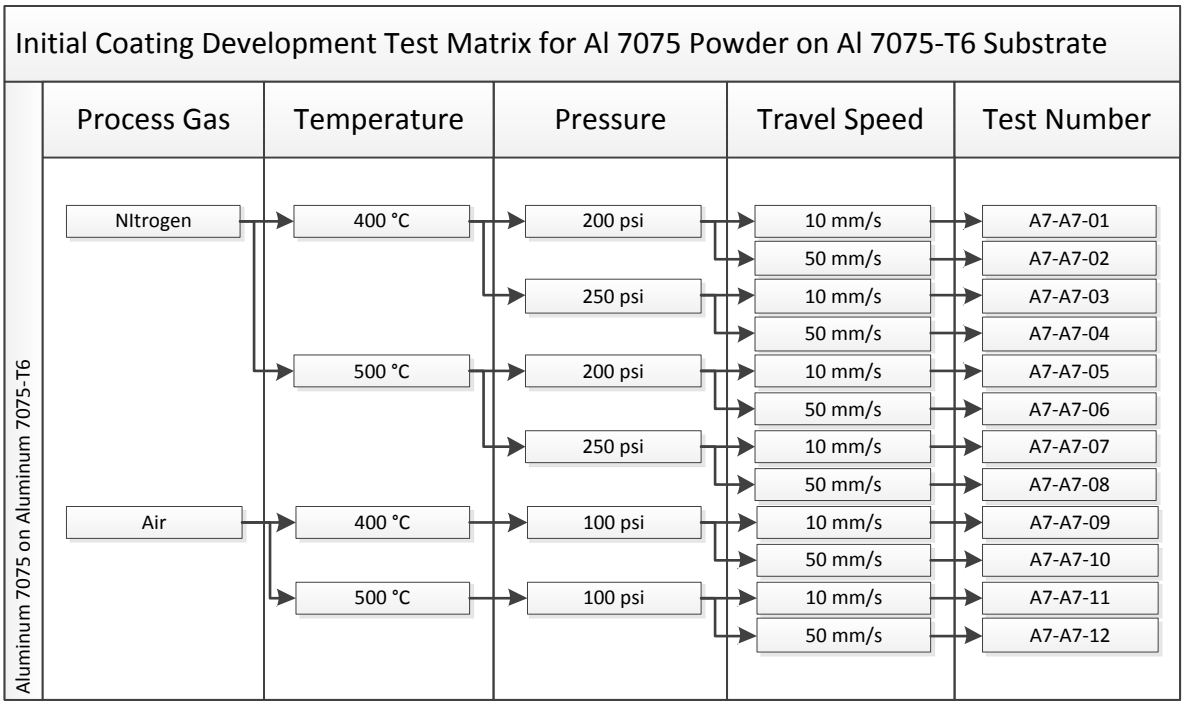

Figure 5.1: Initial coating development test matrix for Al 7075 powder on Al 7075-T6 substrates.

As a point of interest, this test matrix also includes trials to be completed using compressed air as a process gas at the maximum available pressure of approximately 100 psi. The acceleration of the particles is related to the applied drag force on the particle,

$$F_d = \frac{1}{2}\frac{P_o}{RT_o\left(1+\frac{k-1}{2}M^2\right)^{\frac{1}{k-1}}}\left(M\sqrt{kR\frac{T_o}{1+\frac{k-1}{2}M^2}}-V_p\right)^2 C_d A$$

which was derived in subsection 2.3.6. This gas nature affects only the variables k and R in this equation. It is known that air is approximately 78% nitrogen, so its gas properties are similar, ie $R_{air} = 0.287\ kj/kgK$ is very close to $R_{nitrogen} = 0.2968\ kj/kgK$ and $k_{air} = k_{nitrogen} = 1.4$ [64]. This should result in air performing in very similar manner to nitrogen. The advantage of using air as the process gas is that it can be supplied in unlimited quantities a very minimal cost (compressor), the disadvantage is that it is only available at a max pressure of approximately 100 psi (varies based on demand).

The initial criterion investigated was whether or not the coating would deposit. The results of this trial can be found in Table 5.3. Coating that were successfully deposited were measured for thickness and then prepared for metallographic examination under the optical microscope. The porosity level and the Vicker's micro-hardness were then determined. The thickness shown in the results is directly comparable as it is based on an equal amount of spray time per unit area i.e. 1 pass at 10mm/s and 5 passes at 50 mm/s.

Table 5.3: Results for initial coating development test matrix for Al 7075 powder on Al 7075-T6 substrate.

Test Number	Deposits (Y/N)	Porosity (%)	Vickers Hardness (300 gram)	Coating Thickness (µm)
A7-A7-01	N	NA	NA	NA
A7-A7-02	N	NA	NA	NA
A7-A7-03	N	NA	NA	NA
A7-A7-04	N	NA	NA	NA
A7-A7-05	Y	0	156±13	41
A7-A7-06	Y	0	164±4	38
A7-A7-07	Y	0	150±8	61
A7-A7-08	Y	0	160±16	64
A7-A7-09	N	NA	NA	NA
A7-A7-10	N	NA	NA	NA
A7-A7-11	N	NA	NA	NA
A7-A7-12	N	NA	NA	NA

Particles sprayed using nitrogen at a gas temperature of 400°C (A7-A7-01 to A7-A7-04) did not deposit; leaving only an evidence of abrasion on the substrate. This result shows that the particles were below the critical velocity, and therefore a higher particle velocity (and/or particle temperature) would be required for adhesion. At 500 °C gas temperature, the critical velocity of the particles was reached and coating deposition began. It should be noted that the increase in stagnation temperature of the gas also influences the temperature of the particles, lowering the required critical velocity. The coatings (A7-A7-05 to A7-A7-08) had porosity that were not measurable and were therefore considered fully dense (see Figure 5.2) for an example of a coating cross-section). The hardness values were also found to be very similar, regardless of gas pressure or traverse velocity. It is expected that the particles deposited at higher pressures would

have increased deformation upon impact which would lead to an increase of work hardening. This increase is empirically associated with a power law (Hollomon's equation), in which the strain hardening exponent for aluminum alloys is low [65]. This results in only a small increase in hardness for a large increase in deformation.

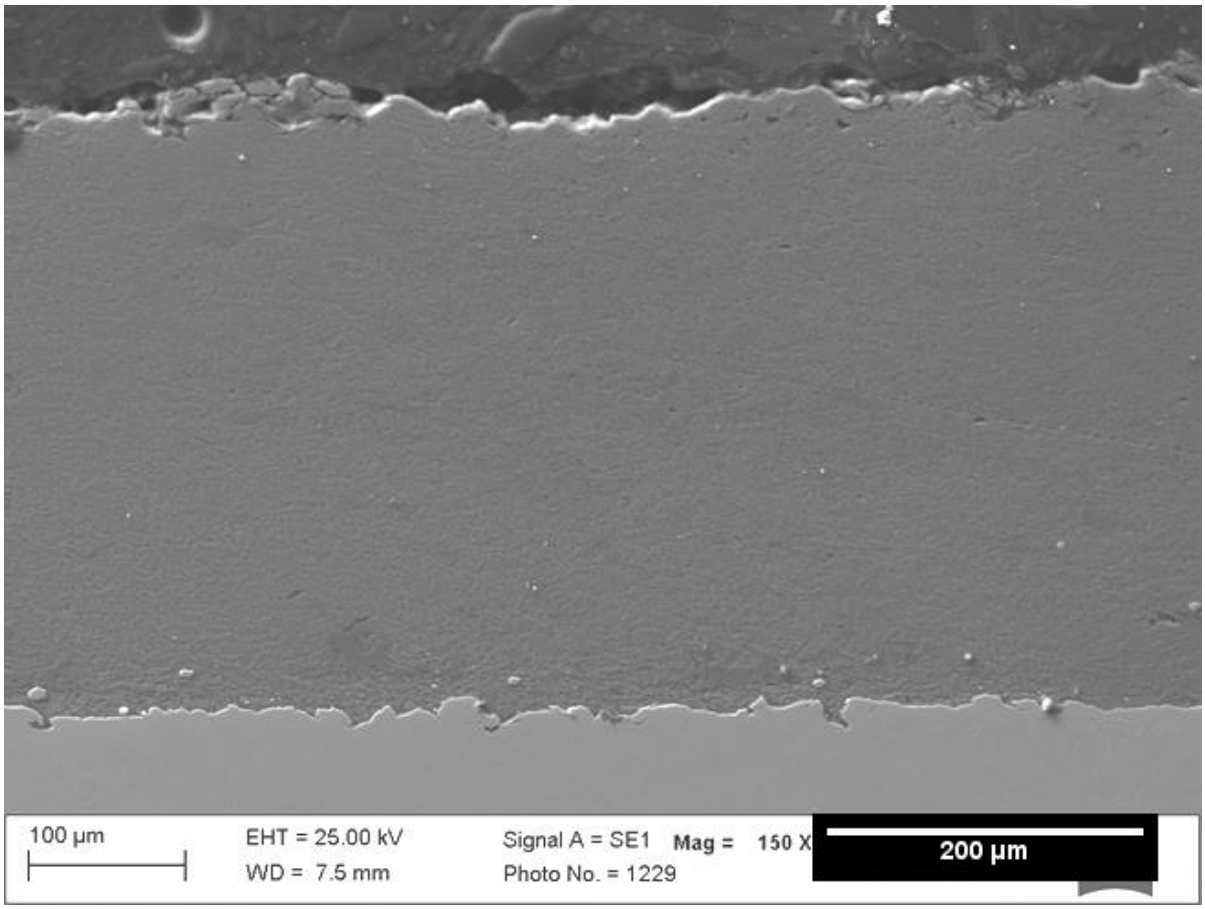

Figure 5.2:Cross-section of aluminum 7075 coating deposited with nitrogen.

Deposition efficiency can be comparatively assessed by the relative coating thicknesses. An equal quantity of powder was sprayed per unit area for each of the coatings; therefore an increase in thickness reflects that a higher percentage of particles were deposited. A jump in deposition efficiency (coating thickness) was present when the gas pressure was increased from 200 psi to 250 psi. This increased gas pressure increases the drag force on the particles by increasing the density of the gas. The higher drag force results in a larger number of particles reaching critical velocity.

Traverse velocity was shown to have a minimal effect on the coating measures that were being investigate. The coatings A7-A7-05 to A7-A7-06 were deposited with the same CGDS parameters, except for traverse velocity (equal spray time by modifying the number of passes), and the resulting thickness, hardness, and porosity of the coatings was found to be very similar. The same trend is seen for the coatings deposited at a higher pressure in A7-A7-07 to A7-A7-08.

Coatings A7-A7-09 to A7-A7-12 were sprayed using air as the carrier gas. These sprays failed to form a deposit on the substrate. It can be concluded as the drag force on the particles was too low to accelerate the particles to the critical velocity. This is likely not a result of the gas nature, but a result of much lower pressure available for compressed air.

5.1.2 Standoff Distance

In the initial testing, a standoff distance of 15 mm was selected based upon manufactures recommendations. It is the goal of this subsection to identify the effect of changing the standoff distance on the coating quality. In the real life application of these coatings, the standoff distance would reduce as coating thickness increases. To test the effect, all other parameters were held constant (see Table 5.4) while only the standoff distance was modified. Three standoff distances were tested and thee results can be found in Table 5.5.

Table 5.4: CGDS parameters held constant for determining standoff distance for Al 7075 powder on Al 7075-T6 substrates.

Parameter Selection	Value
Gas Temperature	500 °C
Gas Pressure	250 psi (1.72 MPa)
Gas Nature	Nitrogen
Traverse Speed	10 mm/s
Step Size	1 mm
Feed Rate	3 rpm
Feed Wheel Type	120 large hole
Powder Feeder Gas Flow Rate	20 SCFH
Powder Feeder Gas Nature	Nitrogen
Nozzle Type	120 mm Standard SS Nozzle
Orifice Diameter	2 mm

Table 5.5: Coating results for determining standoff distance for Al 7075 powder on Al 7075-T6 substrates.

Standoff Distance (mm)	Deposits (Y/N)	Porosity (%)	Coating Thickness (µm)	Comments
10	Y	0	76	NA
20	Y	0	62	NA
30	N	N/A	0 to 30	Poor Quality

The results of Table 5.5 show that coatings had the highest deposition with a small (10 mm) standoff distance. Increasing the distance to 30 mm severely deteriorates the quality of the coating, leaving pits in the coating that penetrate nearly to the substrate. This phenomenon is likely due to the increased interaction of the gas flow with the ambient atmosphere. This interaction would result in unpredictable flow characteristics and particle velocities and temperatures. A 10 mm is the minimum standoff distance recommended from the manufacturer (Centerline (Windsor) Ltd.). With a 5 mm buffer added in order to accommodate the thickness of the deposited coatings, a standoff distance of 15 mm was deemed appropriate and used throughout the remainder of this study.

5.1.3 Effect of CGDS on Heat Treatment of Aluminum 7075-T6 Substrate

In the literature review it was stated that aluminum 7075 gains its strength through the formation of precipitates during heat treatment (see subsection 2.1.3). These precipitates may transform if exposed to high temperatures, resulting in a change of hardness in the material. Hardness tests were used as a qualitative way to identify these changes in the microstructure of the substrate.

It was determined in subsection 5.1.1 that in order for aluminum 7075 powder to deposit, the gas temperature must remain high. Coatings were deposited at 500°C at different pressures and traverse velocities, with all other parameters held constant at values found in Table 5.6. A test matrix showing the varied parameters can be found in Figure 5.3.

Table 5.6: CGDS parameters held constant to test the effect of CGDS on the hardness of Al 7075-T6 substrates.

Parameter Selection	Value
Gas Temperature	500 °C
Gas Pressure	250 psi (1.72 MPa)
Gas Nature	Nitrogen
Traverse Speed	10 mm/s
Step Size	1 mm
Feed Rate	3 rpm
Feed Wheel Type	120 large hole
Powder Feeder Gas Flow Rate	20 SCFH
Powder Feeder Gas Nature	Nitrogen
Standoff Distance	15 mm
Nozzle Type	120 mm Standard SS Nozzle
Orifice Diameter	2 mm

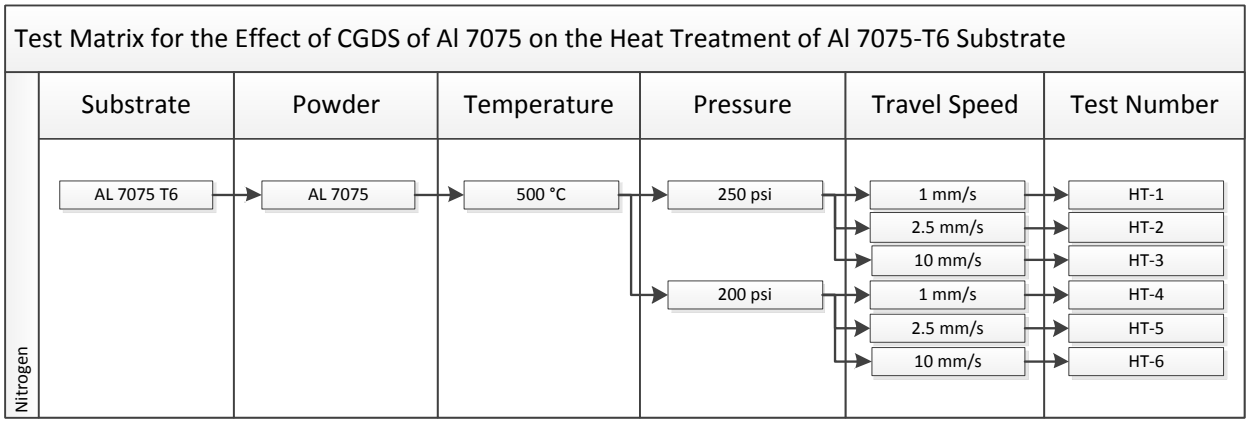

Figure 5.3: Test matrix for the effect of CGDS on the hardness of Al 7075-T6 substrates.

Hardness tests were taken in two locations; directly under the coating/substrate interface and in an area far from the coating. An unsprayed sample is tested as a control. A reduction in the hardness of the substrate will indicate that the microstructure has changed and the heat treatment has been affected. The results showing the effect of CGDS on the heat treatment of Al 7075-T6 can be found in Table 5.7. A graphical representation (Figure 5.4) clearly shows that the substrate is substantially softened.

Table 5.7: Results of the test matrix for the effect of CGDS on the hardness of Al 7075-T6 substrates.

Sample	Distance from Coating/ Substrate Interface (μm)	Average Hardness (VH_{300g})	Standard Deviation (VH_{300g})
7075	NA	195.8	±4.0
HT-1	125	159	±3.1
	900	170.6	±2.8
HT-2	125	175.8	±2.3
	900	173.8	±4.4
HT-3	125	180.2	±3.1
	900	185	±2.2
HT-4	125	173.4	±3.0
	900	179.2	±2.9
HT-5	125	182.6	±2.1
	900	181	±5.0
HT-6	125	180.8	±2.6
	900	181.8	±5.5

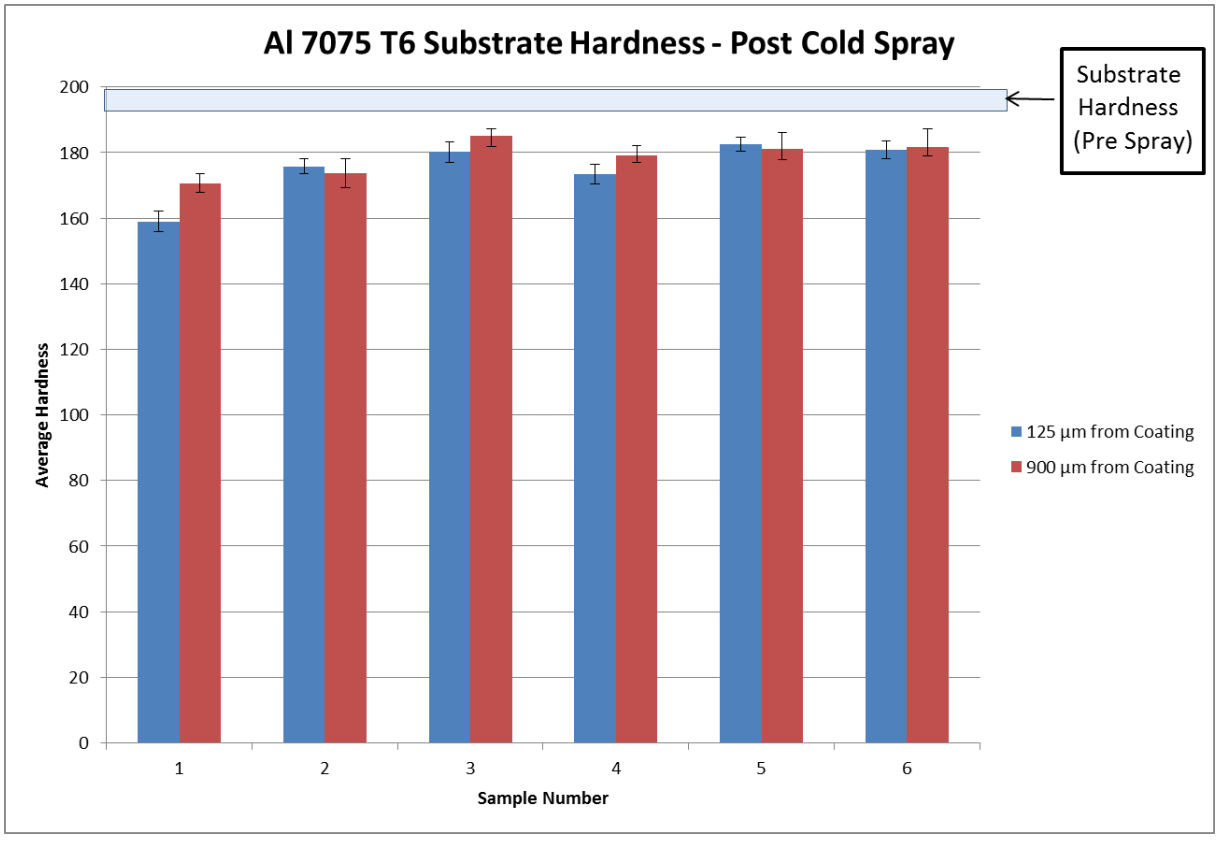

Figure 5.4: Graph showing results of test matrix for the effect of CGDS on the hardness of aluminum 7075-T6 substrates (n=10).

The softening of the substrate indicates that the temperature has coarsened or dissolved the precipitates that are responsible for the hardness of this alloy. The temperature of the substrate is directly related to the stagnation temperature of the gas. Therefore the gas temperature can be reduced to eliminate the effect on the heat treatment of the substrate. However, it was previously concluded that gas temperatures lower than 500°C cannot accelerate particles above their critical velocity using nitrogen. Therefore, in order to achieve the critical velocity at a lower gas temperature, a gas with a higher speed of sound must be used.

5.1.4 Effect of CGDS on Heat Treatment of Aluminum 7075-T6 Substrate using Helium as the Process Gas

To eliminate the effect on the heat treatment of Al 7075-T6, the process gas was switched from nitrogen to helium. It is known that velocity of the gas is related to the speed of sound and the Mach number of the flow. The Mach number is determined by the area ratio of the nozzle it does not change. The speed of sound is bound by the equation,

$$C = \sqrt{kRT}$$

For the same temperature of gas, helium has a much higher speed of sound compared to that of nitrogen. This can be seen as $R_{helium} = 2.0771\ kJ/kgK$ is much larger compared to $R_{nitrogen} = 0.2968\ kJ/kgK$ and $k_{helium} = 1.667$ is larger compared to $k_{nitrogen} = 1.4$. As a result of this much higher speed of sound, it may be possible to achieve critical velocities at gas temperatures below that which affects the hardness of the substrates.

As a guideline for determining the maximum temperature that the aluminum 7075-T6 substrate should reach, a table for the maximum forming temperatures of aluminum alloys was consulted (Figure 5.5). The maximum allowable for Al 7075-T6 is shown to be 165°C for 45 minutes (highlighted in blue). In order to identify the maximum process gas temperature, other parameters were held constant (at values found in Table 5.8) while the gas temperature was modified. A pressure of 200 psi was used for these tests as it was the highest possible pressure that could be used while maintaining desired gas temperatures when using helium. Substrate temperatures were then recorded directly below the substrate surface for gas temperatures of 150°C, 200°C, and 250°C.

ALLOY	CONDITION	MAXIMUM CUMULATIVE TIME – HOURS 1/						
		250°F (121°C)	275°F (135°C)	300°F (149°C)	325°F (165°C)	350°F (177°C)	375°F (191°C)	600°F (316°C)
2014	–T6XX –W	32 4/ 32 4/	32 4/ 32 4/	10 32 4/	10 10	2 1	1/2 3/	3/
2024 2124 2219	–T6X, –T72 –T8XX	32 4/ 32 4/	32 4/ 32 4/	10 10	10 10	1 7	1/2 2	3/ 3/
2090	–T6X –T8X	1 1	1 1	1 1	3/4 3/4	3/4 3/4	3/4 3/4	3/ 3/
6061	–T6XX	32 4/	32 4/	10	10	3	3/4	3/
7075	–T6XX	32 4/	8	2	3/4	3/	3/	3/
7178	–W –T76XX	10 32 4/	1 10	3/ 4	3/ 1	3/ 1/2	3/ 3/	3/ 3/
7049 7075	–T73XX	32 4/	32 4/	10	3	3/4	3/	3/
7050 7075 7175	–T74XX	32 4/	8	2	3/4	3/	3/	3/
7079	–T6XX	10	1	3/	3/	3/	3/	3/
8090	–T8X	2/	2/	10	3/	3/	3/	3/

NOTES: 1/ The sum of fractional times at different temperatures must not exceed one, e.g., for a 6061 part exposed at 300°F (149°C) for 5 hours, another 5 hours at 325°F (163°C) or another 1–1/2 hours at 350°F (177°C) is acceptable.

2/ Do not form or straighten at this temperature to avoid orange peel or excessive residual stresses.

3/ Do not form or straighten at this temperature to avoid overheating and loss in strength.

4/ Times in excess of 32 hours require review by Material and Process (Dept. 679) prior to exceeding 32 hours exposure.

Figure 5.5: Maximum temperature allowances for aluminum alloys.

Table 5.8: CGDS parameters held constant for determining gas temperature for the deposition of Al 7075 powder on Al 7075-T6 substrates using helium.

Parameter Selection	**Value**
Gas Pressure	200 psi (1.38 MPa)
Gas Nature	Helium
Traverse Speed	10 mm/s
Step Size	1 mm
Feed Rate	3 rpm
Feed Wheel Type	120 large hole
Powder Feeder Gas Flow Rate	20 SCFH
Powder Feeder Gas Nature	Helium
Standoff Distance	15 mm
Nozzle Type	120 mm Standard SS Nozzle
Orifice Diameter	2 mm

The results from the temperature tests are shown in Figure 5.6. It is known from literature and the results of the previous subsections that a higher temperature gas stream will result in increased deposition efficiency. To maximize the deposition rate and reduce gas consumption, coatings should be deposited at the highest temperature possible without exceeding the maximum allowable substrate temperature.

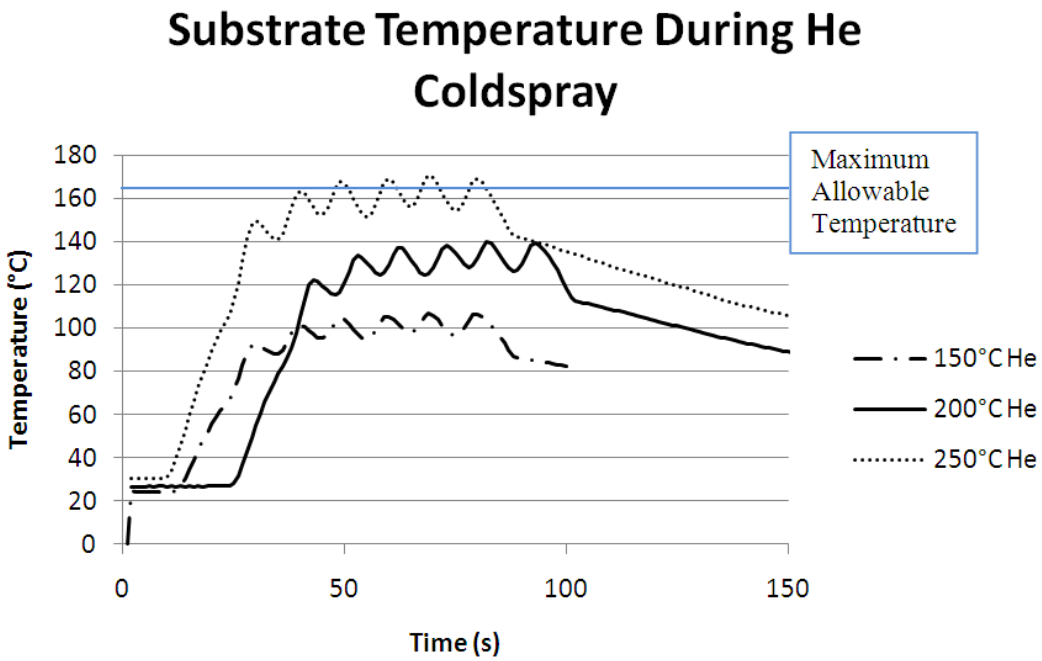

Figure 5.6: Al 7075-T6 substrate temperatures during the CGDS spraying of Al 7075 powder using helium.

The curve for a gas temperature of 250°C in Figure 5.6 shows that the temperature of the substrate directly under the nozzle reaches slightly above the guidelines established in Figure 5.5. The guidelines states that this temperature may be held for up to 45 minutes, in this case it is an instantaneous reading that drops down immediately after the nozzle has passed. Therefore a gas temperature of 250°C was chosen as a parameter for further testing and verification.

In order to verify that the substrate hardness was not affected by the temperature of the sprays, hardness values were taken at the coating surface and center of the plate. Table 5.9 shows the resulting hardness values from the 250°C spray. These results show that the spray process does not affect the heat treatment of the substrate. The hardness of the sprayed sample was unaffected in the middle, and increased slightly near the surface. This increase in hardness is due to work hardening from the impacting particles.

Table 5.9: Al 7075-T6 hardness after the CGDS deposition of Al 7075 powder using helium at 250°C.

Substrate	Hardness (HV_{300g})	
	Mean	Standard Deviation
As Received	175	±4
Sprayed (Near Coating)	185	±4
Sprayed (Middle)	176	±3

5.1.5 Determination of the Powder Feed Rate of Aluminum 7075 Powder using Helium as the Process Gas

In order to reduce the cost of helium, aluminum 7075 powder, and deposition time, the coatings should be deposited at the highest deposition rate and highest deposition efficiency possible. To determine the amount of powder that should be fed into the nozzle, the powder feed rate was varied from 2 to 9 RPM (in 1 RPM increments) while other parameters were held constant (values found in Table 5.10). The coatings were analyzed and the results are found in Table 5.11.

Table 5.10: CGDS parameters held constant for determining powder feed rate for Al 7075 powder on Al 7075-T6 substrates using helium.

Parameter Selection	Value
Gas Pressure	200 psi (1.38 MPa)
Gas Temperature	250 °C
Gas Nature	Helium
Traverse Speed	25 mm/s
Step Size	1 mm
Feed Wheel Type	120 large hole
Powder Feeder Gas Flow Rate	20 SCFH
Powder Feeder Gas Nature	Helium
Standoff Distance	15 mm
Nozzle Type	120 mm Standard SS Nozzle
Orifice Diameter	2 mm

Table 5.11: Results of tests to determine powder feed rate of Al 7075 powder on Al 7075-T6 substrates using helium.

Powder	Thickness (µm)		Hardness (HV_{300g})		Porosity (Area %)	
Feeder RPM	Mean	Standard Deviation	Mean	Standard Deviation	Mean	Standard Deviation
2	196	28	148	5	0.040	0.058
3	381	12	145	12	0.044	0.019
4	502	14	153	6	0.057	0.046
5	587	35	148	5	0.060	0.022
6	711	15	157	3	0.036	0.023
7	713	12	156	4	0.244	0.099
8	754	17	160	9	0.376	0.331
9	747	36	152	9	0.461	0.164

The thickness of the coatings is shown in Figure 5.7. The thickness of the coatings increases linearly with powder feed rates below 7 RPM. At which point, the coating thickness shows a minimal rate of return for increased powder consumption. This leads to the conclusion that at 6 RPM the flow is saturated with powder and is unable to accelerate any more powder to a critical velocity- reducing the deposition efficiency. It is worth noting that at 9 RPM the coating thickness takes a small dip, indicating that any increasing powder flow beyond this point would be detrimental to the spray process.

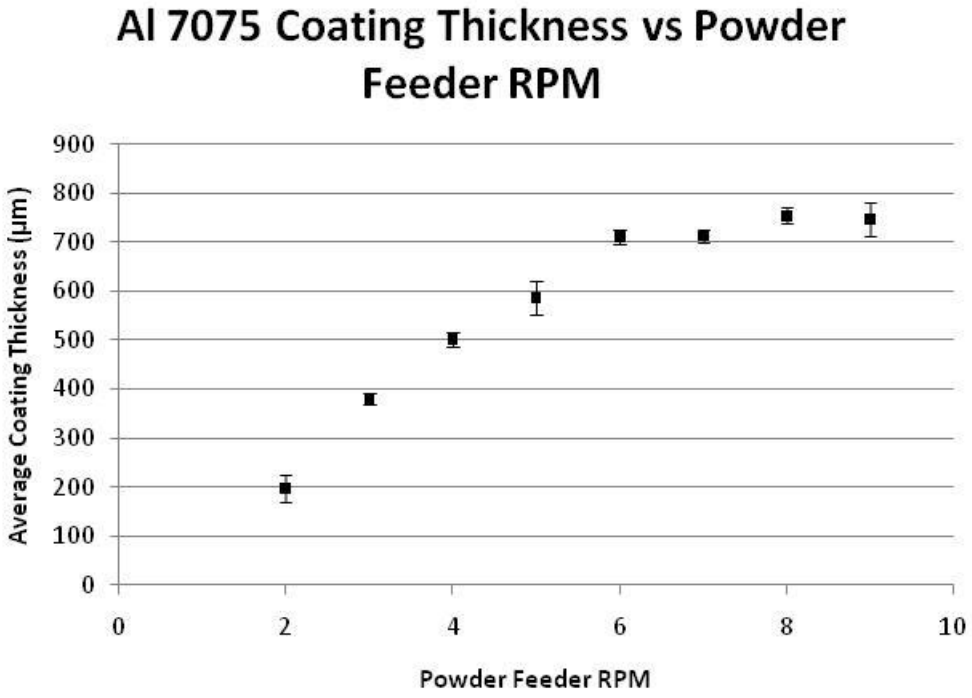

Figure 5.7: Aluminum 7075 coating thickness versus powder feeder RPM for CGDS with helium (n=10).

The hardness values are relatively similar for all of the coatings (Figure 5.8). The coating hardness, in all cases, is lower than that of the bulk material. This can be explained by the lack of heat treatment on the coating. As was discussed in the literature review, this aluminum alloy relies on the precipitates formed during heat treatment for its strength. The porosity of the coatings are all very low (<1 percent) but an increase of porosity is seen above 6 RPM (Figure 5.9). This would be a result of oversaturation of powder in the bulk flow, resulting in slightly lower particle velocities.

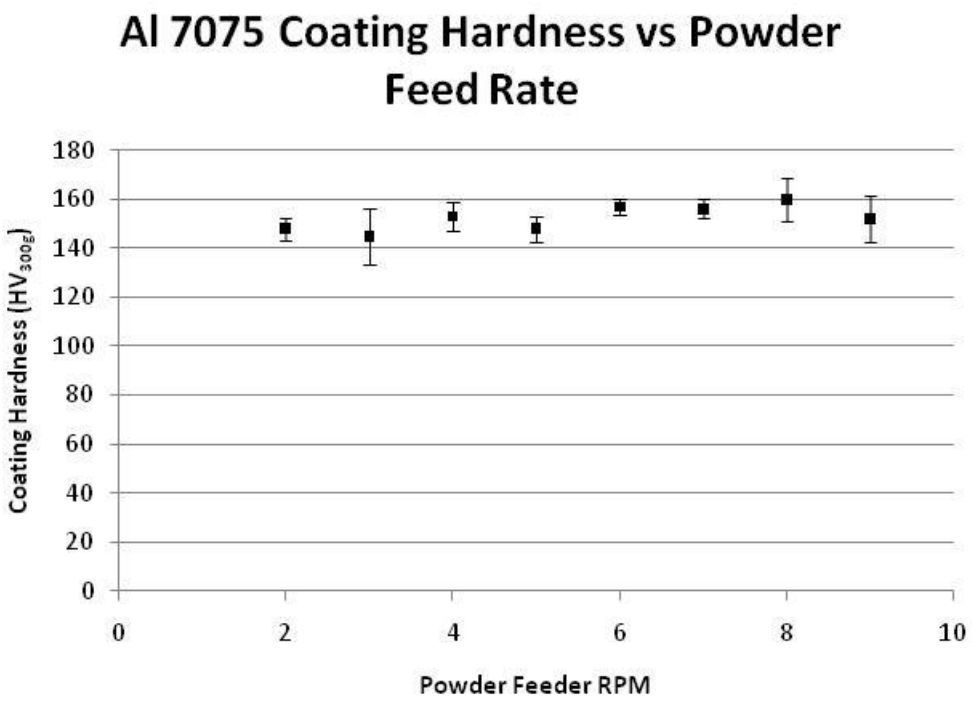

Figure 5.8: Aluminum 7075 coating hardness versus powder feeder RPM for CGDS with helium (n=10).

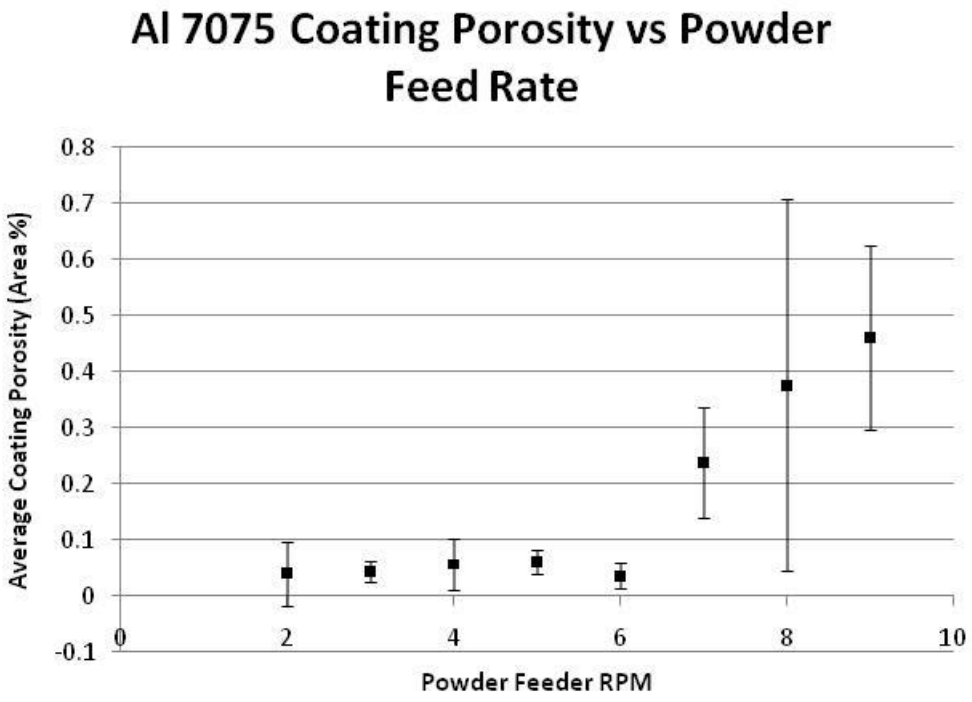

Figure 5.9: Aluminum 7075 coating porosity versus powder feeder RPM for CGDS with helium (n=10).

The results shown in Figure 5.7, Figure 5.8, and Figure 5.9 lead to the conclusion that a powder wheel RPM of 6 is the optimal rate for powder feeding. Above this RPM only a minimal thickness increase is attained for a large increase in powder, as well as a slight decrease in the coating density. Spraying below this RPM would an inefficient use of helium; which is a very costly part of this procedure.

5.1.6 Summary of the CGDS Parameters for the Deposition of Al 7075 powder on Al 7075-T6 Substrates

The gas nature, temperature, pressure, powder feed rate, and standoff distance were investigated in the previous subsections and qualified deposition parameters were determined. These parameters aimed to deposit a dense coating in the most efficient way possible while staying in the limitations of the equipment. The travel speed was shown to have a negligible effect on coating quality, only affecting the thickness per pass. Step size was chosen to be as low as possible (limitation of the system) in order to have the smoothest surface finish possible.

Powder feeding parameters such as powder feed gas flow rate and powder feeder gas nature are thought to have a minimal effect on coating quality as long as they can fluidize the powder for transport and not affect the main gas flow. Values for these parameters were chosen based on experience. Nozzle type was limited by the nature of the powder and orifice diameter was set by the system. A full set of parameters that will be used to deposited aluminum 7075 powder on aluminum 7075-T6 substrates, for the characterization of repairs, can be found in Table 5.12.

Table 5.12: Summary of qualified CGDS parameters for the deposition of Al 7075 powder on Al 7075-T6 substrates.

Parameter Selection	Value
Gas Pressure	200 psi (1.38 MPa)
Gas Temperature	250 °C
Gas Nature	Helium
Traverse Speed	25 mm/s
Step Size	1 mm
Feed Rate	6 RPM
Feed Wheel Type	120 large hole
Powder Feeder Gas Flow Rate	20 SCFH
Powder Feeder Gas Nature	Helium
Standoff Distance	15 mm
Nozzle Type	120 mm Standard SS Nozzle
Orifice Diameter	2 mm

5.2 Coating Development of Aluminum 2024 Powder on Aluminum 2024-T3 Substrates

A procedure similar to that used in section 5.1 was performed in order to determine a set of parameters qualified for deposition of aluminum 2024 powder on aluminum 2024-T3 substrates. All substrates were prepared using the parameters found in Table 5.1.

5.2.1 Pressure, Temperature, and Traverse Velocity

The first parameters investigated were temperature, pressure, and traverse velocity. The standoff distance, nozzle type, orifice diameter, powder feeder wheel, powder feeder gas rate, and powder feed rate were held constant at values recommended by the CGDS supplier (Centerline (Windsor) Ltd.). These values can be found in Table 5.13.

Table 5.13: CGDS parameters held constant for the initial coating development of Al 2024 powder on Al 2024-T3 substrates.

CGDS Parameter	Value
Standoff Distance	15 mm
Nozzle Type	120 mm SS Nozzle
Orifice Diameter	2 mm
Powder Feeder Wheel	120 Large Hole
Powder Feeder Gas Rate	20 SCFH
Powder Feed Rate	3 RPM
Step Size	1 mm

A high and low for each of the variable categories was chosen based on recommended ranges from the manufacturer. A matrix showing the test plan can be found in Figure 5.10. This test matrix also includes trials to be completed using air as a process gas at the maximum available pressure of approximately 100 psi.

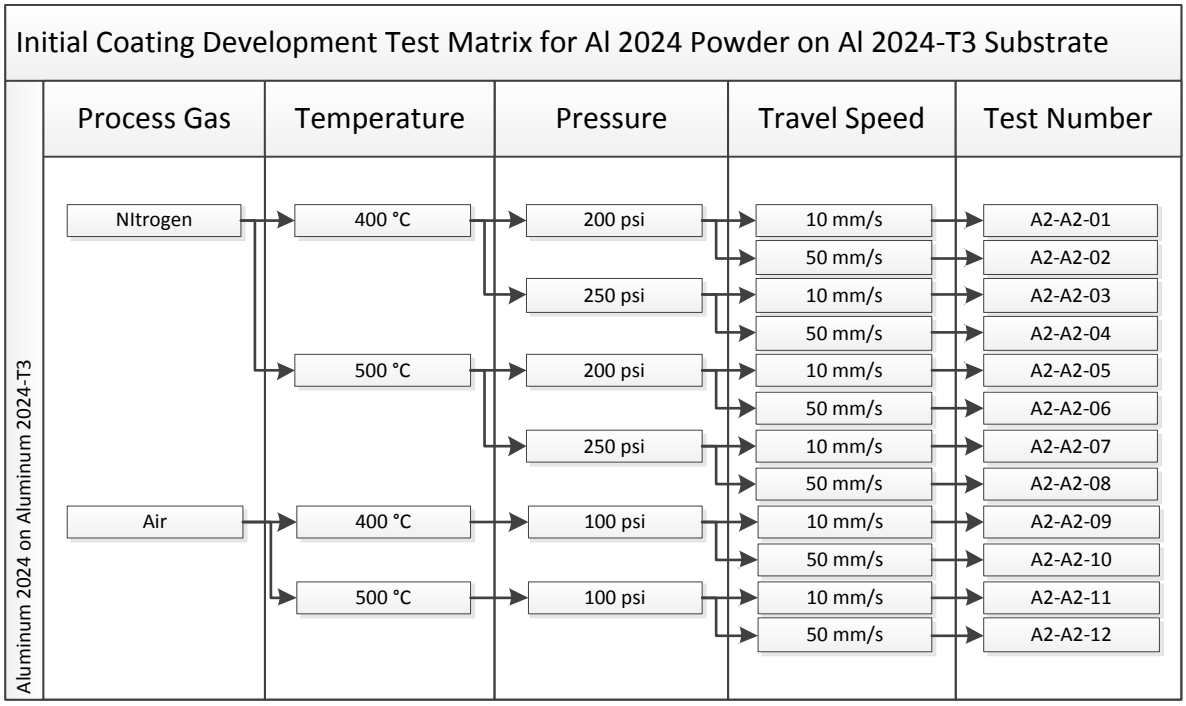

Figure 5.10: Initial coating development test matrix for Al 2024 powder on Al 2024-T3 substrate.

The results of this trial can be found in Table 5.14. Each of these trials resulted in near instantaneous clogging of the nozzle and/or orifice. It is believed that the low hardness and high percentage of satellite particles was the cause of this clogging.

Table 5.14: Results for initial coating development test matrix for Al 2024 powder on Al 2024-T6 substrates.

Test Number	Deposits (Y/N)	Porosity (%)	Vickers Hardness (300 gram)	Coating Thickness (μm)
A2-A2-01	N	NA	NA	NA
A2-A2-02	N	NA	NA	NA
A2-A2-03	N	NA	NA	NA
A2-A2-04	N	NA	NA	NA
A2-A2-05	N	NA	NA	NA
A2-A2-06	N	NA	NA	NA
A2-A2-07	N	NA	NA	NA
A2-A2-08	N	NA	NA	NA
A2-A2-09	N	NA	NA	NA
A2-A2-10	N	NA	NA	NA
A2-A2-11	N	NA	NA	NA
A2-A2-12	N	NA	NA	NA

Further testing with the stainless steel nozzle using Al 2024 powder was halted at this point as it was damaging equipment that was required for the work of others.

5.2.2 Polymer Nozzle Trials

In an attempt to prevent the nozzle from clogging, trials with the polymer nozzle were attempted. The polymer nozzle, designed for pure aluminum powders, is limited to temperature of 350°C. For these tests, the parameters found in Table 5.15 were held constant. The test matrix of the parameters varied is found in Figure 5.11.

Table 5.15: CGDS parameters held constant for the polymer nozzle coating development of Al 2024 powder on Al 2024-T3 substrates.

CGDS Parameter	Value
Standoff Distance	15 mm
Nozzle Type	Polymer Nozzle
Orifice Diameter	2 mm
Powder Feeder Wheel	120 Large Hole
Powder Feeder Gas Rate	20 SCFH
Powder Feed Rate	3 RPM
Step Size	1 mm

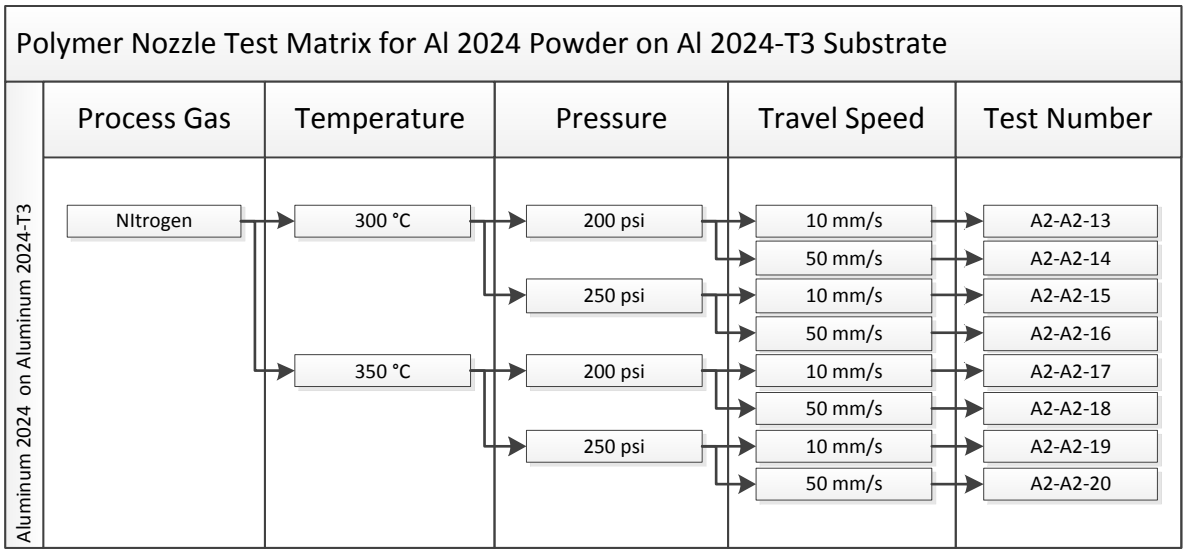

Figure 5.11: Coating development test matrix for Al 2024 powder on Al 2024-T3 substrates using the polymer nozzle.

The results of this test can be found in Table 5.16. After spraying, no evidence of clogging was found in the polymer nozzle itself, but some clogging was seen in the orifice. As a result of the low gas temperatures available, all coatings sprayed with the polymer nozzle resulted in a burnishing of the substrate without deposition.

Table 5.16: Results for initial coating development test matrix for Al 2024 powder on Al 2024-T3 substrates.

Test Number	Deposits (Y/N)	Porosity (%)	Vickers Hardness (300 gram)	Coating Thickness (μm)
A2-A2-13	N	NA	NA	NA
A2-A2-14	N	NA	NA	NA
A2-A2-15	N	NA	NA	NA
A2-A2-16	N	NA	NA	NA
A2-A2-17	N	NA	NA	NA
A2-A2-18	N	NA	NA	NA
A2-A2-19	N	NA	NA	NA
A2-A2-20	N	NA	NA	NA

5.2.3 Summary of the CGDS Parameters for the Deposition of Al 2024 Powder on Al 2024-T3 Substrates

It appears that aluminum 2024 powder requires a critical velocity higher than can be accomplished with the polymer nozzle using nitrogen. The use of the stainless steel nozzle resulted in near instantaneous clogging of the nozzle and orifice. At this point in the research, the use of helium gas was to be investigated, but was halted due to the damage this powder was causing the equipment. It was therefore concluded, that the aluminum 2024 powder (F27131 Poudres Hermillon) could not be deposited using the current system.

5.3 Coating Development of Pure Aluminum Powders on 4130 Steel Substrates

The development of pure aluminum coatings for the restoration of damaged pure aluminum IVD was undertaken prior to the coating development of pure aluminum for aluminum alloy component repair. Information that was acquired in the previous sections was used to streamline the development process. All substrates were prepared using the parameters found in Table 5.17 .

Table 5.17: Surface preparation parameters for 4130 steel substrates.

Parameter	Value
Abrasive	Ferroscilicate
Size	20 mesh
Process Gas	Filtered/Dry Air
Spraying Pressure	60 psi (410 kPa)
Spray Angle	45°
Standoff Distance	2 inch (51 mm)
Post Treatment	Vibratory Ethanol Bath

5.3.1 Temperature and Pressure

In order to determine which temperatures and pressures are suitable for this application, the other parameters were held constant while these parameters were modified. These values can be found in Table 5.18.

Table 5.18: CGDS parameters held constant for the initial coating development test matrix for pure aluminum powder on 4130 steel substrates.

CGDS Parameter	Value
Standoff Distance	15 mm
Nozzle Type	Polymer Nozzle
Orifice Diameter	2 mm
Powder Feeder Wheel	120 Large Hole
Powder Feeder Gas Rate	20 SCFH
Powder Feed Rate	4 RPM

This test also aims to identify the effect of traverse velocity on the resulting coatings. A high and low for each of the variable categories was chosen based on recommended ranges from the manufacturer and accumulated knowledge. A step size of 1 mm was chosen for the 20 mm/s traverse velocity while a 4 mm step was chosen for the 80 mm/s traverse velocities. This was done in order to ensure the same deposition time for all coatings. A matrix showing the test plan can be found in Figure 5.12. This test matrix also includes trials to be completed using air as a process gas at the maximum available pressure of approximately 100 psi.

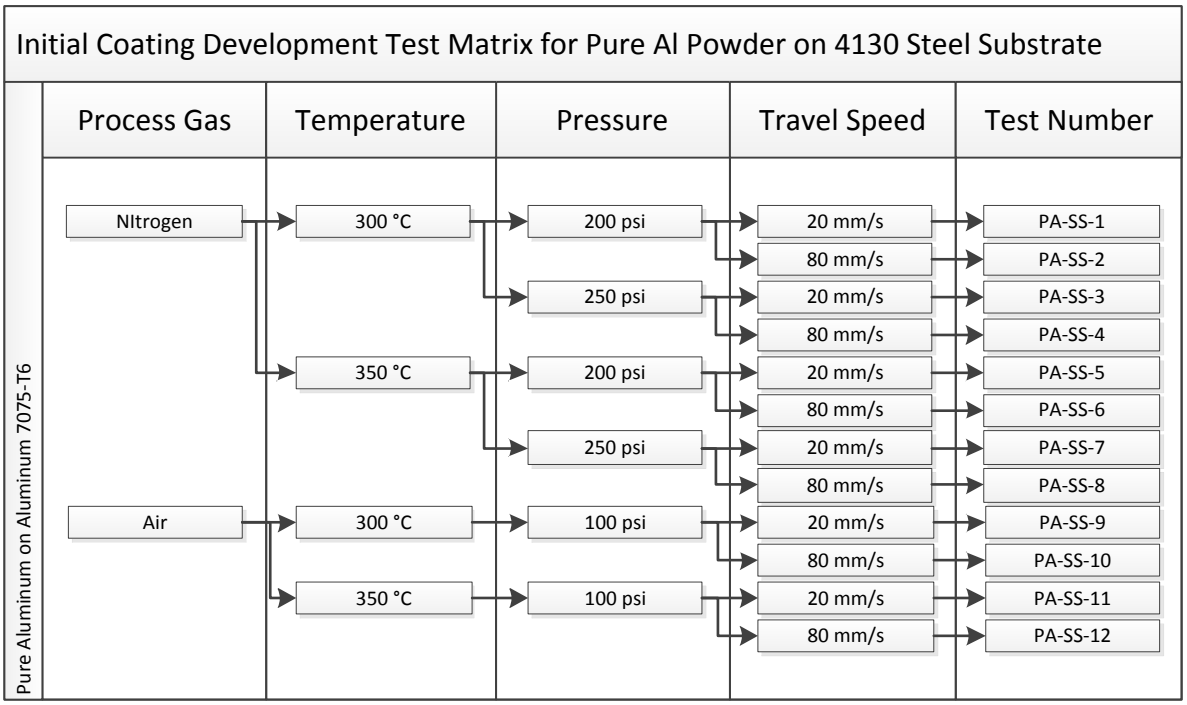

Figure 5.12: Initial coating development test matrix for pure aluminum powder on 4130 steel substrates.

The results of this test can be found in Table 5.19. It should be noted, that the results of the thickness measurements are not included in this result. At the time of testing, issues involving the feeding of the pure aluminum powder were prominent. Coating thickness varied ±100% during a single test due to the rate at which powder was feeding. The problem was isolated to being a result of humidity in the powder, which left the pure aluminum powder extremely clumpy. The traverse velocity, coating thickness, and powder feed rate were investigated in the upcoming subsections.

Table 5.19: Results for initial coating development test matrix for pure aluminum powder on 4130 steel substrates.

Test Number	Deposits (Y/N)	Porosity (%)	Vickers Hardness (300 gram)
PA-SS-1	Y	<1	60±4
PA-SS-2	Y	<1	56±3
PA-SS-3	Y	<1	60±1
PA-SS-4	Y	<1	57±5
PA-SS-5	Y	<1	50±3
PA-SS-6	Y	<1	59±3
PA-SS-7	Y	<1	52±8
PA-SS-8	Y	<1	53±2
PA-SS-9	N	NA	NA
PA-SS-10	N	NA	NA
PA-SS-11	N	NA	NA
PA-SS-12	N	NA	NA

The humidly issue was dealt immediately after this test. From this point on, all powder was stored in a low humidly (<25%) chamber. It should be noted, that even with the poor powder feeding behavior, all the coatings appeared to have very low porosity.

The testing for pure aluminum was run simultaneously with other projects on many different substrates. In those projects, it was determined that the highest rate of deposition happened with the highest temperature and pressure, which agrees with the literature and the results from the previous sections. Therefore, pure aluminum coatings were to be deposited using 350 C and 250 psi. It was found that the low pressure air could not deposit any coatings, for the same reasons stated in the previous sections.

5.3.2 Traverse Velocity with the 120 Large Hole Feeding Wheel

Class 1 pure aluminum IVD coatings have a thickness usually falls within the range of 25 μm to 50 μm (minimum of 25 μm, no maximum given). Therefore the repairs must also fall within this thickness range. A series of coatings were deposited at different traverse velocities while holding

all other parameters constant to determine the traverse velocity resulting in proper thickness. The results of these tests can be found in Figure 5.13.

Table 5.20: CGDS parameters held constant for the initial trial to determine traverse velocity for pure aluminum powder for the restoration of damaged pure aluminum IVD coatings.

Parameter Selection	Value
Gas Pressure	250 psi (1.7 MPa)
Gas Temperature	300 °C
Gas Nature	Nitrogen
Step Size	1 mm
Feed Rate	4 rpm
Feed Wheel Type	120 Large Hole
Powder Feeder Gas Flow Rate	20 SCFH
Powder Feeder Gas Nature	Nitrogen
Standoff Distance	15 mm
Nozzle Type	Polymer Nozzle
Orifice Diameter	2 mm

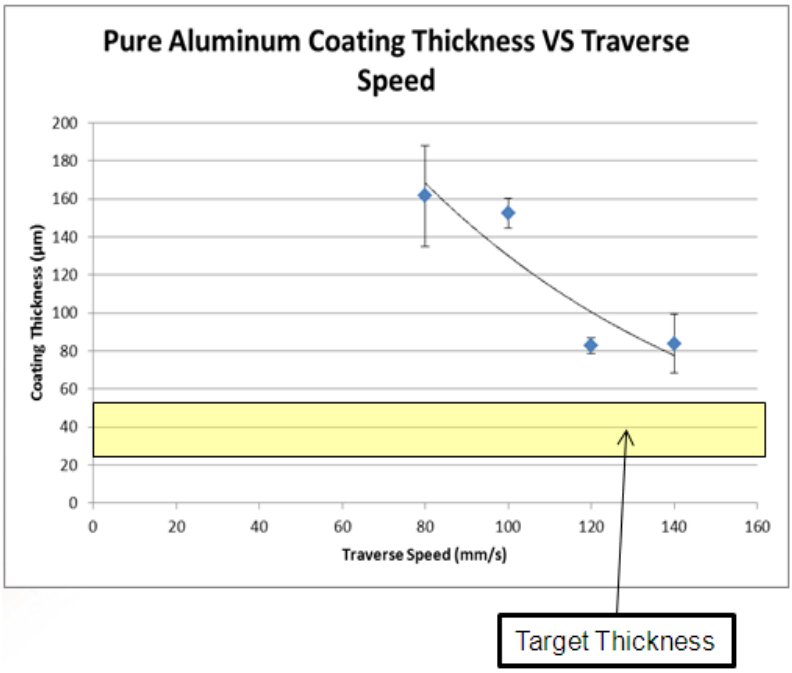

Figure 5.13: Pure aluminum coating thickness with the 120 large hole wheel (n=10).

Above 140 mm/s it was observed that the deposited coating was no longer coherent. At these velocities, individual pulses from the holes in the powder feed wheel were visible, which left discontinuities in the coatings. Below 140mm/s, the coatings were deposited without discontinuities, but the coating thickness was beyond that which was desired. Reduction of the powder feeding rate would lower the thickness of the coatings, but would increase the effect of pulses, which lowers the maximum traverse velocity.

It was then determined that it was not possible to deposit 25 to 50 μm pure aluminum CGDS coatings with the 120 hole large wheel without having discontinuity in the coating. In order to rectify this issue, a powder feeding wheel of 320 small holes was procured. This would allow the traverse velocity to be increased above the 140mm/s, as the powder pulses would be much smaller and closer together, almost acting as a continuous flow.

5.3.3 Powder Feeding Rate with the 320 Small Hole Feeding Wheel

Before investigating the traverse velocity required to produce coatings of desired thickness, a powder feed rate for the new powder feed wheel was determined. The trials were done in a similar manner as the aluminum 7075, in which all parameters were held constant (Table 5.23) except for the powder feeding rate. The goal of this subsection was not to gain the proper coating thickness, but to determine the maximum quantity of powder that can be fed while maintaining deposition efficiency and coating quality.

Table 5.21: CGDS parameters held constant to determine the powder feed rate for pure aluminum powder for the restoration of damaged pure aluminum IVD coatings.

Parameter Selection	Value
Gas Pressure	250 psi
Gas Temperature	300 °C
Gas Nature	Nitrogen
Step Size	1 mm
Traverse Velocity	10
Feed Wheel Type	120 Large Hole
Powder Feeder Gas Flow Rate	20 SCFH
Powder Feeder Gas Nature	Nitrogen
Standoff Distance	15 mm
Nozzle Type	Polymer Nozzle
Orifice Diameter	2 mm (78.7 thou)

Initial trials showed a linear relationship between feeder rpm and coating thickness (Figure 5.14). The linear relationship indicates that as more powder is being fed, a proportional amount of powder is being deposited, i.e. the deposition efficiency remains constant. It was then concluded that the coatings should be deposited at the highest powder feed rate possible in order to save on gas consumption and spray time.

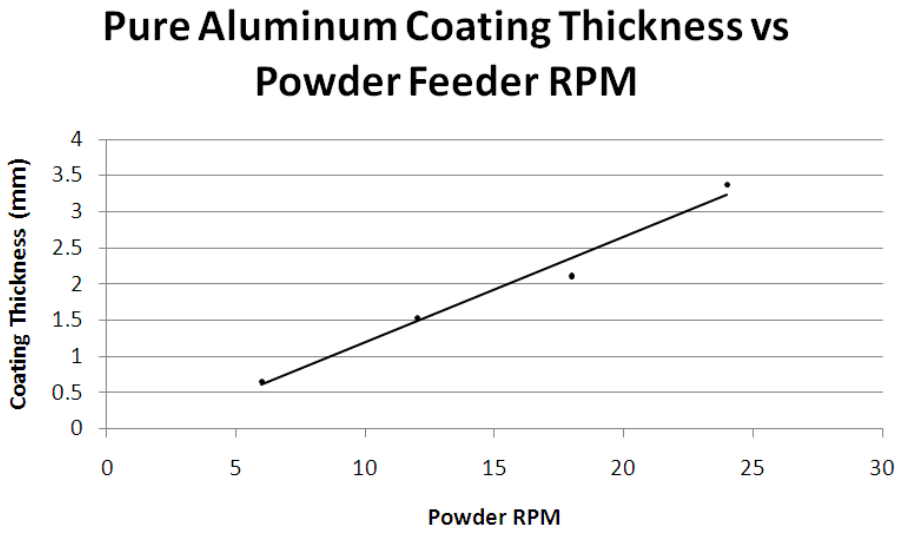

Figure 5.14: Pure Al Coating Thickness vs. Powder Feeder RPM using 320 Hole Wheel

In order to determine what feed rate to use, coating quality must also be investigated. Porosity measurements were taken from the coating thickness samples (shown in Table 5.22). A jump in porosity occurred between 12rpm and 16 rpm and a refined rpm tests was completed to find the feed rate at which the coating quality begins to deteriorate. The results show a clear degradation of coating quality above 14 RPM. Therefore, this was chosen for the powder feed rate for the velocity tests.

Table 5.22: Coating quality results for determining powder feed rate with the 320 small hole wheel for pure aluminum coatings.

Powder Feeder RPM	Porosity (%)	
	Mean	Standard Deviation
6	1.5	±0.4
12	1.7	±1.1
13	1.9	±0.3
14	1.4	±0.7
15	3.1	±0.5
16	3.3	±1.0
17	3.7	±0.6
18	3.0	±0.9
24	3.4	±1.4

The pure aluminum coatings found during these tests were slightly higher than those previously recorded. The reason for this is not entirely clear; it may be a result of manual selection of contrast parameters when determining porosity or a problem with the powder itself. What was clear in this experiment is that a jump in porosity is seen at above 14 rpm. It should also be noted that in order to have powder flow properly with this new wheel, a powder feeder gas flow rate of 25 SCFM was required. This is due to the reduced size of the feeding holes and the clumpy nature of aluminum powders.

5.3.4 Traverse Velocity with the 320 Small Hole Feeding Wheel

As discussed, depositing a coating of proper thickness is a crucial component of this project. It has been shown that the traverse velocity has a minimal effect on coating quality, but does affect the coating thickness. In order to determine the velocity required to reach the proper thickness,

a series of trials at different velocities were performed while holding the remaining parameters constant at values previously determined (Table 5.23).

Table 5.23: CGDS parameters held constant for determining traverse velocity for pure aluminum powder for the restoration of damaged pure aluminum IVD coatings.

Parameter Selection	Value
Gas Pressure	250 psi
Gas Temperature	300 °C
Gas Nature	Nitrogen
Step Size	1 mm
Feed Rate	14 RPM
Feed Wheel Type	320 small hole
Powder Feeder Gas Flow Rate	25 SCFH
Powder Feeder Gas Nature	Nitrogen
Standoff Distance	15 mm
Nozzle Type	Polymer Nozzle
Orifice Diameter	2 mm (78.7 thou)

The thickness of the coatings can be seen in Figure 5.15. With the new powder feeding wheel it was possible to reach the thickness of Class 1 IVD coatings. A traverse velocity of 190mm/s to 260mm/s would result in a coating in the desired 25 to 50 μm range.

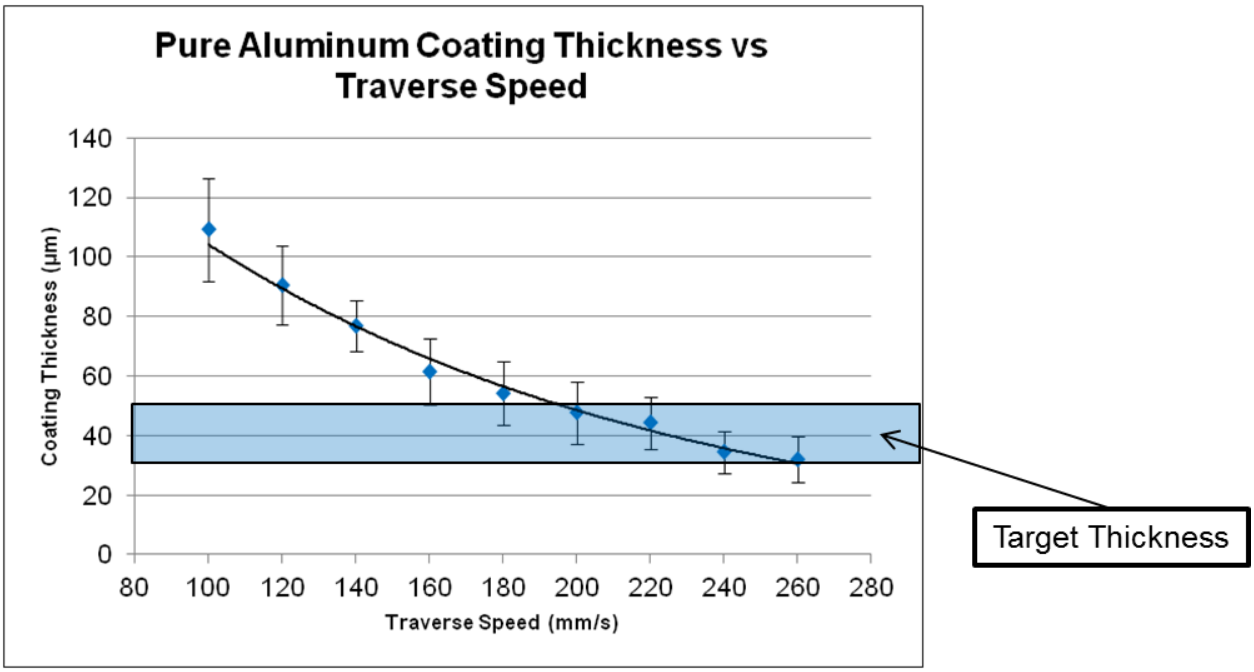

Figure 5.15: Pure aluminum coating thickness based on traverse velocity (n=10).

5.3.5 Summary of the CGDS Parameters for the Deposition of Pure Aluminum Powder on 4130 Steel Substrates

The gas temperature, pressure, powder feed rate, and traverse velocity were investigated in the previous subsections and qualified parameters were determined. These parameters aimed to deposit a dense coating in the most efficient way possible while staying in the limitations of the equipment. The remaining parameters were chosen based on knowledge accumulated within this study. A full set of parameters that will be used to deposited pure aluminum on 4130 steel, for the characterization of repairs, can be found in Table 5.24. An image of a cross-section of the coatings can be found in Figure 5.16.

Table 5.24: Summary of qualified CGDS parameters for the deposition of pure aluminum powder on 4130 steel for the restoration of damaged pure aluminum IVD coatings.

Parameter Selection	Value
Gas Pressure	250 psi (1.72 MPa)
Gas Temperature	350 °C
Gas Nature	Nitrogen
Traverse Velocity	190-260 mm/s
Step Size	1 mm
Feed Rate	14 RPM
Feed Wheel Type	320 small hole
Powder Feeder Gas Flow Rate	25 SCFH
Powder Feeder Gas Nature	Nitrogen
Standoff Distance	15 mm
Nozzle Type	Polymer Nozzle
Orifice Diameter	2 mm

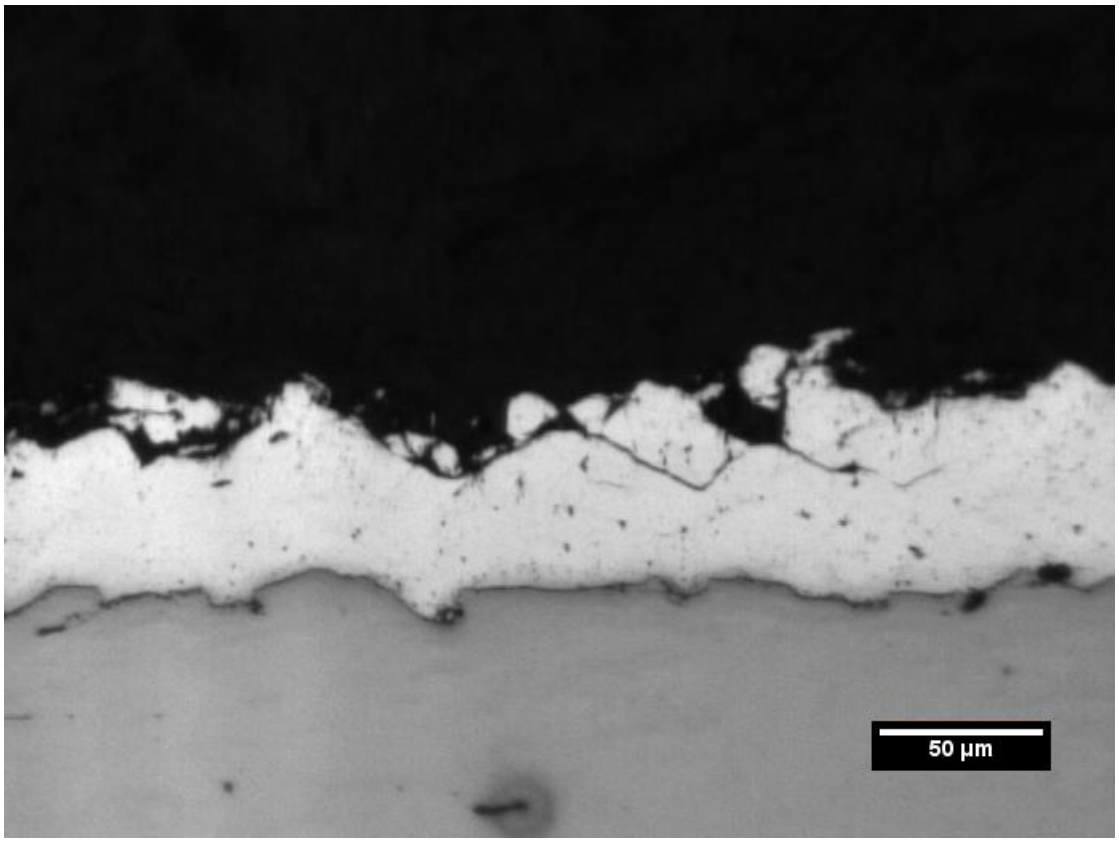

Figure 5.16: Cross-section of a pure aluminum coating deposited on 4130 steel.

5.4 Coating development of Pure Aluminum Powder on Aluminum 7075 and Aluminum 2024 Substrates

In the previous section, CGDS parameters were determined for the deposition of pure aluminum on 4130 steel. According to literature, the substrate material should only have an effect on the first layer of particles deposited, after which particles are deposited on previously deposited particles [41]. Therefore, the parameters previously determined for 4130 steel were assumed suitable for both aluminum alloy substrates. A summary of these parameters can be found Table 5.25 and the surface preparation variables can be found in Table 5.1.

Table 5.25: Summary of qualified CGDS parameters for the deposition of pure aluminum powder on aluminum 7075 and aluminum 2024 substrates.

Parameter Selection	Value
Gas Pressure	250 psi
Gas Temperature	300 °C
Gas Nature	Nitrogen
Step Size	1 mm
Feed Rate	14 RPM
Feed Wheel Type	320 small hole
Powder Feeder Gas Flow Rate	25 SCFH
Powder Feeder Gas Nature	Nitrogen
Standoff Distance	15 mm
Nozzle Type	Polymer Nozzle
Orifice Diameter	2 mm (78.7 thou)

The traverse velocity was determined to have a negligible effect on the coating quality and only have an effect on coating thickness. The required thickness of the coatings will vary depending on the depth of the damage, and would be determined for each repair.

5.4.1 Effect of CGDS on Heat Treatment of Aluminum 7075-T6 and Aluminum 2024-T3 Substrates

In the literature review it was stated that aluminum 7075 and aluminum 2024 gain strength through the formation of precipitates during heat treatment. These precipitates may transform if exposed to higher temperatures (see Section 2.1.3). In order to verify that the substrate microstructure was not affected by the temperature of the sprays, hardness values were taken near the coating surface and inside the substrate for the tests shown in Figure 5.17 (all other parameters can be found in Table 5.25).

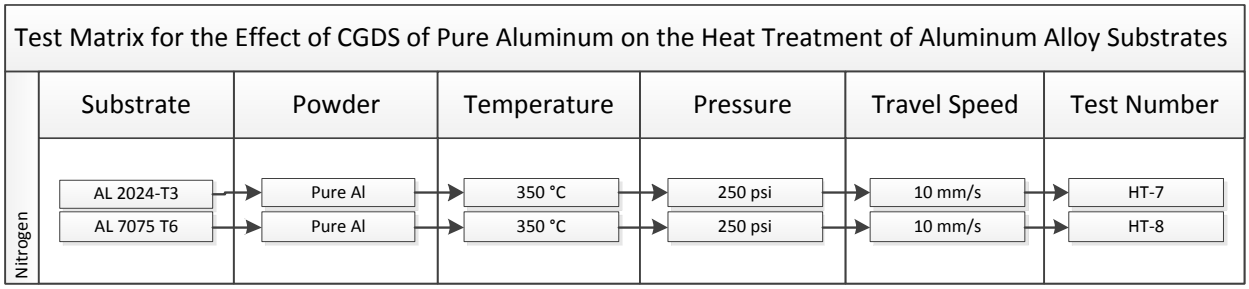

Figure 5.17: Test matrix for the effect of CGDS of pure aluminum powder on the heat treatment of Al 2024-T3 and Al 7075-T6 substrates.

The results of the hardness tests can be found in Table 5.26. Hardness tests were used as a qualitative way to identify changes in the microstructure of the substrate. The hardness values for these tests did not change, and therefore it can be concluded that the coating process had no effect on the heat treatment of the substrates. An example of a dense pure aluminum coating can be found in Figure 5.18.

Table 5.26: Results of Test matrix for the effect of CGDS of pure aluminum on the heat treatment of Al 7075-T6 and Al 2024 substrates.

Sample	Distance from Coating where Hardness Value was Taken (μm)	Average Hardness (VH_{300g})	Standard Deviation (VH_{300g})
2024 Control	NA	170	±4.3
HT-7	5	172.8	±5.4
	350	170.6	±2.8
7075 Control	NA	195.8	±4.0
HT-8	5	197.4	±2.7
	350	199.8	±2.4

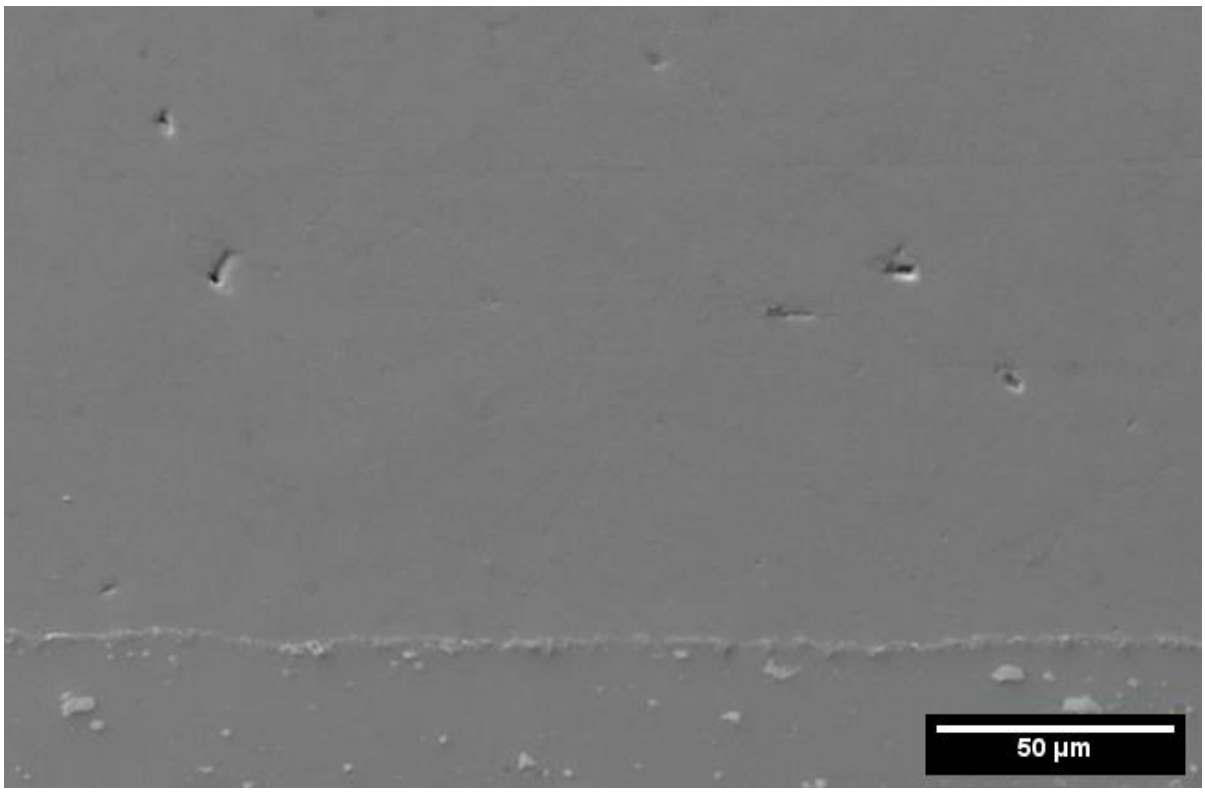

Figure 5.18: Pure aluminum coating deposited with nitrogen on aluminum 7075-T6 substrate.

5.5 Coating development of Aluminum 7075 Powder on 4130 Steel

In the previous sections, CGDS parameters were determined for the deposition of aluminum 7075 powder on aluminum 7075-T6 substrates, using both helium and nitrogen. The reason

helium gas was used was to lower the temperature that the substrate was exposed to. The 4130 steel substrates do not have this temperature limitation and therefore helium is not necessary. In order to determine which gas temperatures and pressures are suitable for this application, the parameters found in Table 5.27 were held constant, while the test plan (Figure 5.19) was executed. All substrates were prepared using the parameters found in Table 5.1.

Table 5.27: CGDS parameters held constant for the initial coating development test matrix for Al 7075 powder on 4130 steel substrates.

CGDS Parameter	Value
Standoff Distance	15 mm
Nozzle Type	Polymer Nozzle
Orifice Diameter	2 mm
Powder Feeder Wheel	120 Large Hole
Powder Feeder Gas Rate	20 SCFH
Powder Feed Rate	4 RPM

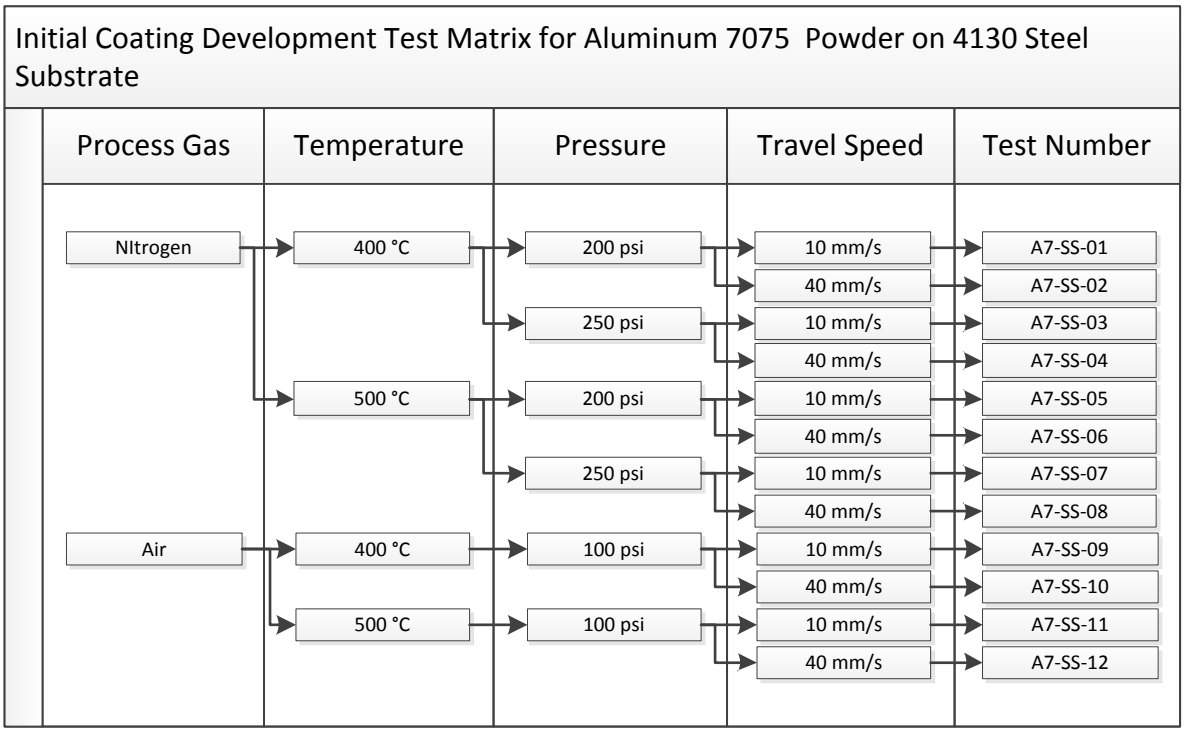

Figure 5.19: Initial coating development test matrix for aluminum 7075 powder on 4130 steel substrates.

This test also aims to identify the effect of traverse velocity on the resulting coatings. A high and low for each of the variable categories was chosen based on recommended ranges from the manufacturer and accumulated knowledge. A step size of 1 mm was chosen the 10 mm/s traverse velocity while a 4 mm step was chosen for the 40 mm/s traverse velocities. This was done in order to ensure the same deposition time for all coatings. This test matrix also includes trials to be completed using air as a process gas at the maximum available pressure of approximately 100 psi. The results of these tests can be found in Table 5.28.

Table 5.28: Results for initial coating development test matrix for aluminum 7075 powder on 4130 steel substrates.

Test Number	Deposits (Y/N)	Porosity (%)	Coating Thickness (μm)
A7-SS-01	N	NA	NA
A7-SS-02	N	NA	NA
A7-SS-03	N	NA	NA
A7-SS-04	N	NA	NA
A7-SS-05	Y	<1	112.4 ±23.0
A7-SS-06	Y	<1	120.4±22.6
A7-SS-07	Y	<1	197.6±13.4
A7-SS-08	Y	<1	189.6±27.3
A7-SS-09	N	NA	NA
A7-SS-10	N	NA	NA
A7-SS-11	N	NA	NA
A7-SS-12	N	NA	NA

The same trends were seen here as in aluminum 7075 on aluminum 7075-T6 substrates. A gas temperature of 500°C is required for the particles to reach the critical velocity. The higher pressure results in thicker coatings. No deposition was present when the process used low pressure air as a carrier gas.

Depositing a coating of proper thickness is a crucial component of this project. In order to determine the velocity required to reach this value, a series of trials at different velocities were performed while holding the remaining parameters constant (Table 5.29). The thickness of the coatings can be seen in Figure 5.20. A traverse velocity of 60 mm/s to 110 mm/s would result in a coating in the desired 25 to 50 μm range.

Table 5.29: CGDS parameters held constant for determining traverse velocity for aluminum 7075 powder for the restoration of damaged pure aluminum IVD coatings.

Parameter Selection	Value
Gas Pressure	250 psi (1.72 MPa)
Gas Temperature	500 °C
Gas Nature	Nitrogen
Step Size	1 mm
Feed Rate	3 RPM
Feed Wheel Type	120 large hole
Powder Feeder Gas Flow Rate	20 SCFH
Powder Feeder Gas Nature	Nitrogen
Standoff Distance	15 mm
Nozzle Type	SS Nozzle
Orifice Diameter	2 mm

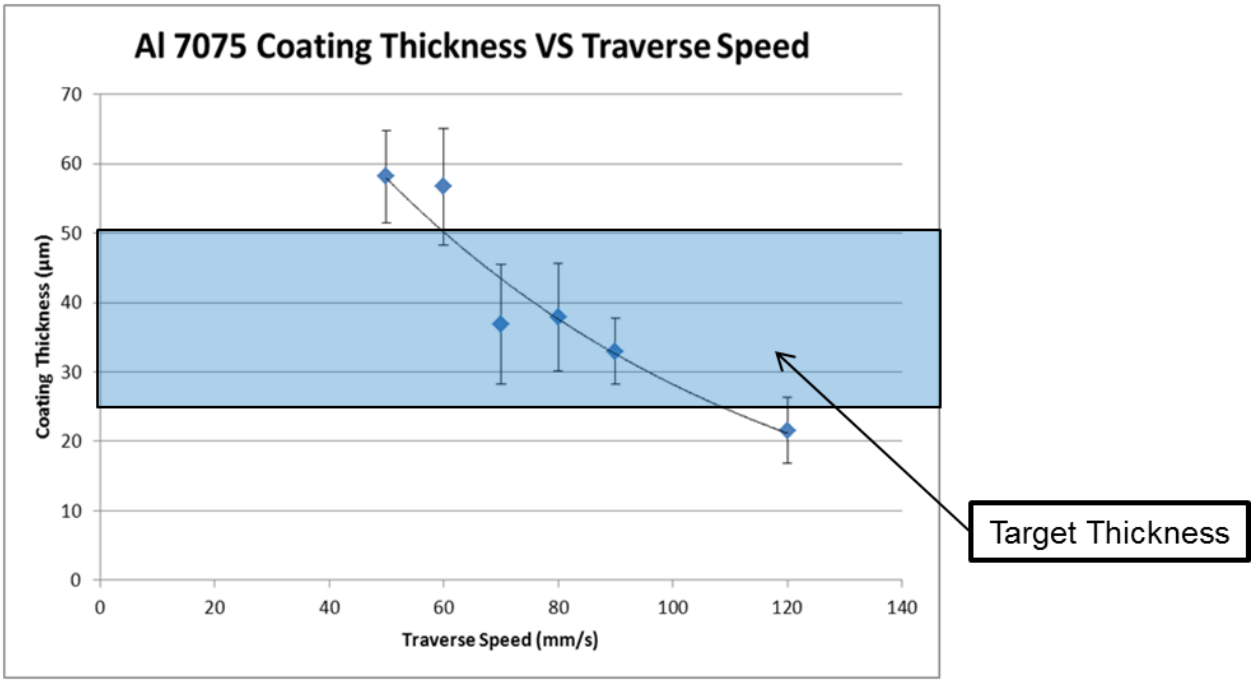

Figure 5.20: Aluminum 7075 coating thickness based on traverse velocity (n=10).

5.5.1 Summary of the CGDS Parameters for the Deposition of Aluminum 7075 Powder on 4130 Steel Substrates

The gas temperature, pressure, and traverse velocity were investigated in this section. These parameters aimed to deposit a dense coating in the most efficient way possible while staying in the limitations of the equipment. The remaining parameters were chosen based on knowledge accumulated within this study. A full set of parameters that will be used to deposited aluminum 7075 powder on 4130 steel, for the characterization of repairs, can be found in Table 5.30. A cross-section of the coating can be found in Figure 5.21.

Table 5.30: Summary of qualified CGDS parameters for the deposition of Al 7075 powder on 4130 steel substrates.

Parameter Selection	Value
Gas Pressure	250 psi (1.72 MPa)
Gas Temperature	500 °C
Gas Nature	Nitrogen
Step Size	1 mm
Traverse Velocity	60mm/s to110 mm/s
Feed Rate	3 RPM
Feed Wheel Type	120 large hole
Powder Feeder Gas Flow Rate	20 SCFH
Powder Feeder Gas Nature	Nitrogen
Standoff Distance	15 mm
Nozzle Type	SS Nozzle
Orifice Diameter	2 mm

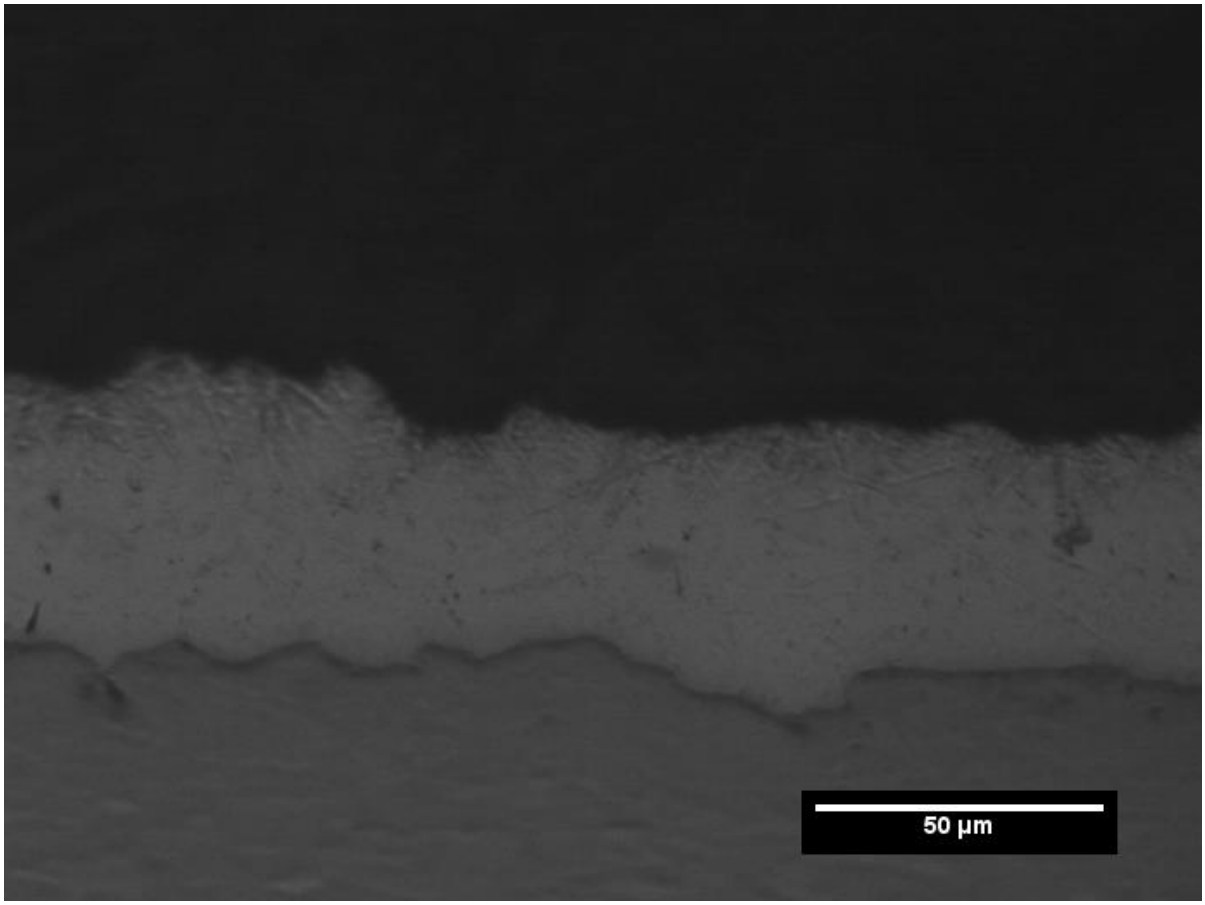

Figure 5.21: Cross-section of aluminum 7075 coating deposited on 4130 steel.

5.6 Coating development of Aluminum 5083 Powder on Aluminum on 4130 Steel

It was found that aluminum 5083 had very similar spraying performance to aluminum 7075, so the parameters found for aluminum 7075 on 4130 steel will act as a starting point for this research. In order to determine which gas temperatures and pressures are suitable for this application, the parameters found in Table 5.31 were held constant, while the test plan (Figure 5.22) was executed. All substrates were prepared using the parameters found in Table 5.1.

Table 5.31: CGDS parameters held constant for the initial coating development test matrix for Al 5083 powder on 4130 steel substrates.

CGDS Parameter	Value
Standoff Distance	15 mm
Nozzle Type	Standard SS Nozzle
Orifice Diameter	2 mm
Powder Feeder Wheel	120 Large Hole
Powder Feeder Gas Rate	20 SCFH
Powder Feed Rate	3 RPM

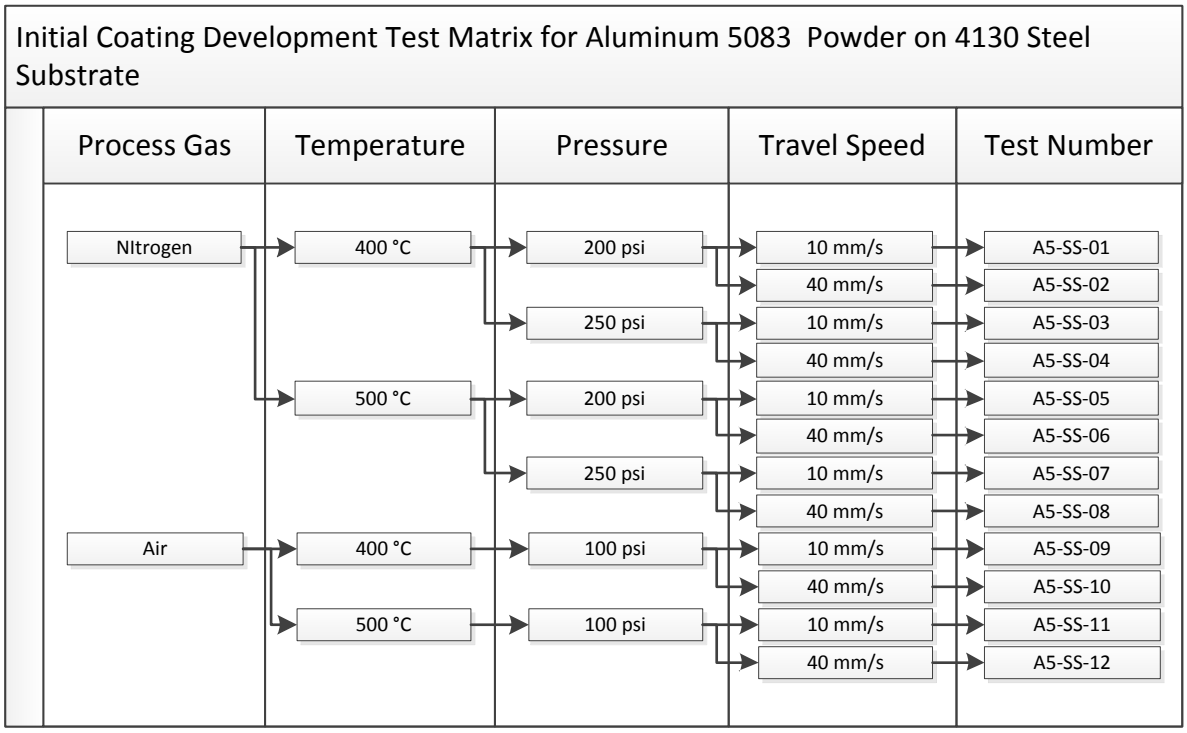

Figure 5.22: Initial coating development test matrix for aluminum 5083 powder on 4130 steel substrates.

This test also aims to identify the effect of traverse velocity on the resulting coatings. A high and low for each of the variable categories was chosen based on recommended ranges from the manufacturer and accumulated knowledge. A step size of 1 mm was chosen the 10 mm/s traverse velocity while a 4 mm step was chosen for the 40 mm/s traverse velocities. This was done in order to ensure the same deposition time for all coatings. This test matrix also includes

trials to be completed using air as a process gas at the maximum available pressure of approximately 100 psi. The results of these tests can be found in Table 5.32.

Table 5.32: Results for initial coating development test matrix for aluminum 5083 powder on 4130 steel substrates.

Test Number	Deposits (Y/N)	Porosity (%)	Coating Thickness (μm)
A5-SS-01	N	NA	NA
A5-SS-02	N	NA	NA
A5-SS-03	N	NA	NA
A5-SS-04	N	NA	NA
A5-SS-05	Y	<1	134.8±21.2
A5-SS-06	Y	<1	127.4±29.2
A5-SS-07	Y	<1	231.6±31.0
A5-SS-08	Y	<1	239.4±66.2
A5-SS-09	N	NA	NA
A5-SS-10	N	NA	NA
A5-SS-11	N	NA	NA
A5-SS-12	N	NA	NA

Analogously to aluminum 7075 powder, the aluminum 5083 powder required a gas temperature of 500°C for the particles to reach the critical velocity and higher gas pressure lead to a thicker coatings. No deposition was present when the process used low pressure air as a carrier gas.

Depositing a coating of proper thickness is a crucial component of this project. In order to determine the velocity required to reach this value, a series of trials at different velocities were performed while holding the remaining parameters constant (Table 5.33). The thickness of the coatings can be seen in Figure 5.23. A traverse velocity of 55 mm/s to 140 mm/s would result in a coating in the desired 25 to 50 μm range.

Table 5.33: CGDS parameters held constant for determining traverse velocity for aluminum 5083 powder for the restoration of damaged pure aluminum IVD coatings.

Parameter Selection	Value
Gas Pressure	250 psi (1.72 MPa)
Gas Temperature	500 °C
Gas Nature	Nitrogen
Step Size	1 mm
Feed Rate	3 RPM
Feed Wheel Type	120 large hole
Powder Feeder Gas Flow Rate	20 SCFH
Powder Feeder Gas Nature	Nitrogen
Standoff Distance	15 mm
Nozzle Type	SS Nozzle
Orifice Diameter	2 mm

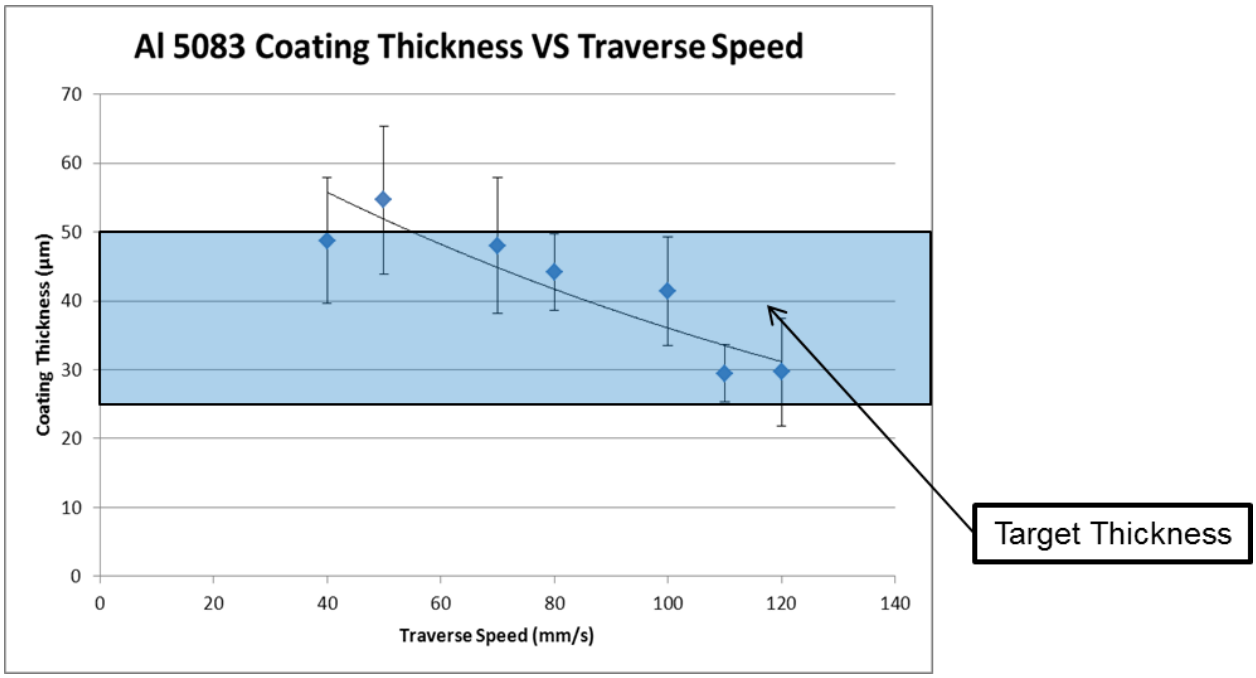

Figure 5.23: Aluminum 5083 coating thickness based on traverse velocity (n=10).

5.6.1 Summary of the CGDS Parameters for the Deposition of Aluminum 5083 Powder on 4130 Steel Substrates

The gas temperature, pressure, and traverse velocity were investigated in this section. These parameters aimed to deposit a dense coating in the most efficient way possible while staying in the limitations of the equipment. The remaining parameters were chosen based on knowledge accumulated within this study. A full set of parameters that will be used to deposited aluminum 5083 powder on 4130 steel, for the characterization of repairs, can be found in Table 5.34. A cross section of the coating can be found in Figure 5.24.

Table 5.34: Summary of qualified CGDS parameters for the deposition of Al 5083 powder on 4130 steel substrates.

Parameter Selection	Value
Gas Pressure	250 psi (1.72 MPa)
Gas Temperature	500 °C
Gas Nature	Nitrogen
Step Size	1 mm
Traverse Velocity	55 mm/s to140 mm/s
Feed Rate	3 RPM
Feed Wheel Type	120 large hole
Powder Feeder Gas Flow Rate	20 SCFH
Powder Feeder Gas Nature	Nitrogen
Standoff Distance	15 mm
Nozzle Type	SS Nozzle
Orifice Diameter	2 mm (78.7 thou)

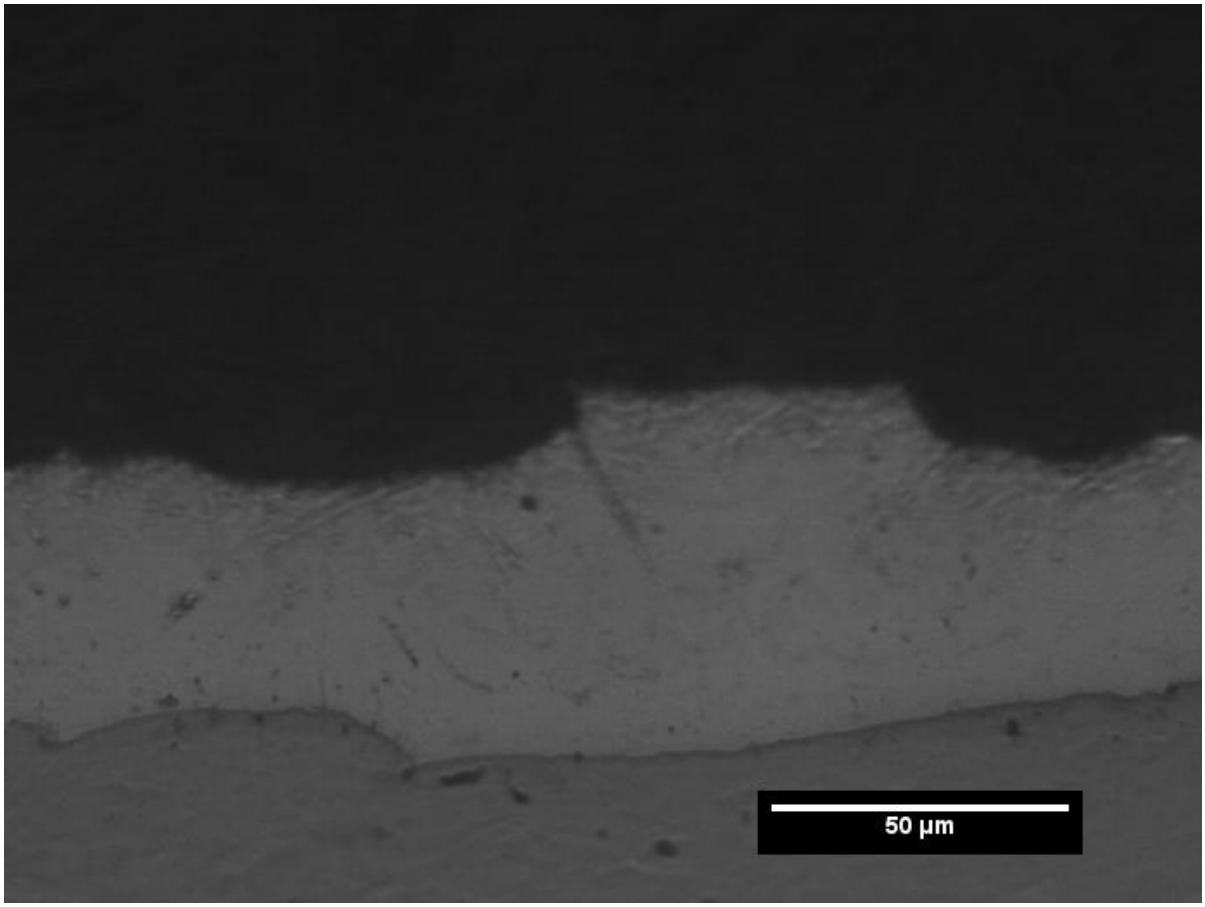

Figure 5.24: Cross section of aluminum 5083 coating deposited on 4130 steel.

6 CHARACTERIZATION OF REPAIRS

This chapter provides the results and discussion of the full characterization of the repairs. The chapter is separated into two sections, one for the restoration of damaged aluminum alloy components and one for the restoration of damaged aluminum IVD. The focus of each of these sections is to evaluate the repaired components under the same scrutiny as the original components using tests standard in the aerospace industry.

6.1 Characterization of CGDS Restorations of Damaged Aluminum Alloy Components

In order determine the suitability of CGDS for the reparation of aluminum alloy aerospace components; the repairs must undergo the same scrutiny as the aerospace components themselves. Adhesion strength, the quality of the anodized layer, corrosion properties, and adhesion properties were examined. The parameters used to deposit these coatings were determined in Chapter 5 and can be found in summary in Table 6.1.

Table 6.1: Summary of CGDS parameters used for the Restoration of Damaged Aluminum Alloy components.

Parameter Selection	Aluminum 7075	Pure Aluminum
Gas Pressure	200 psi (1.38 MPa)	250 psi (1.72 MPa)
Gas Temperature	250 °C	350°C
Gas Nature	Helium	Nitrogen
Traverse Speed	25 mm/s	10 mm/s
Step Size	1 mm	1 mm
Feed Rate	6 RPM	14 RPM
Feed Wheel Type	120 large hole	320 Small hole
Powder Feeder Gas Flow Rate	20 SCFH	25 SCFH
Powder Feeder Gas Nature	Helium	Nitrogen
Standoff Distance	15 mm	15 mm
Nozzle Type	SS Nozzle	Polymer Nozzle
Orifice Diameter	2 mm	2 mm

All sample surfaces are prepared through grit blasting. Issues with the consistency of adhesion results were found before ensuring that surfaces are prepared in the exact same manner every time with brand new blasting medium. The parameters for grit blasting are given in Table 6.2. After grit blasting, the substrate was cleaned using acetone and compressed air.

Table 6.2: Summary of grit blasting parameters used for the Restoration of damaged aluminum alloy components.

Parameter	Metric
Pressure	344 kPa (50 psi)
Gas Nature	Compressed Air
Grit Nature	Black Alumina
Size	80 Grit
Angle	45°

6.1.1 Anodization Behavior and Wear Resistance

In order to test the quality of the hardcoat anodized layer, panels were deposited with pure aluminum and aluminum 7075 powders, hardcoat anodized, and tested in accordance with ASTM D4060-11 [63]. For these trials the substrate is aluminum 7075-T6 as only the anodized layer is being tested. Two pure aluminum and one aluminum 7075 coatings were tested.

The as-deposited pure aluminum coatings can be seen in Figure 6.1. A substantial amount of pitting can be seen on the coating surface compared to the aluminum 7075 coatings (Figure 6.2). Both coatings were machined so that the surfaces were parallel and smooth (Figure 6.3 and Figure 6.4). The size and consistency of the chips (Figure 6.5) show that the coatings machined in a similar manner as bulk material.

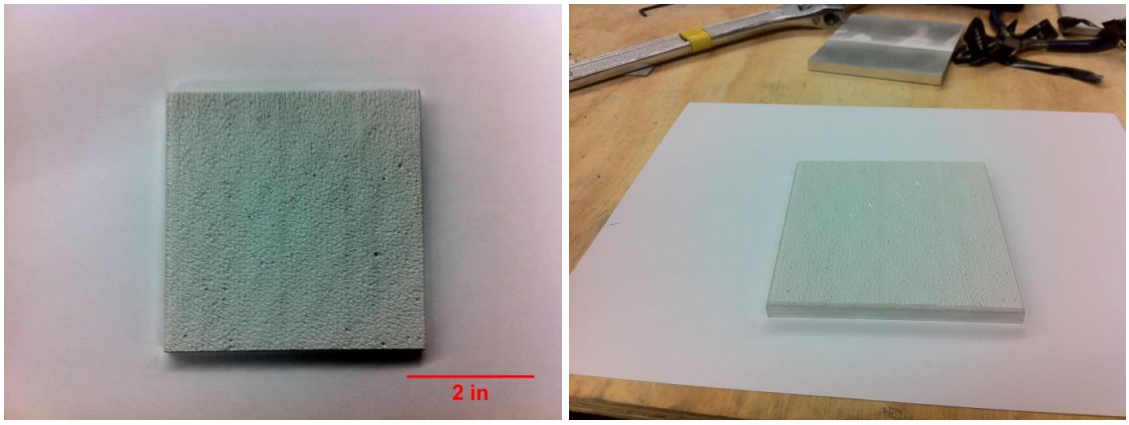

Figure 6.1: As deposited CGDS pure aluminum Taber abrasion panel.

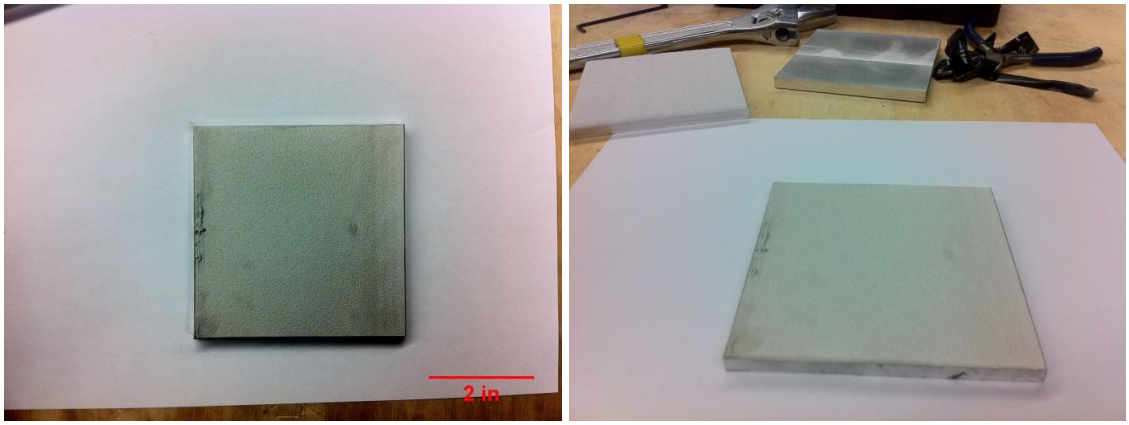

Figure 6.2: As deposited CGDS aluminum 7075 Taber abrasion panel.

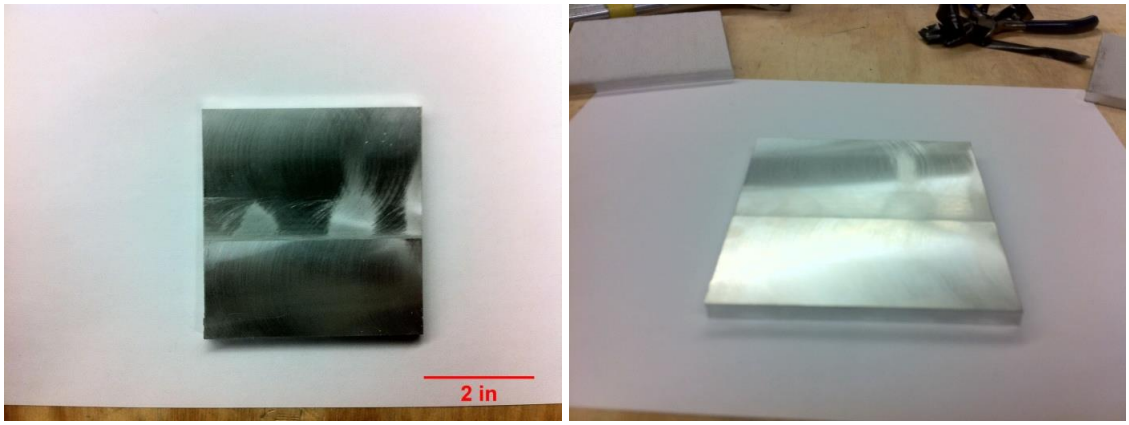

Figure 6.3: Machined CGDS pure aluminum Taber abrasion panel.

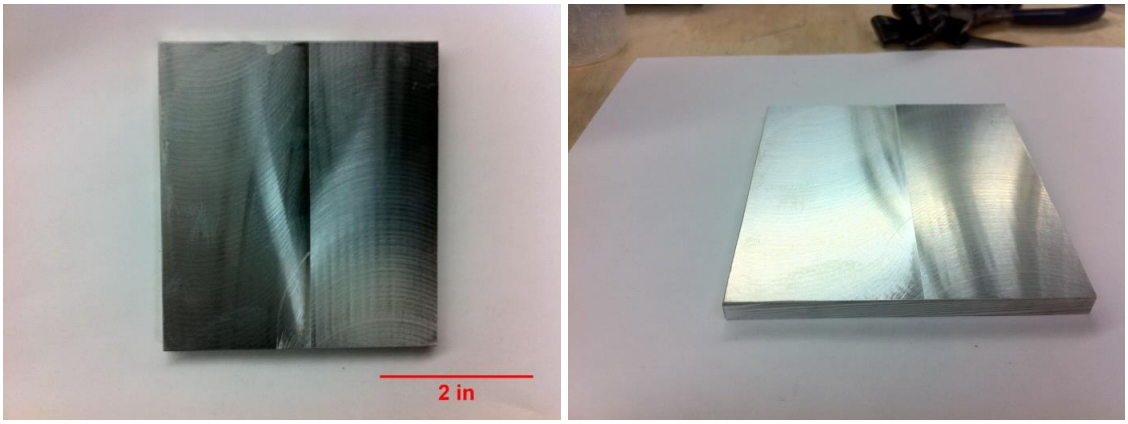

Figure 6.4: Machined CGDS aluminum 7075 Taber abrasion panel.

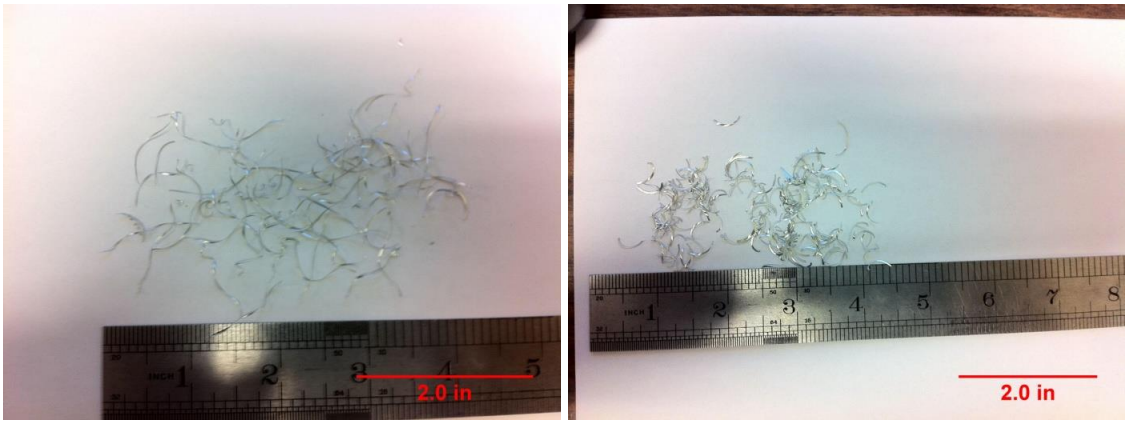

Figure 6.5: Pure aluminum chips (left) and aluminum 7075 (right).

A Type III Class 1 hardcoat anodization process was performed on the coatings, This process resulted in an anodized layer on both the CGDS coated side and the substrate side of the test coupon (see Figure 6.6). The abrasion testing was done on the anodized layer on the CGDS coating. The results from the initial round of testing are found Table 6.3. The pure aluminum coatings fared better than the Al 7075 samples, losing 70 (1100-1) and 62 (1100-2) mg in 11,000 cycles compared to 426 mg. For the pure aluminum coatings, the wear pattern appears to be even for both samples (Figure 6.7).

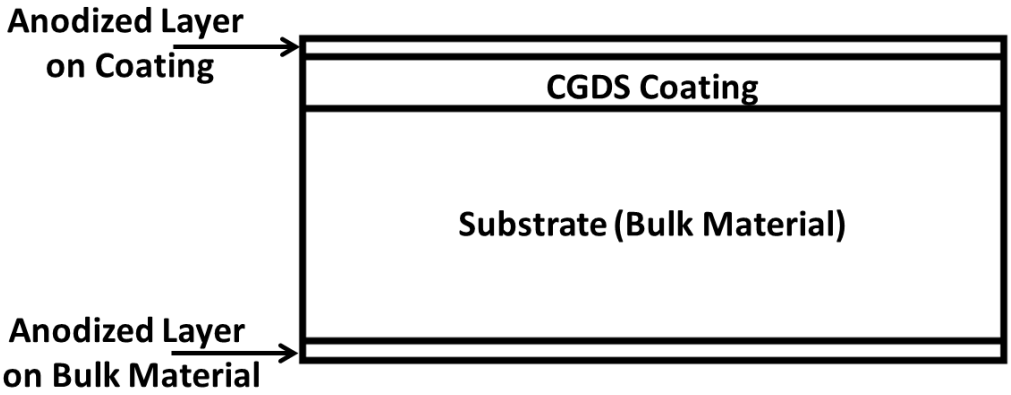

Figure 6.6: Schematic showing arrangement of layers in anodized Taber abrasion samples.

Table 6.3: Taber wear results from initial round of testing (set 1).

Coating Material	Wear (mg)	Cycles
Pure Aluminum	70	11000
Pure Aluminum	62	11000
Aluminum 7075	426	11000

Figure 6.7: Pure aluminum Taber abrasion panels after testing.

Figure 6.8 shows the cross section of the undamaged area of the pure aluminum coatings. Both 1100-1 (left) and 1100-2 (right) show a uniform oxide layer of approximately 45 microns. This consistency between both samples (at multiple points) shows that the hardcoat anodization was

successful. After wear (Figure 6.9), the oxide layer was shown to have been reduced by about 10 microns.

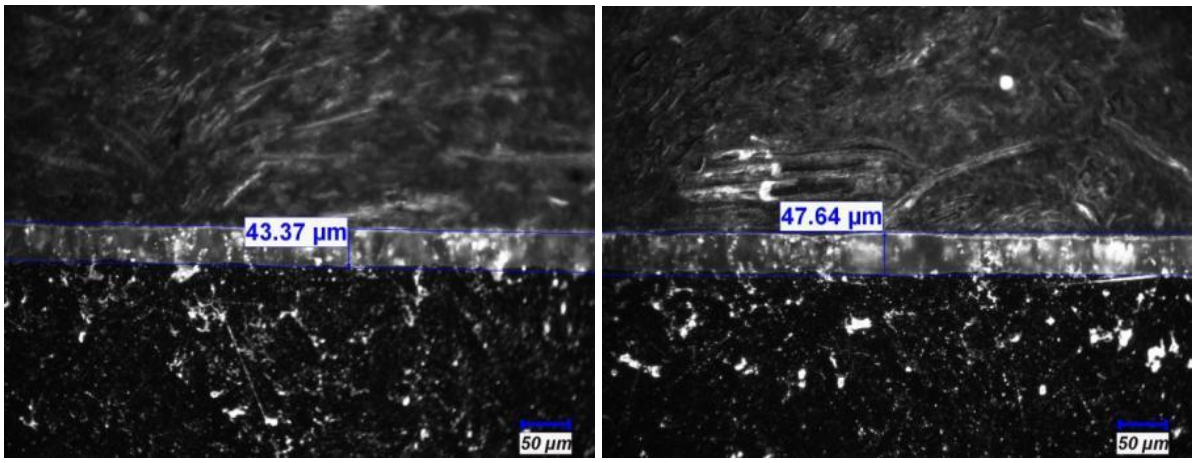

Figure 6.8: Cross-section of undamaged pure aluminum coatings (left: Sample 1100-1. right: Sample 1100-2).

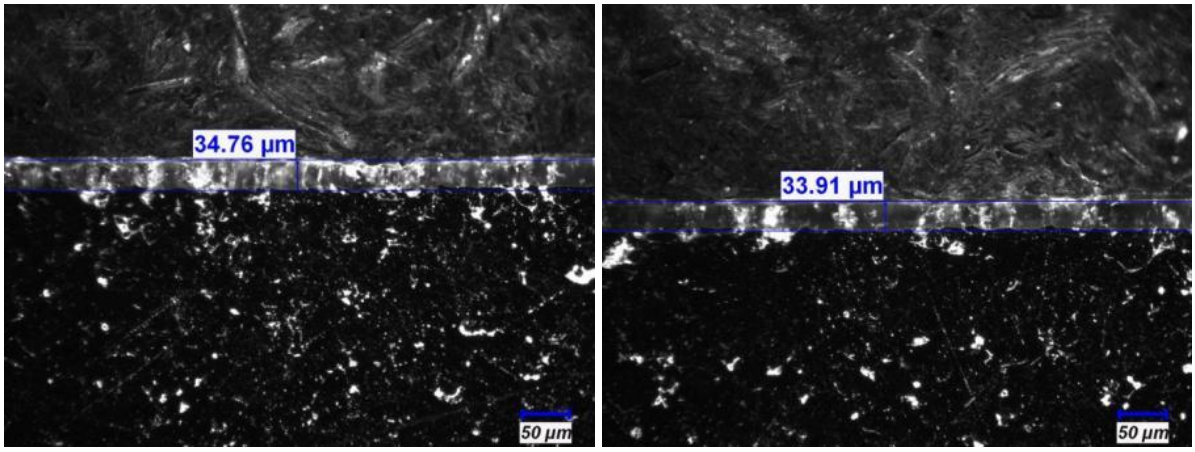

Figure 6.9: Section of worn pure aluminum coatings (left: Sample 1100-1. Right: Sample 1100-2)

The mass loss of the aluminum 7075 coatings during the Taber abrasion test were an order of magnitude higher than that of the pure aluminum coatings. A visual investigation of the Taber panel (Figure 6.10) shows that the wear pattern is uneven. It is clear that the coating on the A side has performed significantly worse than the coating on the B side.

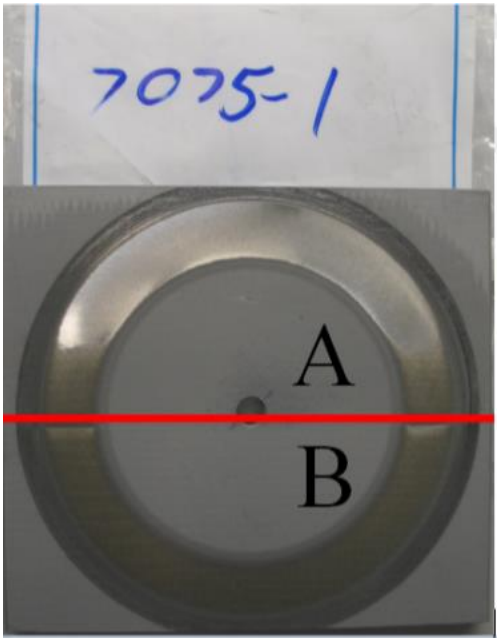

Figure 6.10: Aluminum 7075 Taber Abrasion Panel after Testing

Figure 6.11 shows cross sections of coatings that were outside of the wear area of the Taber abrasion test (undamaged). The coating on the left is from the area that visibly endured less wear during the wear test (side B) and the coating on the right is from the area that endured more wear (side A). These optical, dark field images show the oxide layer that was created during the hardcoat anodization process. The oxide layer was found to be fairly consistent throughout the sample, with a thickness of approximately 50 microns (2 mil) for side B and 60 microns for side A.

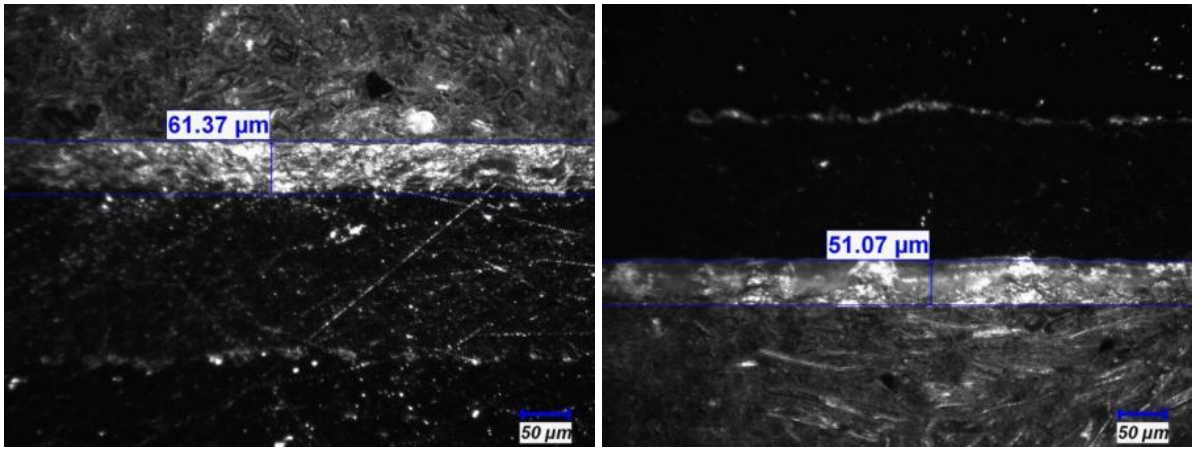

Figure 6.11: Cross Section of Undamaged Coatings, Section A (left) and Section B (right)

The cross-section shown in Figure 6.12 shows the damage caused by the wear test. The damage in side B did not penetrate through the oxide layer. This oxide layer had been worn to approximately 16 microns at its thinnest point. The side A coating, on the other hand, shows damage that has penetrated the oxide layer, the fully dense aluminum 7075 coating, and into the substrate. This result is unexpected, since initially the oxide layer in side A was of the same thickness as side B. It leads to the suspicion that either the quality of the oxide layer was somehow compromised in side A, or the Taber abrasion apparatus was not performing as desired. It seems plausible that the equipment was somehow exerting more force on side A, resulting in significantly increased wear.

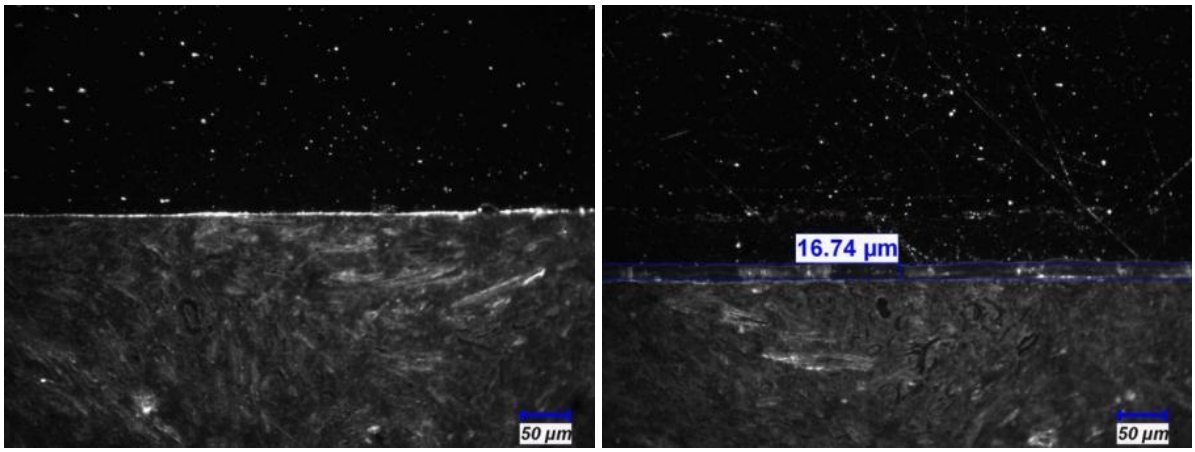

Figure 6.12: Cross Section of Damaged Coating from Section A (left) and Section B (right)

The pure aluminum coatings did not meet the required mass loss specified by industry, but could potentially benefit from lapping (polishing) prior to testing. The aluminum 7075 coating test results were suspected to be invalid due to malfunctioning testing equipment. For these reasons the tests were repeated. This time making sure to lap the surfaces and ensuring the integrity of the Taber testing apparatus. This test was performed using two aluminum 7075 and two pure aluminum coatings. The mass loss values can be found in Table 6.4. These values are drastically different than the initial round of Taber abrasion testing.

Table 6.4: Mass loss during Taber abrasion testing (set 2).

Coating Material	Wear (mg)	Cycles
Pure Aluminum	1004	10000
Pure Aluminum	550	6500
Aluminum 7075	100	11000
Aluminum 7075	90	11000

The results for pure aluminum in Set 1 were close to the desired mass loss results of 40mg in 10000 cycles. It was believed that by polishing (lapping) the anodized surface before testing that the desired mass loss level could be reached. In contrast to the expectation, a substantial increase in mass lost was seen in the Set 2 samples. A comparison of normalized results can be seen in Figure 6.13.

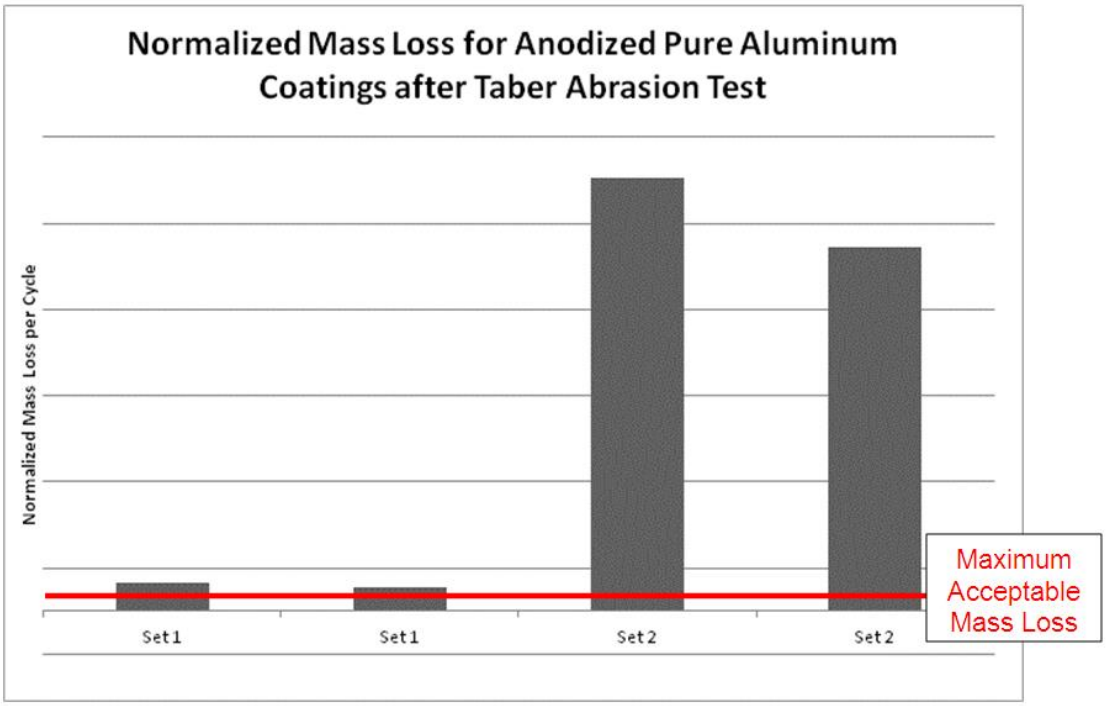

Figure 6.13: Normalized mass loss for anodized pure aluminum coatings after Taber abrasion testing.

The coatings from Set 1 had a uniform layer of alumina on the top of the coating which can be seen in Figure 6.14[right]. This is comparable to anodized coatings found on bulk material which can be found in Figure 6.14[left]. Coatings from Set 2 are shown to have excessive porosity, and very uneven oxide growth (Figure 6.15). It is clear that the abrasive wheel passed easily though

the oxide layer and into the coating (Figure 6.16). This inconsistency in coating quality while maintain operating parameters was not expected.

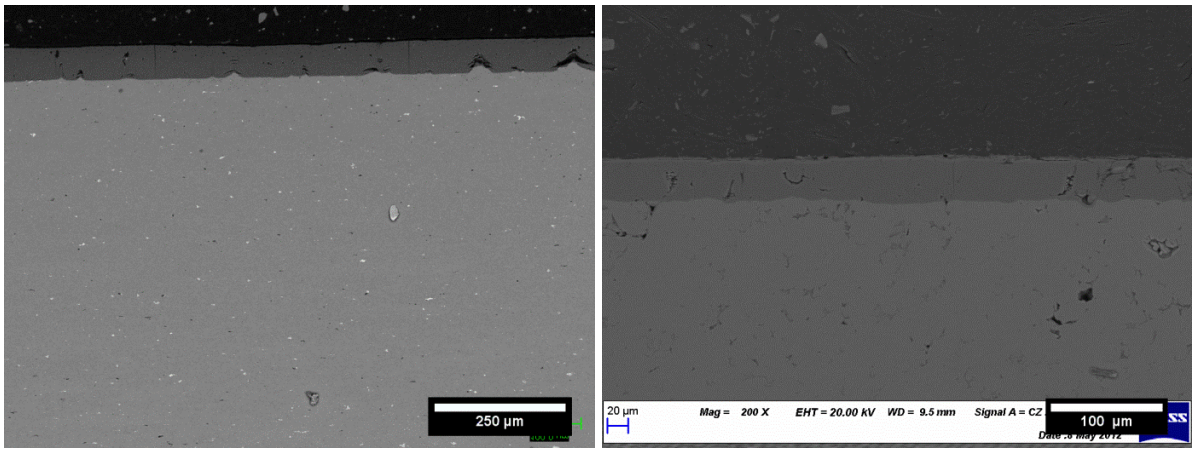

Figure 6.14: Anodized layer on bulk aluminum 7075 (left), anodized layer on pure aluminum coating from the first set of Taber abrasion tests[Set 1] (right).

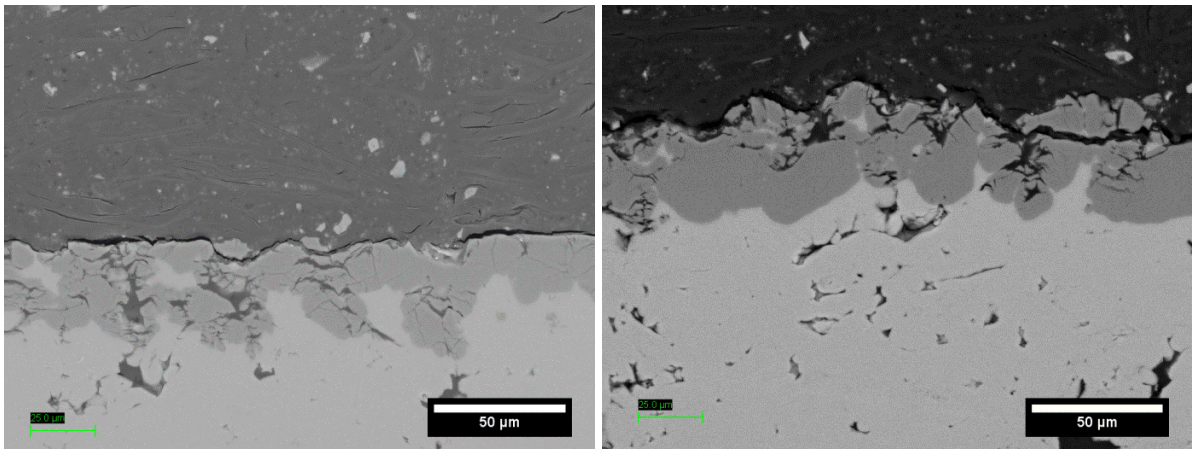

Figure 6.15: Set 2 - Pure aluminum coatings: SEM images of non-worn coatings showing poor quality alumina layer.

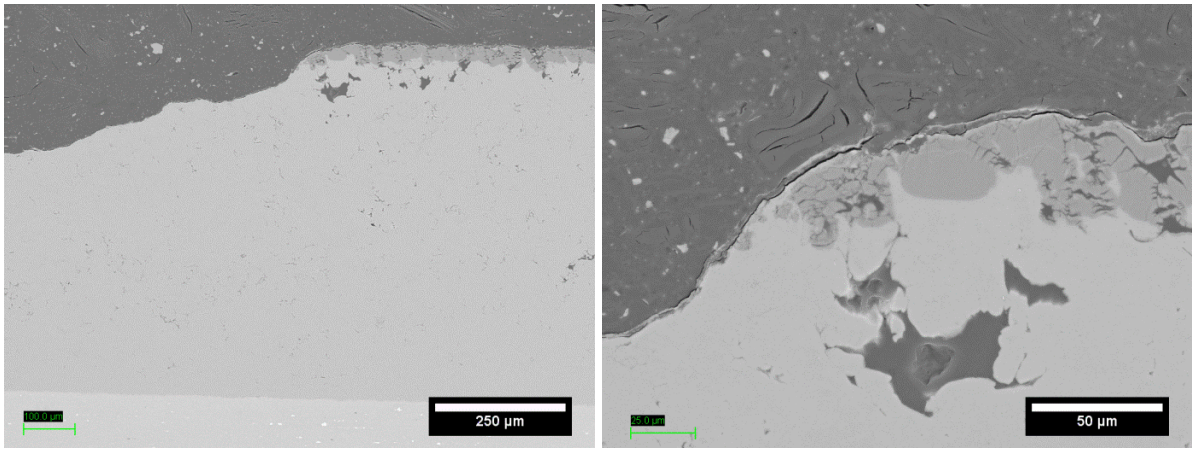

Figure 6.16: Set 2 - Pure aluminum coatings: SEM image of non-worn and worn coating (left), zoom of intersection between worn and non-worn (right).

In order to investigate further, hardness testing of the alumina layer on the coating, the coating, the substrates, and the alumina layer on the substrates were done. The hardness results for pure aluminum coatings (Figure 6.17) show that the hardness of the alumina on the coatings is comparable (or higher) to that of the alumina layer formed on the bulk material. This shows that the problem is not related to the quality of the coating alumina itself, but is related to the quality of the CGDS coating itself (i.e. porosity, cohesion, and metallurgical bonding). An increase in substrate alumina layer hardness was seen in Set 2, the reason for this is not known, as the components were procured from the same supplier and anodized by the same facility.

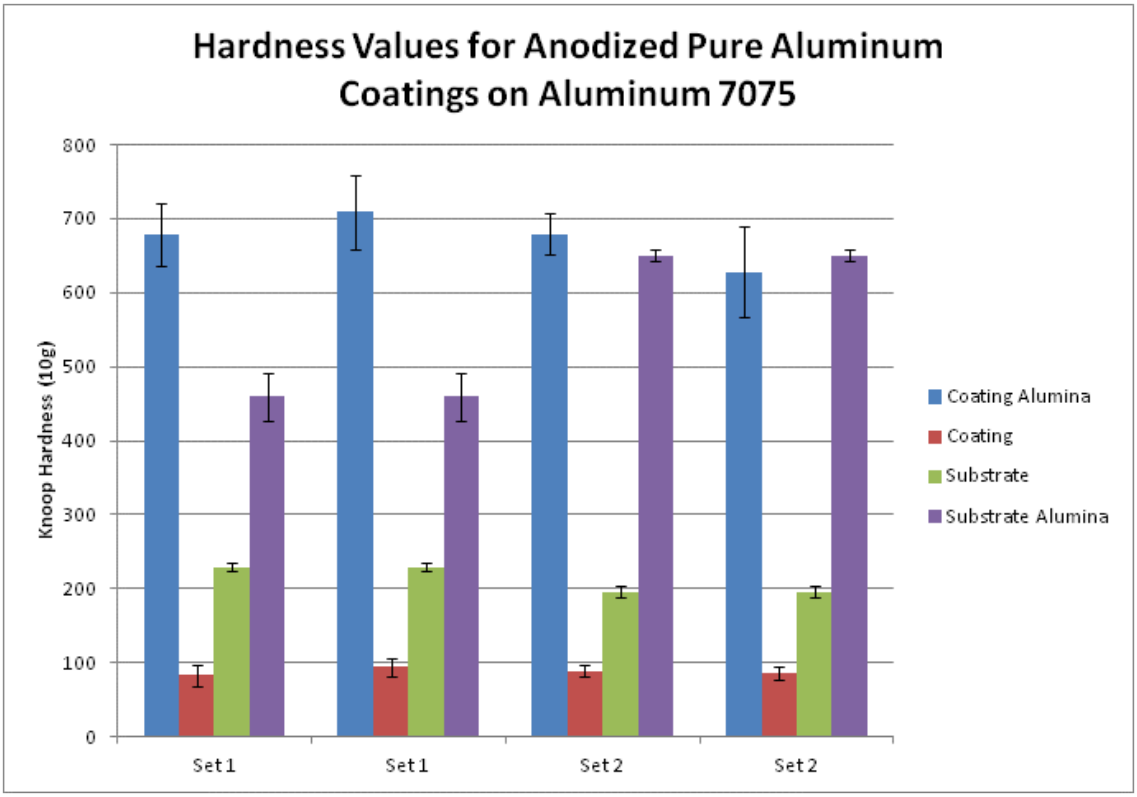

Figure 6.17: Knoop hardness values for anodized pure aluminum coatings on aluminum 7075 substrates (n=10).

The mass loss results for aluminum 7075 coatings from the first set (Set 1) of Taber abrasion testing were much higher than the maximum acceptable mass loss of 40 mg in 10000 cycles. Two additional Taber abrasion panels were tested (data presented in Table 6.4). The results of these trials were much closer to the maximum accepted mass loss (see Figure 6.18). Imaging shows that there are pores inside the alumina layer, as well as horizontal cracks at the surface (Figure 6.19[a]). These cracks are not seen in the worn samples (Figure 6.19[b]), indicating that the coatings are fracturing along these cracks and material is being removed. Additional metallurgical bonding could potentially decrease this phenomenon.

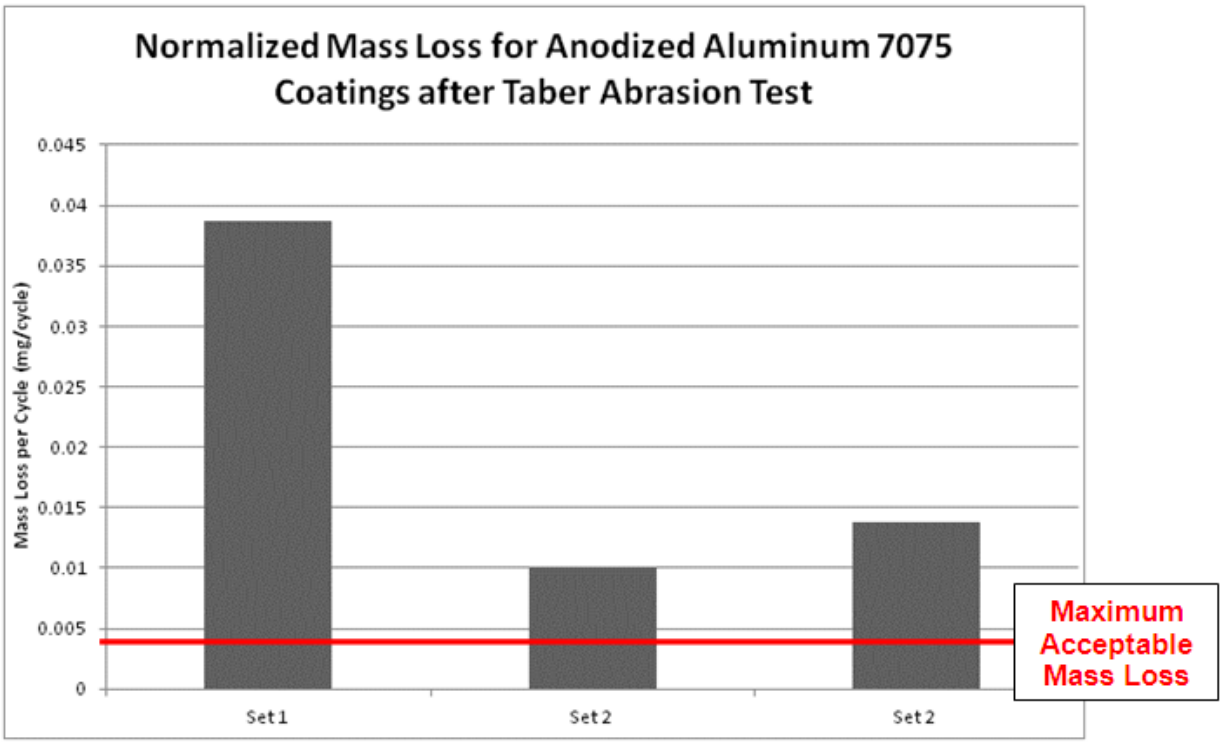

Figure 6.18: Normalized mass loss for anodized aluminum 7075 coatings after Taber abrasion testing.

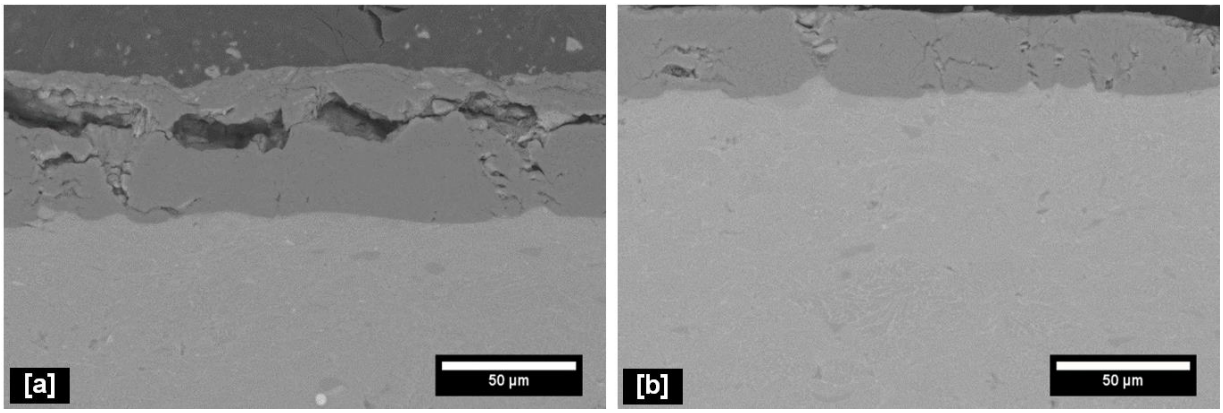

Figure 6.19: Set 2 - Aluminum 7075 coating: SEM image of as-anodized alumina layer with horizontal cracking [a], SEM image of alumina layer after Taber test [b].

The hardness results show that the hardness of the alumina layer on the CGDS coating is comparable to that of alumina layer on the bulk material (Figure 6.20). This demonstrates that the problem is, in all likelihood, not related to the quality of the alumina itself, but rather is

related to the as-sprayed aluminum 7075 coating quality (i.e. porosity, cohesion, and metallurgical bonding).

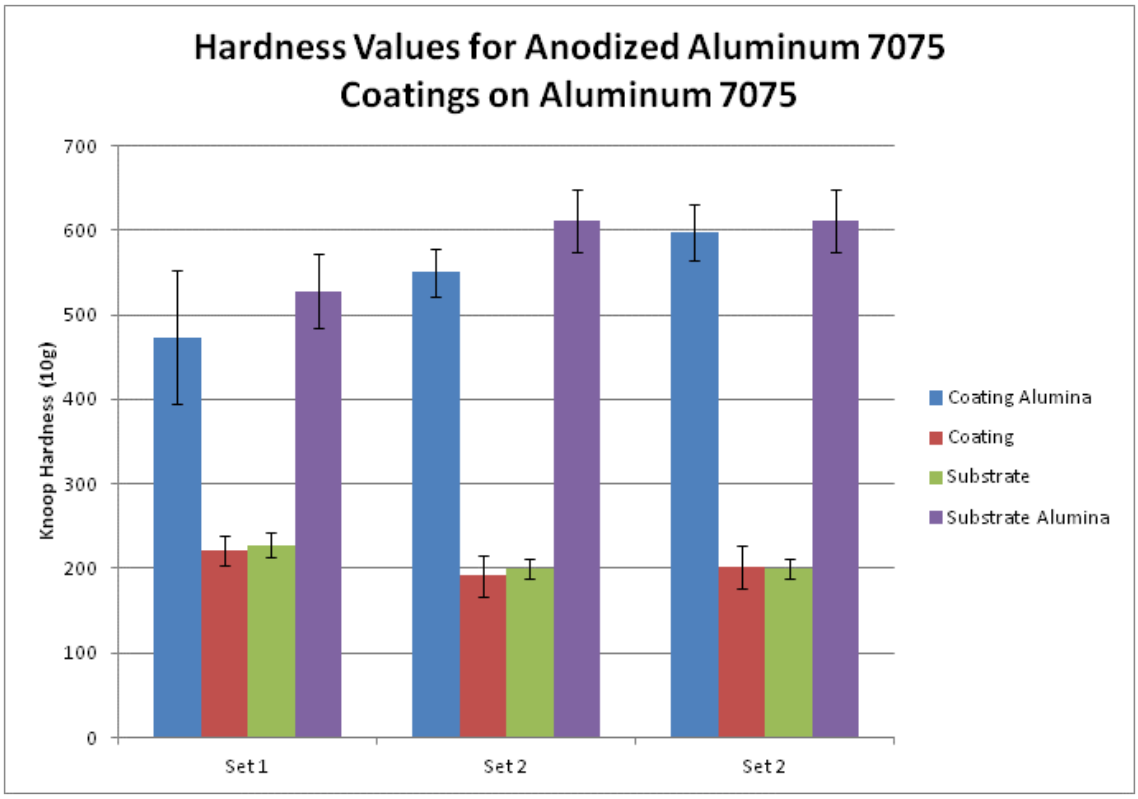

Figure 6.20: Knoop hardness values for anodized aluminum 7075 coatings on aluminum 7075 substrates (n=10).

At the current time, the reasoning for the poor performance of the anodized layers under the Taber abrasion testing is not completely understood. Issues with the consistency of the system and quality control of the powder may have resulted in the flaws in the second set of pure aluminum coatings. It is believed that with an improvement in spray consistency and with further refinement of deposition parameters and powder selection, specifically tailored to improve the results from this test, the coatings could reach desired mass loss levels.

6.1.2 Corrosion Testing

In order to determine the corrosion resistance of the repaired areas, corrosion testing was done in accordance with ASTM B-117 [61]. Pure aluminum was used to repair aluminum 7075-T6

and aluminum 2024-T3 substrates, while aluminum 7075 was used to repair aluminum 7075-T6. Prior to corrosion testing, half of the samples were subjected to a Type II Class 1 anodization with a Type I Class 1A chromate conversion coating. The other half was coated with only a Type I Class 1A chromate conversion coating.

Substrates, with the simulated damage outline in Section 4.5.1, were repaired using the parameters listed in Table 6.1. Figure 6.21 (left) shows a milled sample prior repairing. This sample was grit blasted (using the parameters in Table 6.2). Coatings were then deposited using CGDS. The entire panel was deposited with a coating thicker than the maximum depth of the damage. Figure 6.21 (right) shows what an aluminum 7075 repair looked like before machining.

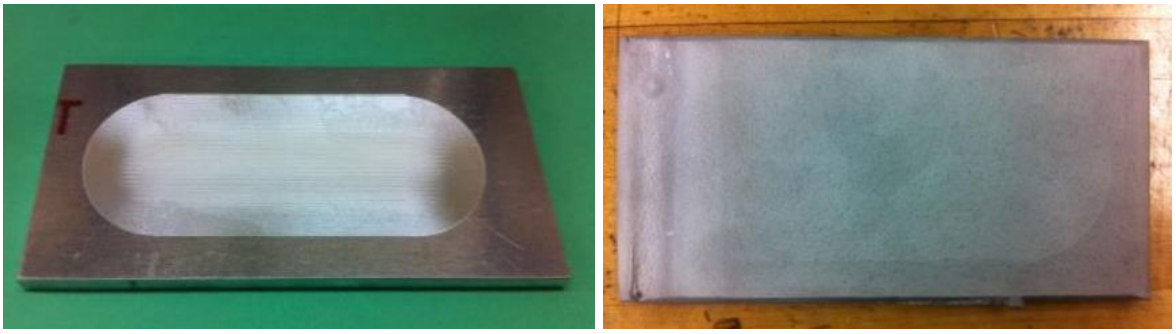

Figure 6.21 Damaged substrate (left) and aluminum 7075 repair before machining (right).

It is apparent in Figure 6.22 (left) that the aluminum 7075 repairs resulted in deformation of the substrate; deforming to approximately 1.25 mm the middle. This was caused by the residual compressive stresses that accumulated during the coating process. The machining of the repaired component to original dimensions relieved some of the stresses and the substrate became nearly flat (Figure 6.22 right). In reality, the component would be much thicker than our test plate and would resist bending. This bowing was not seen in pure aluminum repairs (Figure 6.23) due to the lower residual stress in the coating.

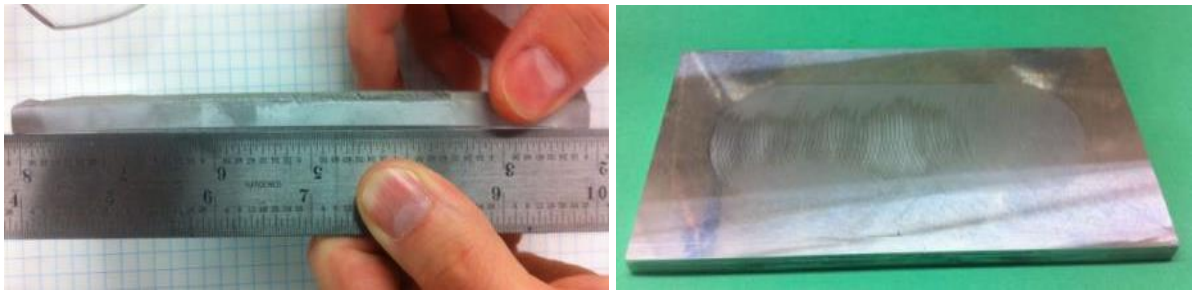

Figure 6.22: Aluminum 7075 repair before machining showing curvature due to residual stresses (left), machined aluminum 7075 repair (right).

Figure 6.23: Pure aluminum repair before machining (left) and after machining (right).

The lower level of residual stress in the pure aluminum repairs can be attributed by the lower velocity of the particles as a result of nitrogen as the carrier gas. It was also deposited at a higher temperature (350°C for pure aluminum versus 250°C for aluminum 7075). This higher temperature could allow for increased stress relief annealing taking place during the deposition process.

The progression of the corrosion tests for Type II Class 1 anodized samples with a Type I Class 1A chromate conversion coating can be seen in Figure 6.24 to Figure 6.28. The yellow colour of the substrates and the repairs seen in these images was a result of the chromate conversion coating. These coating can have different colours depending on the substrate material and morphology.

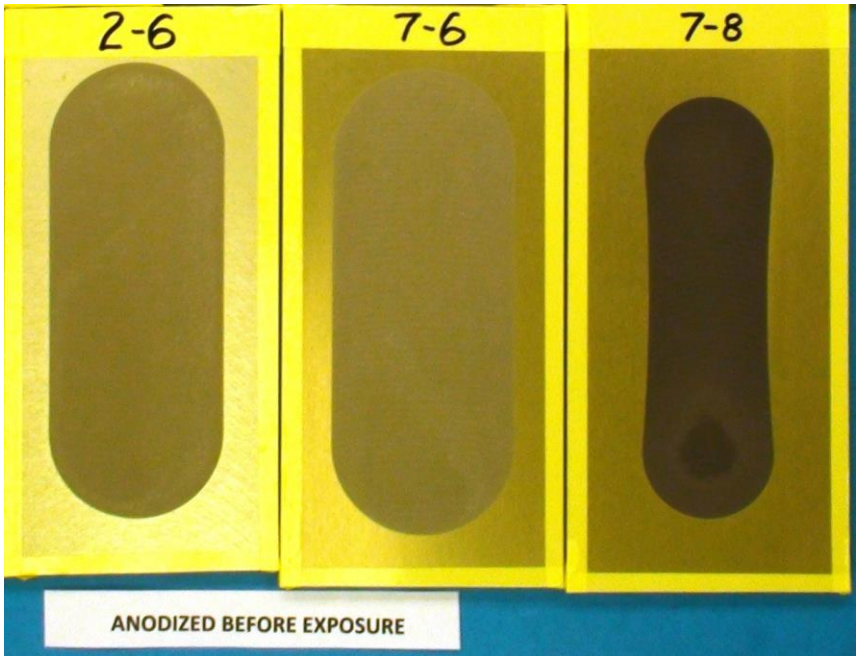

Figure 6.24: **Anodized**: Pure aluminum repair on aluminum 2024-T3 (left), pure aluminum repair on aluminum 7075-T6 (middle), aluminum 7075 repair on aluminum 7075-T6 (right) before exposure.

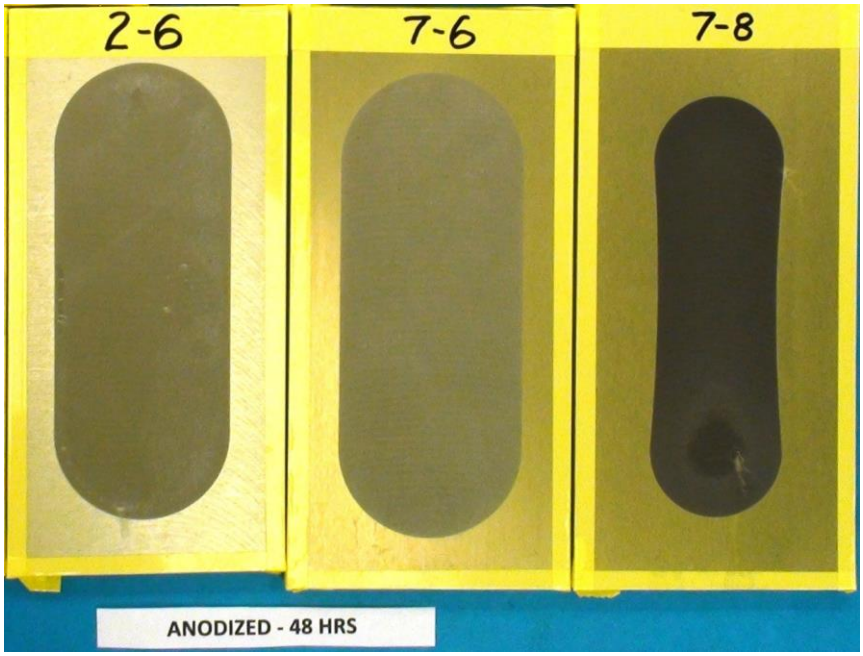

Figure 6.25: **Anodized**: Pure aluminum repair on aluminum 2024-T3 (left), pure aluminum repair on aluminum 7075-T6 (middle), aluminum 7075 repair on aluminum 7075-T6 (right) after 48 hours of exposure.

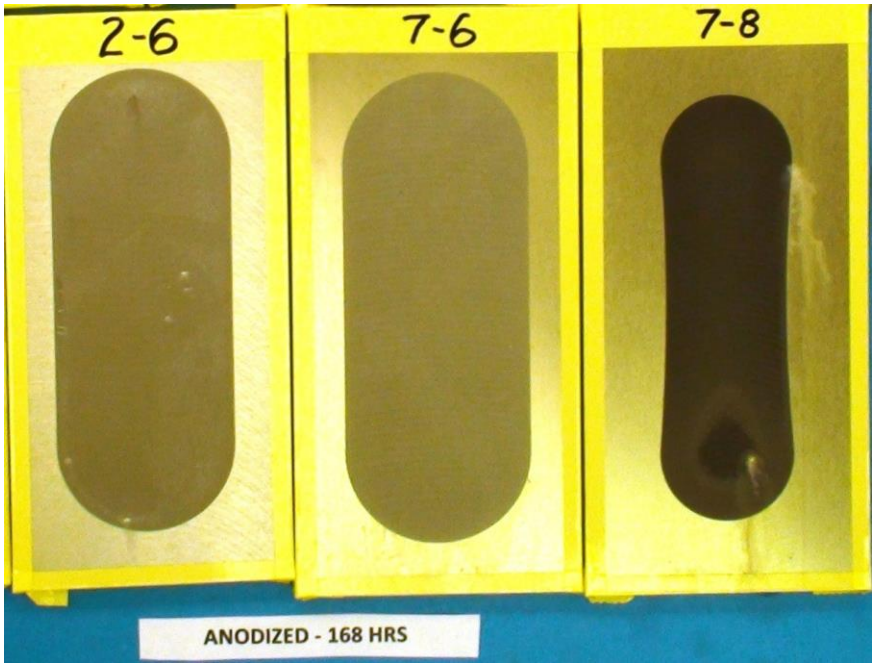

Figure 6.26: **Anodized**: Pure aluminum repair on aluminum 2024-T3 (left), pure aluminum repair on aluminum 7075-T6 (middle), aluminum 7075 repair on aluminum 7075-T6 (right) after 168 hours of exposure.

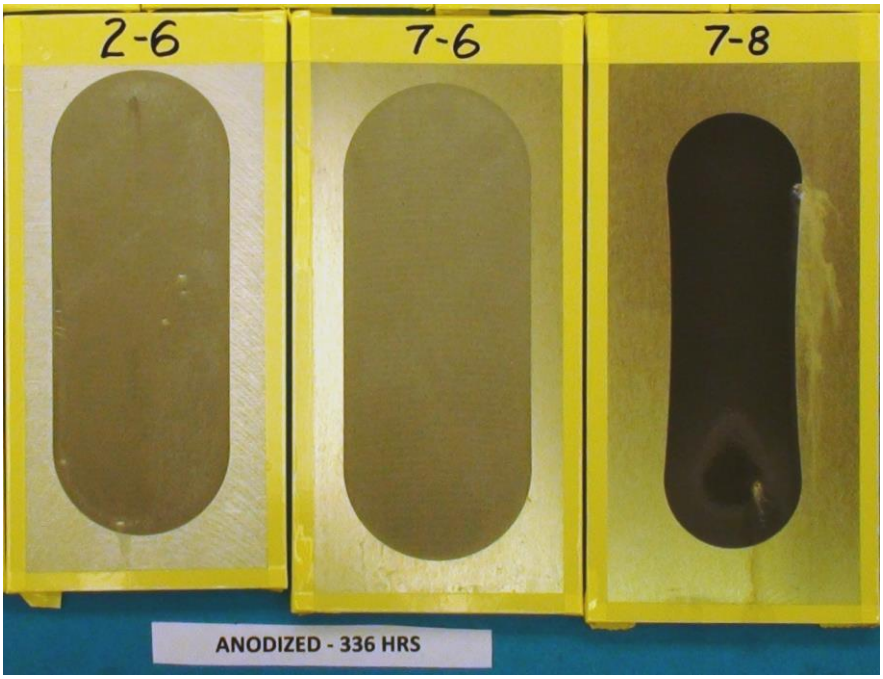

Figure 6.27: **Anodized**: Pure aluminum repair on aluminum 2024-T3 (left), pure aluminum repair on aluminum 7075-T6 (middle), aluminum 7075 repair on aluminum 7075-T6 (right) after 336 hours of exposure.

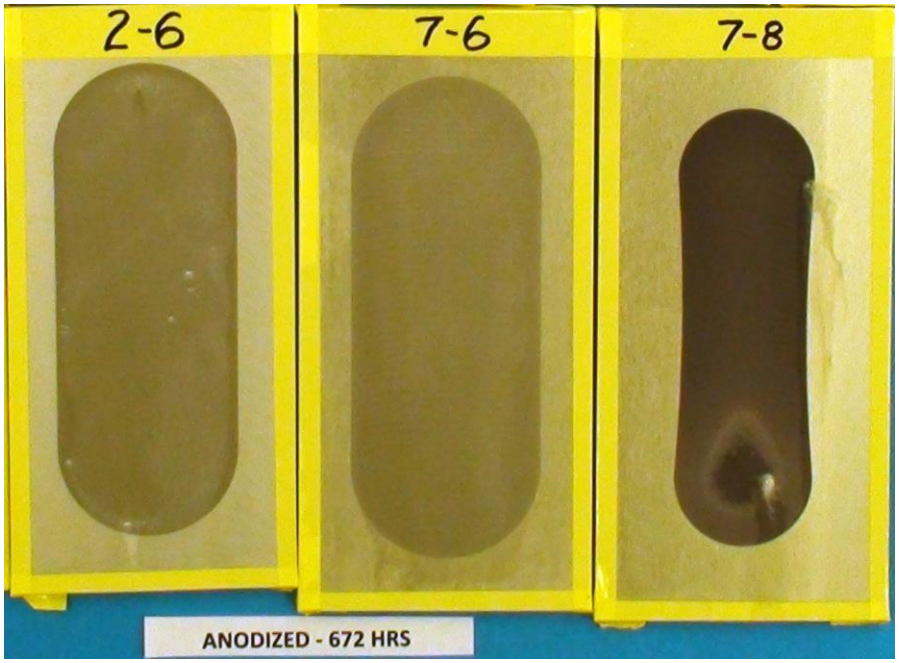

Figure 6.28: **Anodized**: Pure aluminum repair on aluminum 2024-T3 (left), pure aluminum repair on aluminum 7075-T6 (middle), aluminum 7075 repair on aluminum 7075-T6 (right) after 672 hours of exposure.

The anodized pure aluminum repairs on aluminum 2024-T3 had minimal visible corrosion products throughout the 672 hour exposure to the neutral salt fog (Figure 6.28 left), although some minor pitting was present. This localized pitting corrosion was attributed to small surface inconsistencies (pit formation during spraying, accidental removal of material during machining, etc) that create concentration points for pitting to occur.

The anodized pure aluminum repairs on aluminum 7075-T6 showed no visible corrosion products after 672 hours of exposure to the neutral salt fog (Figure 6.28 middle). The pits present in the aluminum 2024-T3 repaired samples were not seen in the pure aluminum repairs on aluminum 7075-T3. Since these two coatings were deposited using the same CGDS parameters, it is unlikely there is a fundamental difference in corrosion behavior of the coatings and supports the conclusion that the pitting seen in the previous repair was a result of the processing.

The anodized aluminum 7075 repair on aluminum 7075-T6 showed minimal corrosion products throughout the exposure with the exception of two areas of localized corrosion (visible in Figure

6.28 right). It is believed that like the pure aluminum repairs, pitting corrosion began at small surface inconsistencies that result from processing. The extent of the corrosion is a result of aluminum 7075 having inherently worse performance in corrosion (particularly pitting corrosion) than pure aluminum (see section 2.1.2). This explains the greater abundance of corrosion products surrounding the pits. It can be noted that there is a darker area present at the bottom the repaired area. This coloration was due to machining. The repaired area could not be machined evenly due to the relaxation of residual stresses during removal of excess coating material.

The progression of the corrosion tests for Samples with a Type I Class 1A Chromate Conversion Coating only can be seen in Figure 6.29 to Figure 6.33.

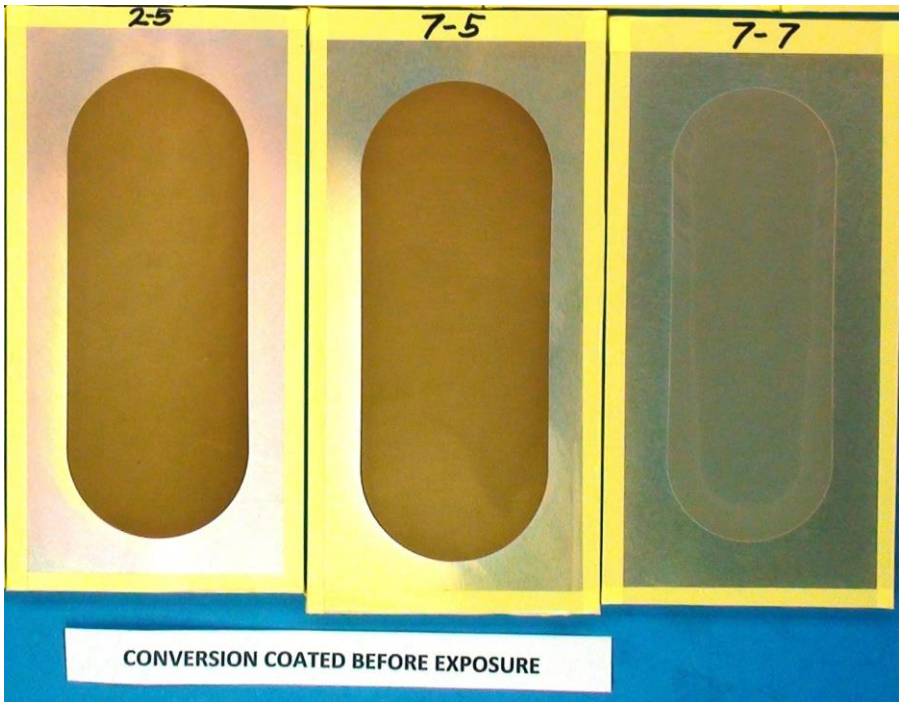

Figure 6.29: **Conversion Coated:** Pure aluminum repair on aluminum 2024-T3 (left), pure aluminum repair on aluminum 7075-T6 (middle), aluminum 7075 repair on aluminum 7075-T6 (right) before exposure.

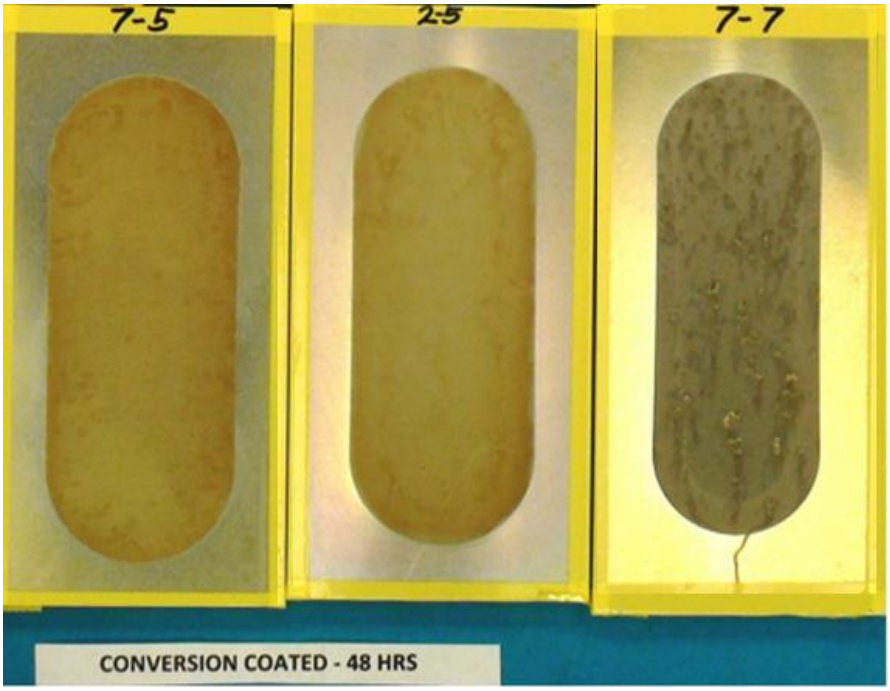

Figure 6.30: **Conversion Coated:** Pure aluminum repair on aluminum 2024-T3 (left), pure aluminum repair on aluminum 7075-T6 (middle), aluminum 7075 repair on aluminum 7075-T6 (right) after 48 hours of exposure. NOTE: The line visible at the bottom of the sample is dripping conversion coating.

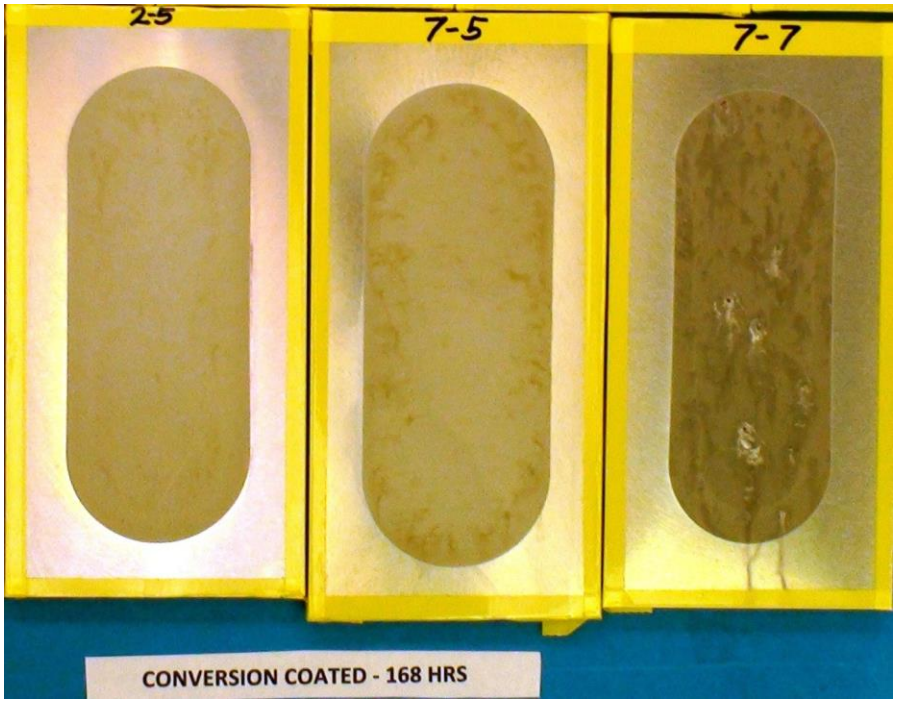

Figure 6.31: **Conversion Coated:** Pure aluminum repair on aluminum 2024-T3 (left), pure aluminum repair on aluminum 7075-T6 (middle), aluminum 7075 repair on aluminum 7075-T6 (right) after 168 hours of exposure. NOTE: The line visible at the bottom of the sample is dripping conversion coating.

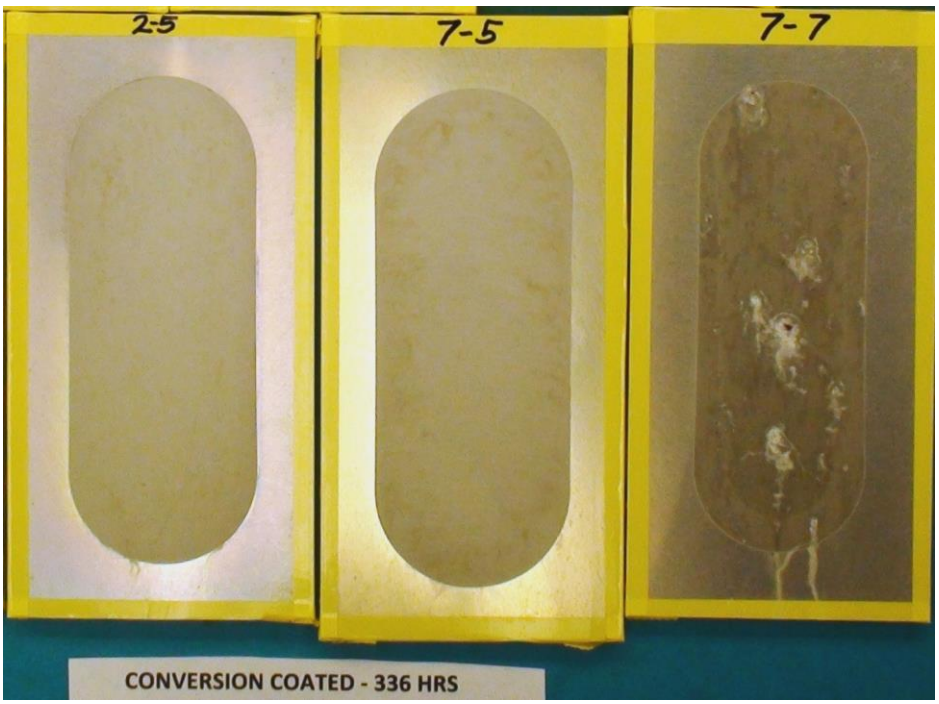

Figure 6.32: **Conversion Coated:** Pure aluminum repair on aluminum 2024-T3 (left), pure aluminum repair on aluminum 7075-T6 (middle), aluminum 7075 repair on aluminum 7075-T6 (right) after 336 hours of exposure.

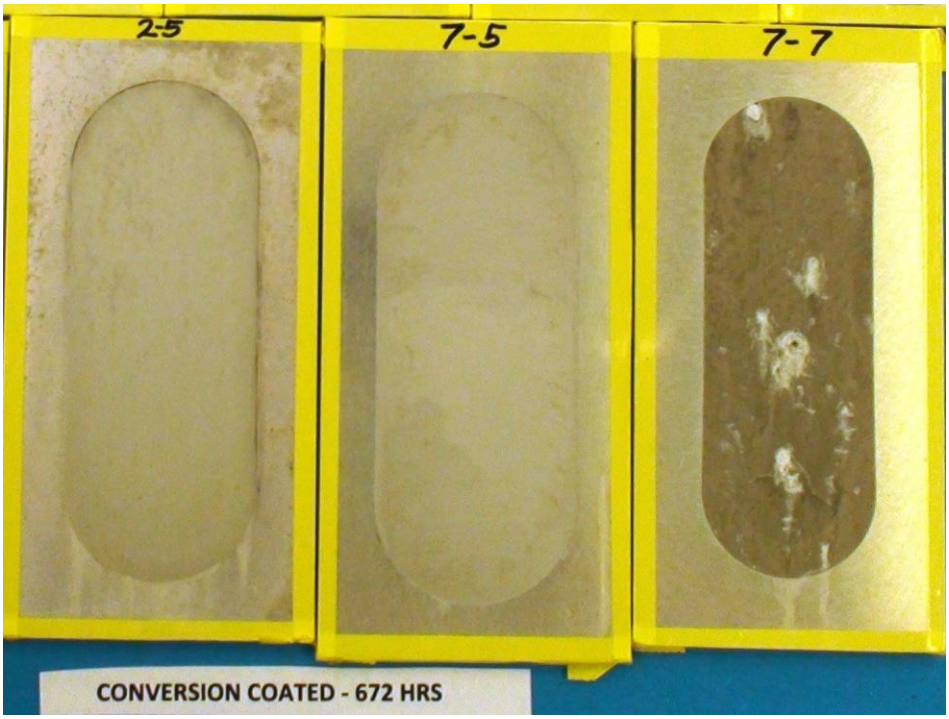

Figure 6.33: **Conversion Coated:** Pure aluminum repair on aluminum 2024-T3 (left), pure aluminum repair on aluminum 7075-T6 (middle), aluminum 7075 repair on aluminum 7075-T6 (right) after 672 hours of exposure.

Similar trends were seen in the conversion coated samples as were seen in the samples that were anodized. The pure aluminum coatings, on both aluminum 7075-T6 and aluminum 2024-T3, showed no evidence of corrosion through the 672 hours of exposure time (Figure 6.33 Left and middle). It is clear that the repaired area performed better than the aluminum 2024-T3.

The conversion coated aluminum 7075 repair shows an abundance of corrosion products at local pitting sites. This is worse than the anodized sample, which is to be expected as the anodization process helps in corrosion performance. This sample may also have a greater number of surface inconsistencies compared to the anodized sample due to processing.

Throughout the testing, all anodized samples remained approximately the same colour from Figure 6.24 to Figure 6.28. This shows that the chromate conversion coating adhered well to the anodized layer. It was clear, that in the samples that received only the chromate conversion coating (Figure 6.29 to Figure 6.33), that the yellow colour faded throughout salt fog exposure.

This shows that the conversion coating did not adhere as well as on the anodized samples, which is to be expected.

These results lead to the conclusion that areas repaired with pure aluminum can have similar, or better, corrosion performance than the aluminum alloy substrates. However, the repaired areas tend to suffer from small surface inconsistencies that lead to pitting corrosion. The process may be further refined in order to eliminate these macroscopic pitting sites though careful machining, refined powder selection and feeding procedures, and technological advancements in equipment (higher pressure and temperatures). The areas repaired with aluminum 7075 powders appear to have similar problems as the pure, but the pitting corrosion is much worse.

6.1.3 Adhesion Strength

The adhesion of the repairs is a crucial factor in the repairs of aerospace components. Without adequate adhesion, the repairs may delaminate from the components, resulting in catastrophic failure. Adhesion tests in accordance with ASTM C633: Standard Test Method for Adhesion of Cohesion Strength of Thermal Spray Coatings [58] were conducted.

In order for the adhesion strength values to represent repaired components, two sets of adhesion tests were taken at different thicknesses. The first test was done at the minimum thickness of 350 μm as required by the ASTM C633 standard. The second one was done at the maximum repair thickness of 1.5 mm (this maximum thickness was determined through discussion with industry). The adhesion strength results are found in Table 6.5.

Table 6.5: Adhesion strength of pure aluminum and aluminum 7075 CGDS coatings on aluminum alloy substrates in MPa.

Coating Material	Substrate Material	1.5 mm Coating Adhesion Strength (MPa)	350 μm Coating Adhesion Strength (MPa)
Aluminum 7075	Aluminum 7075-T6	25.5 ±10.1	32.1±8.1
Pure Aluminum	Aluminum 7075-T6	30.4 ±3.0	40.5±4.4
Pure Aluminum	Aluminum 2024-T3	45.1±4.5	42.1±6.2

The results of the adhesion strength testing show that aluminum 7075 CGDS coatings on aluminum 7075-T6 had the lowest adhesion strength of the trials. This was unexpected as the aluminum 7075 powder was deposited using helium, which should result in a much higher particle velocity than nitrogen. An increased particle velocity should result in better metallurgical and mechanical bonding. The increased velocity would also result in higher compressive residual stresses in the coating, which is known to decrease adhesion. Therefore, the lower adhesion may be explained by the large amount of residual stress in the coating. The residual stresses also accumulate as the coating thickness increases, which explains why the thin coatings have higher adhesion than the thick coatings.

The pure aluminum coatings on aluminum 7075-T6 had lower adhesion than the pure aluminum coatings on aluminum 2024-T3. This can be explained by the lower hardness of the aluminum 2024-T3 substrate. This lower hardness would result in more mechanical anchoring. Both of these coatings can attribute their higher adhesion strength over the aluminum 7075 coatings as a result of the lower residual stress in the coatings.

In order for these results to be interpreted, they must be compared to a known industry standard. In Boeing standard D6-51343: Thermal Spray Repair of Exterior Clad Aluminum Skins, a minimum adhesion of 2000 psi is required. It can be seen in Figure 6.34 that all adhesion strength values recorded in this testing were above this minimum value. It can therefore be concluded that according to existing industry standards for thermal spray repair of aerospace components (clad aluminum skins), the repairs in this research would have adequate adhesion.

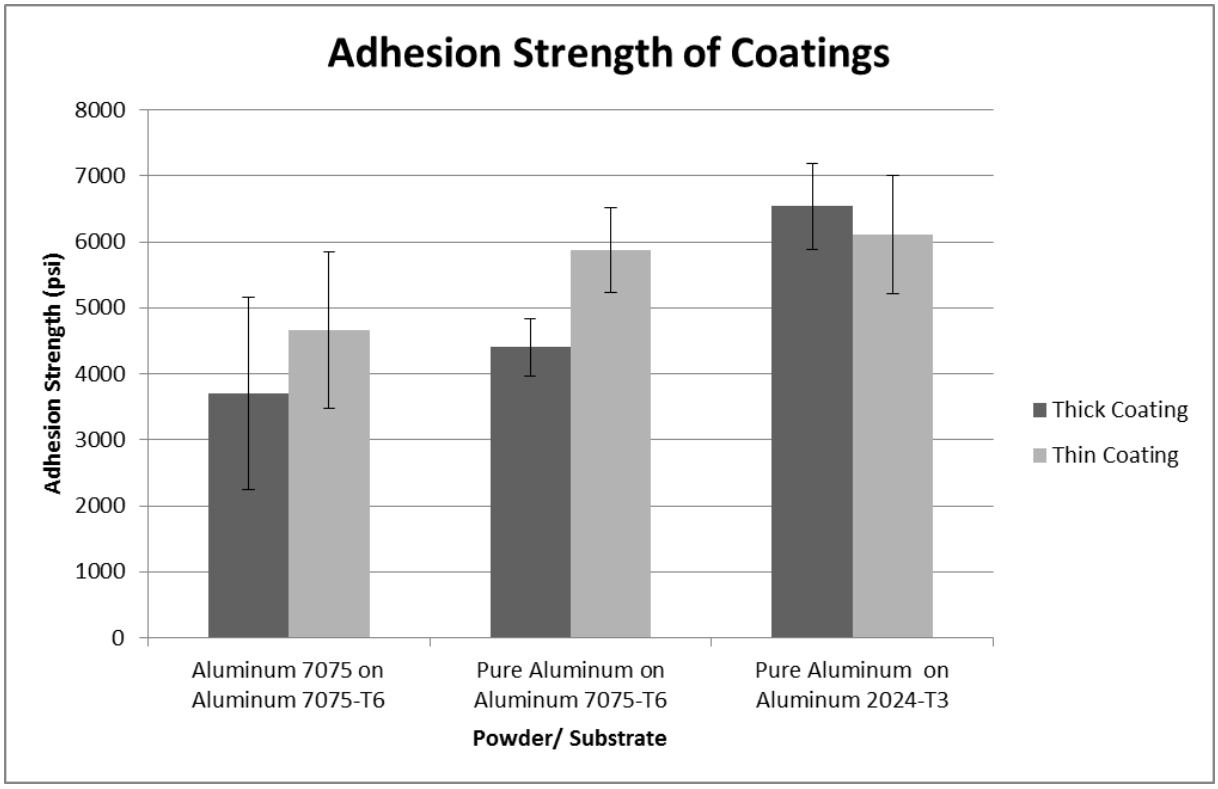

Figure 6.34: Adhesion strength of pure aluminum and aluminum 7075 CGDS coatings on aluminum alloy substrates (n=5).

6.2 Characterization of CGDS Restorations of Damaged Aluminum IVD Coatings

In order determine the suitability of CGDS for the reparation of aluminum alloy aerospace components; the repairs must undergo the same scrutiny as the aerospace components themselves. Adhesion strength, corrosion properties, and surface finish properties were examined. The parameters used to deposit these coatings were determined in Chapter 5 and can be found in summary in Table 6.6.

Table 6.6: Summary of CGDS parameters used for the restoration of damaged aluminum IVD coatings.

Parameter Selection	Pure Aluminum	Aluminum 7075	Aluminum 5083
Gas Pressure	250 psi (1.72 MPa)	250 psi (1.72 MPa)	250 psi (1.72 MPa)
Gas Temperature	350°C	500°C	500°C
Gas Nature	Nitrogen	Nitrogen	Nitrogen
Traverse Speed	190-260 mm/s	60-110 mm/s	55-140 mm/s
Step Size	1 mm	1 mm	1 mm
Feed Rate	14 RPM	3 RPM	3 RPM
Feed Wheel Type	320 Small hole	120 Large Hole	120 Large Hole
Powder Feeder Gas Flow Rate	25 SCFH	20 SCFH	20 SCFH
Powder Feeder Gas Nature	Nitrogen	Nitrogen	Nitrogen
Standoff Distance	15 mm	15 mm	15 mm
Nozzle Type	Polymer Nozzle	SS Nozzle	SS Nozzle
Orifice Diameter	2 mm	2 mm	2 mm

All sample surfaces are prepared through grit blasting. Issues with the consistency of adhesion results were found before ensuring that surfaces are prepared in the exact same manner every time with brand new blasting medium. The parameters for grit blasting can be Table 6.7. After grit blasting, the samples were submerged in ethanol and placed in an ultrasonic bath for approximately 10 minutes. The samples remained in the ethanol until spraying to avoid oxidation.

Table 6.7: Summary of grit blasting parameters used for the Restoration of damaged aluminum IVD coatings.

Parameter	Metric
Pressure	344 kPa (50 psi)
Gas Nature	Compressed Air
Grit Nature	Ferrosilicate
Size	20 Grit
Angle	45°

6.2.1 Adhesion Testing

The initial adhesion test that all aluminum IVD coatings are subjected to is glass bead burnishing. Glass bead burnishing creates residual stresses in the coatings, which will expose areas of poor adhesion through delamination. The parameters for the glass beading are in accordance with MIL-DTL-83488D [8] and are found in Table 6.8.

Table 6.8: Parameters used for glass beading coatings after deposition.

Property	Metric
Pressure	50 psi
Gas Nature	Compressed Air
Bead Nature	Spherical Glass
Size	100-170 Mesh
Type	No 10
Angle	45°

The coatings did not delaminate during glass beading. Cross sections of the coatings were also taken to see the effect of the glass beading process (shown in Figure 6.35, Figure 6.36, and Figure 6.37). These cross sections show no delamination from the substrate. The close contact of the coating to substrate after glass beading leads to the conclusion that the coatings meet the glass bead burnishing standard.

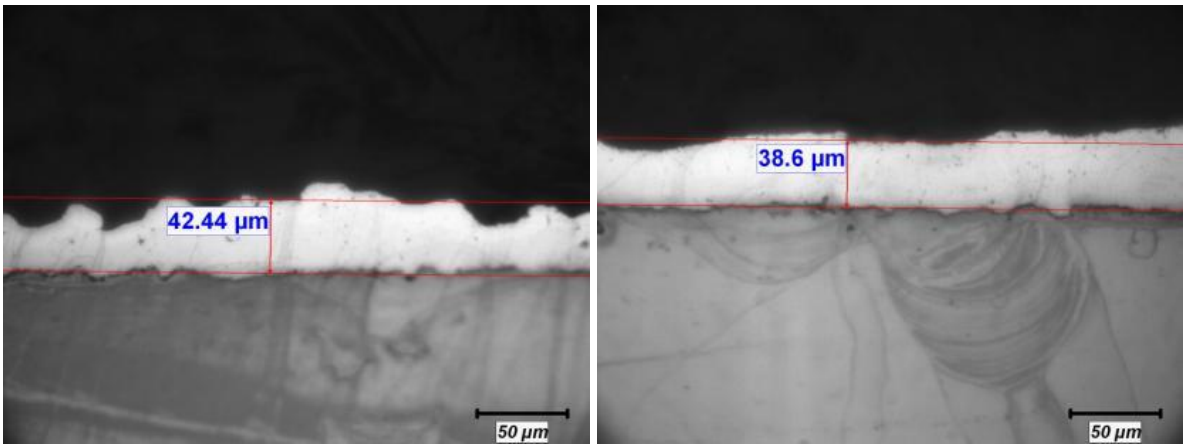

Figure 6.35: CGDS coatings of pure aluminum without (left) and with (right) glass bead burnishing test.

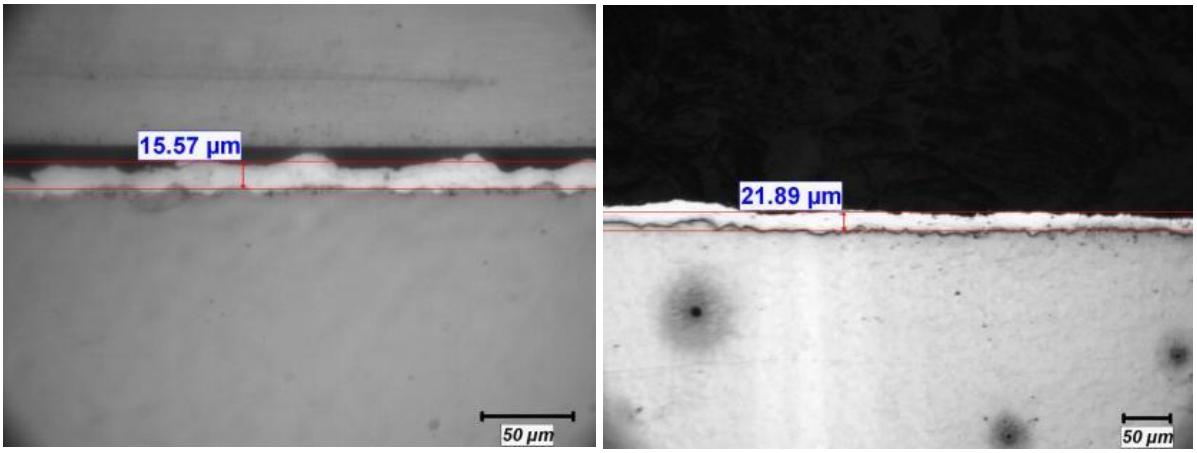

Figure 6.36: CGDS coatings of aluminum 7075 without (left) and with (right) glass bead burnishing test.

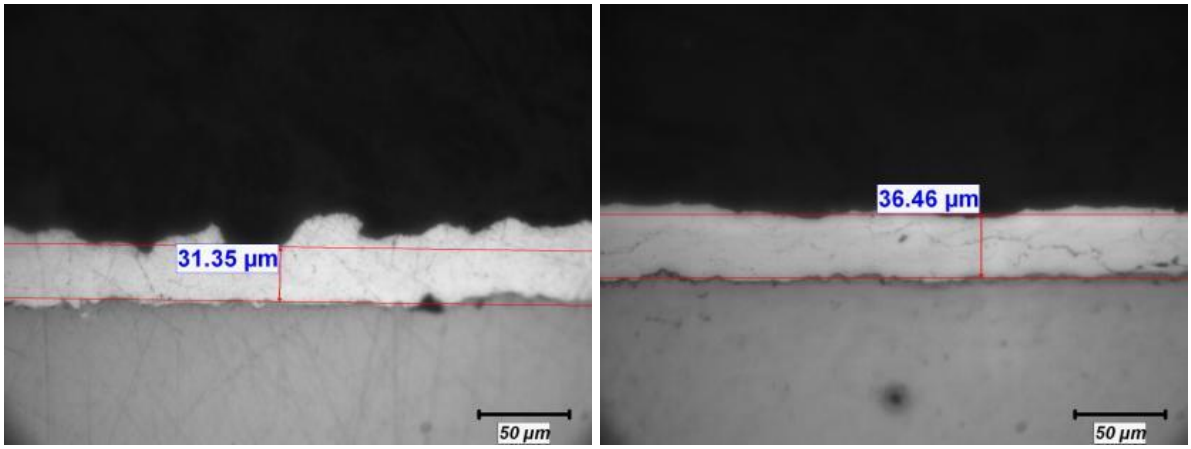

Figure 6.37: CGDS coatings of aluminum 5083 without (left) and with (right) glass bead burnishing test.

The second method used to evaluate the adhesion of the coatings is strip rupture testing. IVD coated panels with simulated damage were repaired with CGDS pure aluminum, aluminum 7075, and aluminum 5083. The coatings were evaluated in two locations, on the bare steel (area being repaired) and on the IVD aluminum (area that the coatings would overlap the aluminum IVD coating).

Pure Aluminum Coating Strip Rupture Results (Set 1)

The strip rupture process for pure aluminum repairs on the bare steel is shown in Figure 6.38, Figure 6.39, Figure 6.40, and Figure 6.41. It can be seen in Figure 6.39 that when the sample is bent to 90°, no delamination is visible, but when the coating is returned to the initial position (Figure 6.40) there is delamination and bubbling visible along the sides of the coating. After the failure of the sample, delamination in the zone surrounding the bent area was observed (Figure 6.41). After further prying of the poorly adhered areas, delamination was seen outside of the immediate fracture area. This delamination travelled mostly along edges of the coating.

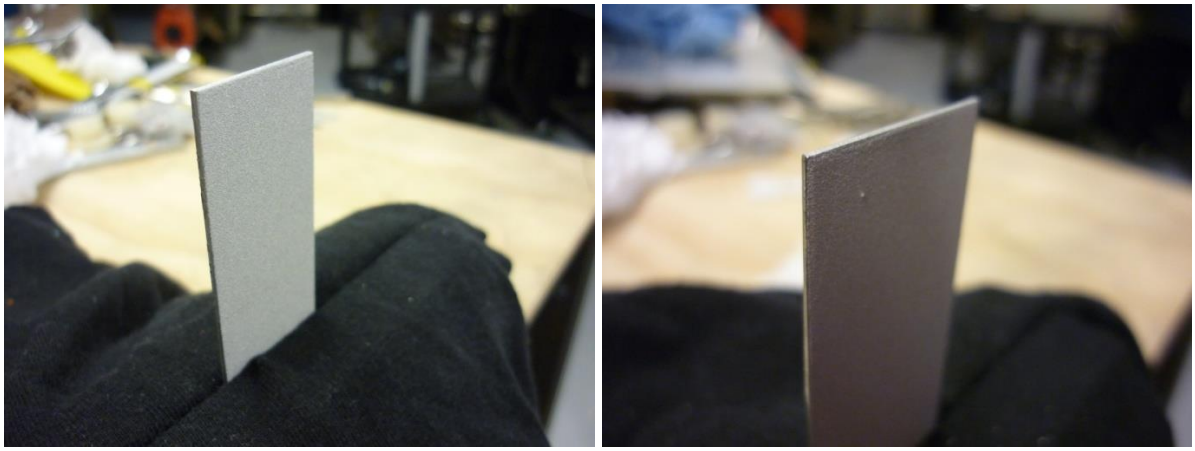

Figure 6.38: Pure aluminum strip rupture samples before bending (coating on bare steel)

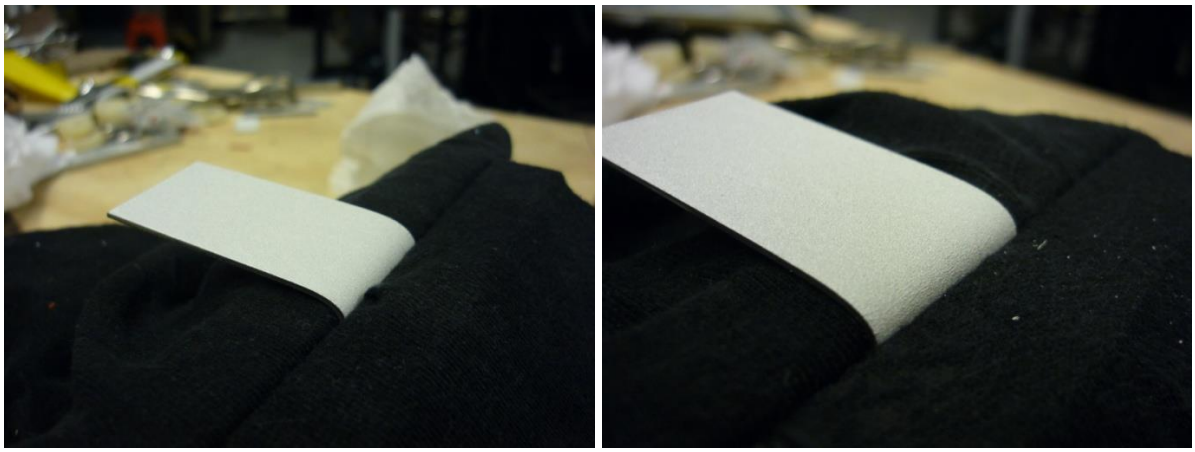

Figure 6.39: Pure aluminum strip rupture samples bent to 90° (coating on bare steel)

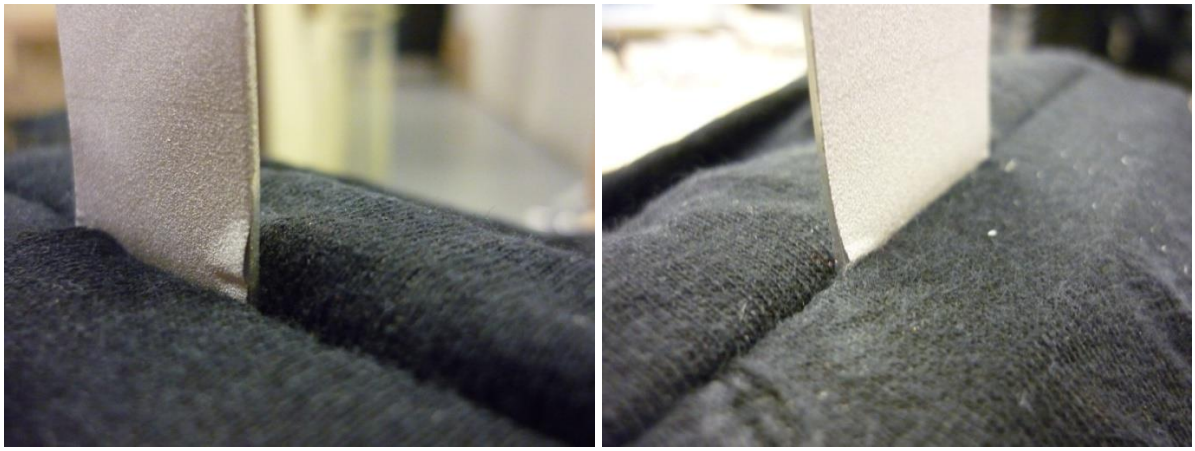

Figure 6.40: Pure aluminum strip rupture samples returned to 0°, showing delamination at the edges (coating on bare steel)

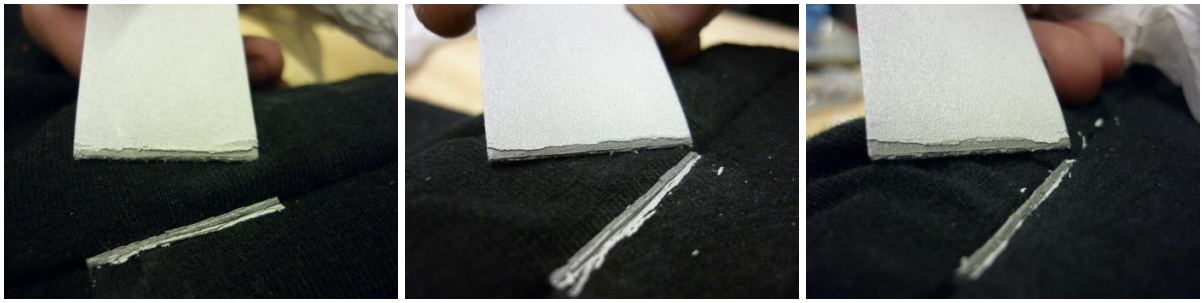

Figure 6.41: Pure aluminum strip rupture samples after testing (coating on bare steel)

The delamination of the coating outside of the bent area leads to the conclusion that the coatings, on bare steel, failed the strip rupture testing according to MIL-DTL-83488D [8]. It was observed that the majority of the coating delamination occurred near the edges of the coating, where the deposition itself may have been affected by edge effects.

There are areas of the repairs that would overlap existing pure aluminum IVD coatings, and therefore strip rupture testing was done on CGDS coatings on IVD aluminum coatings. The results for pure aluminum coatings on aluminum IVD coatings can be found in Figure 6.42, Figure 6.43, and Figure 6.44.

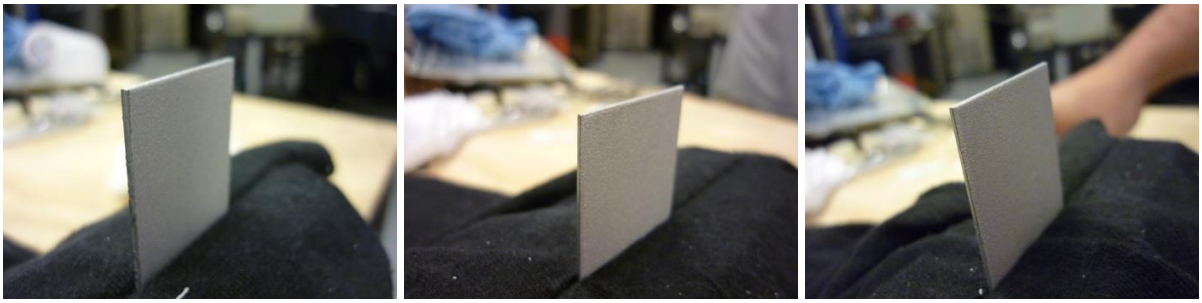

Figure 6.42: Pure aluminum strip rupture samples prior to bending (coating on aluminum IVD coating).

Figure 6.43: Pure aluminum strip rupture samples bent to 90° (coating on aluminum IVD coating).

Figure 6.44: Pure aluminum strip rupture samples after rupture (coating on aluminum IVD coating).

For the pure aluminum sprayed onto the IVD coated areas, adhesion was shown to be much stronger than on bare steel. Little, to no, delamination was observed outside of the immediate area surrounding the break. After prying at the poorly adhered areas of the coating, no further delamination occurred.

Aluminum 7075 Coating Strip Rupture Results (Set 1)

The strip rupture process for aluminum 7075 repairs on the bare steel is shown in Figure 6.45, Figure 6.46, Figure 6.47, and Figure 6.48. It can be seen in Figure 6.46, that when the sample is bent to 90°, no delamination is visible, but when the coating is returned to the initial position (Figure 6.47) there is a small zone delamination in the region that was bent and along the edges. After the failure of the sample, a small amount of delamination in the zone surrounding the bent area was observed. After further prying of the poorly adhered areas, some delamination was seen outside of the immediate fracture area, mostly along edges of the coating.

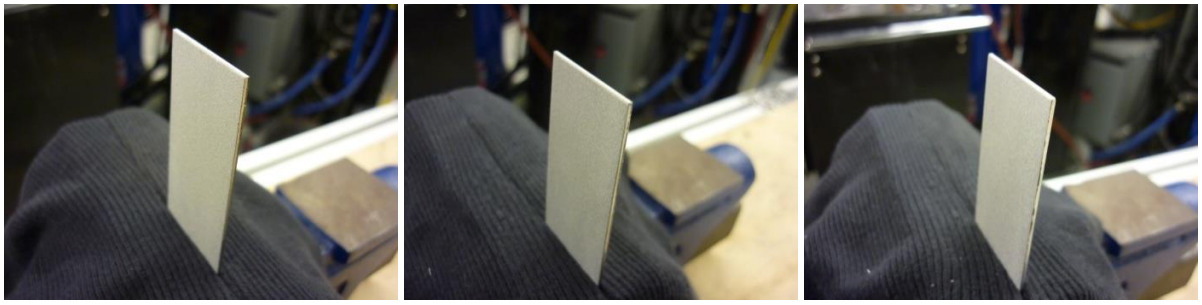

Figure 6.45: Aluminum 7075 strip rupture samples before bending (coating on bare steel).

Figure 6.46: Aluminum 7075 strip rupture samples bent to 90° (coating on bare steel).

Figure 6.47: Aluminum 7075 strip rupture samples returned to 0°, showing delamination at the edges (coating on bare steel)

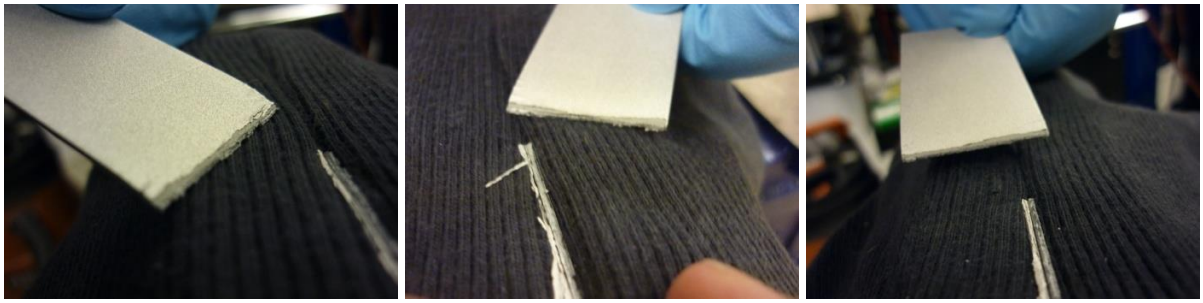

Figure 6.48: Aluminum 7075 strip rupture samples after testing (coating on bare steel).

The delamination of the aluminum 7075 coating outside of the bent area was much less severe than the pure aluminum coatings. It was observed that the majority of the coating delamination occurred near the edges of the coating, where the deposition itself may have been affected by the flow dynamics. In order to improve this test to ensure it qualifies under MIL-DTL-83488D [8], the test was redone to see if this effect could be eliminated.

There are also areas of the repairs that would overlap existing pure aluminum IVD coatings, and therefore strip rupture testing was done on CGDS coatings on IVD aluminum coatings. The results for aluminum 7075 coatings on aluminum IVD coatings can be found in Figure 6.49, Figure 6.50, and Figure 6.51.

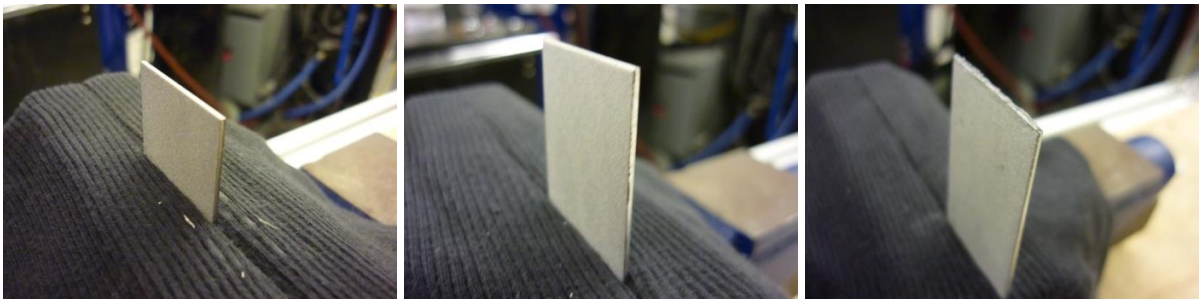

Figure 6.49: Aluminum 7075 strip rupture samples prior to bending (coating on aluminum IVD coating).

Figure 6.50: Aluminum 7075 strip rupture samples bent to 90° (coating on aluminum IVD coating).

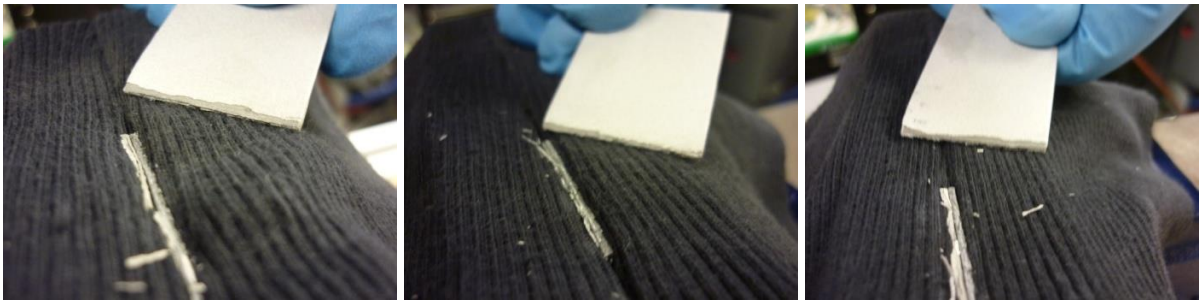

Figure 6.51: Aluminum 7075 strip rupture samples after rupture (coating on aluminum IVD coating).

For the aluminum 7075 coatings sprayed onto the IVD coated areas, adhesion was shown to be even better than bare steel. Little, to no delamination was observed outside of the immediate area surrounding the break. After prying at the poorly adhered areas of the coating, no further delamination occurred.

Aluminum 5083 Coating Strip Rupture Results (Set 1)

The strip rupture process for aluminum 5083 repairs on the bare steel is shown in Figure 6.52, Figure 6.53, and Figure 6.54. It can be seen in Figure 6.53, that when the sample is bent to 90°, no delamination is visible, but when the coating is returned to the initial position there is a small zone delamination in the region that was bent and along the edges. After the failure of the sample, a small amount of delamination in the zone surrounding the bent area was observed. After further prying of the poorly adhered areas, some delamination was seen outside of the immediate fracture area, mostly along edges of the coating.

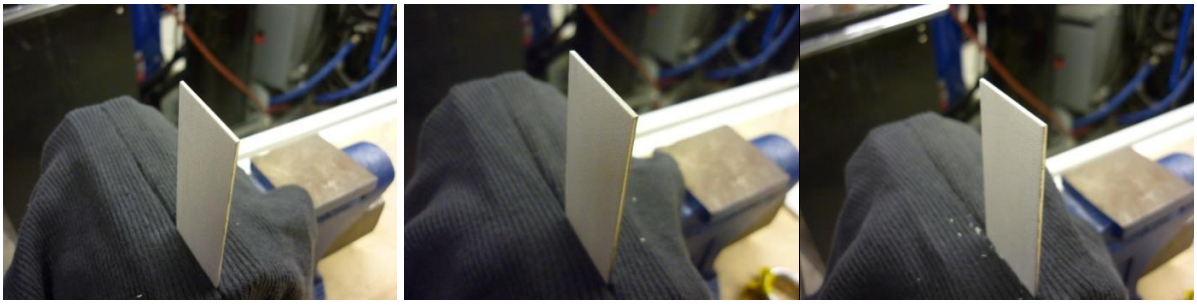

Figure 6.52: Aluminum 5083 strip rupture samples before bending (on bare steel).

Figure 6.53: Aluminum 5083 strip rupture samples bent to 90° (coating on bare steel).

Figure 6.54: Aluminum 5083 strip rupture samples after testing (coating on bare steel).

The delamination of the aluminum 5083 coatings outside of the bent area was much less severe than the pure aluminum coatings (similar to aluminum 7075). It was observed that the majority of the coating delamination occurred near the edges of the coating, where the deposition itself may have been affected by edge effects. In order to improve this test to ensure it qualifies under MIL-DTL-83488D [8], the test was redone to see if this effect could be eliminated.

There are also areas of the repairs that would overlap existing pure aluminum IVD coatings, and therefore strip rupture testing was done on CGDS coatings on IVD aluminum coatings. The results for aluminum 5083 coatings on aluminum IVD coatings can be found in Figure 6.55, Figure 6.56, and Figure 6.57.

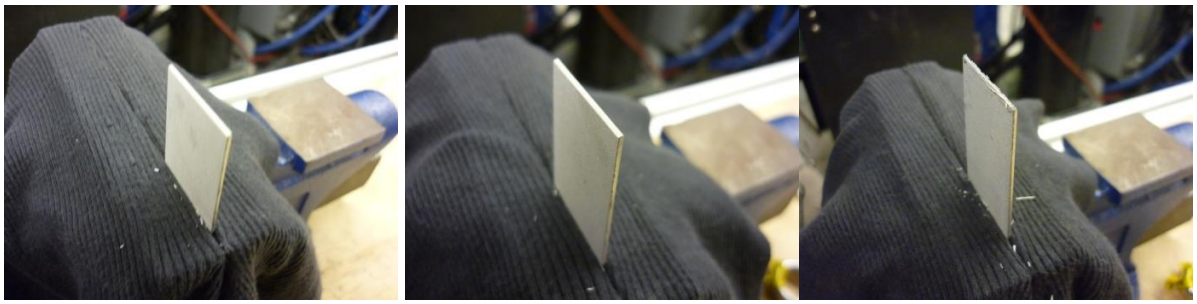

Figure 6.55: Aluminum 5083 strip rupture samples prior to bending (coating on aluminum IVD coating).

Figure 6.56: Aluminum 5083 strip rupture samples bent to 90° (coating on aluminum IVD coating).

Figure 6.57: Aluminum 5083 strip rupture samples after rupture (coating on aluminum IVD coating).

For the aluminum 5083 coatings sprayed onto the IVD coated areas, adhesion was shown to be even better than bare steel. Little, to no delamination was observed outside of the immediate area surrounding the break. After prying at the poorly adhered areas of the coating, no further delamination occurred.

Second Set of Strip Rupture Testing

In order to avoid the edge effects during spraying, a one inch strip was deposited on along the center of a 1.5 inch strip rupture panel (see Figure 6.58). An apparatus was developed to allow for the samples to be bent to 90 degrees consistently along the same line without touching the coating itself (Figure 6.59). The bottom of the fixture holds the sample in the same way the vice would in the original set up. The coating on the top of the sample would remain untouched since the fixture was milled so that only the sides would be in contact (Figure 6.60). This set up effectively creates a consistent "bend to break" with a small bending radius regardless of operator or sample material.

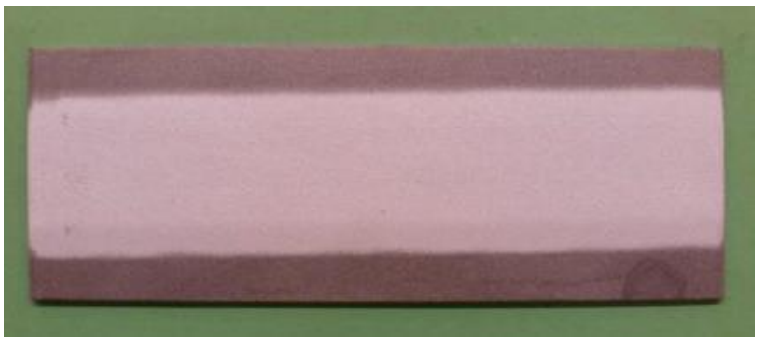

Figure 6.58: Modified strip rupture panel showing coating in the middle.

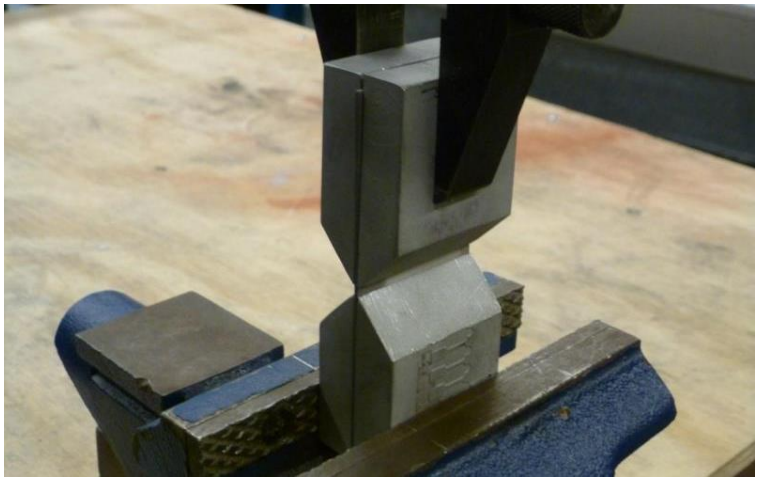

Figure 6.59: Strip rupture fixture for second set of testing.

Figure 6.60: Milled fixture for coating side of sample.

The repairs shown on the top left of Figure 6.61, Figure 6.62, and Figure 6.63 are the coatings after spraying (as-sprayed condition). This surface is fairly smooth and level, but uniformity is improved in the glass beaded sample (bottom left). The glass beaded sample also shows no signs of delamination from the glass bead process, which confirms the glass bead abrasion test from earlier.

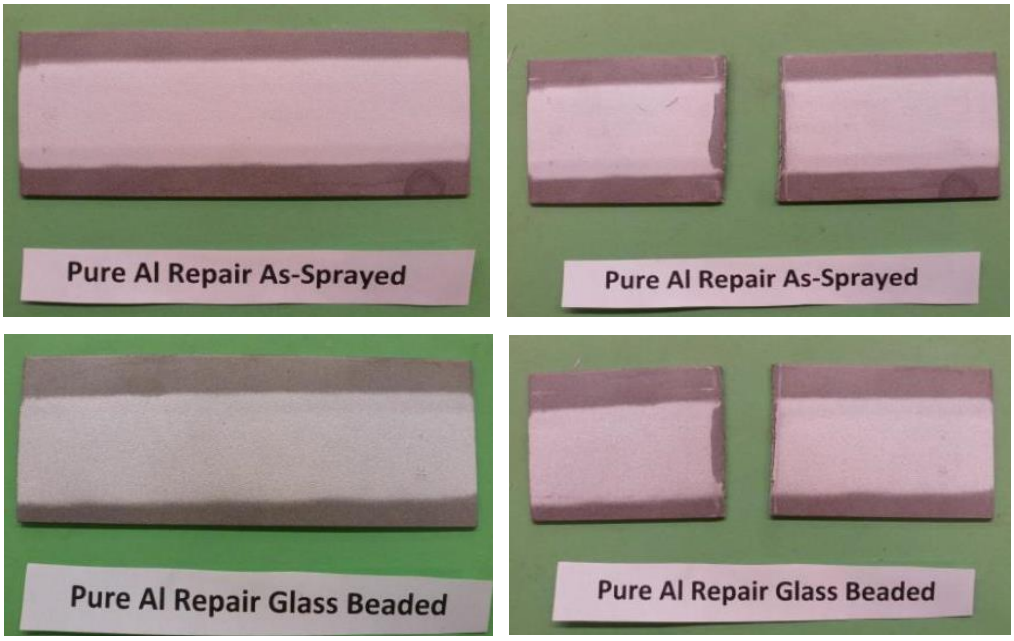

Figure 6.61: Pure aluminum coating strip ruptures results (set 2).

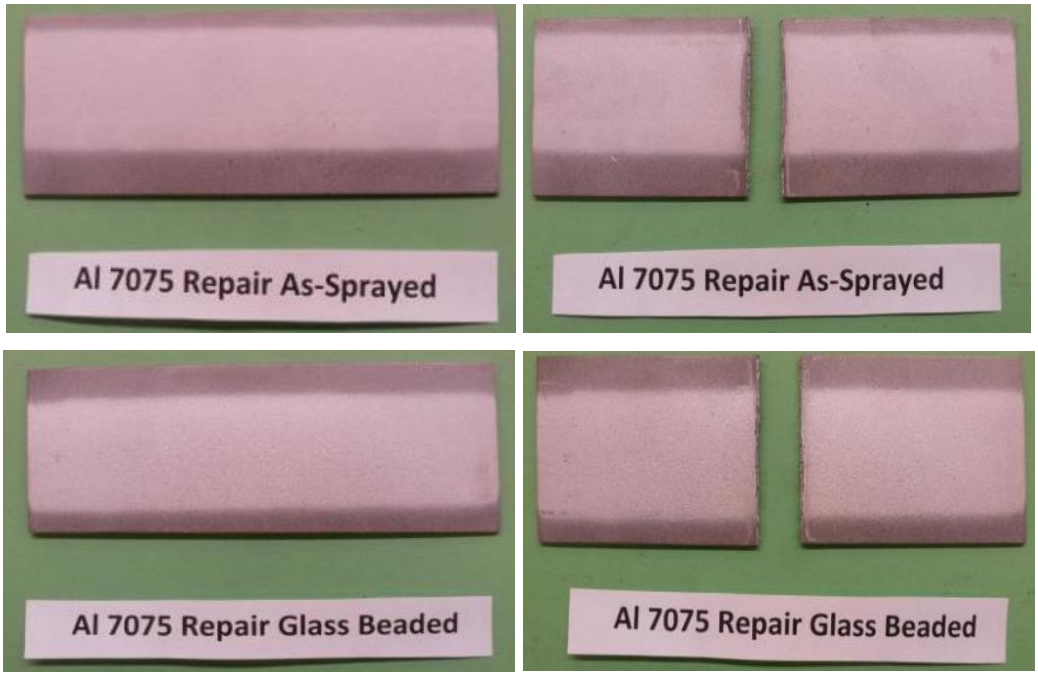

Figure 6.62: Aluminum 7075 coating strip ruptures results (set 2).

Figure 6.63: Aluminum 5083 coating strip ruptures results (set 2).

Figure 6.64: Al 7075 Coating Showing No Delamination when Bent to 90 Degrees

With all three aluminum alloys, delamination was seen in the rounded areas after the rupture. The coating in this area fails due to the brittle nature of cold sprayed coatings. As the sample is bent back and forth, the substrate surface is repeatedly transformed from an internal to external bend radius. This drastically changes the surface area to which the coating is adhered too. This geometry change is handled in the substrate through plastic deformation. The coatings are brittle due to cold working that occurs during the coating process and the lower cohesive strength between particles. This leaves the coating cracked and flaking in this expanded/ contracted area. The coatings showed no signs of delamination or cracking at first bend (Figure 6.64); only after being compressed and expanded again does the damage occur.

The pure aluminum coatings demonstrated the poorest strip rupture performance, which is to be expected as it is sprayed at the lowest particle velocity due to temperature limitations. This delamination, again, is only on the rounded part directly adjacent to the rupture site. There does not seem to be a drastic difference between glass beaded adhesion and as-sprayed adhesion, though a slight improvement is seen for Al 7075 (Figure 6.62).

The peeling of the coatings along the edges is no longer observed. This is an improvement of experimental design, not spray quality. By spraying a pattern on the substrates that did not go along the edge, the edge effects were eliminated. This reduced inconsistency in the coating quality and more accurately imitates a real life repair scenario. It should be noted, that before photographing, all damaged areas were picked with a pin to dislodge any easily removable coatings as was suggested by in the MIL-DTL-83488D [8].

For all of the coatings, some delamination occurs at the rounded area of the bend to break test. This delamination does not continue further into the coating. The coating shows no signs of delamination when bent to 90 degrees. From these results, and consultation within industry, the adhesion of the coatings measured by the strip rupture testing was deemed adequate.

6.2.2 Surface Roughness

As was stated in the general research objectives, the final repairs must have roughness values similar to that of existing pure aluminum IVD coatings. The IVD aluminum panels that were

received by the University of Ottawa were glass-beaded before arrival. The glass beading process used by Boeing has been simulated and the relevant parameters are shown in Table 6.8. Ra roughness value is the "Arithmetic Average of Absolute Values" and was chosen as it is the most commonly used convention. The roughness values of the coatings, before and after glass beading, can be found in Table 6.9.

Table 6.9: Surface roughness (Ra) of coatings before and after glass beading procedure.

Coating Material	**Surface Roughness Ra (μm)**	
	As Sprayed	Glass Bead
IVD Aluminum	N/A	1.752
Pure Aluminum	8.167	4.962
Aluminum 7075	2.964	2.849
Aluminum 5083	5.550	3.411

The glass beaded CGDS coatings are approaching that of the pure aluminum IVD coatings, with aluminum 7075 coatings being the closest. Surface roughness topology for selected samples was performed with a VHX-1000 Digital Microscope from Keyence Canada Inc. These images are created automatically by the microscope by "compiling images of different focus positions". Figure 6.65 shows a 3D image of the pure aluminum surface after glass beading. In this image, pock marks left by the glass beading procedure can be seen. Comparing this to the aluminum 7075 or 5083 images (Figure 6.66 and Figure 6.67, respectively), it is clear that the craters on the pure aluminum are larger and deeper. This is due to the hardness difference between pure aluminum and Al 7075 or Al 5083.

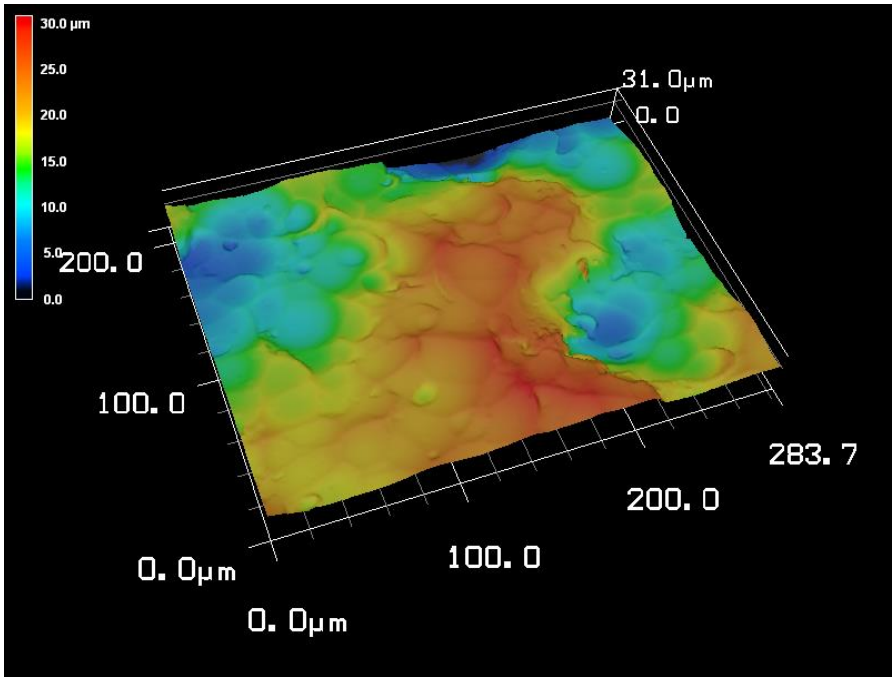

Figure 6.65: Topology of CGDS pure aluminum coatings after glass beading.

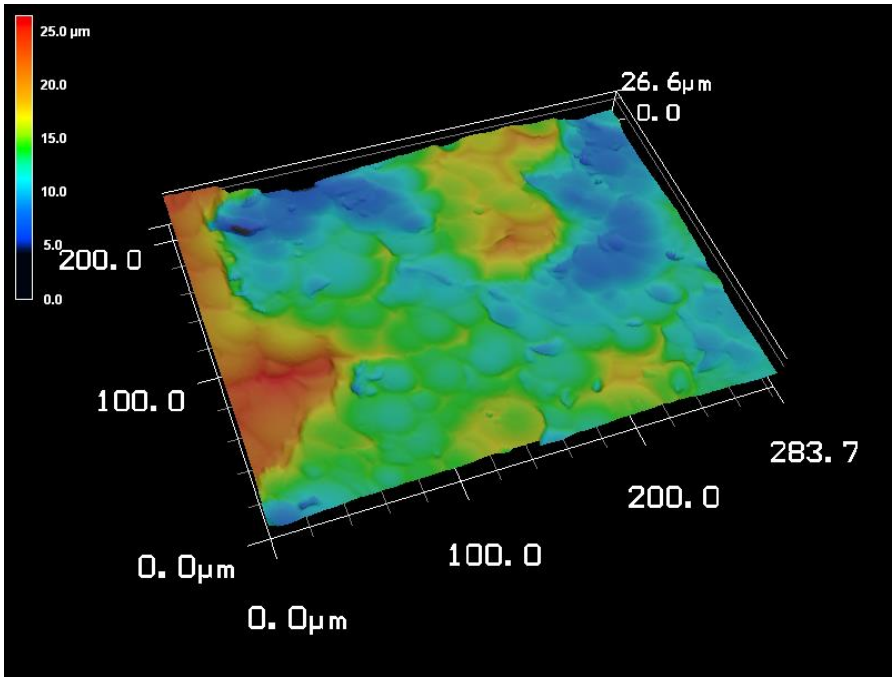

Figure 6.66: Topology of CGDS aluminum 7075 coatings after glass beading.

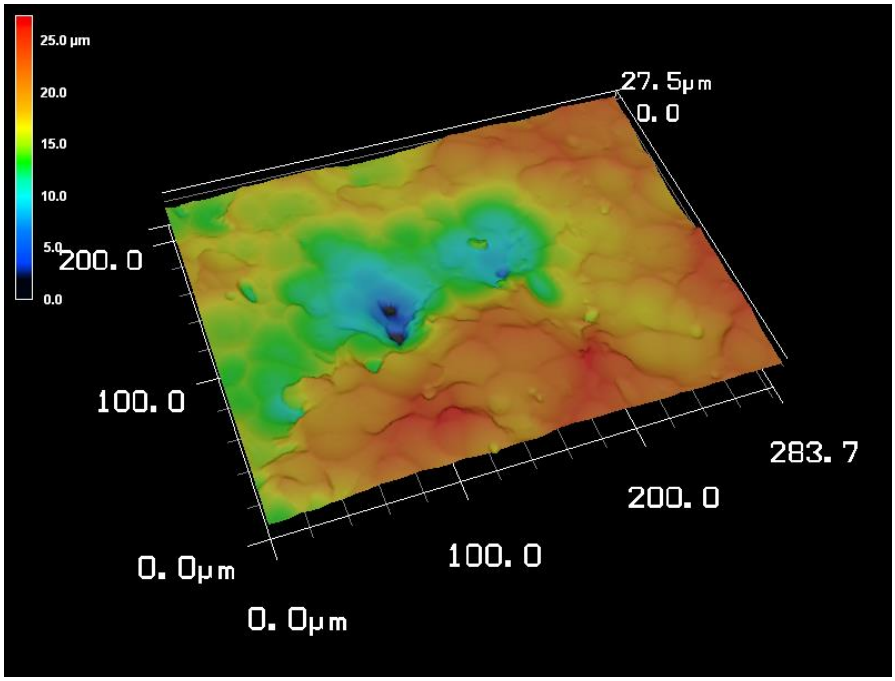

Figure 6.67: Topology of CGDS aluminum 5083 coatings after glass beading.

The roughness values attained for the CGDS coatings were slightly higher than that of aluminum IVD coatings, it is believed that this result is because of a glass beading procedure that is overly harsh, leaving large pits in the surface. It is likely that using the correct glass beading procedure/ equipment available in industry, the exact roughness values could be attained.

6.2.3 Corrosion Testing

In order to test the corrosion resistance of the repairs the samples were placed in a neutral salt spray chamber for corrosion testing according to ASTM B-117. According to the MIL-DTD-83488D standard, a class 1 aluminum coating with a Type II conversion coating must be tested up to 672 hours. A test fails if corrosion products of the substrate are visible (red for the steel). White corrosion of the aluminum layer is not considered a cause for rejection.

The 3"x6" samples were cut from the damaged IVD samples with the damage located in the middle of the sections and the entire samples were sprayed. The samples were then conversion coated (Type II). Half of the samples sprayed had an 'X' scored through the coating and into the

substrate. This was done to verify that the aluminum coating offers proper sacrificial corrosion protection to the steel if the repaired area is ever damaged. This protection occurs because aluminum is more active (i.e. has a more negative corrosion potential) than the steel, which induces a galvanic current that protects the steel while creating a preferential dissolution of the aluminum near the scribe.

The results of for the pure aluminum coatings can be found in Figure 6.68. The uniform coloring of the specimens prior to testing suggests that conversion coating adhered well to the repaired samples. Both the scored and non-scored samples showed no corrosion products after 672 hours. The corrosion properties of the pure aluminum repairs met, and exceeded, the requirements for Class 1, Type II -coatings specified in MIL-DTL-83488D - 4.4.3) [8].

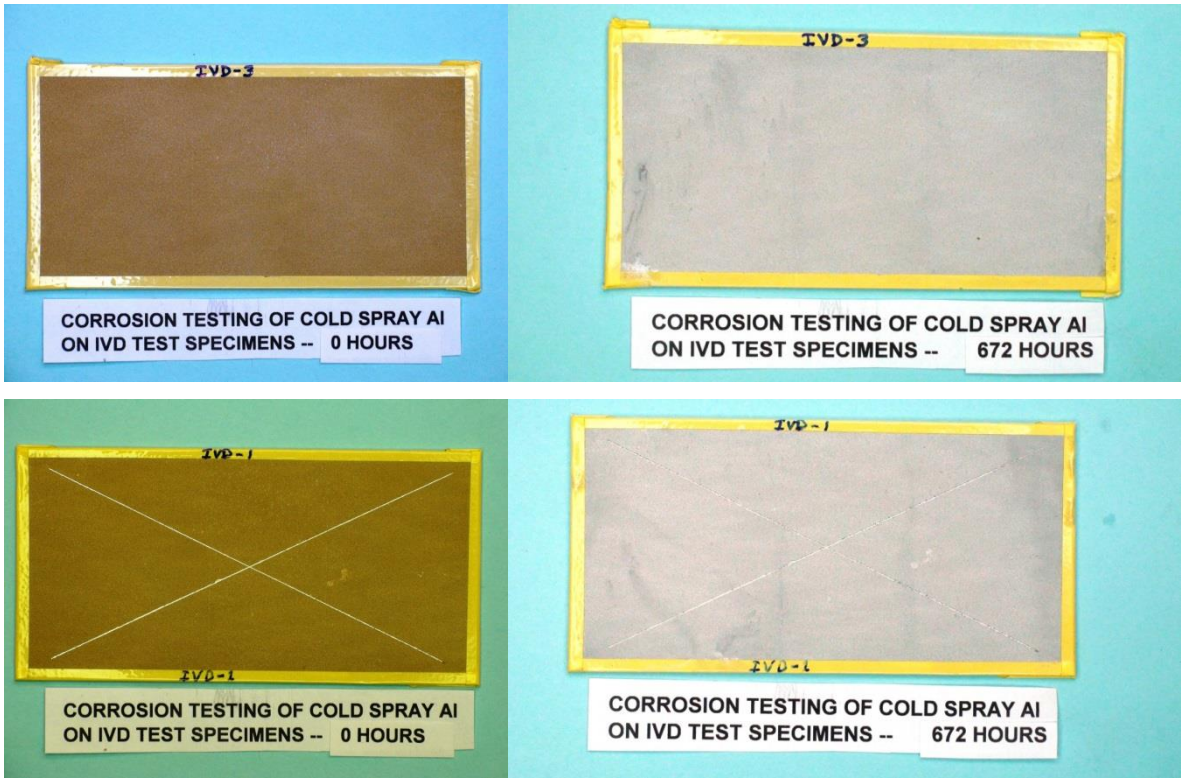

Figure 6.68: Corrosion results of CGDS pure aluminum repairs of damaged pure aluminum IVD coatings.

The results of for the aluminum 7075 coatings can be found in Figure 6.69. The uniform coloring of the specimens prior to testing suggests that conversion coating adhered well to the repaired samples. These repairs showed more corrosion products than the pure aluminum. The

increase in pitting corrosion can be attributed to the higher copper content of the aluminum 7075. In the unscratched sample, white corrosion is seen at the interface of the damaged area and the IVD aluminum. Substantial corrosion products are formed in the scratched sample at a discontinuity in the coating. This is a remnant of a bubble that was formed in the IVD coated aluminum from the off gassing of the masking tape. This defect is clearly visible before corrosion testing and should not be considered for the validity of this test. .

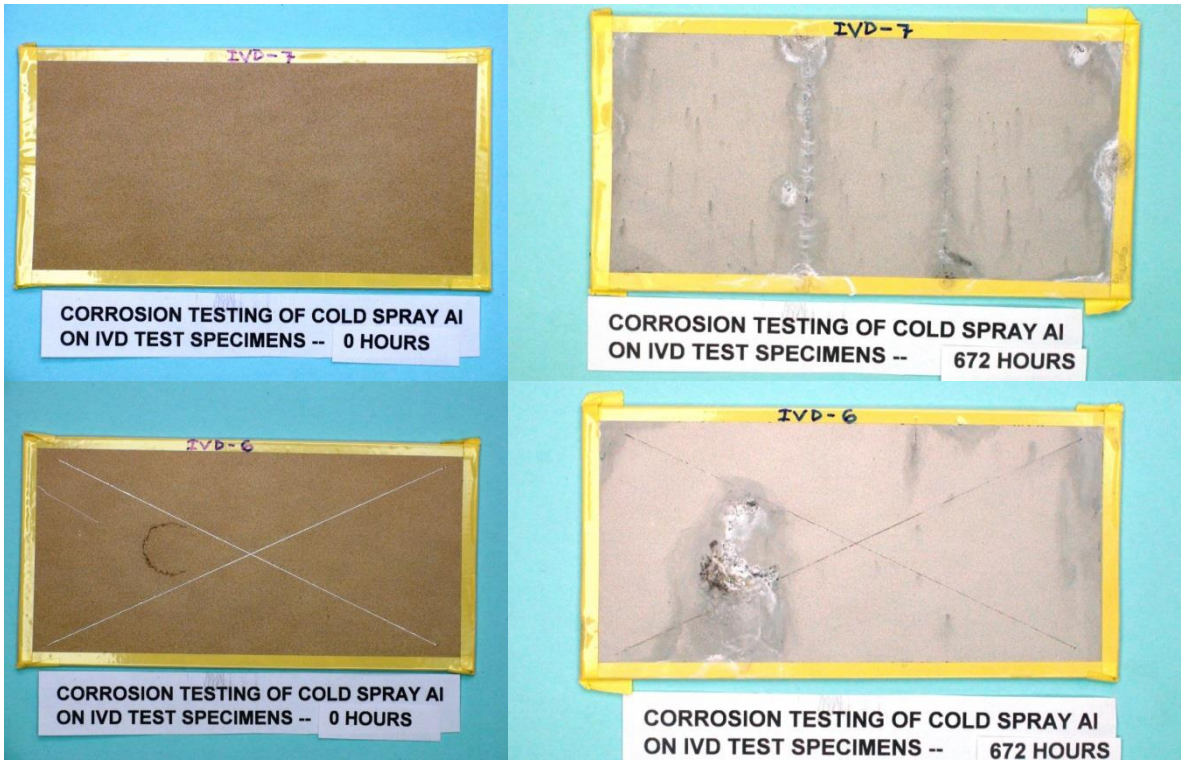

Figure 6.69: Corrosion results of CGDS aluminum 7075 repairs of damaged pure aluminum IVD coatings.

The results of for the aluminum 5083 coatings can be found in Figure 6.70. The uniform coloring of the specimens prior to testing suggests that conversion coating adhered well to the repaired samples. Both the scored and non-scored samples showed no corrosion products after 672 hours. The corrosion properties of the aluminum 5083 repairs met, and exceeded, the requirements for Class 1, Type II coatings specified in MIL-DTL-83488D - 4.4.3) [8]. It is clear that after a period of time in the salt fog chamber, the Type II chromate conversion coating had been removed from all coatings, as the after pictures are no longer brown/yellow.

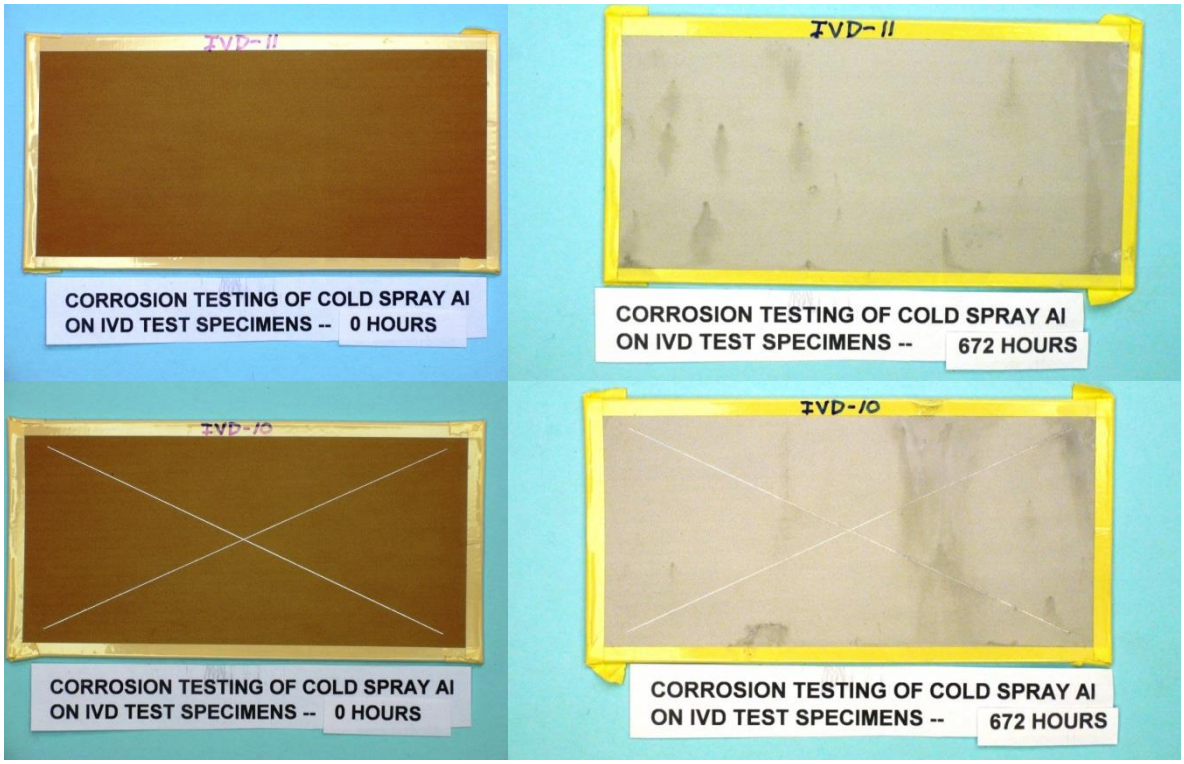

Figure 6.70: Corrosion results of CGDS aluminum 5083 repairs of damaged pure aluminum IVD coatings.

The corrosion resistance of the coatings was deemed acceptable for all coatings according to the MIL-DTL-83488D - 4.4.3. This standard only specifies up to 672 hours, but the test was continued to 1000 hours. A full record of the corrosion tests up to 1000 hours can be found in Appendix IV.

7 CONCLUSIONS AND FUTURE WORK

The results of this research proved the feasibility of using CGDS as a process for the restoration of damaged aluminum IVD coatings and has motivated companies in the aerospace industry to continue on a path of commercialization. The CGDS coatings have met the same level scrutiny as was required of the IVD coatings when they replaced toxic cadmium coatings in the late 1980s. It was found that pure aluminum, aluminum 7075, and aluminum 5083 powders were able to be successfully deposited as dense uniform coatings using commercially available low pressure CGDS equipment. The coating adhesion, demonstrated through glass bead abrasion and strip rupture testing, was shown to meet the current industrial standards. The corrosion testing of the repairs, especially the pure aluminum, was determined to meet current industrial standards as no red rust of the steel components was present. These results have led this project into a new tertiary stage of testing - as a qualification of the process for industrial application with The Boeing Company.

The use of CGDS was also shown in this research to be a very promising as a process for the restoration of aluminum alloy aerospace components. It was found that pure aluminum and aluminum 7075 powders were able to be successfully deposited using commercially available CGDS equipment. At the time of this research, it was determined that aluminum 2024 was unable to be deposited due to clogging issues. This material, in the future, could be used for restorations if another powder source could be found. A powder with fewer satellite particles could result in less damage to the equipment. Improvements in the equipment itself, such as higher temperature limits in the polymer nozzle, could also improve the outlook of using this material.

The adhesion strength of the repaired aluminum components was found to be well above the accepted range for thermally sprayed repairs according to industrial standards. The repairs were subjected to a highly corrosive environment and showed only minor pitting. These sites could be reduced in the future with improved machining techniques and attention to surface detail prior to exposure to the salt fog. The only requirement that the repaired components did not meet was the wear performance of the anodized layer, measured thought Taber abrasion testing. The results of this test, at times, approached the desired results and it is believed that if the

quality and consistency of the coatings could be improved, the test could attain the desired results.

Overall, there is still work to be done in optimizing the CGDS coatings to provide the best results for all necessary industrial tests. The parameters used for this characterization were found only by focusing on creating dense, well depositing, coatings. It is now known that creating a coating that creates a more resilient anodized layer is of the utmost importance for the restoration of aluminum alloy components. Issues with coating consistency were found and through experience it has been determined that this is likely a result of powder consistency. Before industrial application, better quality control between powder batches must be instituted.

REFERENCES

[1] A. S. Warren, “Developments and Challenges for Aluminum – A Boeing Perspective,” *Mater. Forum*, vol. 28, pp. 24–31, 2004.

[2] M. Peters and C. Leyens, “Aerospace and Space Materials,” *Mater. Sci. Eng.*, vol. III.

[3] N. Barrington and M. Black, “Section 1: Industrial Applications - Aerospace materials and manufacturing processes at the millennium,” in *Aerospace Materials*, B. Cantor, H. Assender, and P. Grant, Eds. IOP Publishing Ltd, 2001.

[4] W. Callister and D. Rethwisch, *Materials Science and Engineering: An Introduction*, Eighth., vol. 8. Wiley, 2008.

[5] V. L. Holmes, J. J. Reilly, M. D. Corp, P. O. Box, S. T. L. Mo, T. Air, and F. Base, “THE SUBSTITUTION OF IVD ALUMINUM FOR CADMIUM,” *Air Force Eng. Serv. Cent.*, 1989.

[6] V. L. Holmes, “IVD Aluminum Coating Application of the Process at Boeing-St . Louis,” *A&M Environ. Technotes*, vol. 7, no. 3, 2002.

[7] V. L. Holmes and M. Bridger, “IVD Aluminum Coating and Application of the Process at Boeing – St . Louis,” pp. 1–23.

[8] U. S. Military, “MIL-DTL-83488D Detail Specification Coating, Aluminum, High Purity,” no. April 1999, pp. 1–10, 1985.

[9] R. C. Dykhuizen and M. F. Smith, “Gas Dynamic Principles of Cold Spray,” vol. 7, no. June, pp. 205–212, 1998.

[10] L. Ajdelsztajn, B. Jodoin, G. E. Kim, and J. M. Schoenung, “Cold Spray Deposition of Nanocrystalline Aluminum Alloys,” *Metall. Mater. Trans. A*, vol. 36, no. March, 2005.

[11] J. R. Davis, “Corrosion of Aluminum and Aluminum Alloys,” *ASM Int.*, 1999.

[12] M. Donachie, *Titanium: a technical guide*, Second. Materials Park, Ohio: ASM International, 2000.

[13] K.-H. Grote and E. K. Antonsson, Eds., *Springer Handbook of Mechanical Engineering*. Berlin, Heidelberg: Springer Berlin Heidelberg, 2009.

[14] H. Ezuber, a. El-Houd, and F. El-Shawesh, “A study on the corrosion behavior of aluminum alloys in seawater,” *Mater. Des.*, vol. 29, no. 4, pp. 801–805, Jan. 2008.

[15] T. Gladman, “Precipitation hardening in metals,” *Mater. Sci. Technol.*, vol. 15, pp. 30–36, Apr. 1999.

[16] I. J. Polmear, “Aluminium Alloys – A Century of Age Hardening,” vol. 28, pp. 1–14, 2004.

[17] F. Campbell, *Elements of metallurgy and engineering alloys*. ASM International, 2008.

[18] J. R. Davis, *ASM Specialty Handbook: Aluminum and Aluminum Alloys*. 1993.

[19] G. E. Totten and D. S. MacKenzie, Eds., *Handbook of Aluminum: Volume 2: Alloy Production and Materials Manufacturing*. CRC Press, 2003.

[20] P. Campestrini, G. Goeminne, H. Terryn, J. Vereecken, and J. H. W. de Wit, “Chromate Conversion Coating on Aluminum Alloys,” *J. Electrochem. Soc.*, vol. 151, no. 2, p. B59, 2004.

[21] M. Kendig, S. Jeanjaquet, R. Addison, and J. Waldrop, “Role of hexavalent chromium in the inhibition of corrosion of aluminum alloys,” *Surf. Coatings Technol.*, vol. 140, no. 1, pp. 58–66, May 2001.

[22] J. Zhao, L. Xia, a. Sehgal, D. Lu, R. L. McCreery, and G. S. Frankel, “Effects of chromate and chromate conversion coatings on corrosion of aluminum alloy 2024-T3,” *Surf. Coatings Technol.*, vol. 140, no. 1, pp. 51–57, May 2001.

[23] U. S. Military, “MIL-DTL-5541F: Detail Specification: Chemical Conversion Coatings on Aluminum and Aluminum Alloys,” no. July. 2006.

[24] U. S. Military, “MIL-A-8625F: Military Specification: Anodic Coatings for Aluminum and Aluminum Alloys,” no. September. 2003.

[25] C. A. Grubbs, “Anodizing of Aluminum,” Alpharetta, Ga.

[26] K. E. Steube, “Thick ion-vapor-deposited aluminum coatings for irregularly shaped aircraft and spacecraft parts,” *J. Vac. Sci. Technol.*, vol. 11, no. 1, p. 362, Jan. 1974.

[27] Y. Andoh, Y. Suzuki, and K. Matsuda, “A new machine for film formation by ion and vapour deposition,” *Nucl. Instruments Methods Phys. Res.*, vol. 6, pp. 111–115, 1985.

[28] R. Tapphorn, H. Gabel, K. Hashimtot, and T. Crowe, “Kinetic Metallization - Repair of IVD Aluminum,” in *Thermal Spray 2012: Proceeding from the International Thermal Spray Conference and Exposition*, 2012, pp. 504–509.

[29] Inovati, “Kinetic Metallization: Coatings Once Thought Impossible: Al-Trans,” 2013. [Online]. Available: http://www.inovati.com/information/Coatings/Al-Trans.php.

[30] J. R. Davis, *Handbook of Thermal Spray Technology*. ASM International, 2004.

[31] Alkhimov, "Gas-Dynamic Spraying Method for Applying a Coating," 53024141994.

[32] T. Schmidt, F. Gärtner, H. Assadi, and H. Kreye, "Development of a generalized parameter window for cold spray deposition," *Acta Mater.*, vol. 54, no. 3, pp. 729–742, Feb. 2006.

[33] M. Grujicic, C. . Zhao, W. . DeRosset, and D. Helfritch, "Adiabatic shear instability based mechanism for particles/substrate bonding in the cold-gas dynamic-spray process," *Mater. Des.*, vol. 25, no. 8, pp. 681–688, Dec. 2004.

[34] E. Irissou, J.-G. Legoux, A. N. Ryabinin, B. Jodoin, and C. Moreau, "Review on Cold Spray Process and Technology: Part I—Intellectual Property," *J. Therm. Spray Technol.*, vol. 17, no. 4, pp. 495–516, Oct. 2008.

[35] H. Assadi, F. Gärtner, T. Stoltenhoff, and H. Kreye, "Bonding mechanism in cold gas spraying," *Acta Mater.*, vol. 51, no. 15, pp. 4379–4394, Sep. 2003.

[36] T. Schmidt, H. Assadi, F. Gärtner, H. Richter, T. Stoltenhoff, H. Kreye, and T. Klassen, "From Particle Acceleration to Impact and Bonding in Cold Spraying," *J. Therm. Spray Technol.*, vol. 18, no. 5–6, pp. 794–808, Aug. 2009.

[37] T. Hussain, D. G. McCartney, P. H. Shipway, and D. Zhang, "Bonding Mechanisms in Cold Spraying: The Contributions of Metallurgical and Mechanical Components," *J. Therm. Spray Technol.*, vol. 18, no. 3, pp. 364–379, Feb. 2009.

[38] F. Gärtner, C. Borchers, T. Stoltenhoff, H. Kreye, and H. Assadi, "Numerical and Microstructural Investigations of the Bonding Mechanisms in Cold Spraying," in *Thermal Spray 2003: Avdancing the Science and Applying the Technology*, 2003, pp. 1–8.

[39] S. V. Klinkov, V. F. Kosarev, and M. Rein, "Cold spray deposition: Significance of particle impact phenomena," *Aerosp. Sci. Technol.*, vol. 9, no. 7, pp. 582–591, Oct. 2005.

[40] M. Grujicic, J. R. Saylor, D. E. Beasley, W. S. DeRosset, and D. Helfritch, "Computational analysis of the interfacial bonding between feed-powder particles and the substrate in the cold-gas dynamic-spray process," *Appl. Surf. Sci.*, vol. 219, no. 3–4, pp. 211–227, Dec. 2003.

[41] P. Richer, B. Jodoin, L. Ajdelsztajn, and E. J. Lavernia, "Substrate Roughness and Thickness Effects on Cold Spray Nanocrystalline Al-Mg Coatings," *J. Therm. Spray Technol.*, vol. 15, no. 2, pp. 246–254, Jun. 2006.

[42] P. C. King, C. Busch, T. Kittel-Sherri, M. Jahedi, and S. Gulizia, “Interface melding in cold spray titanium particle impact,” *Surf. Coatings Technol.*, vol. 239, pp. 191–199, Jan. 2014.

[43] T. H. Van Steenkiste, J. R. Smith, and R. E. Teets, “Aluminum coatings via kinetic spray with relatively large powder particles,” *Surf. Coatings Technol.*, vol. 154, no. 2–3, pp. 237–252, May 2002.

[44] J. Wu, H. Fang, S. Yoon, C. Lee, and H. Kim, “Critical Velocities for High Speed Particle Deposition in Kinetic Spraying,” *Mater. Trans.*, vol. 47, no. 7, pp. 1723–1727, 2006.

[45] C.-J. Li, W.-Y. Li, and H. Liao, “Examination of the Critical Velocity for Deposition of Particles in Cold Spraying,” *J. Therm. Spray Technol.*, vol. 15, no. 2, pp. 212–222, Jun. 2006.

[46] F. Raletz, M. Vardelle, and G. Ezo’o, “Critical particle velocity under cold spray conditions,” *Surf. Coatings Technol.*, vol. 201, no. 5, pp. 1942–1947, Oct. 2006.

[47] T. Schmidt, F. Gaertner, and H. Kreye, “New Developments in Cold Spray Based on Higher Gas and Particle Temperatures,” *J. Therm. Spray Technol.*, vol. 15, no. December, pp. 488–494, 2006.

[48] C.-J. Li, W.-Y. Li, Y.-Y. Wang, G.-J. Yang, and H. Fukanuma, “A theoretical model for prediction of deposition efficiency in cold spraying,” *Thin Solid Films*, vol. 489, no. 1–2, pp. 79–85, Oct. 2005.

[49] S. V. Klinkov and V. F. Kosarev, “Measurements of Cold Spray Deposition Efficiency,” *J. Therm. Spray Technol.*, vol. 15, no. 3, pp. 364–371, Sep. 2006.

[50] D. L. Gilmore, R. C. Dykhuizen, R. A. Neiser, T. J. Roemer, and M. F. Smith, “Particle Velocity and Deposition Efficiency in the Cold Spray Process,” vol. 8, no. December, pp. 576–582, 1999.

[51] T. Schmidt, F. Gaertner, and H. Kreye, “New Developments in Cold Spray Based on Higher Gas and Particle Temperatures,” *J. Therm. Spray Technol.*, vol. 15, no. 4, pp. 488–494, Dec. 2006.

[52] Fox and McDonald, *Introduction to Fluid Mechanics*, 8th ed. 2011.

[53] J. G. Legoux, E. Irissou, and C. Moreau, “Effect of Substrate Temperature on the Formation Mechanism of Cold-Sprayed Aluminum, Zinc and Tin Coatings,” *J. Therm. Spray Technol.*, vol. 16, no. 5–6, pp. 619–626, Oct. 2007.

[54] K. Taylor, B. Jodoin, and J. Karov, “Particle Loading Effect in Cold Spray,” *J. Therm. Spray Technol.*, vol. 15, no. 2, pp. 273–279, Jun. 2006.

[55] R. Morgan, P. Fox, J. Pattison, C. Sutcliffe, and W. O'Neill, "Analysis of cold gas dynamically sprayed aluminium deposits," *Mater. Lett.*, vol. 58, no. 7–8, pp. 1317–1320, Mar. 2004.

[56] M. Dorfman, "Thermal Spray Basics," *Adv. Mater. Process.*, pp. 47–50, 2002.

[57] T. C. Hanson and G. S. Settles, "Particle Temperature and Velocity Effects on the Porosity and Oxidation of an HVOF Corrosion-Control Coating," *J. Therm. Spray Technol.*, vol. 12, no. September, pp. 403–415, 2003.

[58] "ASTM C 633 - 01: Standard Test Method for Adhesion or Cohesion Strength of Thermal Spray Coatings," vol. 03, no. July. ASTM, pp. 1–7, 2001.

[59] P. E. Plantz, "Explanation of Data Reported by Microtrac Instruments," 2008.

[60] B. Jodoin, L. Ajdelsztajn, E. Sansoucy, a. Zúñiga, P. Richer, and E. J. Lavernia, "Effect of particle size, morphology, and hardness on cold gas dynamic sprayed aluminum alloy coatings," *Surf. Coatings Technol.*, vol. 201, no. 6, pp. 3422–3429, Dec. 2006.

[61] "ASTM B117-11: Standard Practice for Operating Salt Spray (Fog) Apparatus," no. C. ASTM, pp. 1–12, 2011.

[62] J. R. Davis, "Corrosion Control by Cathodic and Anodic Protection," in *Corrosion: Understanding the Basics*, ASM International, 2000, pp. 407–427.

[63] "ASTM D4060 - 10: Standard Test Method for Abrasion Resistance of Organic Coatings by the Taber." ASTM, pp. 1–5, 2011.

[64] Sonntag, Borgnakke, and VanWylen, *Fundementals of Thermodynamics*, Fifth. 1998.

[65] A. W. Bowen and P. G. Partidge, "Limitations of the Hollomon strain-hardening equationt," *J. Appl. Phys.*, vol. 7, pp. 969–978, 1974.

APPENDIX I: Maximum Exposure Temperature/ Time for Aluminum Alloys

ALLOY	CONDITION	MAXIMUM CUMULATIVE TIME – HOURS 1/						
		250°F (121°C)	275°F (135°C)	300°F (149°C)	325°F (165°C)	350°F (177°C)	375°F (191°C)	600°F (316°C)
2014	–T6XX –W	32 4/ 32 4/	32 4/ 32 4/	10 32 4/	10 10	2 1	1/2 3/	3/
2024 2124 2219	–T6X, –T72 –T8XX	32 4/ 32 4/	32 4/ 32 4/	10 10	10 10	1 7	1/2 2	3/ 3/
2090	–T6X –T8X	1 1	1 1	1 1	3/4 3/4	3/4 3/4	3/4 3/4	3/ 3/
6061	–T6XX	32 4/	32 4/	10	10	3	3/4	3/
7075 7178	–T6XX –W –T76XX	32 4/ 10 32 4/	8 1 10	2 3/ 4	3/4 3/ 1	3/ 3/ 1/2	3/ 3/ 3/	3/ 3/ 3/
7049 7075	–T73XX	32 4/	32 4/	10	3	3/4	3/	3/
7050 7075 7175	–T74XX	32 4/	8	2	3/4	3/	3/	3/
7079	–T6XX	10	1	3/	3/	3/	3/	3/
8090	–T8X	2/	2/	10	3/	3/	3/	3/

NOTES: 1/ The sum of fractional times at different temperatures must not exceed one, e.g., for a 6061 part exposed at 300°F (149°C) for 5 hours, another 5 hours at 325°F (163°C) or another 1–1/2 hours at 350°F (177°C) is acceptable.

2/ Do not form or straighten at this temperature to avoid orange peel or excessive residual stresses.

3/ Do not form or straighten at this temperature to avoid overheating and loss in strength.

4/ Times in excess of 32 hours require review by Material and Process (Dept. 679) prior to exceeding 32 hours exposure.

Figure AI.1: Table showing the maximum exposure temperatures and times for aluminum alloys.

APPENDIX II: Mounting procedure of FM1000 on samples

1. Machine minimal thickness off of coatings to ensure surface is flat.
2. Remove the FM1000 glue from freezer and put in a stove at 160-180°F (70-80°C) for 45min to 1h. This will ensure there is no humidity in the glue.
3. Grit blast the uncoated bond plug with Al_2O_3 80 mesh at an angle of 45 degree, at a pressure of 50 psi and a distance of 2-5".
4. Preheat the stove to 375°F (190°C) (this will guarantee a minimum temperature of 350°F everywhere in the oven).
5. Sand the faces of machined sample on a 240 grit paper without applying pressure in a slow figure eight shape. Clean the face with compress air to remove all dust and residue. The goal of this step is to have raw metal. Do not touch the surface with fingers.
6. Place the coated sample on the bottom part of the fixture.
7. Carefully place disk of glue on each sample.
8. Put the opposite sample gently on the FM1000 glue.
9. Ensure that the two bond plugs are aligned perfectly.
10. Use a torque wrench at a torque of 3.0 Nm to tighten the samples.
11. Place the fixture in the oven for at least 2 hours at 375°F.
12. After 2 hours of curing, stop the stove and let it cold down by keeping the stove door closed.
13. When the fixtures are cold, remove the samples from the oven. The glue should have changed to yellow. Disassemble all the sample of the fixture without imposing forces on the samples. (Take them gently by the two sides and without tension, compression or shear force).
14. Test the samples.

APPENDIX III: Powder Analysis

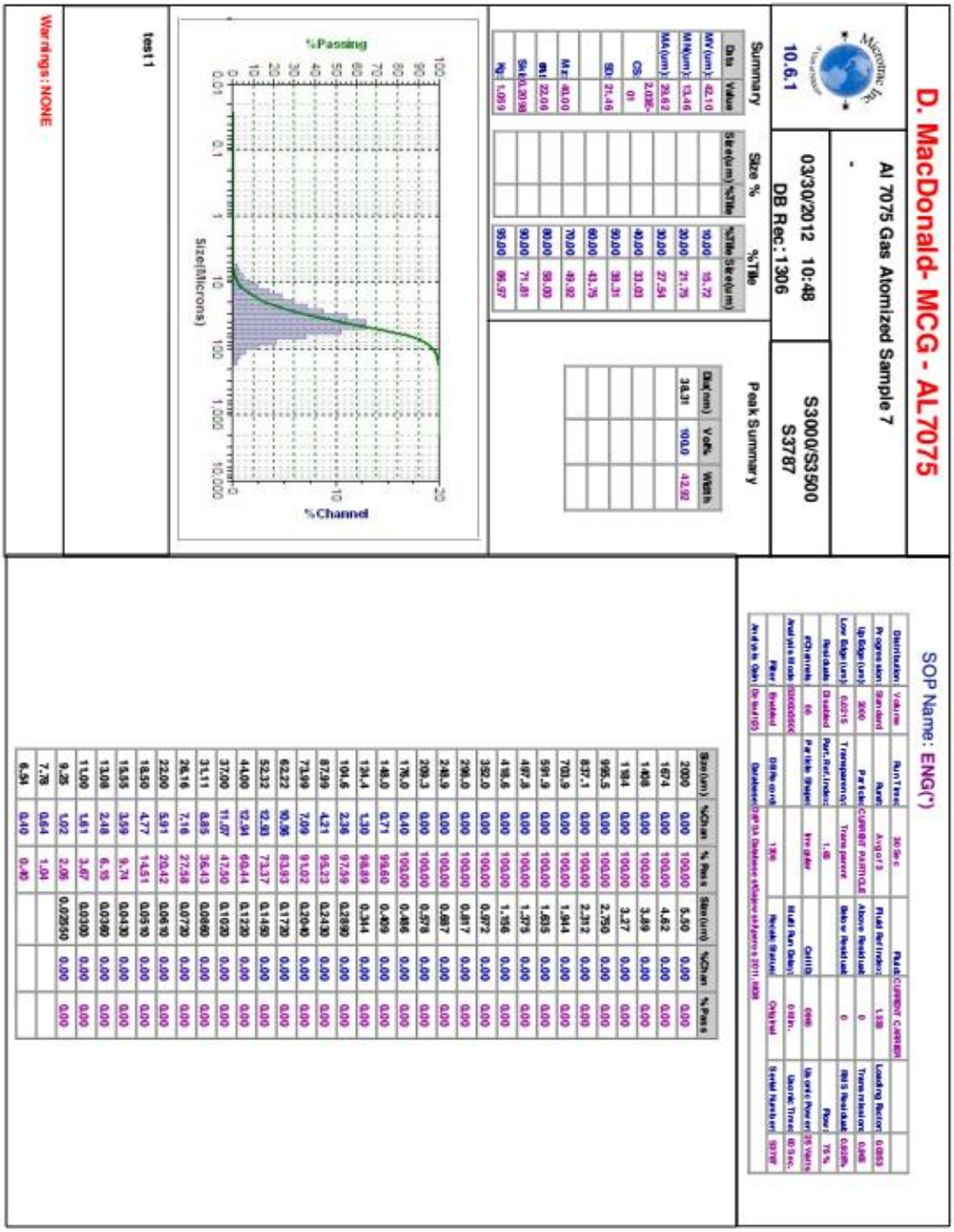

Figure AIII.1:Aluminum 7075 powder analysis results.

D. MacDonald- MCG - PUREAL

Microtrac Inc

10.6.1

PUREAL Sample 5

-

03/30/2012 11:19

DB Rec: 1318

S3000/S3500

S3787

SOP Name: ENG(*)

Distribution:	Volume	Run Time:	30 Sec	Fluid:	CURRENT CARRIER		
Progression:	Standard	Runs:	Avg of 3	Fluid Ref Index:	1.333	Loading Factor:	0.0317
Up Edge(um):	2000	Particle:	CURRENT PARTICLE	Above Residual:	0	Transmission:	0.966
Low Edge(um):	0.0215	Transparency:	Transparent	Below Residual:	0	RMS Residual:	1.268%
Residuals:	Disabled	Part. Ref. Index:	1.65			Flow:	75 %
#Channels:	66	Particle Shape:	Irregular	Cell ID:	0.966	Usonic Power:	25 Watts
Analysis Mode:	S3000/3500			Multi Run Delay:	0 Min.	Usonic Time:	60 Sec.
Filter:	Enabled	DB Record:	1318	Recalc Status:	Original	Serial Number:	S3787
Analysis Gain:	Default(2)	Database:	D:\PSA Databases\Gajewski\Iperos 2011.MDB				

Summary

Data	Value
MV(um):	29.33
MN(um):	14.36
MA(um):	22.52
CS:	2.66E-01
SD:	13.51
Mz:	27.69
σι:	14.36
Ski:	0.346
Kg:	1.155

Size(um)	%Tile

%Tile	Size(um)
10.00	13.29
20.00	16.57
30.00	19.44
40.00	22.28
50.00	25.35
60.00	28.85
70.00	33.16
80.00	39.08
90.00	49.58
95.00	61.27

Peak Summary

Dia(nm)	Vol%	Width
25.35	100.0	27.03

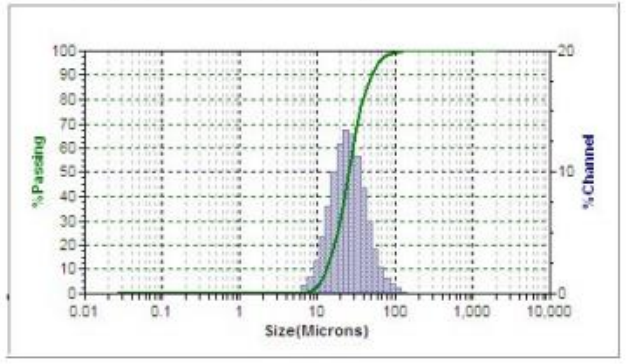

test 2

Warnings: NONE

Size(um)	%Chan	% Pass	Size(um)	%Chan	% Pass
2000	0.00	100.00	5.50	0.00	0.00
1674	0.00	100.00	4.62	0.00	0.00
1408	0.00	100.00	3.89	0.00	0.00
1184	0.00	100.00	3.27	0.00	0.00
995.5	0.00	100.00	2.750	0.00	0.00
837.1	0.00	100.00	2.312	0.00	0.00
703.9	0.00	100.00	1.944	0.00	0.00
591.9	0.00	100.00	1.635	0.00	0.00
497.8	0.00	100.00	1.375	0.00	0.00
418.6	0.00	100.00	1.156	0.00	0.00
352.0	0.00	100.00	0.972	0.00	0.00
296.0	0.00	100.00	0.817	0.00	0.00
248.9	0.00	100.00	0.687	0.00	0.00
209.3	0.00	100.00	0.578	0.00	0.00
176.0	0.00	100.00	0.486	0.00	0.00
148.0	0.10	100.00	0.409	0.00	0.00
124.4	0.46	99.90	0.344	0.00	0.00
104.6	0.75	99.44	0.2890	0.00	0.00
87.99	1.26	98.69	0.2430	0.00	0.00
73.99	2.16	97.43	0.2040	0.00	0.00
62.22	3.68	95.27	0.1720	0.00	0.00
52.32	5.93	91.59	0.1450	0.00	0.00
44.00	8.70	85.66	0.1220	0.00	0.00
37.00	11.36	76.96	0.1020	0.00	0.00
31.11	13.13	65.60	0.0860	0.00	0.00
26.16	13.44	52.47	0.0720	0.00	0.00
22.00	12.36	39.03	0.0610	0.00	0.00
18.50	10.03	26.67	0.0510	0.00	0.00
15.55	7.21	16.64	0.0430	0.00	0.00
13.08	4.64	9.43	0.0360	0.00	0.00
11.00	2.69	4.79	0.0300	0.00	0.00
9.25	1.42	2.10	0.02550	0.00	0.00
7.78	0.68	0.68			
6.54	0.00	0.00			

Figure AIII.2: Pure aluminum powder analysis results.

D. MacDonald- MCG - AL5083

Microtrac Inc

10.6.1

Al 5083 Gas Atomized Sample 3

-

03/30/2012 10:21

DB Rec: 1298

S3000/S3500

S3787

SOP Name: ENG(*)

Distribution:	Volume	Run Time:	30 Sec	Fluid:	CURRENT CARRIER		
Progression:	Standard	Runs:	Avg of 3	Fluid Ref Index:	1.333	Loading Factor:	0.0157
Up Edge(um):	2000	Particle:	CURRENT PARTICLE	Above Residual:	0	Transmission:	0.967
Low Edge(um):	0.0215	Transparency:	Transparent	Below Residual:	0	RMS Residual:	0.760%
Residuals:	Disabled	Part. Ref. Index:	1.65			Flow:	75 %
#Channels:	66	Particle Shape:	Irregular	Cell ID:	0.966	Usonic Power:	25 Watts
Analysis Mode:	S3000/3500			Multi Run Delay:	0 Min.	Usonic Time:	60 Sec.
Filter:	Enabled	DB Record:	1298	Recalc Status:	Original	Serial Number:	S3787
Analysis Gain:	Default(2)	Database:	C:\PSA Databases\Gajewski\Aperos 2011.MDB				

Summary

Data	Value
MV(um):	21.89
MN(um):	5.20
MA(um):	12.88
CS:	4.66E-01
SD:	13.04
Mz:	19.83
σz:	14.01
Ski:	0.351
Kg:	1.161

Size %		%Tile	
Size(um)	%Tile	%Tile	Size(um)
		10.00	6.20
		20.00	8.87
		30.00	11.73
		40.00	14.73
		50.00	17.83
		60.00	21.24
		70.00	25.26
		80.00	30.76
		90.00	41.09
		95.00	54.21

Peak Summary

Dia(nm)	Vol%	Width
17.83	100.0	26.08

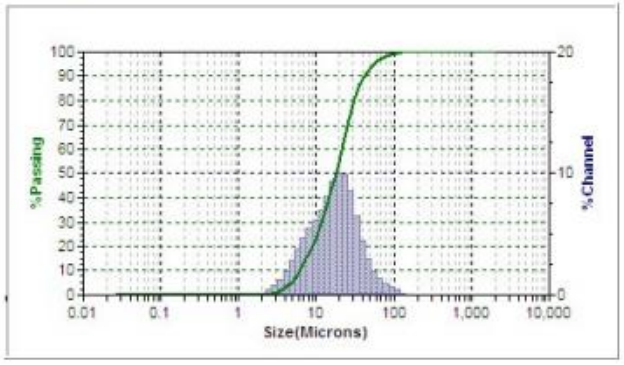

-

Warnings: NONE

Size(um)	%Chan	% Pass	Size(um)	%Chan	% Pass
2000	0.00	100.00	5.50	2.85	7.46
1674	0.00	100.00	4.62	1.98	4.61
1408	0.00	100.00	3.89	1.31	2.63
1184	0.00	100.00	3.27	0.82	1.32
995.5	0.00	100.00	2.750	0.50	0.50
837.1	0.00	100.00	2.312	0.00	0.00
703.9	0.00	100.00	1.944	0.00	0.00
591.9	0.00	100.00	1.635	0.00	0.00
497.8	0.00	100.00	1.375	0.00	0.00
418.6	0.00	100.00	1.156	0.00	0.00
352.0	0.00	100.00	0.972	0.00	0.00
296.0	0.00	100.00	0.817	0.00	0.00
248.9	0.00	100.00	0.687	0.00	0.00
209.3	0.00	100.00	0.578	0.00	0.00
176.0	0.00	100.00	0.486	0.00	0.00
148.0	0.10	100.00	0.409	0.00	0.00
124.4	0.44	99.90	0.344	0.00	0.00
104.6	0.66	99.46	0.2890	0.00	0.00
87.99	0.95	98.80	0.2430	0.00	0.00
73.99	1.35	97.85	0.2040	0.00	0.00
62.22	1.96	96.50	0.1720	0.00	0.00
52.32	2.96	94.54	0.1450	0.00	0.00
44.00	4.51	91.58	0.1220	0.00	0.00
37.00	6.54	87.07	0.1020	0.00	0.00
31.11	8.58	80.53	0.0860	0.00	0.00
26.16	9.90	71.95	0.0720	0.00	0.00
22.00	10.00	62.05	0.0610	0.00	0.00
18.50	9.35	52.05	0.0510	0.00	0.00
15.55	8.16	42.70	0.0430	0.00	0.00
13.08	7.02	34.54	0.0360	0.00	0.00
11.00	6.13	27.52	0.0300	0.00	0.00
9.25	5.43	21.39	0.02550	0.00	0.00
7.78	4.69	15.96			
6.54	3.81	11.27			

Figure AIII.2:Aluminum 5083 powder analysis results.

APPENDIX IV: Full Corrosion Results for CGDS Restorations of Damaged Aluminum IVD Coatings

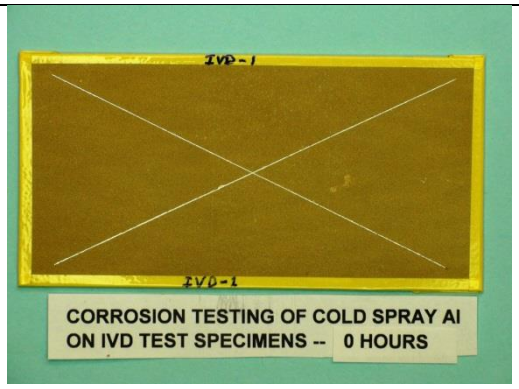

0 Hours

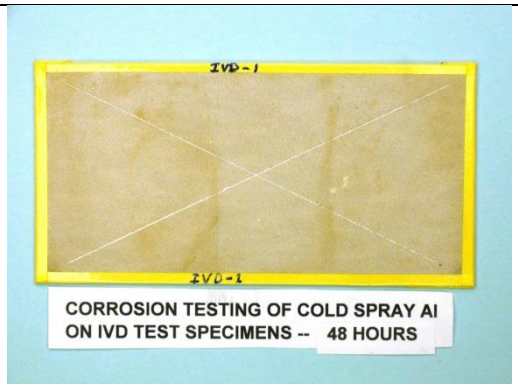

48 Hours

168 Hours

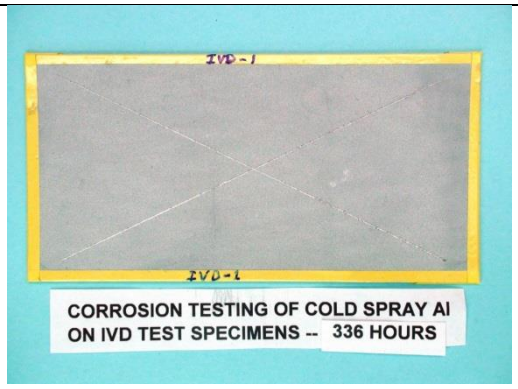

336 Hours

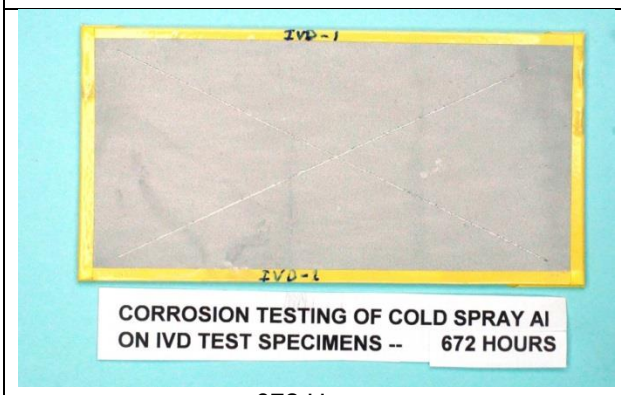

672 Hours

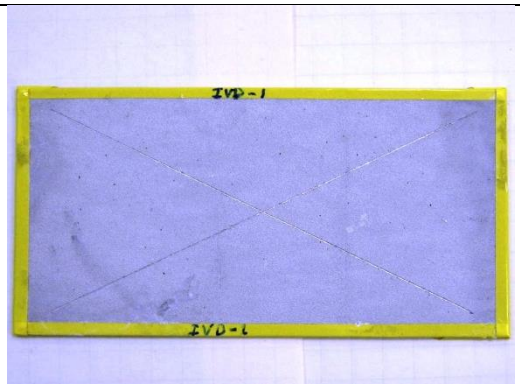

1000 Hours

Figure AIV.1: Full corrosion results for pure aluminum restoration of damaged aluminum IVD coating (Sample 1).

0 Hours

48 Hours

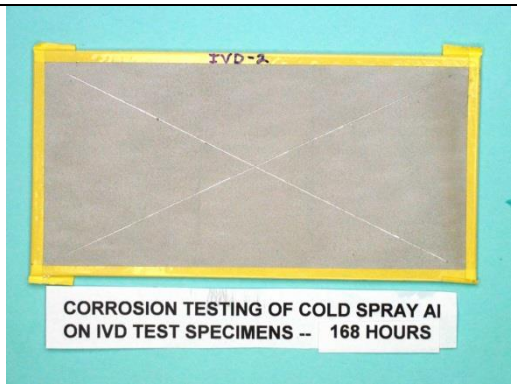

168 Hours

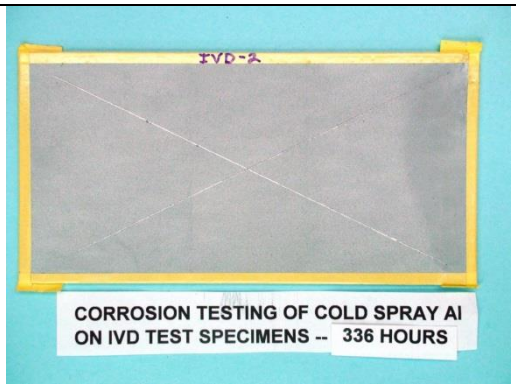

336 Hours

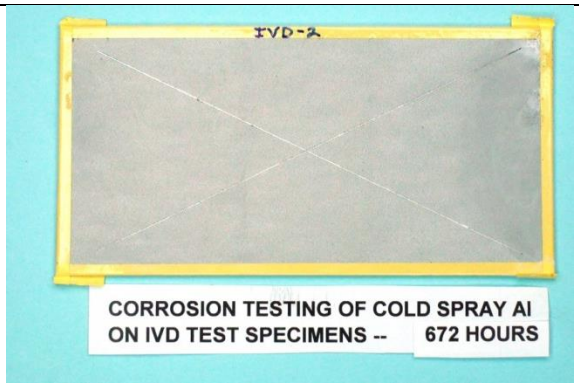

672 Hours

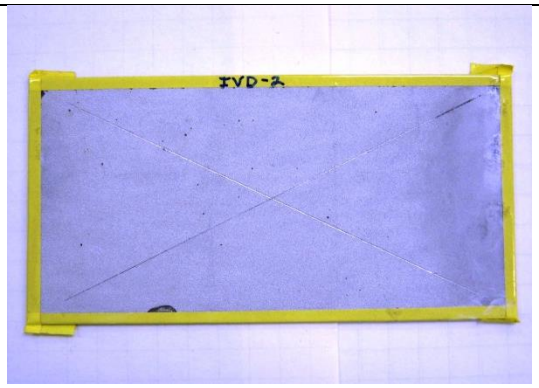

1000 Hours

Figure AIV.2: Full corrosion results for pure aluminum restoration of damaged aluminum IVD coating (Sample 2).

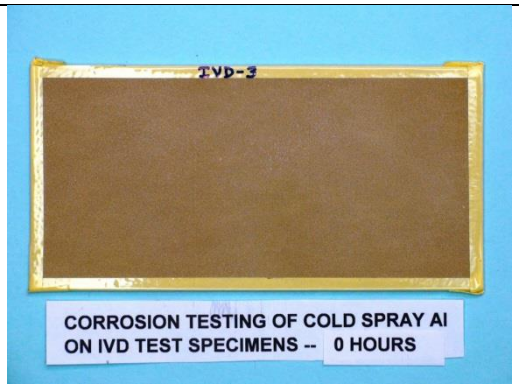

0 Hours

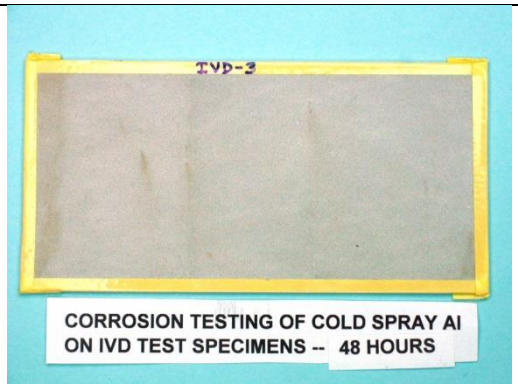

48 Hours

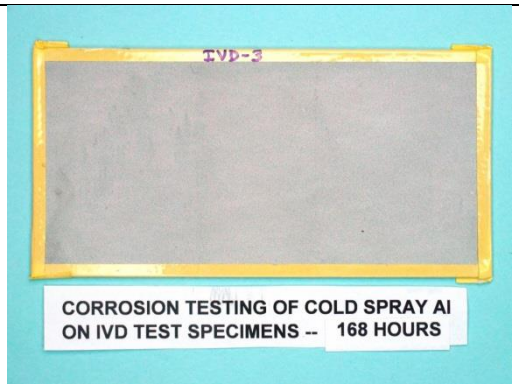

168 Hours

336 Hours

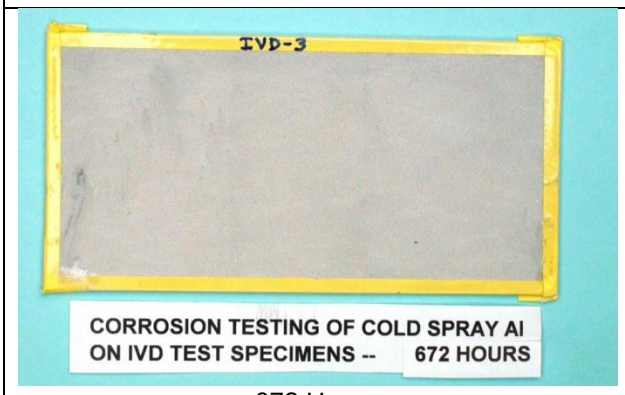

672 Hours

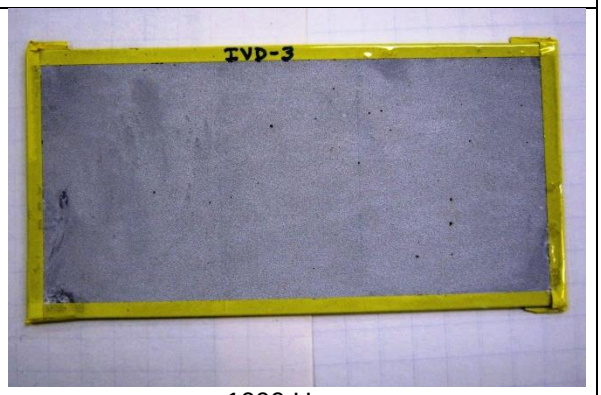

1000 Hours

Figure AIV.3: Full corrosion results for pure aluminum restoration of damaged aluminum IVD coating (Sample 3).

0 Hours

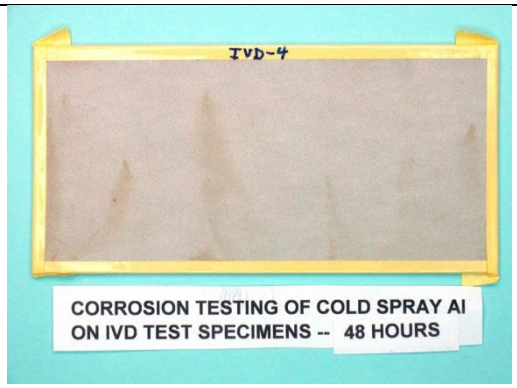

48 Hours

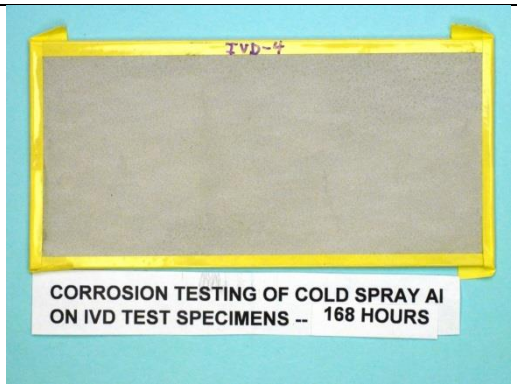

168 Hours

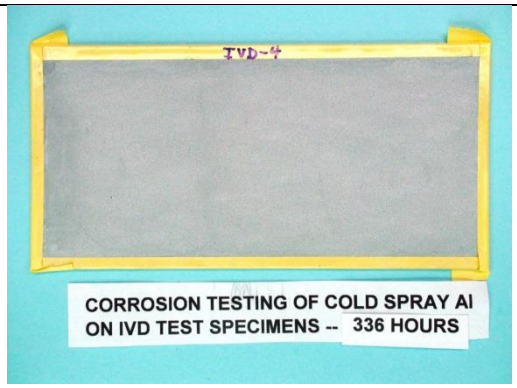

336 Hours

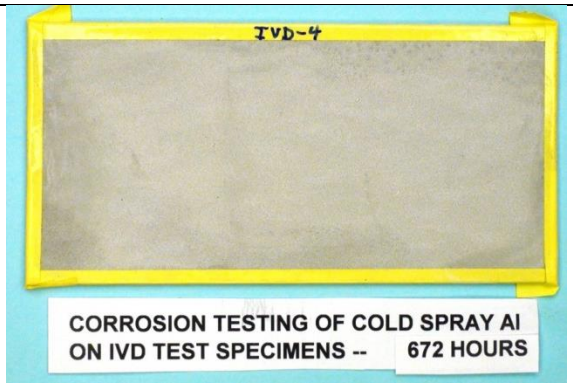

672 Hours

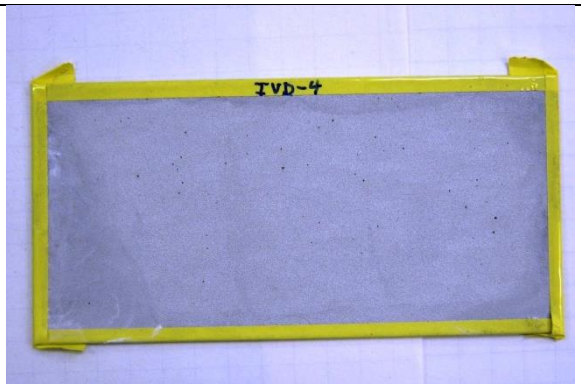

1000 Hours

Figure AIV.4: Full corrosion results for pure aluminum restoration of damaged aluminum IVD coating (Sample 4).

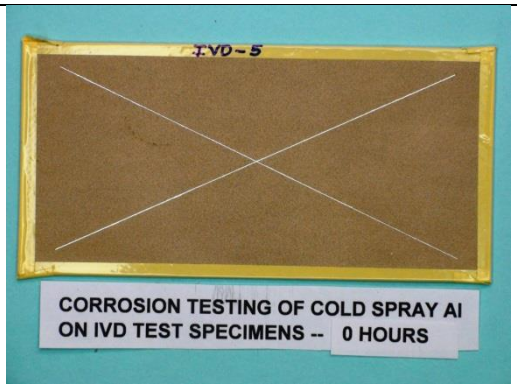

0 Hours

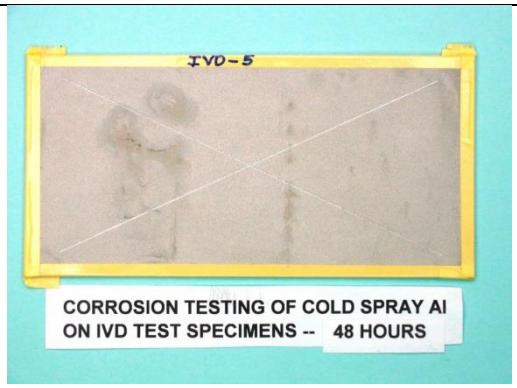

48 Hours

168 Hours

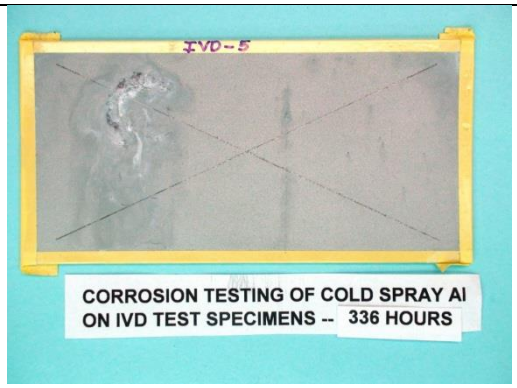

336 Hours

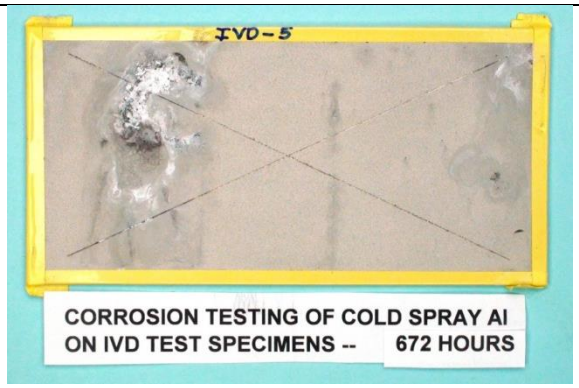

672 Hours

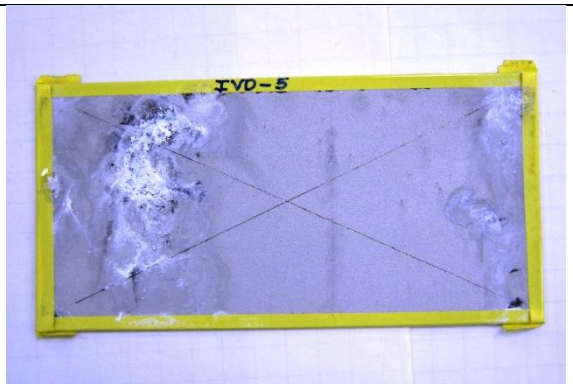

1000 Hours

Figure AIV.5: Full corrosion results for aluminum 7075 restoration of damaged aluminum IVD coating (Sample 5).

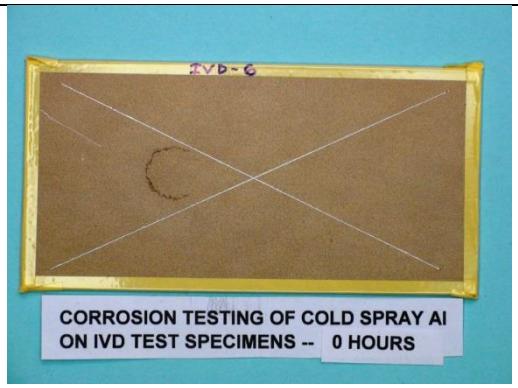

0 Hours

48 Hours

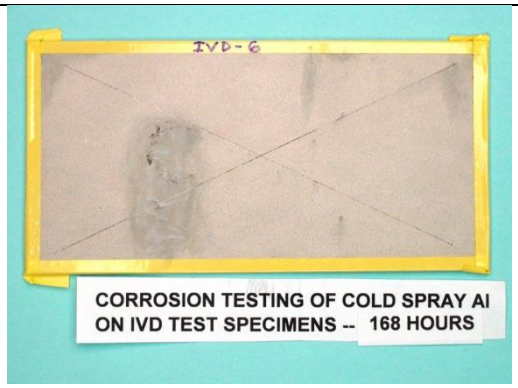

168 Hours

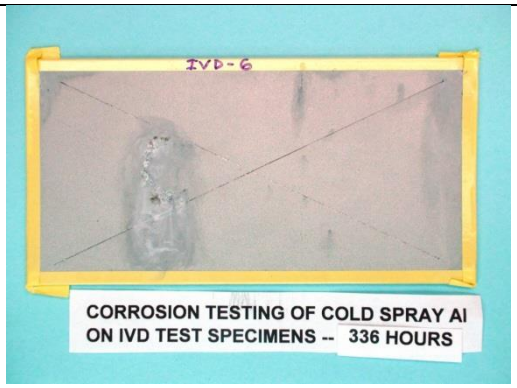

336 Hours

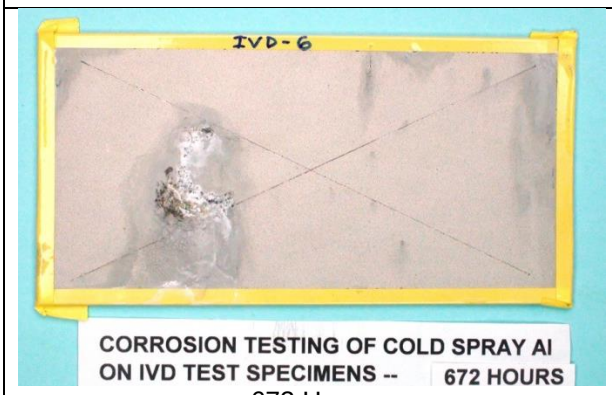

672 Hours

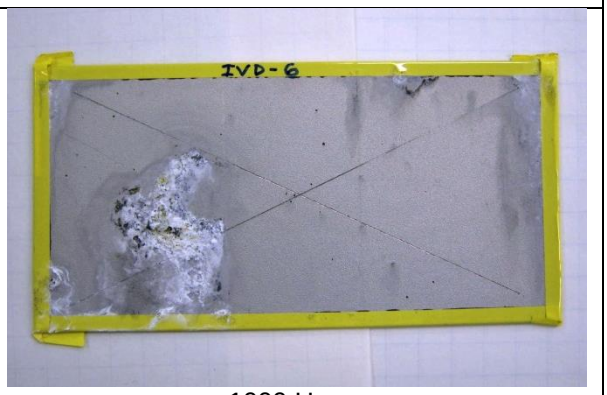

1000 Hours

Figure AIV.6: Full corrosion results for aluminum 7075 restoration of damaged aluminum IVD coating (Sample 6).

0 Hours

48 Hours

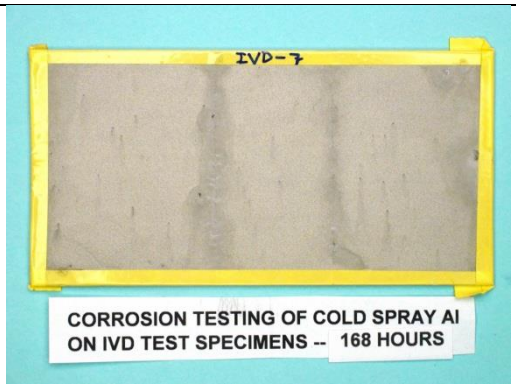

168 Hours

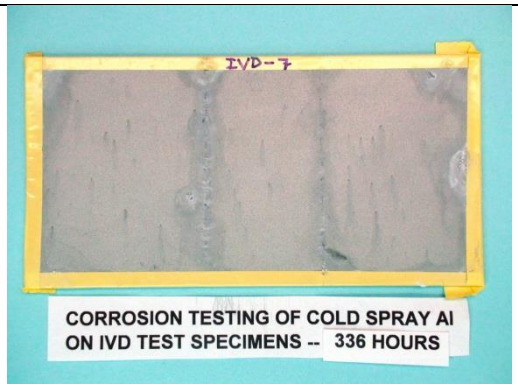

336 Hours

672 Hours

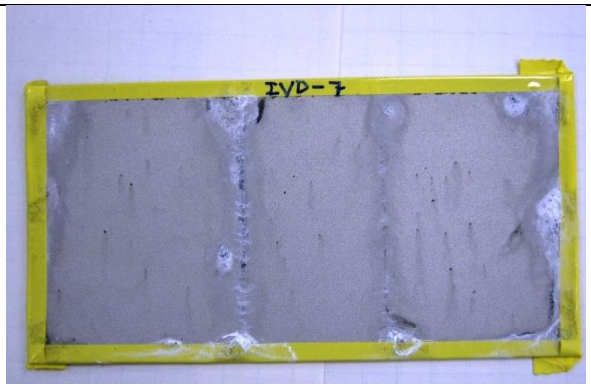

1000 Hours

Figure AIV.7: Full corrosion results for aluminum 7075 restoration of damaged aluminum IVD coating (Sample 7).

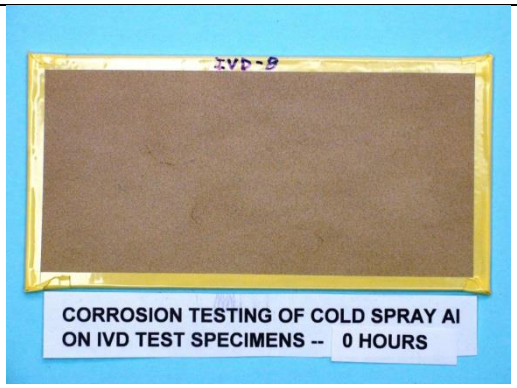

0 Hours

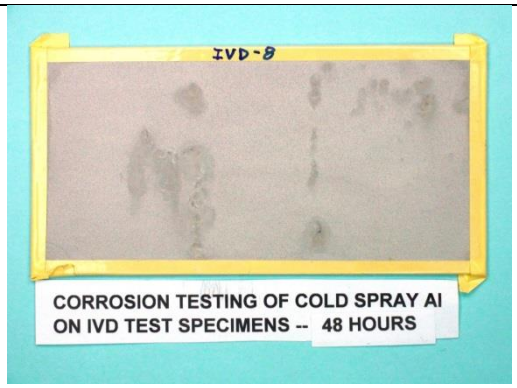

48 Hours

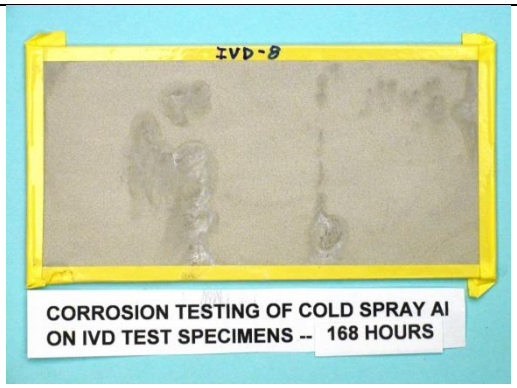

168 Hours

336 Hours

672 Hours

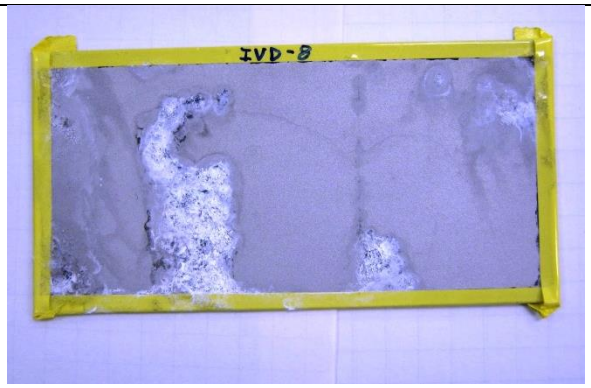

1000 Hours

Figure AIV.8: Full corrosion results for aluminum 7075 restoration of damaged aluminum IVD coating (Sample 8).

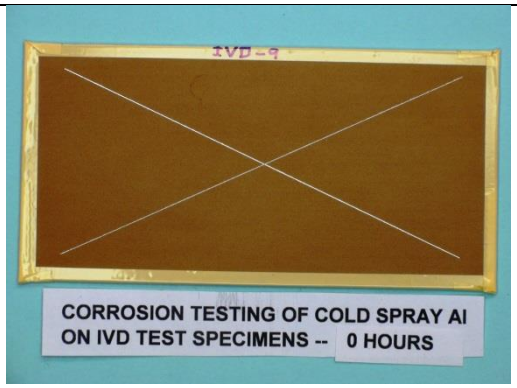

0 Hours

48 Hours

168 Hours

336 Hours

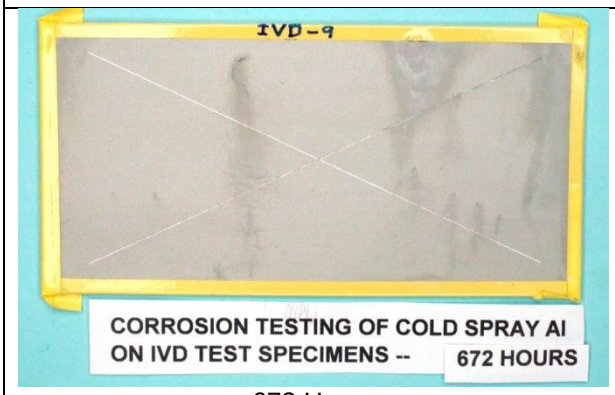

672 Hours

1000 Hours

Figure AIV.9: Full corrosion results for aluminum 5083 restoration of damaged aluminum IVD coating (Sample 9).

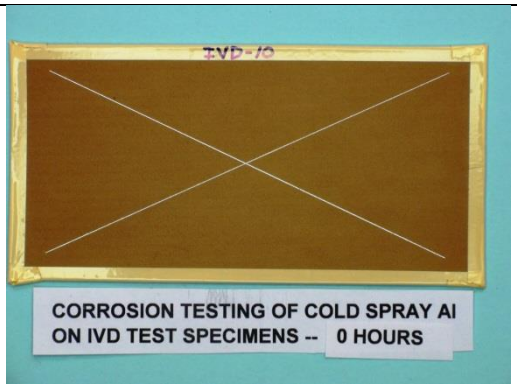

0 Hours

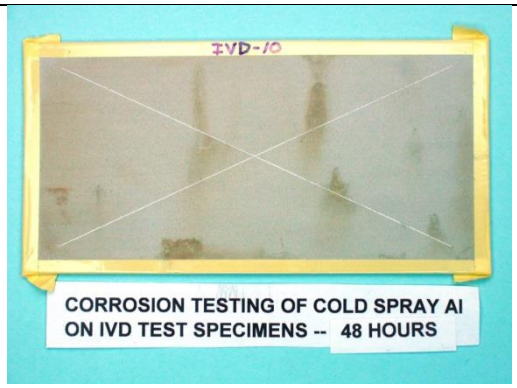

48 Hours

168 Hours

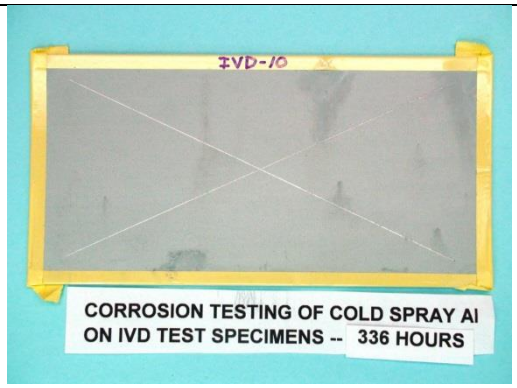

336 Hours

672 Hours

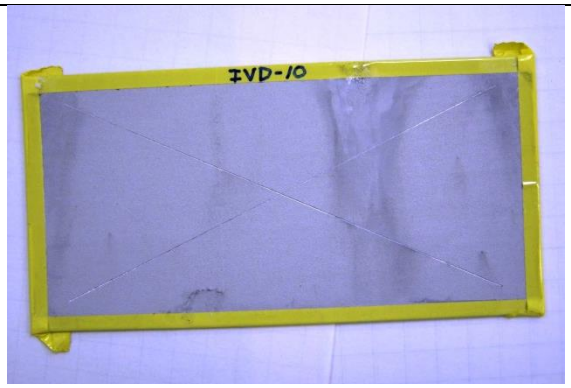

1000 Hours

Figure AIV.10: Full corrosion results for aluminum 5083 restoration of damaged aluminum IVD coating (Sample 10).

0 Hours

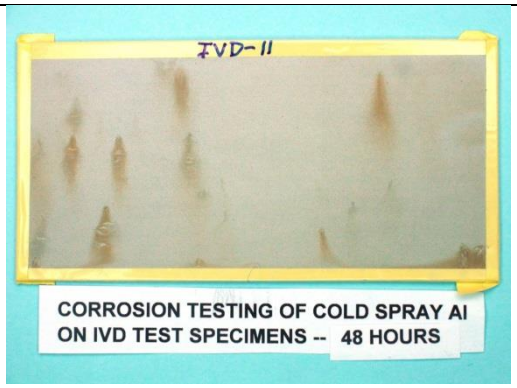

48 Hours

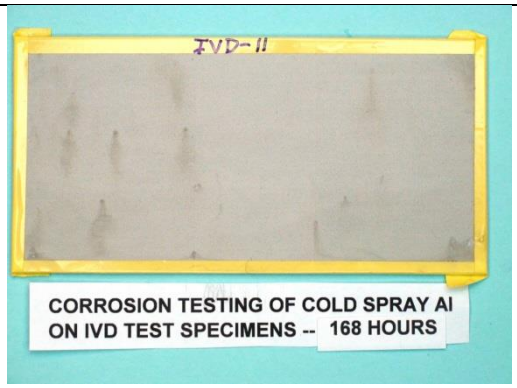

168 Hours

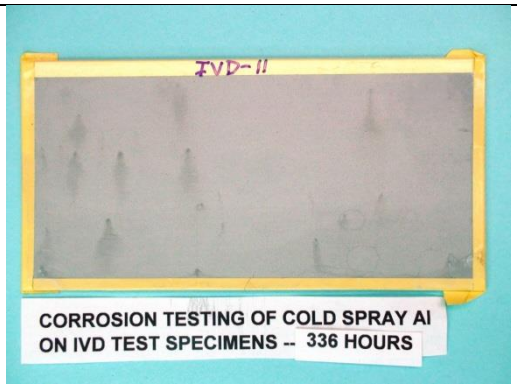

336 Hours

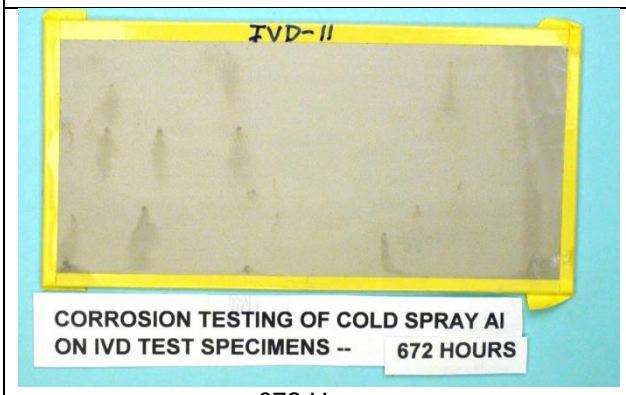

672 Hours

1000 Hours

Figure AIV.11: Full corrosion results for aluminum 5083 restoration of damaged aluminum IVD coating (Sample 11).

0 Hours

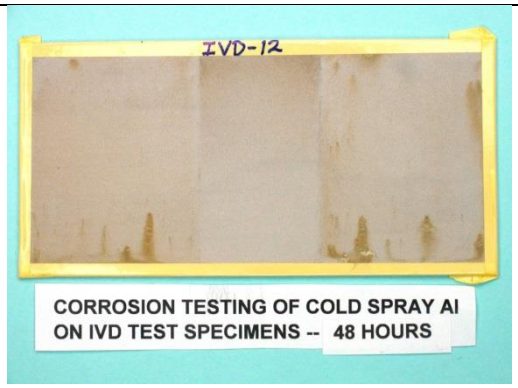

48 Hours

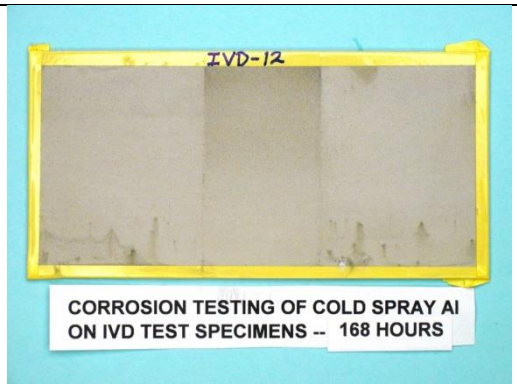

168 Hours

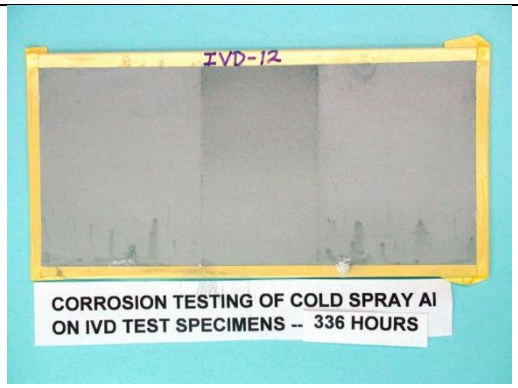

336 Hours

672 Hours

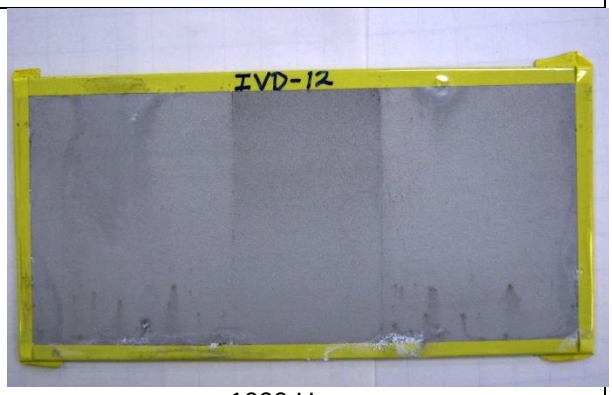

1000 Hours

Figure AIV.12: Full corrosion results for aluminum 5083 restoration of damaged aluminum IVD coating (Sample 12).